Università degli Studi di Napoli "Federico II"

Facoltà di Scienze Matematiche, Naturali e Fisiche
Dipartimento di Scienze Fisiche

Dottorato di Ricerca
in
Fisica Fondamentale ed Applicata
XV Ciclo

Mauro Sereno

The Gravitational Lens Equation

Candidato
Mauro Sereno

Tutor
Ch.mo Prof. Massimo Capaccioli

Coordinatore del XV ciclo
Ch.mo Prof. Antonino Sciarrino

Al prof. Ruggiero de Ritis

Contents

Prefazione

Questo lavoro di tesi discute approfondimenti teorici ed applicazioni cosmografiche dell'*equazione della lente gravitazionale*. Questa è l'equazione fondamentale del lensing gravitazionale, la teoria che descrive la deflessione della luce causata da campi gravitazionali. Le proprietà della lente e la geometria del sistema sorgente-lente-osservatore concorrono alla scrittura dell'equazione, derivata nelle approssimazioni di ottica geometrica per la propagazione della luce, e di campo debole e piccole velocità per la lente sottile. Derminate con osservazioni astronomiche le caratteristiche di alcuni degli elementi che partecipano al fenomeno, si può risalire alle proprietà dei rimanenti.

L'equazione della lente viene derivata nell'ambito di una teoria della gravità che determini le traiettorie dei raggi luminosi in spazi-tempi curvi. La teoria usualmente adottata è la relatività generale. Lo sviluppo tecnologico dell'astronomia di questi anni invita comunque a sottoporre a verifica sperimentale teorie della gravità che, sebbene ancora basate sul principio di equivalenza, differiscano dalla relatività generale nelle equazioni di campo. La prima parte di questa tesi sviluppa la teoria del lensing gravitazionale in una generica teoria della gravità. Eventuali divergenze tra diverse teorie emergono quando si considerino ordini superiori. In particolare, il contributo del campo gravito-magnetico e le correzioni post-post-Newtoniane alle quantità caratteristiche del lensing gravitazionale saranno esplicitamente considerati.

I risultati fondamentali ed i teoremi più importanti ricavati dallo studio della mappa del lensing saranno estesi in modo da includere l'effetto delle correnti di massa sulla curvatura dello spazio-tempo. Le caratteristiche di alcuni dei modelli di lente più comunemente impiegati in astrofisica saranno esaminate.

La seconda parte della tesi considera applicazioni fenomenologiche dell'equazione della lente gravitazionale. Note le proprietà della lente e della sorgente, osservazioni astronomiche di fenomeni di lensing gravitazionale possono fornire significative informazioni sull'ambiente in cui i sistemi di lensing si immergono, l'universo. Assumendo che l'universo evolva in accordo con la relatività generale, considereremo la possibilità di determinare il suo contenuto energetico tramite osservazioni di archi luminosi giganti e di conteggi numerici di galassie di fondo in ammassi di galassie che agiscano da lente sulle galassie retrostanti. Questo studio si inserisce nell'ambito dei due maggiori problemi della cosmologia osservativa moderna: la stima della materia oscura e la

caratterizzazione dell'energia oscura, i due ancora poco definiti componenti dell'universo proposti per spiegare gli attuali dati sperimentali.

Il secondo problema osservativo considerato è la caratterizzazione della distanze cosmologiche nell'universo reale. L'equazione della lente, reiterata per successivi campi deflettenti, permette di derivare la relazione tra la distanza ed il redshift in universi disomogenei su piccola scala. La convinzione, andatasi maturando negli ultimi anni, di un universo in espansione accellerata è principlamente basata su misure di distanza di luminosità. L'impatto del lensing gravitazionale su questa conclusione sarà valutato.

Introduction

Historical remarks

Gravitational lensing is the deflection of light by a gravitational field. This topic was first considered by Isaac Newton in the Query 1 of the first edition of his *Opticks* "Do not Bodies act upon Light at a distance, and by their action bend its Rays; and is not this action strongest at the least distance?" [131]. However, he did not seem to have really studied the problem, which was carried further almost three generations later. John Michell in 1783 [125] and Pierre-Simon Laplace in 1796 [110] independently investigated the action of a body on the very light it emits. So, they anticipated the existence of black holes, sufficiently massive stars which are invisible since they capture their own light. Around 1784, Michell's considerations stimulated Henry Cavendish to calculate the deflection of light from a distant source by a foreground gravitational field. He assumed the corpuscular theory of light and Newton's law of gravitation. His result was reported on an " isolated scrap" of paper but it was not published [220]. The next closest calculation is due to Johann von Soldier in 1801 [207]. He pointed out "Thus when a light ray passes by a celestial body it will, instead of going on in a straight direction, be forced by its attraction to describe a hyperbola whose concave side is directed against the attracting body". He also calculated that a ray grazing the sun would be deflected by 0.84 arcseconds. This is one of the first known calculations of the history of gravitational lensing. No more queries without an answer and mysterious scrap, finally a number.

More than 100 years later, Albert Einstein in 1911 [57] employed the equivalence principle to re-derive the von Soldner's estimate; he also spurred astronomers to investigate this question. A century before, von Soldier concluded that the perturbation of light rays was beyond the possibilities of the observational astronomy of the time, but, in a century, a small number can become large. The Einstein's suggestion aroused interest [142, 172], but the experiments planned to obtain an observational evidence were unlucky. An Argentinian expedition to observe the total eclipse in Brazil in 1912 was rained out. In 1914, German astronomers, headed by Erwin Freundlich, went in Crimea but they were arrested by Russians, just after the World War I broke out. In a confinement there is not much light, but it is still more difficult to do astronomy. It

was a further theoretical development and not an experimental observation to show that the deflection angle is actually twice the early prediction of both von Soldner and Einstein. In 1915, in fact, by applying the full field equations of general relativity, Einstein [58] found that a light ray grazing the sun experiences a deflection of 1.7 arcseconds. During the solar eclipse of May 29, 1919, immediately following World War I, Arthur Eddington, in collaboration with Frank Dyson, measured the displacement of stars close to the sun to within 30% of the value predicted by Einstein. This experiment was the first and, until 1979, only observational evidence of gravitational lensing. It soon became the most famous test of general relativity and was the basis of Einstein's huge popularity. One may argue that, without the World War I, the history of men would have been different, and, maybe, the Einstein's fortune too. On the contrary, we must also note that the relationship between Einstein and the World War II did not concern gravitational lensing at all.

The conditions for multiple light paths connecting a source and an observer were also explored. In 1912, Einstein considered the possibility of double images of a background star lensed by a foreground star but he did not publish his results [172]. Similar considerations were performed by Eddington in 1920 [56] and Chwolson in 1924 [40], who also mentioned the reversed mirror image. Chwolson first noted that in case of perfect alignment of the source and of the foreground star, a ring-shaped image of the background star, centred on the foreground star, would result. *Ubi maior minor cessat*, since Einstein in 1936 [59] obtained the same result, such rings are known as Einstein rings and not Chwolson rings. In the same paper, Einstein also concluded that there is little chance of observing lensing phenomena caused by stellar-mass lenses since the angular image splitting is too small to be resolved by an optical telescope. Anyway, as Fritz Zwicky put in evidence in 1937 [230], this limitation does not regard all gravitational lensing system. Zwicky first recognized the potential of galaxies as gravitational lenses, since they "offer a much better chance than stars for the observation of gravitational lens effects"[1]. In a second letter [231], Zwicky estimated the probability of lensing by galaxies and concluded that it is on the order of one per cent for a source at reasonably large redshift.

It was not until the early 1960s that the topic of gravitational lensing began to be reconsidered with the papers by Liebes and Refsdal, who derived the basic equations of gravitational lensing by a point-mass. Liebes [112] also considered various applications, such as galactic star-star lensing and lensing of stars in the Andromeda galaxy. In 1964, Refsdal [151] also argued that geometrical optics can be a good approximation to deal

[1] Curiously, the last two works we have mentioned, [59, 230], were, directly or indirectly, influenced by Rudi Mandl, a Czech electrical engineer who approached various scientists with his idea that a foreground star may act as a gravitational lens for light coming from a background star. The not too warm acknowledgement of Einstein was in a letter to the editor of Science: "Let me also thank you for your cooperation with the little publication, which Mister Mandl squeezed out of me. It is of little value, but it makes the poor guy happy" [142].

gravitational lensing effects. In a second paper [152], he described the difference in arrival time between two paths connecting source and observer and how the Hubble constant could in principle be measured through gravitational lensing of a variable source. In the same year, Shapiro [184] also pointed out the measurability of the retardation of light signals in the gravitational fields of massive bodies.

From the late sixties to early seventies, then, the influence of gravitational lenses on the newly discovered quasars [170] was considered. Quasars in fact revealed as an ideal class of sources for gravitational lensing observations. They are bright enough to be detected. Since their optical emission region is very compact, they can be considered point-like sources and, when deflected by intervening galaxies (which is more probable since they are distant), they can be multiply imaged with high magnifications. In those years, gravitational lensing was considered as a fairly esoteric business by the majority of the scientific community. On the other hand, some astrophysicists considered it as a kind of panacea for any unexplained phenomenon. Someone tried to explain quasars as strongly magnified active galaxies, but the basic conclusion was that the whole quasar phenomenon cannot be explained. Also, in 1973, Press and Gunn [147] considered statistical effects of a lens population on background sources and the possibility for detecting a cosmologically significant density of condensed objets.

Other theoretical progresses were obtained in the seventies, when the formalism of gravitational lensing was more fully developed. The uniform lens was explored in 1972 by Clark [42]. Bourassa and coworkers [19, 20, 21] studied the transparent gravitational lens investigating a spheroidal mass distribution; they also gave the first discussion of caustics. Cooke and Kantowski [43] calculated time delay for multiply imaged quasars and separated it into two parts: the geometrical part, due to the different length of light paths, and the potential part, due to the gravitational potential.

The breakthrough in gravitational lensing came in 1979, when it became an observational science. Walsh, Carswell and Weymann [210] accidentally detected the first multiply imaged quasar Q0957+561. It has two images at a redshift of 1.41, 6.1 arseconds apart. Shortly thereafter, the detection of the lensing galaxy at a redshift of 0.36 confirmed the lensing nature of the system. Other evidences of the gravitational lensing nature of the phenomenon are the similarity of the spectra of the two images, the constancy in the flux ratio between the images in very different wave-bands, a detailed correspondence between various knots of emission in the two radio images. The discovery of this system triggered an enormous output of publications.

A different feature of lensing by galaxies was studied by Chang and Refsdal [36]. They considered the light curve of a background quasar that is lensed by individual stars in a lens galaxy. Altough the image separation is not observable, the perturbation of lensing by the galaxy as a whole can be detected by the corresponding change in magnification. This phenomenon was first observed in the multiply imaged quasar QSO 2237+0305 [92]. This regime of lensing is now known as *microlensing*, a

term introduced by Paczyńsky in 1986, and refers to a problem already considered by Einstein: lenses of stellar masses produce splitting angles of about a microarcsecond which cannot be detected. Paczyńsky [133] considered another microlensing scenario as a possible test for the existence of faint compact objects in the Halo of the Milky Way. He showed that at any given time one in a million stars in the Large Magellanic Cloud might be measurably magnified by the gravitational lens effect on an intervening star in the Halo. Mass lenses between 10^{-6} $M_\odot$ and 10^2 $M_\odot$ induce events with time scale between two hours and two years. The proposed experiment required to frequently sample millions of light curve, but only six years after the suggestion, three experiment reported successful detections of the microlensing signature [2, 7, 202]. This field has developed into a useful tool for studying the nature and distribution of mass in the Galaxy. Microlensing observations represent one of the rare cases in the history of gravitational lensing in which a theoretical prediction inspired a systematic search so that the detection was not a serendipitous discovery.

Another type of lensed cosmological images is obtained when the source does not involve an effectively point-like quasar component. For instance, either the diffuse lobe of a radio galaxy or the optical image of a galaxy are smooth and extended sources. Radio sources with a finite extent nearly aligned with a quite axial-symmetric mass distribution can be imaged in a nearly full Einstein ring. The first example was discovered in 1988 [84], when the extended radio lobe MG 1131+0456, at a redshift of 1.13, turned out to be imaged in a ring with a diameter of about 1.75 arcseconds by a foreground galaxy. By now, many other Einstein rings have been observed. The sources often have both an extended and a compact component, multiply imaged with separations of the order of the ring size. These systems provide many constraints on the lens and permit to model the mass distribution of galaxies at moderate redshifts.

Compact clusters can produce spectacular luminous *arcs* several tens of arcseconds in length. The source is usually a low-density galaxy at high redshift. These configurations have been predicted long before their detection. In 1936 [163], Russel[2], was, maybe, the first to study lensing effects on extended sources; he also plotted a magnified and tangentially elongated image. However, no program to search for these phenomena was planned and even a couple of arcs seen on photographic plates were not commented before 1986: as noted in [142], in astronomy there is "a strong tendency to recognize only things one knows". As a matter of fact, the first claim of giant luminous arcs came as a surprise in 1986. Lynds & Petrosian [118] and Soucail et al. [188] independently discovered this new gravitational lensing phenomenon: magnified, distorted and strongly elongated images of background galaxies lying behind a foreground cluster of galaxies. Soon, more examples of long and thin arcs, curved around the cluster centre and with lengths up to about 20 arcseconds, were found in the central parts of

[2]Henry Norris Russel was an Einstein's Princeton colleague. Sometimes, it is very useful for a physicist to see a genius everyday.

very massive clusters of galaxies. In 1987, Paczyński [135] first interpreted such arcs as images of background galaxies strongly distorted by the gravitational tidal field close to the cluster centre; later [190], the spectroscopic measurements of the redshifts of such arcs confirmed this hypothesis. These lensing events provide a tool to study objects that would be otherwise too fair to be detectable. Because of the lens induced magnification, it is possible to take spectra and study galactic and stellar population at high redshift.

Clusters also coherently distort the images of other faint background galaxies further from the cluster centre. The distortions are mostly weak, and the corresponding images are referred as *arclets* [65, 199]. These observations can be used to map the lensing potential over the whole extent of the lens. The study of the coherent deformation of the shapes of extended background sources, known as *weak lensing*, allows to reconstruct parameter-free, two dimensional mass maps of the lensing cluster.

Plan of the thesis

The above impressive list of theoretical insights and very broad range of phenomena have made the gravitational lensing a very useful astrophysical tool. All participants to a gravitational lensing system, the *lens*, the *source*, the *background* in which the system is embedded and a *theory of gravity*, which describes the phenomenon, can be investigated by an *observer* who detects the phenomenon by interacting with the transmitter of the information, the *light*. The *gravitational lens equation* relates all these players. Gravitational lensing applications may be classified following and extending the Zwicky's ideas, already formulated in 1937. They are

i) Lensing provides a test for theories of gravity. A theory of gravity determines the space-time in which the gravitational lensing system is embedded. Space-time arises from a background and from a lens, which acts as a weak perturbation on the background. We will assume that light propagates in space-time according to the geometrical optics approximation.

ii) Lensing acts as a gravitational telescope on distant sources, physical objects that emit light. Lensing induces a magnification effect which enables to observe objects which are too distant or intrinsically too faint to be observed without lensing. Source properties well below the resolution or sensitivity limits of current technological capabilities can be inferred for highly magnified sources.

iii) Lensing can be used to measure the lens mass distribution. The lens is a matter perturbation. A matter density variation, either positive or negative, with respect to a homogeneous background induces light deflection. Without being explicitly stated, we will consider positive matter perturbations. Gravitational

lensing depends only on the mass distribution of the lens, and is independent of both luminosity and dynamical properties.

Furthermore, as a fourth point, first addressed by Resfdal in sixties:

iv) Lensing can constrain the age, the scale and the overall properties of the universe. The distances between observer and lens, observer and source, and lens and source, which enter the lens equation, are measured with respect to the background and contain information on the cosmological model.

The work presented in this thesis addresses some theoretical elaborations of the gravitational lensing equation and some cosmological applications. The first part of the thesis faces the point *i*.

The measurement of the light deflection at the solar limb is one of the main check of general relativity. However, the impressive development of observational capabilities will make it possible, in a near future, to detect higher-order effects, such as the action of the gravito-magnetic field and the post-post-Newtonian correction. On the basis of such effects, it is possible to perform a comparison between general relativity and other viable theories of gravity. In Chapter 1, we derive the gravitational lensing equation in a generic theory of gravity in the standard framework of weak-field, thin-screen gravitational lensing theory.

In Chapter 2, we extend the lens mapping to a generic theory of gravity by including the gravito-magnetic effect. By introducing new definitions and correcting previous ones, we develop a proper formalism which allows to generalize results and theorems already known in literature. These results are proposed for the first time.

Chapter 3 considers the gravito-magnetic effect on some specific gravitational lens models of astrophysical interest. We mainly consider the case of a deflector in rigid rotation. The post-post-Newtonian correction is considered for the point-like deflector. Many of these results are also proposed for the first time.

We here list the main references. For theories of gravity:

- Will, C.M., *Theory and Experiment in Gravitational Physics*, rev. ed., 1993, Cambridge University Press, Cambridge; [221].

- Ciufolini, I., Wheeler, J.A., *Gravitation and Inertia*, 1995, Princeton University Press, Princeton; [41].

For the standard hypotheses of gravitational lensing, a complete discussion can be found in:

- Schneider, P., Ehlers, J., Falco, E.E., *Gravitational Lenses*, 1992, Springer-Verlag, Berlin; [172].
- Petters A.O., Levine H., Wambsganss J., *Singularity Theory and Gravitational Lensing*, 2001, Birkhäuser, Boston; [142].

For a treatment of higher order effects, we remind:

- Sereno, M., *Gravitational lensing by spinning and radially moving lenses*, 2002, Phys. Lett. A., in press, [astro-ph/0209148]; [179].
- Sereno, M., *Gravitational lensing in metric theories of gravity*, 2002, Phys. Rev. D, submitted; [180].
- Sereno, M., Cardone, V.F., *Gravitational lensing by spherically symmetric lenses with angular momentum*, 2002, A&A in press; [astro-ph/0209297]; [181].

The second part of the thesis faces the point *iv*.

In Chapter 4, we explore a method to determine what the universe is made of. Once the properties of the lens and of the source are known and once we assume a theory of gravity, we can determine, through the gravitational lens equation, some properties of the background universe from detailed observation of gravitational lensing phenomena. We consider clusters of galaxies acting as lenses on background galaxies. In the framework of general relativity, we will consider as some observable quantities depend on the geometry of the universe. The Chapter is mainly based on:

- Sereno, M., *Probing the dark energy with strong lensing by clusters of galaxies*, 2002, A&A, 393, 757; [178].

The light emitted by any source in the universe is affected by every matter perturbation in the universe. So, the measured distances to cosmic sources are affected by gravitational lensing produced by the intervening inhomogeneities. The multi-plane gravitational lens equation can account for this effect. In Chapter 5, we study the distance–redshift relation and the effect of gravitational lensing when determining cosmological parameters from measurements of distances. The discussion follows:

- Sereno, M., Covone, G., Piedipalumbo, E., de Ritis, R., *Distances in inhomogeneous quintessence cosmology*, 2001, MNRAS, 327, 517; [182].
- Sereno, M., Piedipalumbo, E., Sazhin, M.V., *Effects of quintessence on observations of Type Ia SuperNovae in the clumpy Universe*, 2002, MNRAS, 335, 1061; [183].

Chapter 1

Gravitational lensing in curved space-times

The principle of equivalence provides a firm foundation to any conceivable theory of gravity. On the other hand, the derivation of Einstein's field equation contains a strong element of guesswork. It is, therefore, very interesting to test metric theories of gravity defined as theories such that [41, 221]: *i)* space-time is a Lorentzian manifold; *ii)* the world lines of test bodies are geodesics; *iii)* the equivalence principle in the medium strong form is satisfied. In these theories, the usual rules for the motion of particles and photons in a given metric still apply, but the metric may be different from that derived from the Einstein's field equation. The basic assumption of the existence of a dynamical space-time curvature, as opposed to flat space-time of special relativity, still holds.

Different metric theories can be compared with suitable tests. Bending and time delay of electromagnetic waves are two important effects predicted by theories of gravity. A full analysis of higher order corrections to the lensing theory makes possible a comparison among the predictions of general relativity and other conceivable theories of gravity, whereas an analysis to the lowest orders might hide some differences.

Intrinsic gravito-magnetism is such an higher-order effect. Mass-energy currents relative to other masses generate space-time curvature. This phenomenon, known as intrinsic gravito-magnetism, is a new feature of general relativity and other conceivable alternative theories of gravity and cannot be deduced by a motion on a static background (for a detailed discussion on gravito-magnetism we refer to [41]). Peculiar and intrinsic motions of the lenses are expected to be small second order effects. However, gravity induced by moving matter is related to the dragging of inertial frames and the effects of mass currents on the propagation of light signals deserve attention from the theoretical point of view. Lensing of light rays by stars with angular momentum has been addressed by several authors with very different approaches. Epstein &

Shapiro [60] performed a calculation based on the post-Newtonian expansion. Ibáñez and coworkers [89, 90] resolved the motion equation for two spinning point-like particles, when the spin and the mass of one of the particles were zero, by expanding the Kerr metric in a power series of gravitational constant G. Dymnikova [55] studied the time delay of signal in a gravitational field of a rotating body by integrating the null geodesics of the Kerr metric. Glicenstein [72] applied an argument based on Fermat's principle to the Lense-Thirring metric to study the lowest order effects of rotation of the deflector. The listed results give a deep insight on some peculiar aspects of spinning lenses but are very difficult to generalize. On the other hand, Capozziello et al. [30] discussed the gravito-magnetic correction to the deflection angle caused by a point-like, shifting lens in weak field regime and slow motion approximation. Asada & Kasai [6] considered the light deflection angle caused by an extended, slowly rotating lens.

The post-post-Newtonian (ppN) corrections to the metric element have also to be considered. The ppN contribution to the deflection angle has been considered, for a point-like deflector, by Epstein & Shapiro in [60].

On the observational side, gravitational lensing is one of the most deeply investigated phenomena of gravitation and it is becoming a more and more important tool for experimental astrophysics and cosmology. The impressive development of technical capabilities makes it possible to obtain observational evidences of peculiar metric theories of gravity in a next future and to test the degree of accuracy of the Einstein's field equations. Furthermore, observations of gravitational lensing phenomena could demonstrate the inertia-influencing effect of masses in motion. In fact, the gravito-magnetic field, predicted in 1896-1918, has not yet a firm experimental measurement.

In this Chapter, I discuss deflection and time delay of light rays in the usual framework of gravitational lensing as summarized in the monographs by Schneider et al. [172] and Petters et al. [142]. The standard assumptions of gravitational lensing, i.e. the weak field and slow motion approximation for the lens and the thin lens hypothesis, allow us to consider higher-order approximation terms in the calculation of lensing quantities. Now, I extend to a cosmological context the results I have already reported in [179, 180], where the post-post-Newtonian (ppN) contribution and the action of the gravito-magnetic field have been considered in the framework of viable theories of gravity.

The Chapter is as follows. In Section 1, the principle of equivalence is stated. It provides a common basis for any viable theory of gravity. The role of the field equation is discussed in Section 2. Section 3 introduces one of the main usual simplification of gravitational lensing theory: in most of the astrophysical systems, light propagates in curved space-times according to the geometrical optics. Section 4 considers the Fermat's principle in conformally stationary space-times; this principle, based on the

equivalence principle and the geometrical optics approximation, is independent of the field equation, and provides a tool to derive the relevant relations in lensing theory. In Section 5, the concept of distance in a curved space-time is discussed. Armed with the definition of cosmological distances, in Section 6, we show as gravitational lensing, in the approximation of geometrical optics, does not alter surface brightness. Section 7 treats the background space-time where the gravitational lensing system is embedded. The space-time, assumed to be homogeneous and isotropic, is described by Robertson-Walker metric. In our approximations, the lens is the only perturbing agent in an otherwise smooth universe. Section 8 lists the main contributes to the energy budget of the universe; besides baryonic matter, photons and neutrinos, two new kinds of source of energy must be considered to account for the today observational constraints: the dark matter and the dark energy. In Section 9, a generalized metric element in the weak field and slow motion approximation is introduced. The approximate metric element, expanded up to the ppN order, and with non diagonal components which include the effects of gravity by currents of mass, describes the gravitational action generated by an isolated mass distribution. The line element holds in most of the viable theories of gravity. In Section 10, we discuss the thin lens. In most of the astrophysical systems, the deflection angle are really small and the geometrical extension of the lens is negligible with respect to the other characteristic distances of the gravitational lensing system. Some features of light sources are presented in Section 11. Following Fermat's principle, the time delay function and deflection angle caused by an isolated mass distribution are derived in, respectively, Sections 12 and 13. The time delay can be separated in two contributes. The geometrical time delay, due to the extra length path a deflected light ray undergoes with respect to the unlensed path, is evaluated in the background universe; the deflection time delay, due to the gravitational potential of the lens, is calculated according to the approximate metric element. By using the Fermat's principle, in Section 13, we select the real light path among the kinematically possible light rays. At last, the lens equation can be stated.

1.1 The equivalence principle

The equivalence principle is at the foundation of any viable theory of gravitation. It is one of the best tested principles in the whole field of physics [41, 220].

The equivalence principle has three important versions. The weak equivalence principle, or Galilei equivalence principle, states that the motion of any freely falling test particle is independent of its composition and structure. A test particle is defined to be electrically neutral, to have negligible gravitational binding energy compared to its rest mass, to have negligible angular momentum, and to be small enough that its coupling to inhomogeneities in external fields can be ignored. The weak equivalence

principle is based on the equality between the inertial mass and the gravitational (passive) mass, so that all test particles fall with the same acceleration. It endows space-time with a family of preferred trajectories, the world lines of freely falling test bodies.

Einstein generalized the Galilei principle from the motion of test particles to all the laws of special relativity. The medium strong form of the equivalence principle, or Einstein equivalence principle, states that, for every point-like event of space-time, there exists a sufficiently small neighbourhood such that, in every freely falling frame in that neighbourhood, all the non-gravitational laws of physics obey the laws of special relativity. Here, neighbourhood means a neighbourhood in space and time small enough such that any effect of the gravitational field is unmeasurable within the limiting accuracy of the used experimental apparatus.

If we replace *all the non-gravitational laws of physics* with *all the laws of physics* we get the very strong equivalence principle.

The Einstein equivalence principle is at the heart of gravitation theory, for it is possible to argue convincingly from its validity that gravitation must be a curved space-time phenomenon, i.e. must satisfy the postulates of metric theories of gravity. Their postulates states: *i)* space-time, endowed with a metric $g_{\alpha\beta}$, is a Lorentzian manifold; *ii)* the world lines of test bodies are geodesics; *iii)* the equivalence principle in the medium strong form is satisfied. General relativity, Brans-Dicke theory and the Rosen bimetric theory satisfy these postulates. General relativity also satisfies the equivalence principle in the very strong version.

From the medium strong equivalence principle, it follows that space-time must be at an event, in suitable coordinates, Minkowskian, that is, described by the metric $\eta_{\alpha\beta} = \mathrm{diag}(1, -1, -1, -1)$. It is assumed the Lorentzian, pseudo-Riemannian character of space-time. The metric $g_{\alpha\beta}$ determines the space-time squared distance between two nearby events,

$$ds^2 = g_{\alpha\beta} dx^\alpha dx^\beta. \tag{1.1}$$

Let us briefly recall the definition of a few basic quantities of tensor calculus on a Riemannian manifold. The connection coefficients (or Christoffel symbols) can be constructed from the first derivatives of the metric tensor,

$$\Gamma^\alpha{}_{\beta\gamma} = \frac{1}{2} g^{\alpha\delta} (g_{\delta\beta,\gamma} + g_{\delta\gamma,\beta} - g_{\beta\gamma,\delta}). \tag{1.2}$$

Gravitational acceleration depends on spatial change in the metric, so that the Christoffel symbols correspond roughly to the gravitational force. The Riemann curvature tensor can be written in terms of the Christoffel symbols,

$$R^\alpha{}_{\beta\gamma\delta} = -2(\Gamma^\alpha{}_{\beta[\gamma,\delta]} + \Gamma^\epsilon{}_{\beta[\gamma}\Gamma^\alpha{}_{\delta]\epsilon}), \tag{1.3}$$

where square brackets denotes the antisymmetryzation. It provides a covariant description of the curvature of the space-time. The Riemann tensor is fourth order, but may be contracted to the Ricci tensor $R_{\alpha\beta}$, or further to the curvature scalar R

$$R_{\alpha\beta} = R^{\gamma}{}_{\alpha\gamma\beta} \ , \ R = R^{\alpha}{}_{\alpha} \tag{1.4}$$

In metric theories of gravity, the equation of motion of any test particle is a geodesic. The equation for a geodesic is,

$$\frac{d^2x^\alpha}{dv^2} + \Gamma^{\alpha}{}_{\beta\gamma}\frac{dx^\beta}{dv}\frac{dx^\gamma}{dv} = 0. \tag{1.5}$$

Once given a space-time, mass energy moves in the same way in all metric theories of gravity. The parameter v is called an affine parameter since a reparameterization $v \to \tilde{v}$ preserves the form of the equation if, and only if, it is an affine transformation $\tilde{v} = av + b$.

1.2 The field equation

Metric theories of gravity retain the whole apparatus of general covariance and recognize the metric tensor as the gravitational field. The space-time structure is preserved and formally the same equation of motion for test particles, Eq. (1.5), as for general relativity holds.

However, the field equations are logically distinct and do not derive from this assumptions. So, they can differ from one theory to another one. A field equation connects the gravitational tensor potential $g_{\alpha\beta}$ with the density of mass energy and its current.

1.2.1 The source of gravitation

The source of gravitation is the energy-momentum tensor $T^{\alpha\beta}$. The meanings of its components, in any local inertial frame, are: T^{00} represents the energy density, the spatial vector cT^{0i} represents the energy flux density and T^{ij} is the spatial stress tensor. The tensor is seen to be symmetric.

For most astrophysical purposes, the perfect fluid approximation holds. Then the energy-matter tensor reduces to

$$T^{\alpha\beta} = (\rho c^2 + p)U^\alpha U^\beta - pg^{\alpha\beta}, \tag{1.6}$$

where c is the speed of light in vacuum, ρ denotes the mass density and p the pressure, both measured by a comoving observer; U^α is the 4-velocity, normalized to one,

$$g_{\alpha\beta}U^\alpha U^\beta = 1. \tag{1.7}$$

By virtue of the conservation laws it expresses, $T^{\alpha\beta}$ has zero covariant divergence.

1.2.2 The Einstein's field equation

The Einstein's field equation states

$$G^{\alpha\beta} \equiv R^{\alpha\beta} - \frac{1}{2}Rg^{\alpha\beta} = \frac{8\pi G}{c^4}T^{\alpha\beta}, \tag{1.8}$$

where G is the Newton constant of gravitation. Eq. (1.8) relates the Einstein tensor $G^{\alpha\beta}$ to the stress-energy-momentum tensor $T^{\alpha\beta}$ of matter and non-gravitational fields.

1.3 Geometrical optics

In curved space-times, Maxwell's equations read

$$F^{\mu\nu}{}_{;\nu} = \frac{4\pi}{c}J^{\mu}, \tag{1.9}$$

$$F_{\mu\nu;\lambda} + F_{\lambda\mu;\nu} + F_{\nu\lambda;\mu} = 0, \tag{1.10}$$

where $F_{\mu\nu}$ is the Maxwell tensor and J^{μ} is the charge current density four-vector; the semicolon denotes the covariant derivative. Except in cases of high symmetry, Maxwell's equations do not have explicit solutions. In particular, plane waves do not exist. In many astrophysical situations, however, and especially in gravitational lensing theory, one can consider the geometrical optics regime. Maxwell's equations are approximately solved by "locally plane" waves, which are nearly plane and monocromathic. Geometrical optics holds when, in a typical Lorentz frame, the wavelength of light is significantly less than the scale over which the light's amplitude, polarization, and wavelength vary and much shorter than the radius of curvature of the space-time through which the light travels. Now, the light beam can be considered as a beam of null mass particles, photons, moving with the speed of light in the medium of propagation. The wave nature of light is ignored since the warps in space-time are much bigger than the wavelength.

In this approximation:

1. Light is propagated along null geodesics of space-time, called light rays, i.e. the 4-momentum of each photon is transported parallely along the photon's world line.

2. The amplitude, polarization, etc., of different light rays do not influence each other. In addition, light rays lie in and are orthogonal to surfaces of constant phase.

3. A light ray's polarization vector is orthogonal to the ray and parallel transported along the ray.

4. The number of photons in a ray bundle is conserved and observer-independent.

These results can be obtained in the framework of metric tensor theories of gravity only using the principle of equivalence and the prescriptions of the minimal coupling [120, 172].

Astrophysical sources are very large with respect to the wavelength of the emitted light, so that, wave effects can be neglected. Also, interference of two or more images of a lensed source is, usually, negligible since time delay between the images are much larger than the coherence length of a light wave. In few instances, however, the geometrical optics approximation breaks down. At caustic crossing events, we need the wave optical treatment to avoid unphysical infinitely high magnifications. Furthermore, in the case of a multiply imaged source near a fold caustic, the time delay between images can become as small as the period of light wave in the optical band. In general, however, the geometrical optics approximation suffices for almost all current astrophysical lensing situations.

1.4 Fermat's principle

In metric theories of gravity, a very intuitively way to characterize the light rays is given by the Fermat's principle. When expressed in a space-time context, it has the following statement:

- A light ray (null geodesics) from a source $\mathcal{S}$ (space-time event) to an observer $\mathcal{O}$ (timelike world line) follows a trajectory that is a stationary value, under first order variation of the paths, of the arrival time τ (measured relative to the observer's proper time), within the set of smooth null curves from $\mathcal{S}$ to $\mathcal{O}$,

$$\delta\tau = 0.$$

This version of the Fermat's principle, conformally invariant, states a stationary property of the (invariant) time of arrival at $\mathcal{O}$, who may be moving relative to $\mathcal{S}$. Furthermore, no preferred parameters on $\mathcal{O}$ or on the path enter the theorem; at the observer, one may use proper time or any monotonic function of it.

The Fermat's principle can also be interpreted using the opposite time-orientation: the observer can be treated as located at a space-time event with past pointing null curves followed from the observer to a source, which is, now, a timelike curve.

The Fermat's principle takes a version of particular interest in stationary space-times [120, 172]. We consider a metric whose components $g_{\alpha\beta}$ are functions of the spatial coordinates x^i only (roman indeces label spatial coordinates). On a null curve, it is

$$ds^2 = g_{\alpha\beta}dx^\alpha dx^\beta = 0;$$

for the future directed curve,

$$dx^0 = cdt = -\frac{g_{i0}}{g_{00}}dx^i + \frac{dl_{\rm P}}{\sqrt{g_{00}}}, \tag{1.11}$$

where ${dl_{\rm P}}^2 \equiv \left(-g_{ij} + \frac{g_{0i}g_{0j}}{g_{00}}\right) dx^i dx^j$ defines the spatial metric [109]. The arrival time of a light ray, whose spatial projection is $\hat{p}$, at an asymptotic observer is given by

$$t = \frac{1}{c}\int_{\hat{p}} \frac{dl_{\rm P}}{\sqrt{g_{00}}} - \frac{g_{i0}}{g_{00}}dx^i. \tag{1.12}$$

Then, the Fermat's principle states

$$\delta \int_p n dl_{\rm P} = 0, \tag{1.13}$$

where the spatial paths $\hat{p}$ are to be varied with fixed endpoints; n is an effective index of refraction defined as

$$n \equiv -\frac{g_{i0}}{g_{00}}e^i + \frac{1}{\sqrt{g_{00}}}, \tag{1.14}$$

where $e^i \equiv \frac{dx^i}{dl_{\rm P}}$ is the unit tangent vector of a ray. This version of the Fermat's principle is formally identical with the classical one

It is easy to generalize the Fermat's principle to conformally stationary space-times, i.e. space-times whose physical metric $\tilde{ds}^2$ is conformal to a stationary (time-independent) metric ds^2,

$$\tilde{ds}^2 = \Omega^2 ds^2, \tag{1.15}$$

where the conformal factor Ω may depend on all four coordinates. Since conformally related metrics have identical light rays up to an affine parameter, one may still apply Fermat's theorem to ds^2 to find the light rays of $\tilde{ds}^2$. The effective refraction index of the metric $\tilde{ds}^2$, except for the conformal factor, equals the one of ds^2.

1.5 Distances

In a generic curved space-time, a theoretical definition of distance is problematic since the dependence of the metric on the temporal coordinate [109]: distances can be defined only locally. Furthermore, also in a conformally stationary metric, there is no preferred notion of the distance between two objects. To overcome these difficulties, distances must be defined by means of practical methods.

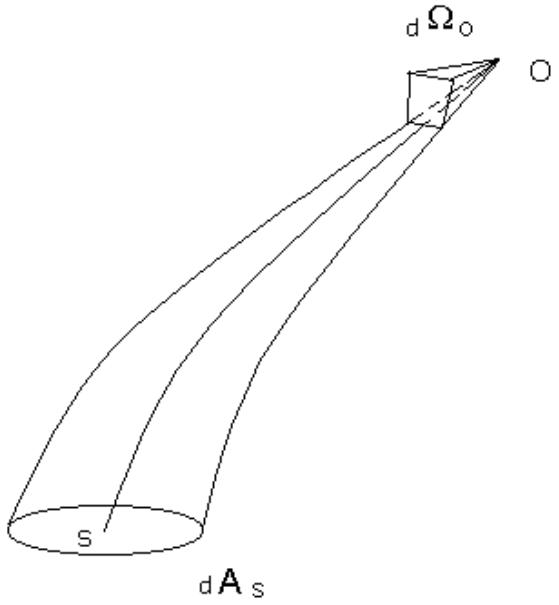

Figure 1.1: A beam of light rays from a source element of area $dA_{\rm S}$ at S with the vertex at the observer O, of size $d\Omega_{\rm O}$.

The distance to an object outside the Galaxy, not counting the measurements of redshifts, can be determined by the photometric method, based on measurements of energetic fluxes, or by the geometrical method, which assumes the knowledge of the sizes of the objects. These methods assume an uniformity of the sources, so that far objects are assumed to be like the nearer ones, easier to observe.

In addition, the distance to a near enough object can be determined either by measuring its parallax, the shift in apparent position in the sky caused by the earth's revolution around the sun, or its proper motion, the shift in apparent position in the sky caused by the object's actual motion relative to the sun. For objects beyond about 10^9 light years, different distances differ from each other.

Distance measures are defined in analogy to relations between measurable quantities in Euclidean space. The *angular diameter distance*, in a cosmological context, is a simple generalization of an intuitive expression that holds in an Euclidean geometry. Here, the angular diameter, δ, of a source of size d at a distance D is

$$\delta = \frac{d}{D} \; ;$$

in curved space-time, the angular diameter distance again satisfies this relation,

$$D_{\rm A} \equiv \frac{d}{\delta} \; . \tag{1.16}$$

The *luminosity distance*, $D_{\rm L}$, is defined as

$$D_{\rm L} \equiv \left(\frac{L}{4\pi S}\right)^{\frac{1}{2}}, \tag{1.17}$$

where L is the bolometric luminosity of the source, S is the total observed flux.

Let us formalize this two definitions in a more general way by showing their link with the propagation of light. Consider a thin beam of light rays emanating from a source-event S and reaching an observation-event O and its neighbourhood. The area $dA_{\rm O}$ of the cross section of the beam at O is well defined independently of an assignment of a 4-velocity at O. On the other hand, the size of the beam at S in terms of a solid angle $d\Omega_{\rm S}$, measured in the tangent 3-space orthogonal to the 4-velocity $U^\alpha_{\rm S}$ at S, depends on $U^\alpha_{\rm S}$ itself. The *corrected luminosity distance* of the source at S with 4-velocity $U^\alpha_{\rm S}$ from the observation event O is defined as

$$D'_{\rm L}(U^\alpha_{\rm S}, O) \equiv \left(\frac{dA_{\rm O}}{d\Omega_{\rm S}}\right)^{\frac{1}{2}}. \tag{1.18}$$

Similarly, interchanging the roles of source and observer, one defines the distance from apparent solid-angular size of S as seen from $(O, U^\rho_{\rm O})$, see Fig. (1.1)

$$D_{\rm A}(U^\alpha_{\rm O}, S) \equiv \left(\frac{dA_{\rm S}}{d\Omega_{\rm O}}\right)^{\frac{1}{2}}. \tag{1.19}$$

The dependence of this distance on the 4-velocity of the observer causes the phenomenon of aberration.

The corrected luminosity distance is strictly related to the luminosity distance. It is easy to show the link between the two definitions by means of the conservation law of photons.

The specific luminosity, L_ω, for a source radiating isotropically, is defined as

$$dN_{\omega_{\rm S}} \equiv d\tau_{\rm S} d\Omega_{\rm S} d\omega_{\rm S} \frac{L_{\omega_{\rm S}}}{4\pi\omega_{\rm S}}, \tag{1.20}$$

where $dN_{\omega_{\rm S}}$ is the number of photons emitted during the the proper time interval, $d\tau_{\rm S}$, into the solid angle $d\Omega_{\rm S}$ with energy in the range $\hbar d\omega_{\rm S}$. According to the photon number conservation, the same photons forming this ray bundle pass through an area $dA_{\rm O}$ orthogonal to the ray direction in an observer's 3-space in proper time $d\tau_{\rm O}$ with energies in the range $\hbar d\omega_{\rm O}$. We can express their number in terms of the specific flux measured by the observer, S_ω,

$$dN_{\omega_{\rm O}} = \tau_{\rm O} dA_{\rm O} d\omega_{\rm O} \frac{S_{\omega_{\rm O}}}{\omega_{\rm O}}. \tag{1.21}$$

Let us define the redshift z,

$$\frac{1}{1+z} \equiv \frac{\omega_0}{\omega_{\rm s}} = \frac{d\tau_{\rm s}}{d\tau_0}, \tag{1.22}$$

where ω_0 is the frequency as measured at the observer and ω_s is the frequency as emitted at the source. Equating Eq. (1.20) and Eq. (1.21) and using the definition of $D_L^{'}$, we get

$$S_\omega = \frac{L_{(1+z)\omega}}{4\pi(1+z)D_L^{'2}}. \tag{1.23}$$

An integration over all frequencies gives the total flux S,

$$S = \frac{L}{4\pi(1+z)^2 D_L^{'2}}. \tag{1.24}$$

Comparing Eq. (1.24) to the definition of the luminosity distance, Eq. (1.17), we obtain the relation between the two distances,

$$D_L = (1+z)D_L^{'}. \tag{1.25}$$

If two events S and O are connected by a light ray and 4-velocities U_S^α, U_O^ρ are given, both distances (1.18) and (1.19) are defined. In any space-time, they are related by the Etherington's reciprocity relation [62, 172]

$$D(U_S^\alpha, O) = (1+z)D(U_O^\rho, S) \tag{1.26}$$

where z denotes the redshift of the source as seen by the observer. From the above relation, it follows

$$D_L = (1+z)^2 D_A. \tag{1.27}$$

1.6 Intensity

Gravitational lensing does not alter surface brightness. This photometric quantity is defined as the radiative energy for unit area, time interval, solid angle and frequency range. Surface brightness is conserved in Euclidean space. A Doppler shift causes a change in surface brightness governed by $I_\nu \propto \nu^3$, so that I_ν/ν^3 is an invariant in special relativity. Now, by the equivalence principle, light can be thought of as propagating along a path that is locally Euclidean, but for which there is a gravitational redshift between the start and end of any given segment of the ray; therefore, the total change in surface brightness just depends on the total frequency change along the path.

Let us consider an extended source, that is an assembly on incoherently radiating point sources. Changing in Eq. (1.23) from $D_L{}'$ to D_A, and using the definition of D_A, Eq. (1.19), we get

$$\frac{dS_\omega}{d\Omega_O} = \frac{dL_{(1+z)\omega}}{4\pi dA_S}\frac{1}{(1+z)^3}. \tag{1.28}$$

In terms of the specific intensity, it is

$$I_\omega(O) = \frac{I_{(1+z)\omega}(S)}{(1+z)^3}. \tag{1.29}$$

Equation (1.29) is a relation between the specific intensity at the observer $I_\omega(O)$ and that at the source $I_{(1+z)\omega}(S)$. So, we have shown as, in any non interacting field, the ratio I_ω/ω^3 is observer-independent and constant on each ray. Integrating on ω, we can obtain the relativistic generalization of the law of constancy of the surface brightness,

$$I(O) = \frac{I(S)}{(1+z)^4}, \tag{1.30}$$

These results have been obtained in the framework of geometrical optics in an arbitrary space-time.

In cosmology, the total frequency change along the path is well approximated by the mean redshift for the object's distance since extra blueshifts caused by falling into the lens potential well are balanced by redshifts on leaving.

1.7 Background space-time

A large portion of modern cosmological theory is built on the Cosmological Principle, the hypothesis that all positions in the universe are essentially equivalent [216]. The universe is assumed to be spatially homogeneous and isotropic. The homogeneity of the universe does not apply to any scale, but only to a smeared-out universe averaged over cells large enough to include many clusters of galaxies, i.e. of diameter $10^8 - 10^9$ light years. Also, the universe appears spherically symmetric about us, so the Cosmological Principle includes the assumption that the smeared universe is isotropic about every point.

The metric element describing such a universe was found independently by H.P. Robertson and A.G. Walker in 1936. Due to the Cosmological Principle, there are coordinates (t, R, θ, ϕ), where t is the cosmic time and (R, θ, ϕ) are comoving coordinates, in which the geometry of the space-time takes the form

$$ds^2 = c^2dt^2 - a^2(t)dS_K^2; \tag{1.31}$$

$a(t)$ is the scaling function or expansion factor (which describes the expansion of the universe). The term $a^2(t)dS_K^2$ is the spatial metric of the universe at cosmic time t. The metric in Eq. (1.31) is known as Robertson-Walker (RW) metric. The factor dS_K^2 is a metric with constant curvature $k = -1, 0$, or 1,

$$dS_K^2 = \frac{dR^2}{1-kR^2} + R^2d\theta^2 + R^2\sin^2\theta d\varphi^2 \tag{1.32}$$

Since for $R \ll 1$ the factor $(1-kR^2)^{-1}$ is approximately unity, the universe is locally flat and its spatial curvature is locally negligible.

The application of the Cosmological Principle to the energy momentum tensor, that describes the average state of cosmic content of energy, shows that it must necessarily take the same form as for a perfect fluid, with a density and a pressure depending on time only. Furthermore, the contents of the universe are, on the average, at rest in the comoving coordinate system.

The cosmological redshift of light emitted from a source at proper time t_s and received by an observer at t_0 can be related to the expansion factor. It is

$$z \equiv \frac{\lambda_0 - \lambda_s}{\lambda_s} = \frac{a(t_0)}{a(t_s)} - 1, \tag{1.33}$$

where λ_s is the wavelength of the light as measured near the source and λ_0 is the wavelength measured by the observer. Near the observer, $z \ll 1$, $c(t_O - t_S) = D$ is the distance; given the RW metric, $v = \left(\frac{\dot{a}}{a}\right)_O D$ is the radial velocity of the source with respect to the observer. By expanding in power series a about t_0, we get the *Hubble law*,

$$z \simeq \frac{v}{c} \simeq \frac{H_0}{c} D, \quad z \ll 1, \quad H_0 \equiv \left(\frac{\dot{a}}{a}\right)_0, \tag{1.34}$$

where H_0 is the *Hubble constant*.

The proper distance is the distance measured by the travel time of a light ray ($ds^2 = 0$). It is defined by $dD_P = cdt$. Hence, the proper distance to a source at radial coordinate R_s, at cosmic time t, takes the form

$$D_P = \int_0^{R_s} \sqrt{g_{RR}} = a(t) \int_0^{R_s} \frac{dR}{(1 - kR^2)^{1/2}}. \tag{1.35}$$

1.7.1 Angular diameter distance in RW metric

The angular diameter distance has a quite simple expression in a homogeneous and isotropic universe. Let us consider an observer at ($R = 0$, $t = t_0$) and a source of proper size d at ($R = R_s$, $t = t_s$). Without any loss of generality, we let us consider light rays from the source to the observer with a fixed radial direction, $\varphi = \varphi_1$, so that, we can rotate the coordinate system in order to place the centre of the luminous source at $\theta = 0$. The coordinates marking the top and the bottom of the object are, respectively, $(R_S, +\frac{d\theta}{2}, \varphi_1)$ and $(R_S, -\frac{d\theta}{2}, \varphi_1)$. Such a source subtends an angle $\delta = d\theta$ as seen at the location of the observer; then, the proper diameter of the source can be determined by setting $t = t_s$ in the RW line element,

$$d = ds = a(t_s) R_s d\theta = a(t_s) R_s \delta$$

and the angular diameter distance is

$$D_A = \frac{d}{\delta} = a(t_s) \cdot R_s = \frac{a_0}{1 + z_s} R_s \ .$$

Let us evaluate the dependence of $D_{\rm A}$ on the redshift [34, 216]. Along a light ray, a, R e t are related by the equation for a null radial geodetic,

$$\frac{dR}{cdt} = \frac{(1-kR^2)^{1/2}}{a(t)}; \tag{1.36}$$

we have

$$R_{\rm s} = {\rm Sinn}\left\{c\int_{t_0}^{t_{\rm s}} \frac{dt}{a(t)}\right\},$$

where "Sinn" is defined as sinh if $k=-1$, as sin if $k=1$, and as the identity if $k=0$. The redshift z and the cosmic time t are related by

$$dt = \frac{a}{\dot{a}}\frac{dz}{1+z} = \frac{1}{H(z)}\frac{dz}{1+z};$$

then, the angular diameter distance reads

$$D_{\rm A}(z_{\rm s}) = \frac{a_0}{1+z_{\rm s}}{\rm Sinn}\left\{\frac{c}{a_o}\int_0^{z_{\rm s}} \frac{dz}{H(z)}\right\}. \tag{1.37}$$

1.7.2 The energy conservation

In general, various distinct components contribute to the total energy density of the universe. The energy-momentum conservation equation, $T^{\mu\nu}_{\ ;\mu} = 0$, determines how the energy density evolves as the universe expands. Let us consider non interacting components with density ρ_i and equation of state $p_i = w_i\rho_i c^2$. In the RW metric, the energy conservation equation reads

$$\dot{\rho}_i = -3H(1+w_i)\rho_i, \tag{1.38}$$

where $H \equiv \frac{\dot{a}}{a}$ is the time dependent Hubble parameter. Eq. (1.38) is solved by

$$\rho_i(z) = \rho_i(0)\exp\left[3\int_1^{1+z}[1+w_i(x)]d\ln x\right]. \tag{1.39}$$

Most of the relevant equations of state in cosmology can be accounted for by a constant w_i. The dominant energy condition [33] states that $T_{\mu\nu}l^\mu l^\nu \geq 0$ and $T^\mu_\nu l^\mu$ is non-spacelike, for any null vector l^μ; this implies that energy does not flow faster than the speed of light. For a perfect-fluid energy momentum tensor, these two conditions become $\rho + p/c^2 = (1+w)\rho \geq 0$ and $|\rho| \geq |p|/c^2$, respectively. Thus, either the density is positive and greater in magnitude than the pressure, or the density is negative and equal in magnitude to a compensating positive pressure[1]. In terms of the equation of state parameter w, we have either $\rho > 0$ and $|w| \leq 1$ or negative density and $w = -1$.

[1] A negative energy density is allowed only if it is in the form of vacuum energy.

For $w_i =$ const., Eq. (1.39) becomes

$$\rho_i \propto a^{-n_i}, \tag{1.40}$$

where the exponent is related to the equation of state parameter by

$$n_i = 3(1 + w_i). \tag{1.41}$$

Massive particles with negligible relative velocities are known as dust or simply matter; they verify $w_{\rm M} \simeq 0$. Their energy density is given by their number density times their rest mass; as the universe expands, since the rest masses are constant and the number density is inversely proportional to the volume, it is $\rho_{\rm M} \propto a^{-3}$. Radiation includes relativistic particles, such as photons and massless neutrinos. Their equation of state is $w_\gamma = 1/3$; since the energy of relativistic particles redshifts as the universe expands, it is $\rho_\gamma \propto a^{-4}$. Vacuum energy does not change with expansion, $\rho_\Lambda \sim$ const. This implies a negative pressure, or positive tension, for a positive vacuum energy ($w_\Lambda = -1$).

It is possible to define a critical density in terms of the Hubble parameter,

$$\rho_{\rm crit} \equiv \frac{3H^2}{8\pi G}; \tag{1.42}$$

the energy density can be measured in units of the critical density by introducing the density parameters

$$\Omega_i \equiv \frac{\rho_i}{\rho_{\rm crit}}. \tag{1.43}$$

1.7.3 The Friedmann's equations

The RW solutions to Einstein's field equation in the rest frame of the comoving fluid are known as Friedmann equations. It is

$$H^2 \equiv \left(\frac{\dot{a}}{a}\right)^2 = \frac{8\pi G}{3}\rho_{\rm T} - \frac{kc^2}{a^2}, \tag{1.44}$$

where $H \equiv \dot{a}/a$ is the time dependent Hubble parameter, and

$$\frac{\ddot{a}}{a} = -\frac{4\pi G}{3}(\rho_{\rm T} + 3\frac{p_{\rm T}}{c^2}). \tag{1.45}$$

Cosmological models having a RW metric and obeying Eqs. (1.44, 1.45) are called Friedmann-Lemaître-Robertson-Walker (FLRW) models.

From Eq. (1.44), we see that for any value of the Hubble parameter, when the total energy density equals the critical value $\rho_{\rm crit}$, the spatial geometry is flat ($k = 0$).

It is useful to describe the curvature as an effective energy density $\rho_{\rm K} \equiv -\frac{3kc^2}{8\pi G}a^{-2}$, so that $w_{\rm K} = -1/3$. Specializing Eq. (1.44) to the present epoch, we see that the space curvature today is related to the total density parameter Ω_0 by

$$-\frac{kc^2}{a_0^2 H_0^2} \equiv \Omega_{\rm K0} = 1 - \Omega_0; \tag{1.46}$$

the subscript zero refers to cosmological quantities evaluated today. According to the definition of $\Omega_{\rm K0}$, we can re-express the angular diameter distance, Eq. (1.37), in a RW metric as

$$D_{\rm A}(z_{\rm s}) = \frac{c}{H_0}\frac{1}{|\Omega_{\rm K0}|^{\frac{1}{2}}(1+z_{\rm s})}{\rm Sinn}\left\{|\Omega_{\rm K0}|^{\frac{1}{2}}\int_0^{z_{\rm s}}\frac{H_0}{H(z)}dz\right\}. \tag{1.47}$$

The expression in Eq. (1.47) is only based on the properties of the RW metric and on the definition of $\Omega_{\rm K0}$. In general relativity, we have $\Omega_{\rm K0} = 1 - \Omega_0$ and the Hubble parameter, Eq. (1.44), can be expressed in terms of the density parameters as

$$H^2 = H_0^2\left\{\Omega_{\rm M0}(1+z)^3 + \Omega_{\rm X0}\exp\left[3\int_1^{1+z}[1+w_{\rm X}(x)]d\ln x\right] + \Omega_K(1+z)^2\right\}, \tag{1.48}$$

where we have only considered pressureless matter, with today energy density parameter $\Omega_{\rm M0}$, and a second component with density $\Omega_{\rm X0}$ and equation of state $w_{\rm X}(z)$.

Besides the Hubble parameter, which describes the observable size of the universe and its age, it is possible to define another number to understand the nature of the RW universe [165, 167]. $q_0 \equiv -H_0^2(\ddot{a}/a)_0$ is called the *deceleration parameter* and probes the equation of state of matter and the cosmological density parameter. In a FLRW universe filled in with fluids with constant equation of state, from Eq. (1.45), we get

$$q_0 = \frac{1}{2}\sum_i(1+3w_i)\Omega_{\rm i0}. \tag{1.49}$$

An accelerating universe ($q_0 < 0$) requires some components with very negative pressure ($w_i < -1/3$).

1.8 The energy budget

Observational cosmology has devoted large efforts in the last years to characterize the energy content of the universe. Galaxy clustering [8, 32] and large-scale structure [139, 204]) observations favour models of a universe with a subcritical matter energy density, $\Omega_{\rm M0} < 1$ [197]. Since, according to balloon-based measurements of the anisotropy of the Cosmic Microwave Background Radiation (CMBR) [9, 48], the total of energy content of the universe nearly equals the critical density [93, 148]), we expect that about 2/3 of the critical density is in form of dark energy (also called quintessence). Furthermore,

evidence coming from type Ia supernovae that the universe is accelerating its expansion [140, 156] demands a new contribute to the total energy density, the *dark energy*, with a strongly negative pressure ($w_{\rm X} \equiv p_{\rm X}/\rho_{\rm X} < -1/3$, where $p_{\rm X}$ and $\rho_{\rm X}$ are, respectively, the pressure and energy density of the dark energy). These observations, together with other constraints coming from the age of the universe, gravitational lensing statistics and Lyα forest, support a geometrically flat universe [82] ($\Omega_{\rm M0} + \Omega_{\rm X0} = 1$, where $\Omega_{\rm X0}$ is the dark energy density parameter of the universe) with $\Omega_{\rm M0} \sim 0.3$-0.4 and a constant equation of state $-1 \leq w_{\rm X} \lesssim -0.4$ [208, 212] at the 68% confidence level or better according to a concordance analysis [212]. A less conservative maximum likelihood analysis suggests a smaller range for the equation of state, $-1 \leq w_{\rm X} \lesssim -0.6$ [12, 141, 212].

1.8.1 Dark matter

There is an overwhelming evidence that most of the mass in the universe is some non-luminous dark matter, of as yet unknown composition.

Zwicky in 1933 [229] proposed the earliest indication of dark matter. He noted that the galaxies in the Coma cluster and other rich clusters of galaxies move so fast that the clusters required about ten to 100 times the mass accounted by the galaxies themselves to keep the galaxies bound. By applying Newton's laws to the motion of galaxies in clusters, one infers a universal mass density of $\Omega_{\rm M0} \simeq 0.1$-$0.3$. Galactic dynamics yields another strong observational evidence for the existence of dark matter. There is simply not enough luminous matter ($\Omega_{\rm LUM} \lesssim 0.01$) observed in spiral galaxies to account for their observed flat rotation curves. From gravitational effects, one infers a galactic dark halo of mass 3-10 times that of the luminous component.

A few theoretical arguments also support the existence of dark matter. If the mass density contributed by the luminous matter were the major contribution to the mass density of the universe, the duration of the epoch of structure formation would be very short, thereby requiring (in almost all theories of structure formation) fluctuations in the CMBR which would be larger than those observed. These considerations imply $\Omega_{\rm M0} \gtrsim 0.3$.

There are many ways in which baryons can hide in dark forms [159]. These are: massive black holes; stellar remnants, such as neutron stars or white dwarf; brown dwarfs; snowballs; clouds of molecular hydrogen. These baryonic dark matter candidates are generally known as MACHOs (Massive Astrophysical Compact Halo Objects). The universal fraction of macroscopic dark matter is still unknown. Direct searches for MACHOs in the Milky Way have been performed by the MACHO and EROS collaborations through microlensing surveys. According to the MACHO group [3], the most likely halo fraction in form of compact objects with a mass in the range

$0.1 - 1$ $M_\odot$ is of about 20%; the EROS collaboration [111] has set a 95% confidence limit that objects less than 1 $M_\odot$ contribute less than 40% of the dark halo. A first attempt to obtain information from sources in the Andromeda galaxy has been performed by the SLOTT-AGAPE collaboration. By using the pixel lensing technique [161] to observe the Andromeda galaxy with the McGraw-Hill telescope, MDM Observatory, Kitt Peak (Arizona, USA), during 1998-1999, five candidate events have been selected [28]. However, the average cosmological fraction in macroscopic dark matter could be significantly different from these local estimates.

Further reasons favour a non-baryonic dark matter, consisting of some new elementary particles [138]. The strongest argument in favour of non-baryonic dark matter comes from big-bang primordial nucleosynthesis, which estimates a baryonic contribution of $\Omega_B \lesssim 0.06$, too small to account for the dark matter in the universe. Although a neutrino species of mass ~ 30 eV could provide the right dark-matter density, N-body simulations of structure formation in a neutrino-dominated universe do a poor job of reproducing the observed structure of the universe. Phase-space arguments also disfavour halos of galaxies made of neutrinos. It appears likely that some non-baryonic, non-relativistic matter is required in the universe. Furthermore, the features in the clustering power spectrum also support collisionless dark matter.

Particle physics can provide candidates. Supersymmetry and theories outside the standard model predict the existence of a new stable elementary particle having weak interactions with ordinary matter. Examples of such a particle, known as WIMPs (Weakly Interacting Massive Particles), are the axion and the neutralino. However, at present, there is no direct accelerator evidence for the existence of supersymmetry.

1.8.2 Dark energy

A positive cosmological constant Λ was introduced initially by Einstein in an attempt to obtain a universe with a static space-time with positive spatial curvature. It is a static, homogeneous energy component with negative pressure, $w_\Lambda = -1$. A time independent cosmological constant can be provided by models which associate Λ with a property of the vacuum, such as the vacuum energy associated with symmetry breaking or vacuum polarization and particle production effects in curved space-time. In 1968, Zeldovich [227] suggested a firm physical mechanism for the generation of a cosmological constant by showing that the vacuum within the quantum framework has properties identical to those of a cosmological constant; the zero-point vacuum fluctuation must have a Lorentz invariant form $p_\Lambda = -\rho_\Lambda c^2$, or equivalently $T^\Lambda_{\mu\nu} = \Lambda g_{\mu\nu}$.

After this first proposal of dark energy, many other candidates have been suggested to close the universe.

Quintessence can be parameterized by an effective equation of state, $p_X = w_X \rho_X c^2$.

The relevant range for $w_{\rm X}$ is between 0, ordinary matter, and -1, true cosmological constant; sources with $w_{\rm X} > 0$ redshift away more rapidly than ordinary matter and, therefore, cause extra deceleration, while $w_{\rm X} < -1$ is unphysical according to the dominant energy condition.

A possibility is represented by a fluid with a constant equation of state ($w_{\rm X} =$ const.), called X-matter [38, 198]. This phenomenological ansatz can describe a dark energy density varying with time, in particular over the redshift range over which the dark energy can be potentially observed.

One interesting idea to model the dark energy density is provided by a dynamical, spatially inhomogeneous, scalar field rolling down an almost flat potential, known as quintessence [29, 50, 149, 160, 162, 165, 219]. In an expanding universe, a spatially homogeneous scalar field with potential $V(\phi)$ and minimal coupling to gravity obeys

$$\ddot{\phi} + 3H\dot{\phi} + V^{'}(\phi) = 0, \tag{1.50}$$

where primes indicate derivatives with respect to ϕ. The energy density is

$$\rho_\phi = \frac{1}{2}\dot{\phi} + V(\phi), \tag{1.51}$$

and the pressure is

$$p_\phi = \frac{1}{2}\dot{\phi} - V(\phi). \tag{1.52}$$

The equation of state turns out

$$w_\phi = \frac{\frac{1}{2}\dot{\phi} + V(\phi)}{\frac{1}{2}\dot{\phi} - V(\phi)}; \tag{1.53}$$

w_ϕ, in general, varies with time. When the field is slowly varying, i.e. $\dot{\phi} \ll V(\phi)$, it is $w_\phi \gtrsim -1$, and the scalar field potential acts like a cosmological constant. Unlike a cosmological constant, this dynamical field can support long-wavelength fluctuations that leave an imprint on both CMBR and large-scale structures. Particle physics theories with dynamical symmetry breaking or non-perturbative effects can generate potentials that support negative pressure.

A motivation for considering quintessence models is to address the *coincidence problem*, the issue of explaining the initial conditions necessary to yield the near coincidence of the densities of matter and the dark energy today. The cosmological constant solution is affected by a fine tuning problem, since the current ratio today is only obtained by a ratio of vacuum density to matter-radiation density to 1 part in 10^{120} at the close of inflation. Since quintessence couples directly to other forms of energy, possible interactions may cause the dark energy to adjust itself naturally to be comparable to the matter density today.

Another scenario alternative to scalar fields is based on a network of light non-intercommuting topological defects [191, 205]. Within a topological defect, the field configuration is in the false vacuum state leading to $p = -\rho c^2$ along any orthogonal direction within the defect. So, $w_{\rm X} = -m/3$, where m is the dimension of the defect: for a tangled cosmic string, $m = 1$; for a domain wall, $m = 2$.

Generally, the equation of state $w_{\rm X}$ evolves with the redshift, and the feasibility of reconstructing its time evolution has been investigated [37, 44, 45, 73, 88, 119, 127, 166, 214, 225]. In gravitational lensing, the cosmological parameters enter the lensing quantities through the angular diameter distances. Since, as can be seen from Eqs. (1.47, 1.48), in FLRW models the distance depends on $w_{\rm X}$ only through a multiple integral on the redshift [119], $w_{\rm X}(z)$ can be determined only given a prior knowledge of the matter density of the universe [70, 73, 217]. In what follows, without being explicitly stated, we will consider only the case of a constant equation of state.

We want only to mention that dark energy is not the only theoretical explanation for an accelerating universe. Theories which go beyond the simplest implications of the principle of equivalence, such as a theory with non-zero torsion, in which the connection is not symmetric, can also support a negative deceleration parameter [31].

1.8.3 Relativistic matter

The energy density in radiation today is really much less than that in matter. There are two obvious candidates for relativistic matter, photons and neutrinos [103]. Photons, which are readily detectable, are mostly in the 2.73° K CMBR. Since the CMBR has an excellent black-body spectrum, its energy is given by the Stefan-Boltzmann law. In terms of the cosmic density parameter, they contribute $\Omega_{\gamma 0} \sim 5{\times}10^{-5}$.

If neutrinos are sufficiently low mass as to be relativistic today, conventional scenarios predict that they contribute approximately the same amount.

In what follows, we will consider the radiation contribution to the energy budget to be negligible.

1.9 Space-time near a gravitational lens

The astrophysical objects that usually act as gravitational lenses are stars, galaxies or group of galaxies (including gas dust and stars) for scales of 100 Kpc and smaller, super-clusters and clusters of galaxies spreading over tens of megaparsec, and the large scale structure of the universe covering scales of hundreds of megaparsec. The matter of large scale structures is concentrated in sheets and filaments that surround large,

roughly spherical under-dense regions, known as voids. It is a common assumption to consider the large scale perturbations effects on a given gravitational lens system as negligible.

Gravitational lenses are supposed to be small local perturbations of the smooth background universe. We assume that a gravitational lens and its lensing effects are weak and localized in a very small portion of sky. Near a deflector, the space-time is nearly flat and can be studied by perturbation methods.

1.9.1 Weak field metric in general relativity

We suppose the metric $g_{\alpha\beta}$ to be close to the flat, Minkowskian metric $\eta_{\alpha\beta}$. It is,

$$g_{\alpha\beta} = \left(1 - \frac{1}{2}h\right)\eta_{\alpha\beta} + h_{\alpha\beta}, \tag{1.54}$$

$$h \equiv \eta^{\alpha\beta}h_{\alpha\beta}, \qquad |h_{\alpha\beta} \ll 1|. \tag{1.55}$$

The effect of the distribution of matter is contained in the perturbation $h_{\alpha\beta}$. In linear approximation with respect to $h_{\alpha\beta}$, we can choose, without loss of generality, the coordinates such that the coordinate gauge condition is satisfied [2]

$$h^{\alpha\beta}{}_{,\beta} = 0. \tag{1.56}$$

The Einstein's gravitational field equation, linearized in $h_{\alpha\beta}$ reads

$$\left(\nabla - \frac{1}{c^2}\frac{\partial^2}{\partial t^2}\right)h^{\alpha\beta} = \frac{16\pi G}{c^4}T^{\alpha\beta}. \tag{1.57}$$

For an isolated source without incoming gravitational radiation, the above equations are solved by the retarded solutions,

$$h^{\alpha\beta}(t, \mathbf{x}) = \frac{-4G}{c^4}\int \frac{T^{\alpha\beta}\left(t - \frac{|\mathbf{y}|}{c}, \mathbf{x} + \mathbf{y}\right)}{|\mathbf{y}|}d^3y, \tag{1.58}$$

We describe the distribution of matter as a perfect fluid matter tensor. We assume that:

- The mass distribution changes its position slowly with respect to the coordinate system, so that the matter velocity is much less than the speed of light, i.e. $v^i \equiv \frac{dx^i}{dt}$ obeys $|\mathbf{v}| \ll c$;

[2] In this approximation, the indices of $h_{\alpha\beta}$ may be raised by means of the background Minkowskian metric $\eta^{\alpha\beta}$ rather than with $g^{\alpha\beta}$.

- matter stresses are also small (the pressure is much smaller than the energy density times c^2), $|p| \ll \rho c^2$.

Then,

$$T^{00} \simeq \rho c^2, \quad T^{0i} \simeq c\rho v^i, \quad T^{ij} \simeq \rho V^i v^j + p\delta^{ij}, \tag{1.59}$$

where terms of relative order $\frac{v^2}{c^2}, \frac{p}{\rho c^2}$ have been neglected.

In this weak field regime and slow motion approximation, space-time is nearly flat near the lens. Up to leading order in c^{-3}, the metric is

$$ds^2 = g_{\alpha\beta}dx^\alpha dx^\beta \approx \left(1 + \frac{2U}{c^2}\right)c^2dt^2 - 8cdt\frac{\mathbf{V}\cdot d\mathbf{x}}{c^3} - \left(1 - \frac{2U}{c^2}\right)d\mathbf{x}^2, \tag{1.60}$$

where we have introduced the retarded potentials

$$U(t,\mathbf{x}) \equiv -G\int \frac{\rho\left(t - \frac{|\mathbf{y}|}{c}, \mathbf{x}+\mathbf{y}\right)}{|\mathbf{y}|}d^3y; \tag{1.61}$$

$$\mathbf{V}(t,\mathbf{x}) \equiv -G\int \frac{(\rho\mathbf{v})\left(t - \frac{|\mathbf{y}|}{c}, \mathbf{x}+\mathbf{y}\right)}{|\mathbf{y}|}d^3y. \tag{1.62}$$

$\mathbf{V}$ is a vector potential taking into account the gravito-magnetic field produced by mass currents. In this approximation, the stresses T^{ij} do not affect the metric. In the near zone of the system, the retardation in Eqs. (1.58) can be neglected; then U reduces to the Newtonian potential,

$$U(t,\mathbf{x}) \simeq -G\int \frac{\rho\,(t,\mathbf{x}+\mathbf{y})}{|\mathbf{y}|}d^3y, \tag{1.63}$$

and

$$\mathbf{V}(t,\mathbf{x}) \simeq -G\int \frac{(\rho\mathbf{v})\,(t,\mathbf{x}+\mathbf{y})}{|\mathbf{y}|}d^3y, \tag{1.64}$$

The *post-Minkowskian* metric in Eq.(1.60) satisfies the weak field condition if, and, only if, in addition to the assumptions just stated, it is

$$|U| \ll c^2; \tag{1.65}$$

then,

$$\left|\frac{\mathbf{V}}{c^3}\right| \lesssim \left|\frac{\mathbf{v}}{c}\right| \cdot \left|\frac{U}{c^2}\right| \ll 1. \tag{1.66}$$

For spherical bodies, $U = -GM/R$, with R distance from the centre of the mass. Eq. (1.65) implies

$$\frac{2GM}{c^2} = R_{\rm S} \ll R;$$

Hence, the neighbourhoods of compact objects as black holes and neutron stars cannot be considered in this approximation. For galaxies clusters $M_{\rm cl} \simeq 10^{15}M_\odot$ and $R_{\rm cl} \simeq$ 1Mpc, so that $|U| \lesssim 10^{-4}c^2$.

1.9.2 A generalized space-time element in metric theories

The weak field metric derived in the slow motion approximation can be extended to the post-post-Newtonian (ppN) order and to general metric theories of gravity [180].

Let us consider the expression of a spatially spherically symmetric metric, in the hypotheses of spherical symmetry only and without any use of the Einstein field equation. In addition, we assume time independence of this metric. It is

$$ds^2 = e^{m(r)}c^2dt^2 - e^{n(r)}dr^2 + r^2(d\theta + \sin^2\theta d\phi^2). \tag{1.67}$$

In 1916, K. Schwarzschild found the solution of the vacuum Einstein's field equation in the form of Eq. (1.67). In isotropic coordinates, the Schwarzschild metric reads

$$ds^2 = \frac{(1 - GM/2r^{'})^2}{(1 + GM/2r^{'})^2}c^2dt^2 - \left(1 + \frac{GM}{2r^{'}}\right)^4 (dr^{'2} + r^{'2}d\theta + r^{'2}\sin^2\theta d\phi^2). \tag{1.68}$$

M is the mass of the source. The new variable $r^{'}$ is defined as

$$r^{'} \equiv \frac{1}{2}\left[r - \frac{GM}{c^2} + \left(r^2 - 2\frac{GM}{c^2}r\right)^{1/2}\right].$$

In what follows, we will drop the apex from the new radial variable.

We expand the metric as power series in the small parameter $\frac{GM}{r}$ up to the ppN order. Then, we multiply the terms of this expansion by dimensionless parameters. This expression can be generalized to an arbitrary mass distribution by replacing $-\frac{GM}{r}$ with the standard Newtonian potential U. It is $U \sim \varepsilon^2$, with ε denoting the order of approximation. Finally, we introduce the nondiagonal components of the metric tensor generated by mass currents. We can write $g_{0i} \sim -4V_i$, where V_i is the gravito-magnetic potential, $V_i \sim Uv \sim \varepsilon^3$. The final expression for the approximate metric element is

$$ds^2 \simeq \left[1 + 2\frac{U}{c^2} + 2\beta\left(\frac{U}{c^2}\right)^2\right]c^2dt^2 - \left[1 - 2\gamma\frac{U}{c^2} + \frac{3}{2}\epsilon\left(\frac{U}{c^2}\right)^2\right]d\mathbf{x}^2 - 8\mu\frac{\mathbf{V}\cdot d\mathbf{x}}{c^3}\,cdt. \tag{1.69}$$

Asimptotically, the metric reduces to the Minkowski one. β and γ are two standard coefficients of the post-Newtonian parametrized expansion of the metric tensor [41, 221]. β is related to nonlinearity of mass contribution to the metric; γ measures space curvature produced by mass. In general relativity, it is $\beta = \gamma = 1$; in the Brans-Dicke theory, $\beta = 1$ and $\gamma = \frac{1+\omega}{2+\omega}$. ϵ and μ are non standard parameters. ϵ takes into account the ppN contribution to the metric [60]; μ quantifies the contribution to the space-time curvature of the mass-energy currents and measures the strength of the intrinsic gravito-magnetic field [41]. In general relativity $\epsilon = \mu = 1$.

The approximated metric element just introduced cannot describe every conceivable metric theory of gravity. In particular, it does not consider preferred frame effects,

violations of conservation of four momentum and preferred location effects.[3] However, the metric in Eq. (1.69) should be obeyed by most metric theories, with differences among them occurring only in the numerical coefficients.

We will assume that during the interaction with light rays, the configuration of an isolated distribution of matter does not change significantly. Then, the metric element can be considered as stationary. This approximation holds for almost all observed gravitational lensing phenomena. Clusters of galaxies have sizes of order a megaparsec and dynamical time scale of order the Hubble time, while light takes a few million years to cross them. A typical spiral galaxy (as Milky Way) takes about 100 million years to complete a rotation, about 10^3 order of magnitude more than the time taken by light to transverse the galaxy.

Furthermore, we can assume that the potential well of the lens does not alter the energies of photons as they cross the deflector; so the redshift of a source's image is unaffected by lensing effect.

1.9.3 Cosmological lenses and background

Gravitational lenses act as small perturbations on a homogeneous and isotropic background universe. The isotropic form of the RW metric is

$$ds^2 = c^2dt^2 - a^2(t)\frac{d\mathbf{x}^2}{\left(1+\frac{k}{4}\mathbf{x}^2\right)^2} \tag{1.70}$$

The geometry of space-time in the neighbourhood of the relevant light rays can be approximated by

$$\begin{aligned} ds^2 = a^2(\tau)\Bigg\{&\left[1+2\frac{U}{c^2}+2\beta\left(\frac{U}{c^2}\right)^2\right]d\tau^2 \\ &-\left[1-2\gamma\frac{U}{c^2}+\frac{3}{2}\epsilon\left(\frac{U}{c^2}\right)^2\right]\frac{d\mathbf{x}^2}{\left(1+\frac{k}{4}\mathbf{x}^2\right)^2}-8\mu\frac{\mathbf{V}\cdot d\mathbf{x}}{c^3}\,d\tau\Bigg\}, \end{aligned} \tag{1.71}$$

where we have introduced the conformal time τ, defined as

$$d\tau = c\frac{dt}{a}. \tag{1.72}$$

Equation (1.71) combines the RW metric with the local metric. Since the universe is locally flat, near the lens the background can be assumed to be endowed with an Euclidean geometry ($k = 0$). In most of the gravitational lensing phenomena, the scale factor a changes negligibly during the time delay between different lensed light

[3] Even by including the complete standard set of ten parameters, the post-Newtonian parameterized expansion cannot include every conceivable metric theory of gravity [41].

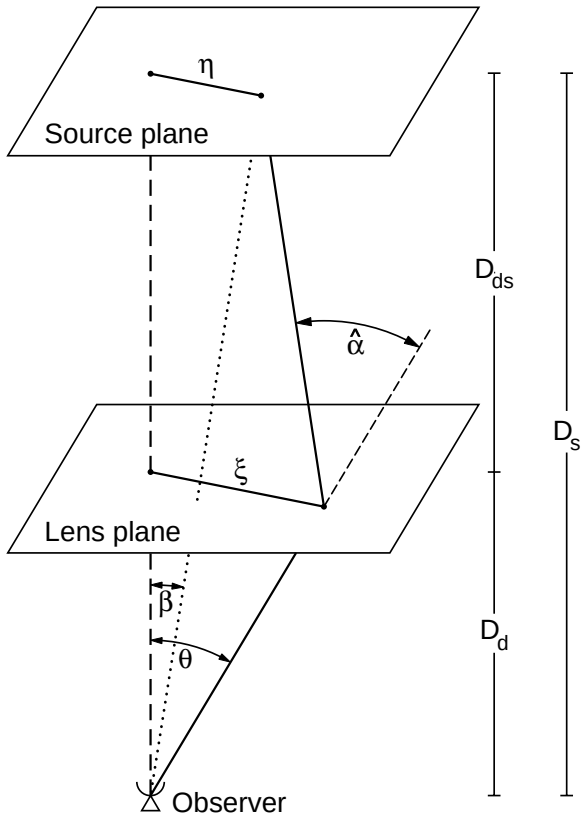

Figure 1.2: Schematic of a gravitational lensing system.

rays connecting source and observer, and during the travel time of light across the lens (both times being very short compared to the Hubble time). So, the scale factor attains approximately the same value at the different cosmic proper times when different light rays reach the lens.

The line element in Eq. (1.71) is conformally stationary, so that the Fermat's principle applies to it in its simpler formulation.

1.10 Thin lenses

Usually, the physical size of a lensing matter distribution along the line of sight, d, is small compared to the distances between lens and observer, or, lens and source [142, 172]. As an example, in practically all cases of known quasar lensing, the observer-deflector and deflector-source separations are of order of $\sim 10^3$ Mpc, while the diameter of a deflector galaxy is roughly $\sim$ 30 Kpc and of a cluster of galaxies is $\sim$ 5 Mpc. For the case of microlensing in the Galactic bulge or towards the Large Magellanic Cloud by foreground stars, the observer-deflector and deflector-source distances are respectively about 5 to 25 Kpc while the separation of binary-star gravitational lens systems ($\sim 10^{-2}$ pc) is lower by $\sim 10^5 - 10^6$ orders of magnitude.

In these situations, given very small deflection angles, $\hat{\alpha} \ll 1$, the extent of the deflector in the direction of the incoming light ray is so small that the value of the transverse gravitational field strength $\nabla_\perp U$ on the actual ray deviates but little from that on the unperturbed (straight) ray. We have that the maximal deviation $\Delta s_{\max} \sim \hat{\alpha} d$ of the ray is small compared to the length scale on which the field changes

$$|\Delta s_{\max} \nabla_\perp \nabla_\perp U| \ll |\nabla_\perp U| \,. \tag{1.73}$$

The lens is geometrically-thin. Since such a thin lens occupies a small portion of the sky, we can treat the lens as lying in the tangent plane to the celestial sphere passing through the lens centre and centred at the observer. This tangent plane is called the lens plane of the system.

It is useful to employ the spatial orthogonal coordinates (ξ_1, ξ_2, l), centred on the lens and such that the l-axis is along the incoming light ray direction $\mathbf{e}_{\text{in}}$. This axis defines the optical axis; we remark that, because of the smallness of angles involved in typical gravitational lensing systems, the exact definition of the optical axis does not matter. The lens plane corresponds to $l = 0$. Since space is approximately Euclidean in the vicinity of the deflector, the vector $\boldsymbol{\xi}$, i.e. the position vector where a light ray impacts the lens plane, see Fig. (1.2), determines proper distances as measured at the lens. The angular diameter distance between the observer and the source will be denoted as D_{d}.

1.11 Light sources

Physical sources emitting light are main players of gravitational lensing. In the usual gravitational lensing situations, only a small cone around the optical axis needs to be considered. Within such a small cone, the celestial sphere through the source can be replaced by the corresponding tangent plane. The light source plane is supposed, for a thin light source, to be approximately orthogonal to the line of sight passing through the lens plane.

In addition, it is assumed that light rays connecting source and observer are negligibly affected by the gravitational fields of the source and observer. In particular, the time delation factor on Earth is $\sim 1 + U_0/c^2$, with $U_0/c^2 \sim 10^{-9}$. So, the gravitational potential at the observer is practically irrelevant in applications of gravitational lensing.

Depending on a source's angular size relative to the Einstein radius, sources are divided in point-like and extended, giving rise to different observable phenomena. Unless contrary stated, light sources will be assumed point-like.

The vector $\boldsymbol{\eta}$, Fig. (1.2), will denote the displacement of the source on the source

plane from the origin, located by the interception with the optical axis. The angular diameter distances between the observer and the source, measured in the homogeneous background, will be referred as $D_{\rm s}$; the distance from the lens to the lens as $D_{\rm ds}$.

1.12 Time delay

We consider the gravitational lens as the only agent of non-trivial perturbations to the ray paths. A light ray follows a smooth curved trajectory, p. Since the deflection angle is very small, we consider, as kinematically possible light rays, piecewise smooth world lines, consisting of a null geodesic of the RW metric from a light source to the lens plane with impact parameter $\boldsymbol{\xi}$, and another such null geodesics from the lens plane to the observer. At some fixed cosmic time t, the spatial paths of lensed light rays are also approximated by piecewise-smooth geodesics of the spatial metric $a^2(t)dS_K^2$. The source is at point $\boldsymbol{\eta}$ on the light source plane at cosmic time $t_{\rm S}$. Since the time delay between paths are assumed to be extremely small, we suppose that light rays impact the lens plane at approximately cosmic time $t_{\rm L}$, equal for all the paths.

In the absence of the lens, there will be a unique null geodesic p_0 connecting the source and the observer. Its projection into the comoving space is a smooth geodesics of dS_K^2.

The projections of p and p_0 form a triangle in the comoving space.

The time delay (as measured in the lens plane at cosmic time $t_{\rm L}$) of the path p relative to the unlensed ray p_0 is

$$\Delta T^{\rm L} = \frac{1}{c}\left(\int_p n_{\rm L} a_{\rm L}\, dl_{\rm P} - \int_{p_0} a_{\rm L} dl_{\rm P}\right), \tag{1.74}$$

where $a_{\rm L} dl_{\rm P}$ is the spatial metric of Eq. (1.71). In what follows, it will be useful to express the refraction index as $n_{\rm L} \equiv 1 - \delta n_{\rm L}$. In Eq. (1.74), $n_{\rm L}$ is the effective refraction index referring to the approximate metric in Eq. (1.69). Equation (1.74) can be re-written as a sum of geometrical and potential time delays

$$\Delta T^{\rm L} = \Delta T^{\rm L}_{\rm geom} + \Delta T^{\rm L}_{\rm pot}.$$

The geometrical time delay, due to the extra path length relative to the unperturbed ray, is

$$\Delta T^{\rm L}_{\rm geom} = \frac{1}{c}\left[\int_p a_{\rm L} dl_K - \int_{p_0} dl_K\right] \equiv \frac{a_{\rm L}}{c}\Delta_{p_0}(p); \tag{1.75}$$

$\Delta_{p_0}(p)$ is the difference between the lengths of p and p_0 relative to dS_K^2; dl_K is the increment of length relative to the spatial metric dS_K^2 of the RW metric.

The potential time delay, due to the retardation of the deflected ray caused by the gravitational field of the lens, is

$$\Delta T^{\rm L}_{\rm pot} = -\frac{1}{c}\int_p \delta n_{\rm L}\; a_{\rm L} dl_{\rm P}. \tag{1.76}$$

Since we consider a locally flat background perturbed by a weak lens ($\delta n_{\rm L} \to 0$ for $|\mathbf{x}| \to \infty$), the spatial metric increment can be evaluated referring to the spatial metric in Eq. (1.71) with $k = 0$.

The time delay $\Delta T^{\rm L}$ measured at the lens is simply related to the time delay ΔT at the observer,

$$\Delta T = (1+z_{\rm d})\Delta T^{\rm L}. \tag{1.77}$$

Furthermore,

$$\Delta T_{\rm geom} = (1+z_{\rm d})\Delta T^{\rm L}_{\rm geom}, \tag{1.78}$$

and

$$\Delta T_{\rm pot} = (1+z_{\rm d})\Delta T^{\rm L}_{\rm pot}, \tag{1.79}$$

where $z_{\rm d}$ is the redshift of the lens.

1.12.1 The effective refractive index

Let us go, now, to evaluate the above quantities with our approximate metric element. The proper arc length is

$$dl_p \simeq \left\{1 - \gamma\frac{U}{c^2} + \left(\frac{3}{4}\epsilon - \frac{\gamma^2}{2}\right)\left(\frac{U}{c^2}\right)^2 + \mathcal{O}(\varepsilon^6)\right\} dl_{\rm eucl}, \tag{1.80}$$

where $dl_{\rm eucl} \equiv \sqrt{\delta_{ij}dx^i dx^j}$ is the Euclidean arc length. Inserting Eq. (1.80) in Eq. (1.14), we get the effective refraction index

$$n_{\rm L} = \left\{1 - (1+\gamma)\frac{U}{c^2} + \left[\frac{3}{2} - \beta + \gamma\left(1 - \frac{\gamma}{2}\right) + \frac{3}{4}\epsilon\right]\left(\frac{U}{c^2}\right)^2 + 4\mu\frac{V_i}{c^3}e^i\right\}\frac{dl_{\rm eucl}}{dl_{\rm P}}. \tag{1.81}$$

The potential time delay at the lens turns out

$$c\Delta T^{\rm L}_{\rm pot} = \int_p \left\{-(1+\gamma)\frac{U}{c^2} + \left[\frac{3}{2} - \beta + \gamma\left(1 + \frac{\gamma}{2}\right) + \frac{3}{4}\epsilon\right]\left(\frac{U}{c^2}\right)^2 + 4\mu\frac{V_i}{c^3}e^i\right\} a_{\rm L} dl_{\rm eucl}. \tag{1.82}$$

1.12.2 Potential time delay

The potential time delay can be considered as the sum of three terms,

$$\Delta T_{\rm pot} = \Delta T^{\rm pN}_{\rm pot} + \Delta T^{\rm ppN}_{\rm pot} + \Delta T^{\rm GRM}_{\rm pot}; \tag{1.83}$$

the first contribution contains the post-Newtonian correction to the time delay,

$$c\Delta T^{\rm pN}_{\rm pot} \equiv -(1+z_{\rm d})\frac{(1+\gamma)}{c^2}\int_p U a_{\rm L} dl_{\rm eucl}; \tag{1.84}$$

the second term is the ppN correction,

$$c\Delta T^{\rm ppN}_{\rm pot} \equiv \frac{1}{c^4}(1+z_{\rm d})\left[\frac{3}{2}-\beta+\gamma\left(1-\frac{\gamma}{2}\right)+\frac{3}{4}\epsilon\right]\int_p U^2 a_{\rm L} dl_{\rm eucl}; \tag{1.85}$$

the third contribution to the time delay derives from the gravito-magnetic field,

$$c\Delta T^{\rm GRM}_{\rm pot} \equiv (1+z_{\rm d})\frac{4\mu}{c^3}\int_p \mathbf{V}\cdot\mathbf{e}\ a_{\rm L} dl_{\rm eucl}\ . \tag{1.86}$$

The thin lens assumption greatly simplifies the calculation of the potential time delay [142, 172]. The actual ray light is deflected, but if the deflection angle is small, it can be approximated as a straight line in the neighbourhood of the lens. This corresponds to the Born approximation, which allows integrating Eq. (1.82) over the unperturbed ray $\mathbf{e}_{\rm in}$. Both $\Delta T^{\rm pN}_{\rm pot}$ and $\Delta T^{\rm GRM}_{\rm pot}$ can be easily expressed in terms of the surface mass density Σ,

$$\Sigma(\boldsymbol{\xi}) \equiv \int \rho(\boldsymbol{\xi}, l)\ dl, \quad dl \equiv a_{\rm L} l_{\rm eucl}; \tag{1.87}$$

we get,

$$c\Delta T^{\rm pN}_{\rm pot} \simeq -2(1+z_{\rm d})(1+\gamma)\frac{G}{c^2}\int_{\Re^2} d^2\xi' \Sigma(\boldsymbol{\xi}')\ln\frac{|\boldsymbol{\xi}-\boldsymbol{\xi}'|}{\xi_0} + \text{const.}, \tag{1.88}$$

and

$$c\Delta T^{\rm GRM}_{\rm pot} \simeq 8(1+z_{\rm d})\mu\frac{G}{c^3}\int_{\Re^2} d^2\xi' \Sigma(\boldsymbol{\xi}')\langle\mathbf{v}\cdot\mathbf{e}_{\rm in}\rangle_l(\boldsymbol{\xi}')\ln\frac{|\boldsymbol{\xi}-\boldsymbol{\xi}'|}{\xi_0} + \text{const.}; \tag{1.89}$$

$\langle\mathbf{v}\cdot\mathbf{e}_{\rm in}\rangle_l$ is the weighted average, along the line of sight, of the component of the velocity $\mathbf{v}$ orthogonal to the lens plane,

$$\langle\mathbf{v}\cdot\mathbf{e}_{\rm in}\rangle_l(\boldsymbol{\xi}) \equiv \frac{\int(\mathbf{v}(\boldsymbol{\xi}, l)\cdot\mathbf{e}_{\rm in})\ \rho(\boldsymbol{\xi}, l)\ dl}{\Sigma(\boldsymbol{\xi})}; \tag{1.90}$$

ξ_0 is a scale-length in the lens plane.

On the contrary, it is not an easy task to perform the integration along the line of sight in the case of $\Delta T^{\rm ppN}_{\rm pot}$; expressions in terms of elementary functions are not known.

1.12.3 Geometrical time delay

Let us evaluate $\Delta_{p_0}(p)$, the very small amount by which the geometrical length of p exceeds that of p_0 relative to the metric dS^2_K. We will consider the Euclidean 3-space $\Re^3$. It is, see Fig. (1.3,)

$$\Delta_{p_0}(p) = l_{\rm L} + l_{\rm L,S} - l_{\rm S}. \tag{1.91}$$

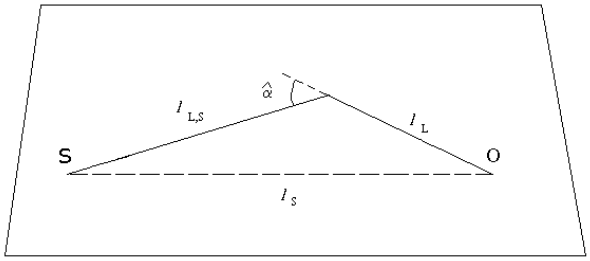

Figure 1.3: The geodesic triangle formed from the projections of p and p_0 into the standard comoving space.

Since $\hat{\alpha} \ll 1$, we have

$$l_{\rm S} \simeq l_{\rm L} + l_{\rm L,S}, \tag{1.92}$$

and

$$1 - \cos\hat{\alpha} = 2\sin^2\frac{\hat{\alpha}}{2} \simeq \frac{\hat{\alpha}^2}{2}. \tag{1.93}$$

The geodesic triangle lies in a two-dimensional (complete simply connected, totally geodesic) submanifold of the standard space, isometric with the Euclidean plane. On this submanifold, the law of cosines takes the form

$$l_{\rm S}^2 = l_{\rm L}^2 + l_{\rm L,S}^2 - 2l_{\rm L}^2 l_{\rm S}^2\cos(\pi - \hat{\alpha}) \tag{1.94}$$

For small angles, Eq. (1.94) reduces to

$$l_{\rm S}^2 \simeq (l_{\rm L} + l_{\rm L,S})^2 - l_{\rm L}l_{\rm S}\hat{\alpha}^2. \tag{1.95}$$

Eq. (1.95) yields

$$(l_{\rm L} + l_{\rm L,S} + l_{\rm S})(l_{\rm L} + l_{\rm L,S} - l_{\rm S}) = (l_{\rm L} + l_{\rm L,S})^2 - l_{\rm S}^2 \simeq l_{\rm L}l_{\rm S}\hat{\alpha}^2. \tag{1.96}$$

Using Eqs. (1.92, 1.96), we can express $\Delta_{p_0}(p)$ as

$$\Delta_{p_0}(p) \simeq \frac{l_{\rm L}l_{\rm L,S}}{l_{\rm L} + l_{\rm L,S} + l_{\rm S}}\hat{\alpha}^2 \simeq \frac{l_{\rm L}l_{\rm L,S}}{2l_{\rm S}}\hat{\alpha}^2. \tag{1.97}$$

The proper lengths can be expressed in terms of the angular diameter distances. For the sides of the geodesic triangle in Fig. (1.3), we get

$$D_{\rm d} \equiv D_{\rm A}(z_{\rm L}) = a_{\rm L}l_{\rm L},\ D_{\rm ds} \equiv D_{\rm A}(z_{\rm L}, z_{\rm S}) = a_{\rm S}l_{\rm L,S},\ D_s \equiv D_{\rm A}(z_{\rm S}) = a_{\rm S}l_S. \tag{1.98}$$

Finally,

$$\hat{\alpha}D_{\rm ds} \simeq \left|\frac{\boldsymbol{\xi}}{D_{\rm d}} - \frac{\boldsymbol{\eta}}{D_{\rm s}}\right|. \tag{1.99}$$

Given Eqs.(1.98,1.99), we can rewrite Eq. (1.97) as

$$\Delta_{p_0}(p) \simeq \frac{1}{a_{\rm L}}\frac{D_{\rm d}D_{\rm s}}{D_{\rm ds}}\left|\frac{\boldsymbol{\xi}}{D_{\rm d}} - \frac{\boldsymbol{\eta}}{D_{\rm s}}\right|^2. \tag{1.100}$$

Finally, the geometrical time delay turns out

$$\Delta T_{\rm geom} = \frac{1 + z_{\rm d}}{2c}\frac{D_{\rm d}D_{\rm s}}{D_{\rm ds}}\left|\frac{\boldsymbol{\xi}}{D_{\rm d}} - \frac{\boldsymbol{\eta}}{D_{\rm s}}\right|^2. \tag{1.101}$$

1.12.4 Time delay function

Adding the geometrical contribution and the potential term, we get the total time delay, measured at the observer, of a kinematically possible light ray with impact parameter $\boldsymbol{\xi}$ in the lens plane, relative to the unlensed one for a single lens plane. The time delay function is

$$\Delta T = \frac{1+z_{\rm d}}{c}\left[\frac{1}{2}\frac{D_{\rm d}D_s}{D_{\rm ds}}\left|\frac{\boldsymbol{\xi}}{D_{\rm d}}-\frac{\boldsymbol{\eta}}{D_{\rm s}}\right|^2-\psi(\boldsymbol{\xi})\right], \tag{1.102}$$

where ψ is the deflection potential up to the order v/c,

$$\psi(\boldsymbol{\xi}) \equiv \frac{2G}{c^2}\left[\int_{\Re^2} d^2\xi' \Sigma(\boldsymbol{\xi}')\left(1+\gamma-4\mu\frac{\langle \mathbf{v}\cdot\mathbf{e}_{\rm in}\rangle_l(\boldsymbol{\xi}')}{c}\right)\ln\frac{|\boldsymbol{\xi}-\boldsymbol{\xi}'|}{\xi_0}\right]+ \tag{1.103}$$

$$\frac{1}{c^5}\left[\frac{3}{2}-\beta+\gamma\left(1-\frac{\gamma}{2}\right)+\frac{3}{4}\epsilon\right]\int U^2 dl.$$

We have neglected the constant in Eq. (1.102), since it has no physical significance [172]. We remind that the time delay function is not an observable, but the time delay between two actual rays can be measured.

1.13 The deflection angle

In order to derive an equation which relates the true position of the source to its observed position on the sky, we must determine the deflection angle, i.e. the difference of the initial and final ray direction. Then, we have to apply the Fermat's principle. For each path p, the time measured on the observer's clock when p arrives locates a surface of arrival times. Actual light rays, given the source position, are characterized by critical points of $\Delta T(\boldsymbol{\xi})$, i.e. $\Delta T(\boldsymbol{\xi})$ is stationary with respect to variations of $\boldsymbol{\xi}$. The minima, maxima and (generalized) saddle points of the arrival time surface characterize those paths followed by the actual light rays. The lens equation is then obtained calculating

$$\nabla_{\boldsymbol{\xi}}\Delta T(\boldsymbol{\xi}) = 0; \tag{1.104}$$

we get

$$\boldsymbol{\eta} = \frac{D_{\rm s}}{D_{\rm d}}\boldsymbol{\xi} - D_{\rm ds}\boldsymbol{\alpha}(\boldsymbol{\xi}); \tag{1.105}$$

$\boldsymbol{\alpha} \equiv -\nabla_{\boldsymbol{\xi}}\psi(\boldsymbol{\xi})$ is the deflection angle.

We can express the total deflection angle as the sum of three terms,

$$\boldsymbol{\alpha} = \boldsymbol{\alpha}^{\rm pN} + \boldsymbol{\alpha}^{\rm ppN} + \boldsymbol{\alpha}^{\rm GRM}. \tag{1.106}$$

Once again, the post-Newtonian and the gravito-magnetic contribution to the deflection angle have a simple expression. It is

$$\boldsymbol{\alpha}^{\rm pN}(\boldsymbol{\xi}) \simeq 2(1+\gamma)\frac{G}{c^2}\int_{\Re^2} d^2\xi' \Sigma(\boldsymbol{\xi}')\frac{\boldsymbol{\xi}-\boldsymbol{\xi}'}{|\boldsymbol{\xi}-\boldsymbol{\xi}'|^2}. \tag{1.107}$$

The equivalence principle, special relativity and Newtonian gravitational theory imply that a photon must feel the gravity field of massive body. They yield only the "1" part of the coefficient in front of Eq. (1.107). This accounts for the deflection of light relative to local straight lines. However, because of space curvature, local straight lines are bent relative to asymptotic straight lines. The contribution proportional to γ in Eq. (1.107) is just the bending due to the g_{ii} components of the space metric in Eq. (1.69); γ measures at the post-Newtonian order the curvature generated by an isolated mass and varies from theory to theory.

The contribution of the gravito-magnetic field to the deflection angle is

$$\boldsymbol{\alpha}^{\rm GRM}(\boldsymbol{\xi}) \simeq -8\mu\frac{G}{c^3}\int_{\Re^2} d^2\xi' \Sigma(\boldsymbol{\xi}')\langle \mathbf{v}\cdot\mathbf{e}_{\rm in}\rangle_l(\boldsymbol{\xi}')\frac{\boldsymbol{\xi}-\boldsymbol{\xi}'}{|\boldsymbol{\xi}-\boldsymbol{\xi}'|^2}. \tag{1.108}$$

The parameter μ tests intrinsic gravito-magnetism in conceivable metric theories of gravity [41].

In the thin lens approximation, the only components of the velocities parallel to the line of sight enter the equations of gravitational lensing. A change in position of the deflector orthogonal to the line of sight can be noticeable in a variation of the luminosity of the source but does not affect the individual light rays, i.e. does not contribute to the gravito-magnetic correction.

For shifting lenses, $\langle \mathbf{v}\cdot\mathbf{e}_{\rm in}\rangle_l(\boldsymbol{\xi}) = v_l$, the gravito-magnetic correction reduces to a multiplicative factor to the zero order expressions. The deflection angle and the related quantities, such as the optical depth, up to order v/c, are derived from the zero-order expressions just by a product by $1-2v_l/c$. For deflector moving towards the observer and far away from the source ($v_l > 0$), the optical depth decreases; for receding lenses ($v_l < 0$), the deflection angle increases. In what follows, we will only consider rotating deflector. Since the velocity $\mathbf{v}$ is the peculiar velocity with respect to the coordinate system, in a cosmological context, the cosmological recession velocity of the deflector does not contribute to the gravito-magnetic correction.

The ppN contribution to the deflection angle has not a simple form in terms of $\Sigma(\boldsymbol{\xi})$. It is

$$\boldsymbol{\alpha}^{\rm ppN}(\boldsymbol{\xi}) \simeq \frac{1}{c^4}\left[\frac{3}{2}-\beta+\gamma\left(1-\frac{\gamma}{2}\right)+\frac{3}{4}\epsilon\right]\nabla_{\boldsymbol{\xi}}\int_p U^2(\boldsymbol{\xi}, l_{\rm eucl})dl_{\rm eucl} \tag{1.109}$$

For β, γ and ϵ of order of the unity, nearly 70% of the bending comes from the standard post-Newtonian parameters β and γ, the remaining 30% arises from the non-standard ϵ coefficient.

For a given deflecting mass, Eq. (1.105) relates source and image positions. A source, with true position $\boldsymbol{\eta}$, can be seen by an observer at positions $\boldsymbol{\xi}$ satisfying the lens equation. Given the matter distribution of the lens, Eq. (1.105) may have more than one solution $\boldsymbol{\xi}$, so that the same source can be seen at several positions in the sky. In general, it is very difficult to determine the images analytically. In order to find all the images of a source for a given matter distribution or to find, for given image positions, a suitable matter distribution, the lens equation is often attacked numerically.

Fermat's principle still holds for reversed light rays, that is for light rays backwards from the observer to the impact point $\boldsymbol{\xi}$. The ray-trace equation (1.105) allows us to determine directly the source position $\boldsymbol{\eta}$ of an image at $\boldsymbol{\xi}$. The lens equation induces a mapping, called lensing map, from a subset of the lens plane into the light source plane,

$$\boldsymbol{\eta}(\boldsymbol{\xi}) = \frac{D_{\mathrm{s}}}{D_{\mathrm{d}}}\boldsymbol{\xi} - D_{\mathrm{ds}}\boldsymbol{\alpha}(\boldsymbol{\xi}); \tag{1.110}$$

the Jacobian matrix of the lensing map is symmetric.

Chapter 2

Properties of the lens mapping

We discuss some general properties of the gravitational lens equation. As seen in Chapter 1, the lens equation induces a lens mapping from the lens plane into the source plane. Including higher order effects does not change the form of the lens equation: only the physical quantities, such as the deflection angle and the time delay, are corrected. In the framework of viable theories of gravity, we want, now, to extend the formalism of the lens mapping by including the gravito-magnetic effect. The gravito-magnetic correction to the lensing quantities turns out to be linear in the surface mass density. So, regarding the lensing effects, a rotating deflector can be identified with a non-rotating one with an appropriately modified surface mass density. Given this analogy, it is easy to generalize standard results, which refer to static deflectors, to rotating deflectors. Furthermore, we can perform such a generalization in the framework of any viable theory of gravity. The ppN contribution, non linear in the mass of the deflector, will not be considered.

The lens mapping can be converted into a dimensionless form by converting the physical variables into a dimensionless form, using appropriate scales. To this aim, a characteristic surface mass density, which nearly distinguishes strong lenses capable of producing multiple images, is introduced. With respect to the usual definition, this characteristic surface mass density contains explicitly the pN parameter γ. Some other quantities, such as the convergence and the deflection potential, will be corrected for the intrinsic motion of the lens mass distribution. The non standard parameter μ will be also included.

Section 1 introduces the dimensionless form of the ray-trace equation and the related dimensionless quantities. All the new definitions which we introduce in this Section are corrected for the dragging of the inertial frames. Viable theories of gravity are included by considering the parameters γ and μ. By introducing the dimensionless Fermat potential, the lens equation can be written as a gradient equation. The magnification of the light source and its geometrical nature are the argument of Section 2,

where the Jacobian matrix of the lens mapping and related quantities, such as shear and convergence, are introduced. Images can be classified according to the properties of the Jacobian matrix. Section 3 treats ordinary images; the orientation and the shape of the image of an extended are discussed. Important counting information on the number of images produced by a transparent, isolated deflector are stated in Section 4, where the condition, for at least one image appears brighter than it would be without the lensing effect, is also considered. In Section 5, some conditions for a lens to be able to produce multiple images are presented. Section 6 treats the critical curves, locus of all formally infinitely magnified images, and the corresponding positions in the source plane, the caustics.

2.1 Basic equations

The lens equation,

$$\boldsymbol{\eta} = \frac{D_{\rm s}}{D_{\rm d}}\boldsymbol{\xi} - D_{\rm ds}\hat{\boldsymbol{\alpha}}(\boldsymbol{\xi}), \tag{2.1}$$

relates the position of a source and the impact vector, in the lens plane, of those rays which connect source and observer. The deflection angle, including the gravitomagnetic effect and neglecting the ppN contribution, reads

$$\hat{\boldsymbol{\alpha}}(\boldsymbol{\xi}) = \frac{2(1+\gamma)G}{c^2}\int_{R^2} d^2\boldsymbol{\xi}'\Sigma(\boldsymbol{\xi}')\left(1 - \frac{4\mu}{(1+\gamma)}\frac{\langle \mathbf{v}\cdot\mathbf{e}_{\rm in}\rangle_l(\boldsymbol{\xi}')}{c}\right)\frac{\boldsymbol{\xi}-\boldsymbol{\xi}'}{|\boldsymbol{\xi}-\boldsymbol{\xi}'|^2}, \tag{2.2}$$

The expression for the deflection angle in Eq. (2.2) is linear in the mass of the deflector. In general, a slowly moving deflector, with surface mass density $\Sigma^{\rm SLMO}$, has the same lensing effect of a really static lens with

$$\Sigma^{\rm STAT}(\boldsymbol{\xi}) = \Sigma^{\rm SLMO}(\boldsymbol{\xi})\left(1 - \frac{4\mu}{(1+\gamma)}\frac{\langle \mathbf{v}\cdot\mathbf{e}_{\rm in}\rangle_l(\boldsymbol{\xi})}{c}\right). \tag{2.3}$$

The lens equation induces a mapping $\boldsymbol{\xi} \to \boldsymbol{\eta}$, called lensing map, from the lens plane to the source plane. It is useful to write Eq. (2.1) in dimensionless form. Let ξ_0 be a length scale in the lens plane and let η_0 be the corresponding length in the source plane, $\eta_0 \equiv \xi_0 D_{\rm s}/D_{\rm d}$. We set the dimensionless vectors,

$$\mathbf{x} = \frac{\boldsymbol{\xi}}{\xi_0}; \quad \mathbf{y} = \frac{\boldsymbol{\eta}}{\eta_0}; \tag{2.4}$$

the length scale is, at this point, arbitrary. For $\xi_0 = D_{\rm d}$, $\mathbf{x}$ e $\mathbf{y}$ are the angular positions of the image and the unlensed source relative to the optical axis.

Let us introduce the corrected critical surface mass density, $\Sigma_{\rm cr}$,

$$\Sigma_{\rm cr} \equiv \frac{c^2 D_{\rm s}}{2(1+\gamma)\pi G D_{\rm d} D_{\rm ds}}, \tag{2.5}$$

usually defined in the case $\gamma = 1$ [142, 172]. We can define the corrected dimensionless surface mass density or *corrected convergence*,

$$k(\mathbf{x}) = \frac{\Sigma(\xi_0\mathbf{x})}{\Sigma_{\rm cr}}\left(1 - \frac{4\mu}{(1+\gamma)}\frac{\langle \mathbf{v}\cdot\mathbf{e}_{\rm in}\rangle_l(\xi_0\mathbf{x})}{c}\right); \tag{2.6}$$

when the deflector is static ($\mathbf{v} = 0$), the corrected convergence reduces to the ratio of the surface mass density to the critical density,

$$k^{\rm pN} \equiv \frac{\Sigma}{\Sigma_{\rm cr}}; \tag{2.7}$$

in general, if we consider the gravito-magnetic field, the velocity of the lens contributes to the total convergence. With these definitions, the lens equation (2.1) reads

$$\mathbf{y} = \mathbf{x} - \boldsymbol{\alpha}(\mathbf{x}), \tag{2.8}$$

where

$$\boldsymbol{\alpha}(\mathbf{x}) = \frac{1}{\pi}\int_{R^2} d^2x' k(\mathbf{x}')\frac{\mathbf{x}-\mathbf{x}'}{|\mathbf{x}-\mathbf{x}'|^2} = \frac{D_{\rm d}D_{\rm ds}}{\xi_0 D_{\rm s}}\hat{\boldsymbol{\alpha}}(\xi_0\mathbf{x}) \tag{2.9}$$

will be referred as the *scaled deflection angle*.

Let us now introduce a dimensionless deflection potential ψ,

$$\hat{\psi} \equiv \frac{D_{\rm s}\xi_0^2}{D_{\rm d}D_{\rm ds}}\psi, \tag{2.10}$$

and a dimensionless Fermat potential ϕ,

$$\hat{\phi} \equiv (1+z_{\rm d})\frac{D_{\rm s}\xi_0^2}{D_{\rm d}D_{\rm ds}}\phi. \tag{2.11}$$

We have

$$\psi(\mathbf{x}) = \frac{1}{\pi}\int_{R^2} d^2x' k(\mathbf{x}')\ln|\mathbf{x}-\mathbf{x}'|, \tag{2.12}$$

and

$$\phi(\mathbf{x},\mathbf{y}) = \frac{1}{2}(\mathbf{x}-\mathbf{y})^2 - \psi(\mathbf{x}) \tag{2.13}$$

From Eq. (2.12), since $\mathcal{G} = \frac{1}{2\pi}\ln(\mathbf{x})$ is the Green's function of the 2-dimensional Laplacian, $\Delta\mathcal{G} = \delta^{(2)}$, it follows that ψ can be expressed as [192]

$$\psi(\mathbf{x}) = 2\mathcal{G} * k, \tag{2.14}$$

where $*$ is the convolution operator. Given the identity $\nabla\ln|\mathbf{x}| = \frac{\mathbf{x}}{|\mathbf{x}^2|}$, it is easy to show that

$$\boldsymbol{\alpha} = \nabla\psi. \tag{2.15}$$

Equation (2.14) can be inverted. We get

$$\Delta\psi = 2k; \tag{2.16}$$

ψ satisfies the 2-dimensional Poisson's equation.

The map $\mathbf{x} \mapsto \mathbf{y}$ can be written as a gradient map,

$$\mathbf{y} = \nabla \left(\frac{1}{2}\mathbf{x}^2 - \psi(\mathbf{x}) \right), \tag{2.17}$$

or, using the Fermat's principle, as

$$\nabla_{\mathbf{x}} \phi(\mathbf{x}, \mathbf{y}) = 0. \tag{2.18}$$

2.2 Magnification

Gravitational light deflection affects the properties of the images of a source. Because of deflection angle of a light ray depends on the ray's impact parameter, the cross sectional area of a light bundle is deformed and distorted by the deflection. In particular, the solid angle subtended by the image, $d\omega$, will differ from the solid angle subtended by the source in the absence of lensing, $d\omega^*$. Since photon number conservation, the flux of the image is determined by this area variation. The flux of an infinitesimal source with surface brightness I_ν, in the absence of gravitational light deflection, is $S^*_\nu = I_\nu d\omega^*$. Since the surface brightness of an image of a lensed source coincides with the surface brightness of the unlensed source, the observed flux is given by $S_\nu = I_\nu d\omega$. Hence, the light deflection induces a change of the flux of the observed image by a factor,

$$|\mu| = \frac{S_\nu}{S^*_\nu} = \frac{d\omega}{d\omega^*}, \tag{2.19}$$

which is independent of the frequency of the radiation. The factor $|\mu(\mathbf{x})|$ quantifies how much gravitational lensing brightens or dims the image $\mathbf{x}$ of an infinitesimally small source.

If a source is much smaller than the angular scale on which the lens properties change, the lens mapping can be locally linearized. Then, the Jacobian matrix of the lens mapping describes how gravitational lensing distorts images. The Jacobian matrix of the map in Eq. (2.8) is [172],

$$A(\mathbf{x}) = \frac{\partial \mathbf{y}}{\partial \mathbf{x}}, \qquad A_{ij} = \frac{\partial y_i}{\partial x_j}. \tag{2.20}$$

Since the ratio of solid angles is given by

$$\frac{d\omega}{d\omega^*} = \left| \frac{d^2x}{d^2y} \right|, \tag{2.21}$$

then, the *magnification factor* reads

$$\mu(\mathbf{x}) = \frac{1}{\det A(\mathbf{x})}. \tag{2.22}$$

The absolute value of the Jacobian determinant is the ratio of an infinitesimal area in the light source plane to its corresponding area in the lens plane. Then, the magnification of a lensed image, $|\mu(\mathbf{x})|$, is the absolute value of the inverse of the Jacobian determinant at the lensed image position.

The total magnification of a point-like light source at $\mathbf{y}$ is

$$\mu_{\rm TOT}(\mathbf{y}) = \sum_{\mathbf{x}} |\mu(\mathbf{x})|, \tag{2.23}$$

where the sums runs over all lensed images $\mathbf{x}$ of $\mathbf{y}$. The magnification of an extended light source with surface brightness profile $I(\mathbf{y})$ is given by

$$\mu_e = \frac{\int I(\mathbf{y})\mu_{\rm TOT}(\mathbf{y})d^2y}{\int I(\mathbf{y})d^2y} \ ,$$

where the integrals are over the source.

Equations (2.13, 2.17, 2.20) imply

$$A_{ij} = \phi_{ij} = \delta_{ij} - \psi_{ij}, \tag{2.24}$$

where subscripts denotes partial derivatives with respect to x_i. ψ_{ij} is the Hessian of ψ and describes the deviation of the Jacobian matrix from the identity due to the gravitational lensing. The matrix A is symmetric. Using Eq. (2.16), the Jacobian matrix can be written as

$$A = \begin{pmatrix} 1-k-\gamma_1 & -\gamma_2 \\ -\gamma_2 & 1-k+\gamma_1 \end{pmatrix}, \tag{2.25}$$

where we have introduced the components of the *shear*

$$\begin{aligned} \gamma_1 &\equiv \frac{1}{2}(\psi_{11} - \psi_{22}), \\ \gamma_2 &\equiv \psi_{12} = \psi_{21}; \end{aligned} \tag{2.26}$$

the magnitude of the shear is defined as

$$\gamma \equiv \sqrt{\gamma_1^2 + \gamma_2^2}. \tag{2.27}$$

The convergence k describes a local effect arising only from the surface mass density within the beam. On the other hand, the additional light deflection caused by matter far away from the light bundle is described by the shear. For asymmetric mass distribution, there is an additional distortion on the light rays along one particular direction.

From Eq. (2.25), we can evaluate the orthogonal invariants of A, i.e. the determinant,

$$\det A = (1-k)^2 - \gamma^2, \tag{2.28}$$

the trace

$$\mathrm{tr}A = 2(1-k) \tag{2.29}$$

and the eigenvalues,

$$a_{1,2} = 1 - k \mp \gamma. \tag{2.30}$$

Both the determinant and the eigenvalues consist of two terms, the first arising from the convergence and the second from the shear.

The magnification factor,

$$\mu(\mathbf{x}) = \frac{1}{(1-k)^2 - \gamma^2}, \tag{2.31}$$

is determined by both isotropic focusing caused by the local matter density k and anisotropic focusing caused by shear. Introducing an *angle of shear*, θ_γ, the shear components can be parameterized as

$$\gamma_1(\mathbf{x}) = \gamma(\mathbf{x}) \cos 2\theta_\gamma(\mathbf{x}), \tag{2.32}$$

$$\gamma_2(\mathbf{x}) = \gamma(\mathbf{x}) \sin 2\theta_\gamma(\mathbf{x}). \tag{2.33}$$

The shear at $\mathbf{x}$ produced along $\theta_\gamma(\mathbf{x})$ is identical to that produced along $\theta_\gamma(\mathbf{x}) + \pi$. Consequently, it suffices to assume $0 \leq \theta_\gamma(\mathbf{x}) < \pi$. Shear does not transform as a vector under rotations of the coordinate frame [138]. The matrix A can be rewritten as

$$A = (1-\kappa) \begin{pmatrix} 1 & 0 \\ 0 & 1 \end{pmatrix} - \gamma \begin{pmatrix} \cos 2\theta_\gamma & \sin 2\theta_\gamma \\ \sin 2\theta_\gamma & -\cos 2\theta_\gamma \end{pmatrix}. \tag{2.34}$$

2.3 Ordinary images

For a given source position $\mathbf{y}$, the images are critical points of the Fermat potential. A critical point of ϕ is non-degenerate, if the Hessian, ϕ_{ij}, is a non-degenerate quadratic form, $\det \phi_{ij} = \det A \neq 0$. These conditions characterize *ordinary images* [142, 172]. For certain values of $\mathbf{x}$, $\det A = 0$: these points are called *critical points* and they forms the *critical curves* in the lens plane. The critical curves are mapped onto *caustics* in the lens plane.

Let us first consider ordinary images.

2.3.1 Classification

Images are located at local extrema and saddle points of the arrival time surface. The index of such a critical point is just the number of negative eingenvalues of the Hessian at that point. In two dimensions, there are three types of non-degenerate critical

points. According to the Morse's lemma [142], the ordinary image is either a local minimum (if the index i is equal to zero), saddle ($i = 1$), or local maximum ($i = 2$). Hence, all nondegenerate light rays are isolated. The type is readily determined by the quadratic form of ϕ at $\mathbf{x}_0$,

$$q(t_1, t_2) = \phi_{11} t_1^2 + 2\phi_{12} t_1 t_2 + \phi_{22} t_2^2, \tag{2.35}$$

where $(t_1, t_2) \in \Re^2$. Then [142],

- Type I: $\mathbf{x}_0$ is a local minimum if and only if $q(t_1, t_2) > 0$ for all $(t_1, t_2) \in \Re^2 - \{0\}$. It is $\det A > 0$ and $\phi_{11} > 0$.

  Since $\gamma < 1 - k \leq 1$, it is $\mu \geq \frac{1}{1-\gamma^2} \geq 1$: the minimum is magnified.

- Type II: saddle point of ϕ. $q(t_1, t_2)$ attains both positive and negative values. A critical poin is a saddle if and only if $\det A < 0$.

- Type III: $\mathbf{x}_0$ is a local maximum if and only if $q(t_1, t_2) < 0$ for all $(t_1, t_2) \in \Re^2 - \{0\}$ if, and only if, it is $\det A > 0$ and $\phi_{11} < 0$. We get

$$(1 - k)^2 > \gamma^2, \; k > 1. \tag{2.36}$$

In what follows, we will use the notation below:

- N = total number of lensed images;
- n_{I} = total number of minimum lensed images;
- n_{II} = total number of saddle lensed images;
- n_{III} = total number of maximum lensed images;

2.3.2 Orientation

The magnification factor μ can be positive or negative; the corresponding images are said to have positive or negative parity. Images of type I and III have positive parity; images of type II have negative parity and are reversed with respect to the source. Given an image at $\mathbf{x}_0$, not on a critical curve, and a displacement vector $\mathbf{x} - \mathbf{x}_0 \equiv \mathbf{X}$ in the lens plane, the corresponding displacement vector in the source plane is

$$\mathbf{Y} \equiv \mathbf{y} - \mathbf{y}(\mathbf{x}_0) \simeq \frac{\partial \mathbf{y}}{\partial \mathbf{x}} (\mathbf{x} - \mathbf{x}_0); \tag{2.37}$$

in other words, $\mathbf{Y}$ is mapped on $\mathbf{X}$,

$$\mathbf{Y} = A\mathbf{X}. \tag{2.38}$$

Since

$$\mathbf{Y}\cdot\mathbf{X} = A\mathbf{X}\cdot\mathbf{X} = \sum_{i,j} A_{ij}X^iX^j, \tag{2.39}$$

the position angle of the image vector differs by no more than $\pi/2$ from that of the source for images of type I, whereas for image of type III, the source and image vectors differ by more than $\pi/2$.

Given two displacement vectors at $\mathbf{y}$, $\mathbf{Y}$ and $\mathbf{Z}$, and the corresponding image vectors $\mathbf{X}$ and $\mathbf{W}$, it is

$$\mathbf{X}\times\mathbf{W} = \frac{1}{\det A}\mathbf{Y}\times\mathbf{Z}. \tag{2.40}$$

Since $|\mathbf{X}\times\mathbf{W}|$ is the area spanned by $\mathbf{Y}$ and $\mathbf{Z}$, Eq. (2.40) restates that the magnification is the area distortion of the lens mapping. The *handness* of two vectors is defined as the sign of

$$\mathbf{Y}\times\mathbf{Z} \equiv Y_1Z_2 - Y_2Z_1. \tag{2.41}$$

Images of type I and III ($\det A > 0$) have positive parity, so that the handness is preserved, whereas for images of type II (negative parity), the handness is reversed.

2.3.3 Shape

The images are distorted in both shape and size. The shapes of the images differ from the shape of the source because light bundles are deflected differentially. Let us consider an infinitesimal circular source bounded by

$$\mathbf{c}(t) = \mathbf{y} + R(\cos t, \sin t). \tag{2.42}$$

At the first order, the corresponding boundary curve of the image is

$$\mathbf{d}(t) \simeq \mathbf{x} + A^{-1}R(\cos t, \sin t); \tag{2.43}$$

the image is an ellipse with semi-axes given by

$$\frac{R}{\mid 1 - \kappa \mp \gamma \mid} = \frac{R}{\mid a_{1,2} \mid}, \tag{2.44}$$

and oriented along and orthogonally to θ_γ [128, 172]. The shear γ describes the tidal gravitational field, which determines the shape distortion, and the anisotropic focusing, which contributes to the magnification. When $\gamma = 0$, the image is still disc-shaped. The convergence k describes the magnification caused by isotropic focusing caused by the local matter density. The area of the image differs by a factor $|\mu| = 1/|\det A|$ from the area of the source. The ellipse reduces to a circle also if $\mathrm{tr}A = 0$, that is $k = 1$. If both $k \simeq 1$ and $|\gamma| \ll 1$, strongly magnified images, morphologically similar to the source, can be produced. When the lens is a cluster of galaxies and the source is a background galaxy, this condition realizes the so called *GRAMORs*[1] [81].

[1] GRAvitazional deflected but MORphologically regular images.

2.4 Some theorems on ordinary images

A gravitational lens is isolated if its lensing effects are negligible at the infinity, as in the case of lenses with a finite total mass. A Fermat potential $\phi(\mathbf{x}, \mathbf{y})$ is isolated if, for all $\mathbf{y}$ not on a caustic, it is subcritical at the infinity: for $|\mathbf{x}| \to \infty$, both the eingenvalues of the Hessian matrix remain positive (moreover, both the shear and the convergence are also subcritical at the infinity) and $\phi(\mathbf{x}, \mathbf{y}) \to \infty$ [142]. These conditions are fulfilled by a lens with both a surface mass density decreasing faster than $|\mathbf{x}|^{-2}$ and a bounded deflection angle [172].

Important counting information has been derived for isolated gravitational lenses [142, 172]. A point $\mathbf{a}$ is a singularity of the deflection potential ψ if, for $\mathbf{x} \to \mathbf{a}$, either $\psi(\mathbf{x}) \to -\infty$ or $\Delta\psi(\mathbf{x}) \to \infty$.

Then, an isolated gravitational lens with a total number of g singularities will produce a finite total number of lensed images of a source at a noncaustic point $\mathbf{y}$ and

1. $n_{\rm I} \geq 1,\ n_{\rm II} \geq n_{\rm III} + g,\ n_{\rm II} \geq n_{\rm I} + g - 1,\ n_{\rm I} + n_{\rm III} = n_{\rm II} - g + 1.$
2. $N = 2(n_{\rm I} + n_{\rm III}) + g - 1 = 2n_{\rm II} - g + 1,\ N \geq g + 1.$
3. For a locally stable lensing map:
   (a) for $|\mathbf{y}|$ sufficiently large, it is $N = g + 1$, with $n_{\rm I} = g + 1$, $n_{\rm II} = g$, $n_{\rm III} = 0$;
   (b) if $|\mathbf{y}| \to \infty$, then all saddle images lie inside a compact set whereas the remaining minimum lensed image $\mathbf{x}_{\rm I}$ satisfies $\mathbf{x}_{\rm I} \to \infty$.

From the above properties on the number of images it immediately follows the *odd number image theorem* for nonsingular lenses: the total number of images, $N = 2(n_{\rm I} + n_{\rm III}) - 1 = 2n_{\rm II} + 1$, is odd.

Under the same assumptions, the *magnification theorem* holds. If an isolated gravitational lens has a positive density perturbation, then its action on any light source will produce a lensed image with magnification of at lest one. In fact, according to the statement of the above theorem, there is, at least, one minimum; therefore $\mu \geq 1$. We stress that this theorem depends on the inequality $\Delta\psi \geq 0$.

2.5 Criteria for multiple imaging

A gravitational lens at distance $D_{\rm d}$ may or may not be sufficiently strong to cause multiple images of a source at distance $D_{\rm s}$ [142, 172].

- If an isolated deflector has at least one singularity, then, by the theorem on the number of images, there are multiple lensed images

- An isolated transparent lens can produce multiple images if, and only if, there is a point $\mathbf{x}$ with $\det A(\mathbf{x}) < 0$. In this case, the number of lensed images is ≥ 3

Proof. If $\det A(\mathbf{x}) > 0$ for all $\mathbf{x}$, the lens mapping is globally invertible and thus cannot cause multiple images. On the other hand, if $\det A(\mathbf{x}_0) < 0$ at $\mathbf{x}_0$, a source at $\mathbf{y}_0 = \mathbf{y}(\mathbf{x}_0)$ has a saddle lensed image. Then, there must be at least two additional images of positive parity.

- Suppose that k is supercritical at a regular point $\mathbf{x}_0$, $k(\mathbf{x}_0) > 1$. Then a source at $\mathbf{y}_0 = \mathbf{y}(\mathbf{x}_0)$ has multiple images.

Proof. Since ψ is isolated, it is $n_{\rm I} \geq 1$. Since $k(\mathbf{x}_0) > 1$, $\mathbf{x}_0$ is either a local maximum, so that $n_{\rm II} \geq n_{\rm III} \geq 1 \Rightarrow N \geq 3$, or a saddle lensed image, so that $N \geq 3$ (since N is odd and $n_{\rm I} \geq 1$).

For a general lens, there is no lower limit to the surface mass density required to produce multiple images; such conditions arise only for symmetric lenses. Nevertheless, a strong lens with $\Sigma > \Sigma_{\rm cr}$ is able to produce multiple images. This condition shows that the surface density scale $\Sigma_{\rm cr}$ does very nearly distinguish those lenses that will produce non-trivial imaging. Gravitational lensing turns out to be very interesting in cosmology since $\Sigma_{\rm cr}$ is of the order of that found in clusters of galaxies and in the central parts of galaxies,

$$\Sigma_{\rm cr} \simeq 3.5 \frac{(D_{\rm ds}/1{\rm Gpc})}{(D_{\rm d}/1{\rm Gpc})(D_{\rm s}/1{\rm Gpc})} {\rm kg\ m^{-2}}. \tag{2.45}$$

2.6 Critical curves and caustics

Points in the lens plane where the Jacobian is singular, $\det A = 0$, form closed curves, the critical curves [142, 172]. They are the locus of all images with formally infinite magnification.

The corresponding locations in the source plane are the caustics [142, 172]; hence, the caustics due to a gravitational lens are the critical values of the associated lensing map. When caustics are curves, the smooth arcs are called folds, while cusps are the points where two abutting fold arcs have coincident tangents with the folds arcs on opposite sides of the double tangent [142, 172].

Sources on caustics are infinitely magnified. However, infinite magnification does not occur in real astrophysical situations. First, each source has a proper finite size, and

its magnification (given by the surface brightness-weighted point-source magnification across its solid angle) remains finite. Second, for point-sources, near critical curves, geometrical optics approximations fails and a wave optics descriptions should be used; then, even point-sources are magnified by a finite value.

Images of sources near caustics are magnified and distorted substantially.

The number of images can change only if the source crosses a caustic. In fact, at other points, the lens mapping is locally invertible and therefore, no images can appear or disappear. Point sources which moves across a caustic have their number of images changed by ± 2, and the two additional images appear or disappear at the corresponding critical curve in the lens plane. Hence, sources inside a caustic are multiply imaged.

Chapter 3

Lens models

The purpose of this Chapter is to determine the gravitational lensing signatures of some commonly used gravitational lens models. Given a lens model, gravitational lensing theory aims at determining the configurations of images of the background source, i.e. their number, locations and magnification, and at characterizing the properties of critical points and caustics. In general, this problem can be solved only numerically, but some gravitational lensing systems allow an analytical approach.

The ray-trace equation for a spherically symmetric non-rotating lens can be reduced to a one-dimensional equation. However the gravito-magnetic field, induced by rotation, breaks this symmetry. Even for very simple mass distributions, we have to consider the full vectorial equation. In general, the inversion of the lens equation becomes a mathematical demanding problem. But the gravito-magnetic effect is an higher-order correction and interesting gravitational lens systems can be studied in some details despite of their complexity using a perturbative approach. This procedure is quite usual in gravitational lensing problems [22, 104].

In this Chapter, we consider gravitational lenses of astrophysical interest. Except for the last section, we will only consider the gravito-magnetic correction to the lensing quantities and neglect the ppN contribution. For simplicity, we will also specialize the parameters of the approximate metric element describing the gravitational action of the lens, introduced in Section 1.9, to general relativity; so, we will assume $\gamma = \mu = 1$ and $\beta = \epsilon = 0$. On the other hand, in the last section we will consider the point-like deflector in a general viable theory of gravity up to the ppN order included. In Section 1, we consider matter distributions with axial symmetry. Following [181], we derive the deflection angle for a spherical body in rigid rotation about a symmetry-axis. Static axially symmetric lenses are treated in Section 2: now, the lens equation is one-dimensional. According to the shape of images close to the critical curves, these are divided in tangential curves or radial critical curves. Some conditions for the existence of multiple images are also listed. We next consider some specific lens models.

In Sections 3 and 4, we discuss thin lenses. The uniform sheet is the argument of Section 3; here no gravito-magnetic field acts. This model will be employed in Chapter 5 to derive the distance–redshift relation ia a locally inhomogeneous universe. The thin exponential disk will be studied in Section 4. We propose original formulae for the deflection angle, corrected for the gravito-magnetic field, for a disk with an arbitrary inclination with respect to the optical axis.

In the following sections, we consider spherically symmetric mass distributions in rigid rotation. The gravitational phenomena connected to intrinsic gravito-magnetism are generated by mass-energy currents relative to other masses. The simplest lens model, the point-like Schwarzschild lens, cannot produce such a peculiar effect since the local Lorentz invariance on a static background does not account for the dragging of inertial frames [41]. General relativity is a classical-nonquantized theory where the classical angular momentum of a particle goes to zero as its size goes to zero. To treat the gravito-magnetic field, we need a further step after the point mass as a lens model; extended lens models have to be considered. To our knowledge, for the first time, the effect of the gravito-magnetic field is considered on the images positions, critical curves and caustics of extended sources. In Section 5, we will discuss the singular isothermal sphere. The deflection potential, the Jacobian determinant and the deflection angle will be corrected for the gravito-magnetic effect. As a second step, we first consider the non rotating case and, then, with a perturbative approach, we derive critical curves, caustics and image positions for a rotating system. In Sections 6 and 7, we treat, respectively, isothermal spheres with a finite core size and power law models. The deflection angle will be corrected for the dragging of inertial frames and critical curves and other features will be discussed for the non rotating case. In Section 8, we consider the homogeneous sphere. We consider light rays from the source to the observer passing inside or outside the sphere. For images outside the lens, we proceed as for the singular isothermal sphere.

We conclude the Chapter by considering the point-like deflector in Section 9. Given the simplicity of this lens model, a full treatment in the framework of metric theories of gravity is possible. The ppN contributions to the deflection potential and to the deflection angle take a very simple form. The point-like deflector is used to consider several astrophysical systems.

3.1 Axially symmetric lenses

Let us consider a class of matter distributions with a spherically-symmetric mass density, $\rho(\mathbf{r}) = \rho(|\mathbf{r}|) \Rightarrow \Sigma(\boldsymbol{\xi}) = \Sigma(|\boldsymbol{\xi}|)$, that rotates anticlokwisely about an arbitrary axis, $\hat{\eta}$, passing through its centre (i.e. a main axis of inertia). To specify the orientation of the rotation axis, we need two Euler's angles: φ is the angle between $\hat{\eta}$ and

the ξ_2-axis; ϑ is the angle between the line of sight, $\hat{l}$, and the line of nodes, located at the intersection of the $l\,\hat{\xi}_1$ plane and the equatorial plane (i.e., the plane orthogonal to the rotation axis and containing the lens centre). Using the axial symmetry about the rotation axis, we find

$$\mathbf{v}\cdot\mathbf{e}_{\rm in}(\xi_1,\xi_2,l) = -\omega(R)\left[\xi_1\cos\varphi + \xi_2\sin\varphi\cos\vartheta\right] \equiv -\omega_2(R)\xi_1 + \omega_1(R)\xi_2, \tag{3.1}$$

where $\omega(R)$ is the modulus of the angular velocity at a distance $R \equiv (R_1^2 + R_2^2)^{1/2}$ from the rotation axis; $\hat{R}_1$ (that, given the spherical symmetry of the system, can be taken along the line of nodes) and $\hat{R}_2$ are the axes on the equatorial plane; ω_1 and ω_2 are the components of the angular velocity along, respectively, the ξ_1- and the ξ_2-axis. We have

$$R_1 = l\cos\vartheta + \xi_1\sin\vartheta, \tag{3.2}$$

and

$$R_2 = -l\cos\varphi\sin\vartheta + \xi_1\cos\varphi\cos\vartheta + \xi_2\sin\varphi. \tag{3.3}$$

Let us assume a rigid rotation, $\omega(R) = \omega =$ const. It is

$$\langle\mathbf{v}\cdot\mathbf{e}_{\rm in}\rangle_l = -\omega_2\xi_1 + \omega_1\xi_2. \tag{3.4}$$

We can, now, evaluate the integral in Eq. (2.2) for $\gamma = \mu = 1$; it is,

$$\alpha_1(\xi,\theta) = \frac{4G}{c^2}\left\{\frac{M(\xi)}{\xi}\cos\theta + \frac{I_{\rm N}(\xi)}{\xi^2}\left(\frac{\omega_2}{c}\cos 2\theta - \frac{\omega_1}{c}\sin 2\theta\right) - M(>\xi)\frac{\omega_2}{c}\right\}; \tag{3.5}$$

$$\alpha_2(\xi,\theta) = \frac{4G}{c^2}\left\{\frac{M(\xi)}{\xi}\sin\theta + \frac{I_{\rm N}(\xi)}{\xi^2}\left(\frac{\omega_1}{c}\cos 2\theta + \frac{\omega_2}{c}\sin 2\theta\right) + M(>\xi)\frac{\omega_1}{c}\right\}. \tag{3.6}$$

ξ and θ are polar coordinates in the lens plane; $M(\xi)$ is the mass of the lens within ξ,

$$M(\xi) \equiv 2\pi\int_0^\xi \Sigma(\xi')\xi' d\xi'; \tag{3.7}$$

$M(>\xi)$ is the lens mass outside ξ, $M(>\xi) \equiv M(\infty) - M(\xi)$; and

$$I_{\rm N}(\xi) \equiv 2\pi\int_0^\xi \Sigma(\xi')\xi'^3 d\xi' \tag{3.8}$$

is the momentum of inertia of the mass within ξ about a central axis. $I_{\rm N}\times\omega_i$ is the component of the angular momentum along the ξ_i-axis.

The gravito-magnetic correction consists of the last two terms in Eqs.(3.5, 3.6), both proportional to some components of the angular velocity. Spherical symmetry is broken. In the first contribution, the angular momentum appears; the second one is proportional to the mass outside ξ and can be significant for lenses with slowly decreasing mass density.

Let us change to dimensionless variables $\mathbf{x}$ and $\mathbf{y}$. We define the dimensionless mass $m(x)$ within a circle of radius x,

$$m(x) = 2\int_0^{|x|} k^{\mathrm{pN}}(x^{'})x^{'}dx^{'}, \tag{3.9}$$

where k^{pN}, defined in Eq. (2.7), is the dimensionless surface density up to the order c^{-2}; it accounts only for the surface mass density. $m(x)$ and $M(\xi)$ are related by

$$m(x) = \frac{M(\xi)}{\xi_0^2\pi\Sigma_{\mathrm{cr}}}. \tag{3.10}$$

Furthermore, we introduce the dimensionless momentum of inertia within x,

$$i_{\mathrm{N}}(x) = 2\int_0^{x} k^{\mathrm{pN}}(x^{'})x^{'3}dx^{'}. \tag{3.11}$$

With these notations, the scaled deflection angle $\boldsymbol{\alpha}(\mathbf{x}) \equiv \frac{D_{\mathrm{d}}D_{\mathrm{ds}}}{\xi_0 D_{\mathrm{s}}}\hat{\boldsymbol{\alpha}}(\boldsymbol{\xi})$ reduces to

$$\alpha_1(\mathbf{x}) = m(x)\frac{x_1}{x^2} + i_{\mathrm{N}}(x)\left[v_2\frac{x_1^2-x_2^2}{x^4} - v_1\frac{2x_1x_2}{x^4}\right] - m(>x)v_2, \tag{3.12}$$

$$\alpha_2(\mathbf{x}) = m(x)\frac{x_2}{x^2} + i_{\mathrm{N}}(x)\left[v_1\frac{x_1^2-x_2^2}{x^4} + v_2\frac{2x_1x_2}{x^4}\right] + m(>x)v_1, \tag{3.13}$$

where

$$v_1 \equiv \frac{\omega_1\xi_0}{c}, \quad v_2 \equiv \frac{\omega_2\xi_0}{c} \tag{3.14}$$

are the circular velocity at the scale length around, respectively, ξ_1 and ξ_2 in units of the speed of light.

3.2 Static axially symmetric lenses

For a non rotating, axially symmetric mass distribution, the lens equation reduces to a one-dimensional form [172, 192]. The plane containing the centre of the lens, the source and the observer is a totally geodesic sub-manifold of the space-time: all light rays from the source to the observer lie in this plane. Now, $k(\mathbf{x}) = k^{\mathrm{pN}}(|\mathbf{x}|)$. The ray trace equation reduces to

$$y = x - \alpha(x), \tag{3.15}$$

and the scaled deflection angle is

$$\alpha(x) = \frac{m(x)}{x}, \tag{3.16}$$

where $x \in R$. Owing to the symmetry, it is enough to consider source positions $y \geq 0$. Since $m(x) \geq 0$, any positive solution x of Eq. (3.15) must have $x \geq y$, and any negative one obeys $-\frac{m(x)}{x} > y$.

From Eq. (2.15), given the axial symmetry, we obtain

$$\alpha = \frac{d\psi}{dx}. \tag{3.17}$$

The Poisson's equation reads

$$\frac{1}{x}\frac{d}{dx}\left(x\frac{d\psi}{dx}\right) = 2k(x). \tag{3.18}$$

As seen before, for static axially symmetric deflectors, $k(x) = k^{\mathrm{pN}}(|x|)$. Substituting in Eq. (3.18) for Eqs. (3.16, 3.17), we obtain

$$\frac{dm}{dx} = 2xk(x), \tag{3.19}$$

as can be verified starting from Eq. (3.9). From Eqs. (3.9, 3.16, 3.17), we obtain

$$\frac{d\psi}{dx} = \frac{2}{x}\int_0^x k(x^{'})x^{'}dx^{'}. \tag{3.20}$$

In the above equation the right hand side is equal to

$$2\frac{d}{dx}\int_0^x k(x^{'})x^{'}\ln\left(\frac{x}{x^{'}}\right)dx^{'};$$

we have

$$\psi(x) = 2\int_0^x k(x^{'})x^{'}\ln\left(\frac{x}{x^{'}}\right)dx^{'}, \tag{3.21}$$

where the additive constant has been put to zero[1].

The Fermat potential can be written as

$$\phi(x,y) = \frac{1}{2}(x-y)^2 - \psi(x), \tag{3.22}$$

and the lens equation is equivalent to

$$\frac{\partial\phi}{\partial x} = 0. \tag{3.23}$$

3.2.1 The Jacobian matrix

The Jacobian matrix A can be obtained by differentiating the deflection angle [172],

$$\alpha_i(\mathbf{x}) = \frac{m(x)}{|x|^2}x_i, \tag{3.24}$$

It is

$$A = \mathcal{I} - \frac{m(x)}{|x|^4}\begin{pmatrix} x_2^2 - x_1^2 & -2x_1x_2 \\ -2x_1x_2 & x_1^2 - x_2^2 \end{pmatrix} - \frac{dm(x)}{dx}\frac{1}{|x|^3}\begin{pmatrix} x_1^2 & x_1x_2 \\ x_1x_2 & x_2^2 \end{pmatrix}, \tag{3.25}$$

[1]The results about the deflection angle hold when $k(x)$ decreases faster than x^{-1}. Then, Eq. (3.21) represents a potential for α [172].

where $\mathcal{I}$ is the 2-dimensional identity matrix. Using Eq. (3.25), we check that the property of the trace, Eq. (2.29), is satisfied. The convergence can be written as

$$k(x) = \frac{m^{'}(x)}{2|x|}, \tag{3.26}$$

where $m^{'} = \frac{dm}{dx}$. From Eq. (2.26), we get the components of the shear,

$$\gamma_1 = \frac{1}{2}(x_2^2 - x_1^2)\left(\frac{2m}{|x|^4} - \frac{m^{'}}{|x|^3}\right), \tag{3.27}$$

$$\gamma_2 = x_1 x_2 \left(\frac{m^{'}}{|x|^3} - \frac{2m}{|x|^4}\right), \tag{3.28}$$

From these relations, we can express the magnitude of the shear, Eq. (2.27), as

$$\gamma^2 = \left(\frac{m}{|x|^2} - k\right)^2; \tag{3.29}$$

By using Eq. (2.28), we evaluate the determinant of A,

$$\det A = \left(1 - \frac{m}{|x|^2}\right)\left(1 + \frac{m}{|x|^2} - 2k\right). \tag{3.30}$$

The determinant can be obtained also using the definition of A, Eq. (2.20). In the symmetric case, we have

$$\det A = \frac{y}{x}\frac{dy}{dx} = \left(1 - \frac{m}{x^2}\right)\left[1 - \frac{d}{dx}\left(\frac{m}{x}\right)\right] = \left(1 - \frac{\alpha(x)}{x}\right)\left(1 - \frac{d}{dx}\alpha(x)\right), \tag{3.31}$$

in agreement with Eq. (3.30).

3.2.2 Critical lines

Critical curves in the lens plane are circles defined by $\det A(x) = 0$. There are two kinds of critical curves, those where $m/x^2 = 1$ (*tangential critical curves*), and those where $\frac{d(m/x)}{dx} = 1$ (*radial critical curves*). As can be seen from the lens equation, Eq. (3.15), tangential curves are mapped onto the point $y = 0$. In fact, if source, observer and lens centre are collinear, light rays are not restricted to a single geodesic plane and ring images can be formed. This property derives from the axial symmetry: any perturbation in the mass distribution or a small rotation of the deflector will remove the degeneracy.

At a critical point, an eingevalue of A reduces to zero. Let us consider a critical point on the x_1-axis, $(x_1 \equiv x, 0)$; it is

$$A = \mathcal{I} - \frac{m(x)}{x^2}\begin{pmatrix} -1 & 0 \\ 0 & 1 \end{pmatrix} - \frac{m^{'}}{|x|}\begin{pmatrix} 1 & 0 \\ 0 & 0 \end{pmatrix}. \tag{3.32}$$

The vector $\mathbf{X}_{\rm t} = (0, 1)$ is tangent to the critical curve, whereas for $x_1 \neq 0$, $\mathbf{X}_{\rm r} = (1, 0)$ is normal to the circle. $\mathbf{X}_{\rm t}$ belongs to the kernel of A if the considered critical curve is tangential; on the other hand, $\mathbf{X}_{\rm r}$ is an eingevector with eingenvalue zero for a radial critical curve. Critical curves are folds. As can be derived from catastrophe theory, the point singularity at $\mathbf{y} = 0$ is unstable [142, 172]. The radial critical curve, inner to the tangential curve, is mapped in a circle centred at the point-like tangential caustic.

At the tangential critical curve, $x = x_{\rm t}$, we have

$$m(x_{\rm t}) = \int_0^{x_{\rm t}} 2xk(x)dx = x_{\rm t}^2 \ . \tag{3.33}$$

The tangential circle is called *Einstein ring*. In angular coordinates, i.e when $\xi_0 = D_{\rm d}$ in Eq. (3.10), it is

$$\theta_{\rm E} = \frac{1}{D_{\rm d}} \left(\frac{M(\theta_{\rm E})}{\pi \Sigma_{\rm cr}} \right)^{\frac{1}{2}} . \tag{3.34}$$

Given Eq. (2.6), from Eq. (3.33) we obtain

$$2 \int_0^{\xi_{\rm t}} \Sigma(\xi) \xi d\xi = \xi_{\rm t}^2 \Sigma_{\rm cr}; \tag{3.35}$$

the total mass $M(\xi_{\rm t})$ inside the Einstein ring reads

$$M(\xi_{\rm t}) = \pi \xi_{\rm t}^2 \Sigma_{\rm cr}; \tag{3.36}$$

so the average surface density $\langle \Sigma \rangle_{\rm t}$ within the tangential curve is equal to the critical density,

$$\langle \Sigma \rangle_{\rm t} = \Sigma_{\rm cr}, \tag{3.37}$$

or using dimensionless quantities, $\langle k \rangle_{\rm t} = 1$. These simple considerations give a practical method to determine the mass of the deflector, if the distances and the angular position $\theta_{\rm E}$ of the tangential curve are known. It is

$$M(\theta_{\rm E}) = \pi (D_{\rm d} \theta_{\rm E})^2 \Sigma_{\rm cr} \approx (1.1 \times 10^{14} M_\odot) \left(\frac{\theta_{\rm E}}{30''} \right)^2 \left(\frac{(D_{\rm d}/1{\rm Gpc})(D_{\rm s}/1{\rm Gpc})}{(D_{\rm ds}/1{\rm Gpc})} \right). \tag{3.38}$$

We want now investigate the image distortion near a critical curve. Images of extended source near caustics are highly elongated. They are called *arcs*. Let us consider a tangential critical curve. We take a point $\mathbf{x}_{\rm c} = (x_{\rm c}, 0)$ very close to the tangential critical line. Then, at $\mathbf{x}_{\rm c}$ it is $m/x_{\rm c}^2 = 1 - \delta$ with $|\delta| \ll 1$. The Jacobian matrix A can be approximated as

$$A \simeq \begin{pmatrix} 2 - m'/x_{\rm c} & 0 \\ 0 & \delta \end{pmatrix}, \tag{3.39}$$

where δ has been neglected in the first diagonal element. Let us consider an ellipse centred at $\mathbf{x}_{\rm c}$ and with semi-axes small compared to the distance of $\mathbf{x}_{\rm c}$ from the critical curve,

$$\mathbf{c}(\varphi) = \mathbf{x}_{\rm c} + \begin{pmatrix} \rho_1 \cos\varphi \\ \rho_2 \sin\varphi \end{pmatrix}.$$

The ray-trace equation maps the ellipse in the image plane onto an ellipse in the source plane,

$$\mathbf{d}(\varphi) = \mathbf{y}_{\rm c} + \begin{pmatrix} (2 - m^{'}/x_{\rm c})\rho_1 \cos\varphi \\ \delta\rho_2 \sin\varphi \end{pmatrix}$$

where $\mathbf{y}_{\rm c} = \mathbf{y}(\mathbf{x}_{\rm c})$. By construction, $\mathbf{c}(\varphi)$ is an image of the source $\mathbf{d}(\varphi)$. $\mathbf{d}(\varphi)$ reduces to a circle when,

$$\mid \rho_2 \mid = \frac{2 - m^{'}/x_{\rm c}}{\delta} \mid \rho_1 \mid, \tag{3.40}$$

The image $\mathbf{c}(\varphi)$ of such a disk shaped source is an arc-like image near the critical curve. Since $|\delta| \ll 1$, it is a tangentially highly elongated, along the x_2-axis, ellipse ($|\rho_2| \gg |\rho_1|$). For this reason, the outer critical curve is called tangential. On the other hand, an extended source near the radial caustic has an image intersecting the inner radial critical curve that is radially stretched.

The eingenvalues of the Jacobian matrix have a simple geometrical interpretation. They describe the image distortion in the radial and tangential directions. Let an ellipse, centred at $\mathbf{x}$ and with axes ρ_1 in the radial direction and ρ_2 in the tangential direction, be the image of an infinitesimal circular source of diameter δ at $\mathbf{y}$. The source subtends an angle $\varphi = \delta/y$, as seen from the centre of the source plane. Given the axial symmetry, the polar coordinate is unchanged, so that, $\varphi = \rho_2/x$. We have $\frac{\delta}{\rho_2} = \frac{y}{x}$. By rewriting y/x by means of Eqs. (3.15, 3.16), we obtain that images are stretched in tangential direction by a factor $\left(\frac{y}{x}\right)^{-1} = \left(1 - \frac{m}{x^2}\right)^{-1}$.

The radial size of the source and of the image are related by $\delta = \frac{dy}{dx}\rho_1$. Hence, images are stretched in the radial direction by a factor $\left(\frac{dy}{dx}\right)^{-1} = \left(1 + \frac{m}{x^2} - 2k\right)^{-1}$. The factor of radial deformation at the Einstein radius is

$$\left.\frac{dy}{dx}\right|^{-1}_{x=x_{\rm t}} = 2\left[1 - k(x_{\rm t})\right]. \tag{3.41}$$

3.2.3 Criteria for multiple images

Besides the conditions for general isolated deflector stated in Section 2.5, axially symmetric lenses exhibit some additional criteria for multiple images [142, 172]. Let us consider a transparent lens with a piece-wise continuous surface mass density, such that

$$0 \leq k(x) \leq k_{\rm max} \quad \forall x, \tag{3.42}$$

and

$$\lim_{x\to\infty} xk(x) = 0. \tag{3.43}$$

It is convenient to introduce the mean surface mass density within x

$$\bar{k}(x) \equiv \frac{2}{x^2}\int_0^x k(x^{'})x^{'}dx^{'} = \frac{m(x)}{x^2}; \tag{3.44}$$

the lens equation can be rewritten as

$$y = x(1 - \bar{k}).$$

Then,

1. A lens can produce multiple images if, and only if, the condition $\frac{dy}{dx} = 1-2k+\bar{k} < 0$ is fulfilled at lest at one point.

   If $\frac{dy}{dx} \geq 0$, $y(x)$ increases monotonically and no multiple images can be produced. On the other hand, since the deflection angle is bounded, $\frac{dy}{dx} \to 1$ for $x \to \pm\infty$. If there is a point where $\frac{dy}{dx} < 0$, then there is a local maximum x_1 and a local minimum $x_2 > x_1$ of $y(x)$. For $y(x_2) < y < y(x_1)$, there are at least three images. $\frac{dy}{dx} < 0$ implies the existence of the radial caustic: point sources inside the caustic circle have three images, while a source outside the radial circle has one image.

2. Multiple images are produced only if $k > 1/2$ at one point.

   In fact, $\frac{dy}{dx} < 0$ implies $k = \frac{1+\bar{k}}{2} - \frac{1}{2}\frac{dy}{dx} > \frac{1+\bar{k}}{2} \geq \frac{1}{2}$. This result follows from the positiveness of the convergence.

3. Assume a deflector with a surface mass density decreasing with x, $k^{'} \leq 0$. Then, multiple images are produced if, and only if, $k(0) > 1$.

   Sufficiency follows from general criteria for multiple images, see Section 2.5. On the other hand, $\frac{dy}{dx} = (1 - \bar{k}) - x\bar{k}^{'}$ for $x \geq 0$. Since

   $$\bar{k}(x) = 2\int_0^1 uk(ux)du,$$

   then

   $$\frac{d\bar{k}}{dx} = 2\int_0^1 u^2 k^{'}(ux)du \leq 0, \text{ and } \bar{k}(x) \leq k(0) \leq 1.$$

   If $k(0) \leq 1$, then $\bar{k}(x) \leq k(0) \leq 1$ and $\frac{dy}{dx} \geq 0$: multiple images cannot occur.

3.3 Uniform sheet

A sheet of continuous matter with constant mass density can approximate the central part of clusters of galaxies with large cores [142]. The gravitational lens potential of a uniform sheet of matter with constant surface mass density Σ_c is solution of

$$\nabla^2_{\mathbf{x}}\psi = 2k_c, \tag{3.45}$$

where $k_c \equiv \Sigma_c/\Sigma_{cr}$ is a constant. The gravitational and Fermat potentials are, respectively,

$$\psi(x) \;=\; \frac{k_c}{2}x^2, \tag{3.46}$$

and

$$\phi(\mathbf{x},\mathbf{y}) \;=\; \frac{|\mathbf{x}-\mathbf{y}|^2}{2} - \frac{k_\mathrm{c}}{2}x^2; \tag{3.47}$$

the lens equation is

$$\mathbf{y} = \mathbf{x}(1-k_\mathrm{c}). \tag{3.48}$$

The determinant of the Jacobian matrix is $(1-k_\mathrm{c})^2$, whereas $A_{11} = 1-k_\mathrm{c}$.

The condition $k_\mathrm{c} \neq 1$ selects the non-critical sheets. Since $\det A \neq 0$, no critical points (hence, caustics) occur. Only one lensed image $\mathbf{x}_0$ of a source at $\mathbf{y}$ occurs at

$$\mathbf{x}_0 = \frac{\mathbf{y}}{1-k_\mathrm{c}}, \tag{3.49}$$

with magnification

$$\mu = \frac{1}{(1-k_\mathrm{c})^2}, \tag{3.50}$$

which is independent of the source position. If $k_\mathrm{c} < 1$, then $\det A > 0$ and $A_{11} > 0$: the lensed image is a minimum and it is magnified; for $k_\mathrm{c} > 1$, the image is a maximum, which is de-magnified[2] for $k_\mathrm{c} > 2$. As $k_\mathrm{c} \to 1$, the lensed image goes to infinity getting infinitely bright.

In the critical case, $k_\mathrm{c} = 1$, the lens equation reduces to $\Delta_\mathbf{x}\phi = -\mathbf{y} = 0$ for all $\mathbf{x}$. If $\mathbf{y} \neq 0$, no lensed image exists. If $\mathbf{y} = 0$, the Fermat potential is constant, $\phi(\mathbf{x},\mathbf{y}) = 0$; then, every point on the lens plane is a degenerate lensed image. A light source at the point-like caustic $\mathbf{y} = 0$ appears as an infinitely bright plane.

3.4 Exponential disk

Spiral galaxies, like our own and M31, contain a prominent, flattened, roughly axisymmetric, disk component composed of Population I stars, gas, and dust. The distribution of surface brightness in spiral galaxies disks obeys the exponential law [66] with a typical length scale $R_\mathrm{D} \simeq 3$ Kpc. In the hypothesis that mass follows light, the surface mass density in the disk plane can be written as

$$S_\mathrm{D}(R) = S_0 \exp\left[-\frac{R}{R_\mathrm{D}}\right]. \tag{3.51}$$

The circular rotation velocity is [15]

$$v_\mathrm{D}^\mathrm{ROT}(R) = 4\pi G S_0 R_\mathrm{D} y^2 \left[I_0(y)K_0(y) - I_1(y)K_1(y),\right] \tag{3.52}$$

where $y \equiv \frac{1}{2}\frac{R}{R_\mathrm{D}}$, and I_n and K_n are the modified Bessel function of, respectively, the first and the second kinds.

[2] The potential ϕ is not isolated.

3.4.1 Tilted disk

Let (R_1, R_2) be the coordinates in the plane of the disk. We define the angles φ and ϑ as in Section 3.1. Now, since the disk is thin, we have to fix the condition $R_3 = 0$. It is

$$l = -\csc\varphi\csc\vartheta + \xi_1\sin\vartheta - \xi_2\cot\varphi\cot\vartheta; \tag{3.53}$$

then, Eqs. (3.2, 3.3) reduce to

$$R_1 = -\xi_2\cot\varphi\cot\vartheta + \xi_1\csc\vartheta, \tag{3.54}$$

and

$$R_2 = \xi_2\csc\varphi. \tag{3.55}$$

Since the disk is thin, the line of sight intercepts the matter distribution in a single point, so that no integration along the line of sight has to be performed. The infinitesimal area dR_1dR_2, at a distance R from the centre, projects itself in an element with surface mass density $\Sigma_{\rm D}$ in the lens plane, defined by

$$S_{\rm D}(R)dR_1dR_2 = \Sigma_{\rm D}(\xi_1,\xi_2)d\xi_1d\xi_2; \tag{3.56}$$

the surface mass density reads

$$\Sigma_{\rm D}(\xi_1,\xi_2) = S_{\rm D}(R_1(\xi_1,\xi_2),R_2(\xi_2))\left|\csc\varphi\csc\vartheta\right|. \tag{3.57}$$

The velocity along the line of sight of the mass element is

$$\mathbf{v}\cdot\mathbf{e}_{\rm in} = -\frac{R_2}{R}v_{\rm D}^{\rm ROT}(R)\cos\vartheta + \frac{R_1}{R}v_{\rm D}^{\rm ROT}(R)\cos\varphi\sin\vartheta. \tag{3.58}$$

3.4.2 Face-on disk

In this case, it is $\vartheta = \pi/2$ and $\varphi = \pi/2$, i.e. the disk plane coincides with the lens plane. Since the orbits are in the lens plane, there is no gravito-magnetic contribution to the gravitational lensing effect. We can apply the formulae for an axially symmetric system. The mass within ξ is

$$M(\xi) = 2\pi\int_0^\xi S_{\rm D}(R)RdR = 2\pi R_{\rm D}^2S_0\left[1-\exp\left(-\frac{R}{R_{\rm D}}\right)\left(1+\frac{R}{R_{\rm D}}\right)\right]; \tag{3.59}$$

then, the deflection angle reads

$$\hat{\alpha}(\xi) = \frac{4GM(\xi)}{c^2\xi} = \frac{8\pi GS_0R_{\rm D}^2}{c^2\xi}\left[1-\exp\left(-\frac{R}{R_{\rm D}}\right)\left(1+\frac{R}{R_{\rm D}}\right)\right]. \tag{3.60}$$

3.4.3 Edge-on disk

Now, let us consider a disk orthogonal to the lens plane. The 2-dimensional surface mass density reduces, by an integration along the line of sight, to a linear density λ in the lens plane. We take the disk in the (l, ξ_1) plane. It is,

$$\lambda(\xi_1) = \int_{-\infty}^{+\infty} S_{\rm D}(\xi_1, l) dl = 2S_0 \int_{\xi_1}^{\infty} \exp\left[-\frac{R}{R_{\rm D}}\right] \frac{RdR}{\sqrt{R^2 - \xi_1^2}} = 2S_0 \xi_1 K_1\left(\frac{\xi_1}{R_{\rm D}}\right). \quad (3.61)$$

Then, the surface mass density in the lens plane reduces to

$$\Sigma_{\rm D}(\xi_1, \xi_2) = \lambda(\xi_1)\delta(\xi_2), \quad (3.62)$$

where $\delta(\xi_2)$ is the Kronecker delta.

The velocity orthogonal to the lens plane must be integrated along the line of sight,

$$\langle \mathbf{v}\cdot\mathbf{e}_{\rm in}\rangle_l = -\frac{2\xi_1}{\lambda(\xi_1)} \int_{\xi_1}^{\infty} |v(R)| S_{\rm D}(R) \frac{RdR}{\sqrt{R^2 - \xi_1^2}}. \quad (3.63)$$

The deflection angle reads

$$\hat{\alpha}_1(\xi_1, \xi_2) = \frac{4G}{c^2} \int_{-\infty}^{+\infty} d\xi_1' \lambda(\xi_1') \left(1 - \frac{2}{c}\langle \mathbf{v}\cdot\mathbf{e}_{\rm in}\rangle_l(\xi_1')\right) \frac{\xi_1 - \xi_1'}{(\xi_1 - \xi_1')^2 + \xi_2^2}, \quad (3.64)$$

$$\hat{\alpha}_2(\xi_1, \xi_2) = \frac{4G}{c^2} \int_{-\infty}^{+\infty} d\xi_1' \lambda(\xi_1') \left(1 - \frac{2}{c}\langle \mathbf{v}\cdot\mathbf{e}_{\rm in}\rangle_l(\xi_1')\right) \frac{\xi_2}{(\xi_1 - \xi_1')^2 + \xi_2^2}. \quad (3.65)$$

3.5 Singular isothermal sphere

Isothermal spheres (ISs) are widely used in astrophysics to model systems on very different scales, from galaxy haloes to clusters of galaxies; also, IS can be adopted to study microlensing by non-compact invisible objects in the Milky Way's halo [168].

The mass profile of a singular isothermal sphere (SIS) can be derived by assuming an ideal isothermal gas in hydrostatic equilibrium; the equation of state is $p = (\rho/m)k_{\rm B}T$, where ρ and m are, respectively, the mass density and the (average) mass of a particle, and $k_{\rm B}$ is the Boltzmann constant. The equation of hydrostatic equilibrium reads

$$\frac{k_{\rm B}T}{m}\frac{d\rho}{dr} = -\rho\frac{GM(r)}{r^2}, \quad (3.66)$$

where $M(r)$ is the total mass interior to radius r. If we multiply Eq. (3.66) through by $r^2(m/k_{\rm B}T)$ and then differentiate with respect to r, we obtain, using the law of conservation of mass,

$$\frac{dM(r)}{dr} = 4\pi r^2 \rho, \quad (3.67)$$

the differential equation

$$\frac{d}{dr}\left(r^2\frac{d}{dr}\ln\rho\right) = -\frac{Gm}{k_{\rm B}T}4\pi r^2\rho. \tag{3.68}$$

This equation can be obtained also in the kinetic theory starting from the Jeans equation[3]. In the stationary, spherically symmetric case, we have

$$\frac{d}{dr}(n\sigma_{\rm r}^2) + \frac{2n}{r}(\sigma_{\rm r}^2 - \sigma_{\rm t}^2) = -n\frac{dU}{dr}, \tag{3.69}$$

where n is the density of particles, and $\sigma_{\rm r}$, $\sigma_{\rm t}$ are, respectively, the radial and transversal velocity dispersions.

For the special case of isotropic velocity dispersion, $\sigma_{\rm r}^2 = \sigma_{\rm t}^2 = \sigma_{\rm v}^2 =$ const., Eq. (3.69) reduces to

$$\sigma_{\rm v}^2\frac{dn}{dr} = -n\frac{GM(r)}{r^2}; \tag{3.70}$$

Eq. (3.70) can identified with Eq. (3.66) for $\rho = nm$, and $k_{\rm B}T = m\sigma_{\rm v}^2$. A solution of Eq. (3.70), with a power law dependence for $\rho(r)$, is

$$\rho(r) = \frac{\sigma_{\rm v}^2}{2\pi G r^2}. \tag{3.71}$$

The density profile, singular at the origin, describes a model known as SIS. Regular solutions of Eq. (3.68) are known only numerically [15].

Since $\rho \propto r^{-2}$, the mass within r, $M(r)$, is proportional to r; the rotational velocity of a test-particle in a circular orbit in the gravitational potential is

$$v_{\rm ROT}^2(r) = \frac{GM(r)}{r} = 2\sigma_{\rm v}^2 = \text{ const.} \tag{3.72}$$

The observed flat rotation curves of spiral galaxies are reproduced.

The projected mass density is

$$\Sigma(\xi) = \frac{\sigma_{\rm v}^2}{2G}\frac{1}{\xi}. \tag{3.73}$$

Then,

$$M^{\rm SIS}(\xi) = \frac{\pi\sigma_{\rm v}^2}{G}\xi, \tag{3.74}$$

$$I_{\rm N}^{\rm SIS}(\xi) = \frac{\pi\sigma_{\rm v}^2}{3G}\xi^3. \tag{3.75}$$

Since the total mass is divergent, we introduce a cut-off radius $R \gg \xi$. The cut-off radius must be much larger than the Einstein radius in order to not significantly affect the lensing behavior. For the SIS, the deflection angle reduces to

$$\hat{\alpha}_1^{\rm SIS}(\xi,\theta) = 4\pi\left(\frac{\sigma_{\rm v}}{c}\right)^2\left\{\cos\theta + \frac{\omega_2}{c}\left[\xi\left(\frac{\cos 2\theta}{3}+1\right) - R\right] - \frac{\omega_1}{c}\xi\frac{\sin 2\theta}{3}\right\}, \tag{3.76}$$

[3]The Jeans equation can be obtained by taking the first moment of the collisionless Boltzmann equation [15].

$$\hat{\alpha}_2^{\rm SIS}(\xi,\theta) = 4\pi\left(\frac{\sigma_{\rm v}}{c}\right)^2\left\{\sin\theta + \frac{\omega_1}{c}\left[\xi\left(\frac{\cos 2\theta}{3}-1\right)+R\right] + \frac{\omega_2}{c}\xi\frac{\sin 2\theta}{3}\right\}. \quad (3.77)$$

The correction couples kinematics, through the angular velocity, and geometry, through the cut-off radius. As can be easily seen, the gravito-magnetic effect is significant when

$$\frac{\omega}{c}R \gtrsim 10^{-3}; \quad (3.78)$$

In particular, in the inner regions ($\xi \ll R$), the above equations reduce to

$$\hat{\alpha}_1^{\rm SIS}(\xi \ll R,\theta) \simeq 4\pi\left(\frac{\sigma_{\rm v}}{c}\right)^2\left\{\cos\theta - \frac{R\omega_2}{c}\right\}, \quad (3.79)$$

$$\hat{\alpha}_2^{\rm SIS}(\xi \ll R,\theta) \simeq 4\pi\left(\frac{\sigma_{\rm v}}{c}\right)^2\left\{\sin\theta + \frac{R\omega_1}{c}\right\}; \quad (3.80)$$

the correction derives from the mass outside the considered radius.

We can model a typical galaxy as a SIS with $\sigma_{\rm v} \sim 200$ km s^{-1}, $R \lesssim 50$ kpc and $J \equiv I_{\rm N}(R)\times\omega \sim 0.1 M_\odot$ kpc^{2}s^{-1}, as derived from numerical simulations [206]. It is,

$$\frac{\omega}{c}R \sim \frac{G}{c^3}J\left(\frac{c}{\sigma_{\rm v}}\right)^2 R^{-2} \sim 10^{-3}. \quad (3.81)$$

The gravito-magnetic correction is quite significant, increases with the ordered motion of the stars (i.e., with the angular momentum) and decreases with the random proper motions (i.e., with the dispersion velocity).

In order to change to dimensionless variables, we introduce a length scale,

$$\xi_0 = R_{\rm E} = 4\pi\left(\frac{\sigma_{\rm v}}{c}\right)^2\frac{D_{\rm d}D_{\rm ds}}{D_{\rm s}} \quad (3.82)$$

We consider a sphere rotating about the ξ_2-axis, $\omega_1 = 0,\ \omega_2 = \omega$. The scaled deflection angle simplifies to

$$\alpha_1^{\rm SIS}(x_1,x_2) = \frac{x_1}{|x|} + L\left(\frac{2x_1^2+x_2^2}{|x|} - \frac{3}{2}r\right), \quad (3.83)$$

$$\alpha_2^{\rm SIS}(x_1,x_2) = \frac{x_2}{|x|} + L\frac{x_1x_2}{|x|}, \quad (3.84)$$

where $L \equiv \frac{2}{3}\frac{\omega R_{\rm E}}{c}$ is an estimate of the rotational velocity and r is the cut-off radius in units of $R_{\rm E}$.

The determinant of the Jacobian matrix reads

$$A^{\rm SIS}(x_1,x_2) = 1 - \frac{1}{|x|} - L\frac{x_1}{|x|}\left(3-\frac{2}{|x|}\right) + L^2\left(\frac{2x_1^2-x_2^2}{|x|^2}\right) \quad (3.85)$$

and the deflection potential is

$$\psi^{\rm SIS}(x_1,x_2) = (1+Lx_1)|x| - \frac{3}{2}Lrx_1. \quad (3.86)$$

The corrected convergence is

$$k^{\rm SIS} = \frac{1+3Lx_1}{2|x|}; \tag{3.87}$$

k is positive when $x_1 > -\frac{1}{3L}$. Since we have introduced a cut-off radius, our expressions hold for $x_1 \lesssim r$: the tighter condition $Lr < \frac{1}{3}$ guarantees $k > 0$ for all points in the lens plane.

3.5.1 Non-rotating sphere

Let us first consider a non-rotating sphere [142, 172]. We obtain

$$k^{\rm pN}(x) = \frac{1}{2|x|}, \tag{3.88}$$

thus

$$m(x) = |x|, \quad \alpha^{\rm pN}(x) = \frac{x}{|x|}; \tag{3.89}$$

the strength of the deflection angle is constant at

$$\left|\hat{\alpha}^{\rm pN}\right| = \frac{4\pi\sigma_{\rm v}^2}{c^2}. \tag{3.90}$$

The lens equation reads

$$y = x - \frac{x}{|x|}. \tag{3.91}$$

Let us consider $y > 0$; for $y < 1$, there are two images, at $x_+ = y + 1$ and $x_- = y - 1$, on opposite sides of the lens centre. It is $x_+ + x_- = 2y$. The lensed image x_+ is a minimum and x_- is a saddle. For $y = 1$, there is one lensed image x_+, which is a magnified minimum, whereas the saddle lensed image x_- disappears at the singularity. For $y > 1$, only one image occurs at $x_+ = y + 1$.

The magnification for an image at x is

$$\mu^{\rm pN} = \frac{|x|}{|x| - 1}. \tag{3.92}$$

The magnifications of the lensed images are

$$\mu_+ = 1 + \frac{1}{y}, \quad \mu_- = \frac{1}{y} - 1; \tag{3.93}$$

They verify the relation $\mu_+ - \mu_- = 2$, i.e. the semi-difference of the lensed image magnification is the magnification of the unlensed light source. In the limit $y \to 1$, the inner image becomes very faint. The total magnification of a point source is

$$\mu_{\rm TOT}^{\rm pN} = \begin{cases} 2/y & (y \leq 1) \\ (1+y)/y & (y > 1) \end{cases}. \tag{3.94}$$

A light source at the origin, $y = 0$, appears as an infinitely bright circle at $x = 1$. The tangential critical curve, $|\xi_{\rm t}| = R_{\rm E}$, is the Einstein radius. The corresponding angle is given by

$$\theta_{\rm E} = 4\pi \left(\frac{\sigma_{\rm v}}{c}\right)^2 \frac{D_{\rm ds}}{D_{\rm s}} \simeq 29'' \left(\frac{\sigma_{\rm v}}{10^3 {\rm km\ s^{-1}}}\right)^2 \frac{D_{\rm ds}}{D_{\rm s}}. \tag{3.95}$$

For a typical cluster of galaxies with a 1-dimensional velocity dispersion $\sigma_{\rm v} = 500\,{\rm km\,s^{-1}}$, and for $D_{\rm s} \simeq 2D_{\rm d}$, the Einstein ring is about 0.5 arcmin.

The set of caustics consists of the point $y = 0$.

From Eq. (3.29), we find

$$\gamma^{\rm pN}(x) = k^{\rm pN}(x) = \frac{1}{2|x|}.$$

The images are stretched in the tangential direction by a factor $|x/y| = |\mu|$, whereas the distortion factor in the radial direction, $|dx/dy|$, is unity.

The deflection potential reduces to

$$\psi(x) = |x|; \tag{3.96}$$

we can now determine the time delay between the two images from Eq. (1.102). It is

$$c\Delta T^{\rm pN} = (1 + z_{\rm d}) \left[4\pi \left(\frac{\sigma_{\rm v}}{c}\right)^2\right]^2 \frac{D_{\rm d} D_{\rm ds}}{D_{\rm s}} 2y. \tag{3.97}$$

Since cosmological distances scale as H_0^{-1}, once measured the time delay and known the lens parameters, the Hubble constant can be measured.

3.5.2 Perturbative analysis

When the gravito-magnetic correction is considered, the inversion of the lens mapping is not an easy task. However, under the condition $L \ll 1$, we can obtain approximate solutions to the first-order in L, given by

$$\mathbf{x} \simeq \mathbf{x}_{(0)} + L\mathbf{x}_{(1)}, \tag{3.98}$$

where $\mathbf{x}_{(0)}$ and $\mathbf{x}_{(1)}$ denote, respectively, the zeroth-order solution, i.e. is a solution of the lens equation for $L = 0$, and the correction to the first-order. Substituting Eq. (3.98) in the corrected lens equation, we obtain the first-order perturbation,

$$x_{(1)1} = x_{(0)}^2 + \left(\frac{3}{2}r - 2x_{(0)} + x_{(0)}^2\right) \frac{x_{(0)1}^2 - x_{(0)}^3}{x_{(0)}^2 (x_{(0)} - 1)}, \tag{3.99}$$

$$x_{(1)2} = \left(\frac{3}{2}r - 2x_{(0)} + x_{(0)}^2\right) \frac{x_{(0)1} x_{(0)2}}{x_{(0)}^2 (x_{(0)} - 1)}. \tag{3.100}$$

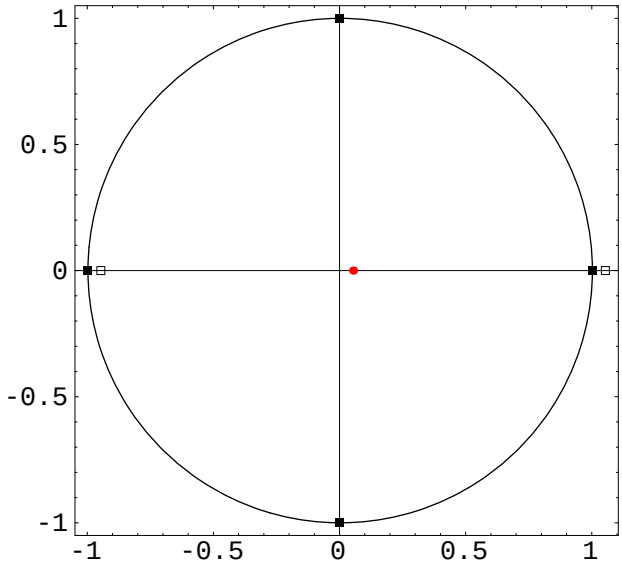

Figure 3.1: A source (the grey circle) inside the caustic of a rotating SIS is multiply imaged in a cross shaped pattern; the four filled box locate the four images. The empty boxes represent the positions of the two unperturbed images. The critical line is also plotted. It is $r = 15$ and $L = 2.5{\times}10^{-3}$.

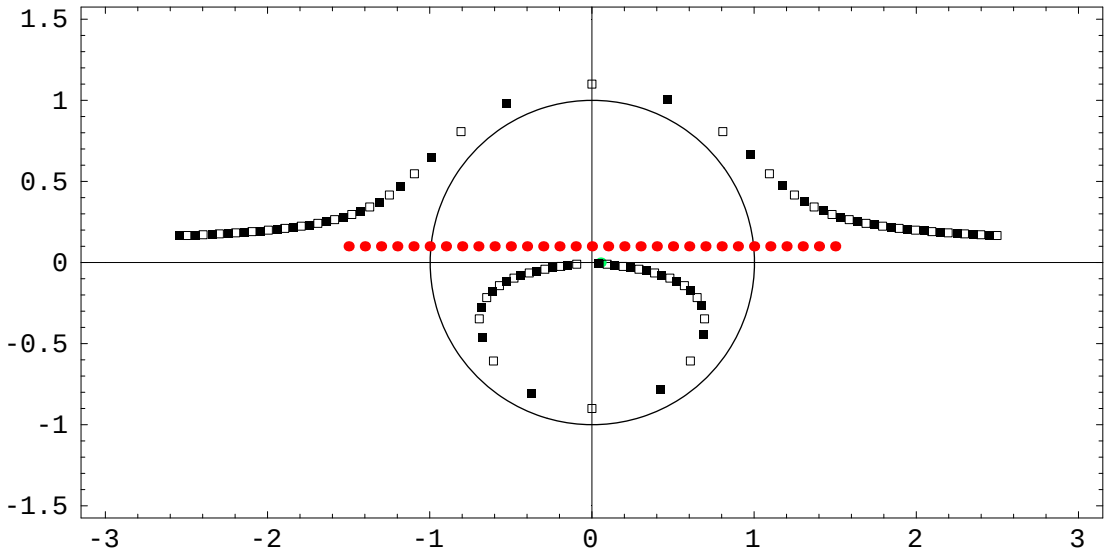

Figure 3.2: A source's track, at $y_2 = 0.1$, and the corresponding images produced by a rotating SIS. The grey circles represent successive positions of the source. For each source position, the centre of the coordinate-axes, the source (grey circle) and the two unperturbed images (empty boxes) lie on a straight line. The images (filled boxes) are anticlockwisely rotated, about the centre, with respect to this line. The critical line is also plotted. It is $r = 15$ and $L = 2.5{\times}10^{-3}$.

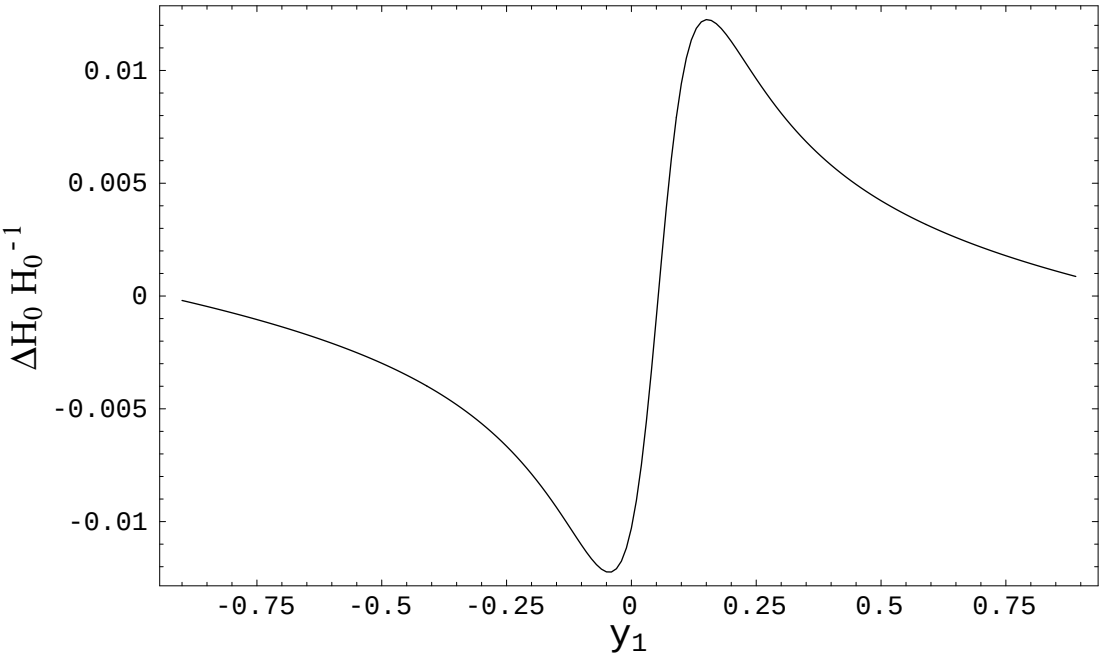

Figure 3.3: Relative variation in the estimate of the Hubble constant for a source moving with $y_2 = 0.1$. It is $r = 15$ and $L = 2.5\times10^{-3}$.

The critical curve is slightly distorted. The solution of $\det A(x_1, x_2) = 0$, with respect to x_2, is

$$\begin{aligned} x_2(x_1) &= \pm\left\{\frac{1}{\sqrt{2}(1-L^2)}\left(1-2x_1^2+2Lx_1+7L^2x_1^2+4L^3x_1+4L^4x_1^2\right.\right. \\ &+ \left.\left.(1+3Lx_1)\sqrt{1-2Lx_1-3L^2x_1^2+8L^3x_1+12L^4x_1^2}\right)^{\frac{1}{2}}\right\} \qquad (3.101) \\ &\simeq \pm\left\{\sqrt{1-x_1^2}+\frac{x_1}{\sqrt{1-x_1^2}}L+\frac{2-4x_1^2+x_1^4}{2(1-x_1^2)^{3/2}}L^2\right\}, \qquad (3.102) \end{aligned}$$

where the above approximate solution holds for $x_1 < 1$. The critical curve intersects the x_1-axis in $x_1 = -\frac{1}{1+L} \simeq -1+L-L^2$ and $x_1 = \frac{1}{1-L} \simeq 1+L+L^2$. The gravito-magnetic correction changes the width of the curve from 2 to $2(1+L^2)$. The maximum height is for $x_1 \simeq L$, when $x_2 \simeq \pm\left(1+\frac{3}{2}L^2\right)$; the total maximum height becomes $2(1+3L^2)$. So, the area of the critical curve slightly grows and its centre shifts of L along the x_1-axis.

By mapping the four extremal points of the critical curve onto the source plane through the lens equation, we can determine the corresponding cusps of the caustic. It is a diamond-shaped caustic with four cusps, centred in $(y_1, y_2) = \left(L(\frac{3}{2}r-1), 0\right)$. The axes, of semi-width $\sim L^2$, are parallel to the coordinate axes. The orientation and the position on the caustic depends on both the strength and orientation of the angular momentum and on the radius of the lens. A source outside (inside) the caustic has two

(four) images. When the source is inside the caustic, it is imaged in a cross pattern, see Fig. (3.1); since the axial symmetry is broken by the gravito-magnetic field, the Einstein ring is no more produced.

In Fig. (3.2), we plot the images of a source moving in the source plane. With respect to the non-rotating case, the images are rotated anti-clockwisely for $L > 0$.

Neglecting the gravito-magnetic correction in the analysis of a gravitational lensing system induces an error in the determination of some quantities. We want to study the case of the Hubble constant. As Refsdal realized in 1964 [152], any gravitational lensing system can be used to determine the Hubble constant. In fact, the geometrical time delay is simply proportional to the path lengths of the rays which scale as H_0^{-1}; the potential time delay, as can be seen from Eq. (2.10), scales as a physical length and has the same scaling H_0^{-1}. We have

$$H_0 \Delta T = \mathcal{F}(\sigma_{\rm v}, ..., z_{\rm d}, z_{\rm s}, \Omega_{i0}). \tag{3.103}$$

The dimensionless function $\mathcal{F}$ depends on the lens parameters and on the cosmological density parameters, but this last dependence is not very strong. A lens model which reproduces the positions and magnifications of the images provides the scaled time delay $H_0\Delta T$ between the images. Therefore, a measurement of ΔT will yield the Hubble constant. Let us consider a rotating galaxy, described by a SIS, with known dispersion velocity and redshift, which multiply images a background quasar, at redshift $z_{\rm s}$. An observer measures the time delay between the two images, $\Delta T = \Delta T^{\rm GRM}$, and their positions, $\mathbf{x}_a$ and $\mathbf{x}_b$; the source position $\mathbf{y}$ is unknown. If, to analyse the data, we use a non rotating lens model, from the position of the images, the non-correct estimated position of the source, through the lens equation, is

$$\mathbf{y}^{\rm STAT} = \sum_{a,b} \mathbf{x}_i - \frac{\mathbf{x}_i}{|\mathbf{x}_i|}; \tag{3.104}$$

the estimated Hubble constant is

$$H_0^{ST} = \frac{1}{\Delta T} F(z_{\rm d}, z_{\rm s}, \sigma_{\rm v}) 2 y^{ST}, \tag{3.105}$$

where $F(z_{\rm d}, z_{\rm s}, \sigma_{\rm v}) \equiv (1 + z_{\rm d}) \left[4\pi \left(\frac{\sigma_{\rm v}}{c}\right)^2\right]^2 \frac{r_{\rm d} r_{\rm ds}}{r_{\rm s}}$ and r is the angular diameter distance in units of c/H_0. Since

$$H_0 = \frac{1}{\Delta T} F(z_{\rm d}, z_{\rm s}, \sigma_{\rm v}) |\phi(\mathbf{x}_a, \mathbf{y}) - \phi(\mathbf{x}_b, \mathbf{y})|, \tag{3.106}$$

the relative error in the determination of the Hubble constant is

$$\frac{\Delta H_0}{H_0} = \frac{2 y^{\rm STAT} - |\phi(\mathbf{x}_a, \mathbf{y}) - \phi(\mathbf{x}_b, \mathbf{y})|}{|\phi(\mathbf{x}_a, \mathbf{y}) - \phi(\mathbf{x}_b, \mathbf{y})|}; \tag{3.107}$$

numerically, we find that the maximum error is $\sim \frac{1}{2} \left|\frac{L}{y_2}\right|$ for a source moving at fixed y_2. In Fig. (3.3), we plot the relative error for a source moving at $y_2 = 0.1$ for $L = 0.0025$ and $r = 15$. These are typical values for a galaxy with $\sigma_{\rm v} \sim 200{\rm Km\ s^{-1}}$, $R \sim 50{\rm Kpc}$ $J \sim 0.04 {\rm M_\odot Kpc\ s^{-1}}$, when $z_{\rm d} = 0.3$ and $z_{\rm s} = 1$. In this case, the error is $\lesssim 1\%$.

3.6 Isothermal sphere with finite core

Analytical solutions of Eq. (3.69), without a central singular cusp, are not known. To obtain a regular profile, let us consider an IS with a finite core radius $r_{\rm c}$, which determines the scale over which the distribution falls off. The mass density is

$$\rho^{\rm IS}(r) = \frac{\sigma_{\rm v}^2}{2\pi G}\left(\frac{1}{r_{\rm c}^2 + r^2}\right), \tag{3.108}$$

with central mass density

$$\rho_0 = \frac{\sigma_{\rm v}^2}{2\pi G}\frac{1}{r_{\rm c}^2}; \tag{3.109}$$

$\sigma_{\rm v}$ is the velocity dispersion at radius much larger than $r_{\rm c}$ [172]. In this model, the velocity dispersion goes to zero at the origin. The surface mass density is

$$\Sigma^{\rm IS}(\xi) = \frac{\sigma_{\rm v}^2}{2G}\frac{1}{(\xi^2 + \xi_{\rm c}^2)^{1/2}}, \quad \xi_{\rm c} \equiv r_{\rm c}. \tag{3.110}$$

We use the same length scale ξ_0 as in Eq. (3.82); ξ_0 can be now expressed as

$$\xi_0 = \frac{2\pi r_{\rm c}^2 \rho_0}{\Sigma_{\rm cr}}.$$

The corresponding dimensionless surface mass density is

$$k^{\rm pN}(x) = \frac{1}{2\sqrt{x^2 + x_{\rm c}^2}}, \tag{3.111}$$

where $x_{\rm c} = \xi_{\rm c}/\xi_0$. We have,

$$M^{\rm IS}(\xi) = \frac{\pi\sigma_{\rm v}^2}{G}\xi_{\rm c}\left\{\left[1 + \left(\frac{\xi}{\xi_{\rm c}}\right)^2\right]^{\frac{1}{2}} - 1\right\}, \tag{3.112}$$

or, in a dimensionless form,

$$m(x) = \sqrt{x^2 + x_{\rm c}^2} - x_{\rm c}; \tag{3.113}$$

without introducing a cut off radius, the total mass diverges.

The projected momentum of inertia is [181]

$$I_{\rm N}^{\rm IS}(\xi) = \frac{\pi\sigma_{\rm v}^2}{3G}\xi_{\rm c}^3\left\{2 + \left[\left(\frac{\xi}{\xi_{\rm c}}\right)^2 - 2\right]\left[1 + \left(\frac{\xi}{\xi_{\rm c}}\right)^2\right]^{\frac{1}{2}}\right\}. \tag{3.114}$$

3.6.1 Non-rotating sphere

Let us consider static spheres. The potential, as derived from Eq. (3.111), is

$$\psi^{\rm pN}(x) = \sqrt{x^2 + x_{\rm c}^2} - x_{\rm c} \ln[x_{\rm c} + \sqrt{x^2 + x_{\rm c}^2}] + \text{ const.} \tag{3.115}$$

where the constant depends on $x_{\rm c}$.

The convergence may or may not to be critical. Since $\frac{d}{dx}k^{\rm pN}(x) < 0$, multiple images can be produced only if

$$k^{\rm pN}(0) = \frac{1}{2x_{\rm c}} > 1,$$

that is, $x_{\rm c} < \frac{1}{2}$. This condition gives a relation between the dispersion velocity and the core radius,

$$\theta_{\rm c} < 2\pi \left(\frac{\sigma_{\rm v}}{c}\right)^2 \frac{D_{\rm ds}}{D_{\rm s}}; \tag{3.116}$$

in order to produce large arcs, a deflector must have a large velocity dispersion, i.e. a large mass, and a small core radius, well below the Einstein ring.

The tangential critical line is located at

$$x_{\rm t} = \sqrt{1 - 2x_{\rm c}}; \tag{3.117}$$

the radial critical line is at

$$x_{\rm r} = \left(\frac{x_{\rm c}}{2}\right)^{1/2} \sqrt{2 - x_{\rm c} - \sqrt{x_{\rm c}}\sqrt{4 + x_{\rm c}}}. \tag{3.118}$$

3.7 Power law models

Power law models can be considered as a generalization of the ISs [172], and are often adopted to model mass distribution in clusters of galaxies by lensing inversion [178]. They include models with smooth and non-singular matter distributions. The surface mass density is

$$\Sigma(\xi) = \Sigma_0 \frac{1 + p(\xi/\xi_{\rm c})^2}{[1 + (\xi/\xi_{\rm c})^2]^{2-p}}. \tag{3.119}$$

$\Sigma_0^{\rm PL}$ is the central surface mass density, $\xi_{\rm c}$ is the core radius, the slope parameter p determines the softness of the mass profile of the lens; for $\xi \gg \xi_{\rm c}$, $\Sigma \simeq \Sigma_0 p \xi^{2(p-1)}$. The total mass diverges, so that a sufficiently large cut-off radius must be introduced. Let us consider values $0 \le p \le 1/2$. For $p = 0$, the distribution is called a Plummer model; a power law model with $p = 1/2$ approximates the isothermal sphere at a large radius. It is [181],

$$M^{\rm PL}(\xi) = \pi \Sigma_0 \xi^2 \left[1 + \left(\frac{\xi}{\xi_{\rm c}}\right)^2\right]^{p-1}, \tag{3.120}$$

and

$$I_{\rm N}^{\rm PL}(\xi) = \frac{\pi\Sigma_0\xi_{\rm c}^4}{p(1+p)}\left\{\left[1+\left(\frac{\xi}{\xi_{\rm c}}\right)^2\right]^{p-1}\left[1+(1-p)\left(\frac{\xi}{\xi_{\rm c}}\right)^2+p^2\left(\frac{\xi}{\xi_{\rm c}}\right)^4\right]-1\right\}. \quad (3.121)$$

3.7.1 Non-rotating sphere

In what follows, we will consider non-rotating models. As a length scale, we choose $\xi_0 = \xi_{\rm c}$. The dimensionless surface mass density becomes

$$k^{\rm pN}(x) = k_0\frac{1+px^2}{(1+x^2)^{2-p}}; \quad (3.122)$$

from Eq. (3.21), we obtain the deflection potential

$$\psi^{\rm pN}(x) = \frac{k_0}{2p}\left[(1+x^2)^p-1\right], \quad p\neq 0, \quad (3.123)$$

which, in the limit $p\to 0$, reduces to

$$\psi^{\rm pN}(x) = \frac{k_0}{2}\ln(1+x^2), \quad p=0. \quad (3.124)$$

The lens equation reads

$$y = x-\alpha^{\rm pN}(x) = x-k_0\frac{x}{(1+x^2)^{1-p}}. \quad (3.125)$$

Roots must be found numerically.

For $k_0>1$, the tangential critical line is located at $x=x_{\rm t}$,

$$x_{\rm t} = \sqrt{k_0^{1/(1-p)}-1}; \quad (3.126)$$

the radial critical curve, $x=x_{\rm r}$, is determined by the equation,

$$1-k_0(1+x_{\rm r}^2)^{p-2}[1+(2p-1)x_{\rm r}^2] = 0. \quad (3.127)$$

which has analytical solutions for $x_{\rm r}$ only for $p=0$ e $p=1/2$, respectively,

$$\begin{aligned} x_{\rm r} &= \sqrt{\sqrt{2k_0+\frac{k_0^2}{4}}-1-\frac{k_0}{2}}, \quad (p=0),\\ x_{\rm r} &= \sqrt{k_0^{2/3}-1}, \quad (p=1/2). \end{aligned}$$

As can be numerically verified, $x_{\rm r}$ increases with k_0 and p [172]. The corresponding caustic in the light source plane is located at $\mid y(x_{\rm r})\mid = y_{\rm r}$, where

$$y_{\rm r} = \frac{2(1-p)x_{\rm r}^3}{1-(1-2p)x_{\rm r}^2}. \quad (3.128)$$

Sources with $\mid y\mid < y_{\rm r}$ have three images, sources with $\mid y\mid > y_{\rm r}$ have only one image. For $0<y<y_{\rm r}$, one image is of type I (located at $x>x_{\rm t}$), one image is of type II (located at $-x_{\rm t}<x<-x_{\rm r}$) and one image is of type III (located at $-x_{\rm r}<x<0$). The magnification of an image is

$$\mu^{\rm pN} = \left[1-\frac{k_0}{(1+x^2)^{1-p}}\right]^{-1}\left[1-\frac{k_0}{(1+x^2)^{2-p}}[1+(2p-1)x^2]\right]^{-1}. \quad (3.129)$$

3.8 The homogeneous sphere

Let us consider a homogeneous sphere of radius R and volume density ρ_0. It is [181]

$$\Sigma(\xi) = 2\rho_0\sqrt{R^2-\xi^2},\ \text{if}\ \xi \le R, \tag{3.130}$$

or $\Sigma(\xi) = 0$ elsewhere;

$$M(\xi) = M_{\rm TOT}\left\{1-\left[1-\left(\frac{\xi}{R}\right)^2\right]^{\frac{3}{2}}\right\},\ \text{if}\ \xi \le R, \tag{3.131}$$

or $M(\xi) = M_{\rm TOT}$ elsewhere, $M_{\rm TOT} \equiv \frac{4}{3}\pi R^3\rho_0$;

$$I_{\rm N}(\xi) = I_{\rm N}^{\rm TOT}\left\{1-\left[1-\left(\frac{\xi}{R}\right)^2\right]^{\frac{1}{2}}\left[1+\frac{1}{2}\left(\frac{\xi}{R}\right)^2-\frac{3}{2}\left(\frac{\xi}{R}\right)^4\right]\right\},\ \text{if}\ \xi \le R, \tag{3.132}$$

or $I_{\rm N}(\xi) = I_{\rm N}^{\rm TOT}$ elsewhere, $I_{\rm N}^{\rm TOT} \equiv \frac{8}{15}\pi R^5\rho_0$;

For light rays outside the lens, $\xi > R$, the deflection angle is

$$\hat{\alpha}_1(\xi,\theta) = \frac{4G}{c^2}\left\{\frac{M_{\rm TOT}}{\xi}\cos\theta + \frac{I_{\rm N}^{\rm TOT}}{\xi^2}\left(\frac{\omega_2}{c}\cos 2\theta - \frac{\omega_1}{c}\sin 2\theta\right)\right\}, \tag{3.133}$$

$$\hat{\alpha}_2(\xi,\theta) = \frac{4G}{c^2}\left\{\frac{M_{\rm TOT}}{\xi}\sin\theta + \frac{I_{\rm N}^{\rm TOT}}{\xi^2}\left(\frac{\omega_1}{c}\cos 2\theta + \frac{\omega_2}{c}\sin 2\theta\right)\right\}. \tag{3.134}$$

Let us consider a lens rotating about the ξ_2-axis ($\omega_1 = 0$, $\omega_2 = \omega$) and a light ray in the equatorial plane, $\theta = 0$. The deflection generated by the gravito-magnetic field is

$$\hat{\alpha}_{\rm GRM} = \frac{4G}{c^3}\frac{J}{\xi^2}. \tag{3.135}$$

The gravito-magnetic correction is significant if

$$\frac{I_{\rm N}^{\rm TOT}}{M_{\rm TOT}}\frac{\omega}{c\,\xi} = \frac{J}{M_{\rm TOT}\ c\,\xi} \gtrsim 10^{-3}, \tag{3.136}$$

where $J \equiv I_{\rm N}\times\omega$ is the angular momentum. To have a non-negligible gravito-magnetic effect, the angular momentum of the lens has to be non-negligible compared to the angular momentum of a particle of mass $M_{\rm TOT}$ and velocity c in a circular orbit of radius ξ around the rotation axis.

Let us change to dimensionless variables. As a natural length scale we introduce

$$\xi_0 = R_{\rm E} = \sqrt{\frac{4GM_{\rm TOT}}{c^2}\frac{D_{\rm d}D_{\rm ds}}{D_{\rm s}}}. \tag{3.137}$$

The scaled deflection angle inside the lens ($x \leq r$, where r is the lens radius in units of the scale length), for a lens rotating about the x_2-axis, becomes

$$\begin{aligned}
\alpha_1(x_1,x_2) &= \frac{x_1}{|x|^2}\left\{1-\left[1-\left(\frac{|x|}{r}\right)^2\right]^{\frac{3}{2}}\right\} \\
&- U\frac{x_1^2-x_2^2}{|x|^4}\left\{\left[1-\left(\frac{|x|}{r}\right)^2\right]^{\frac{3}{2}}\left[1+\frac{3}{2}\left(\frac{|x|}{r}\right)^2\right]-1\right\} \\
&- \frac{5}{2}U\frac{1}{r^2}\left[1+\frac{3}{2}\left(\frac{|x|}{r}\right)^2\right], \qquad (3.138)\\
\alpha_2(x_1,x_2) &= \frac{x_2}{|x|^2}\left\{1-\left[1-\left(\frac{|x|}{r}\right)^2\right]^{\frac{3}{2}}\right\} \qquad (3.139)\\
&- 2U\frac{x_1x_2}{|x|^4}\left\{\left[1-\left(\frac{|x|}{r}\right)^2\right]^{\frac{3}{2}}\left[1+\frac{3}{2}\left(\frac{|x|}{r}\right)^2\right]-1\right\},
\end{aligned}$$

where $U \equiv \frac{J}{cM_{\rm TOT}R_{\rm E}}$ is the ratio between the angular momentum of the lens and that of a particle of mass $M_{\rm TOT}$ and velocity c in a circular orbit at the Einstein radius.

Outside the lens radius ($x > r$), the scaled deflection angle reads

$$\begin{aligned}
\alpha_1(x_1,x_2) &= \frac{x_1}{|x|^2}+U\frac{x_1^2-x_2^2}{|x|^4}, \qquad (3.140)\\
\alpha_2(x_1,x_2) &= \frac{x_2}{|x|^2}+2U\frac{x_1x_2}{|x|^4}. \qquad (3.141)
\end{aligned}$$

The determinant of the Jacobian matrix is

$$\det A = 1-\frac{1}{|x|^4}-4U\frac{x_1}{|x|^6}-4U^2\frac{1}{|x|^6}. \qquad (3.142)$$

The deflection potential can be expressed as

$$\psi(x_1,x_2) = \ln|x| - U\frac{x_1}{x^2}. \qquad (3.143)$$

3.8.1 Non-rotating sphere

Let us first consider the non-rotating case, $U = 0$. The dimensionless surface mass density is

$$k^{\rm pN}(x) = \frac{3}{2}\frac{1}{r^2}\left[1-\left(\frac{x}{r}\right)^2\right]^{\frac{1}{2}}. \qquad (3.144)$$

The scaled deflection angles reduces to

$$\boldsymbol{\alpha}^{\rm pN}(\mathbf{x}) = \begin{cases} \frac{\mathbf{x}}{x^2}\left[1-\left(1-\left(\frac{x}{r}\right)^2\right)^{\frac{3}{2}}\right], & x<r \\ \frac{\mathbf{x}}{x^2}, & x\geq r \end{cases}. \qquad (3.145)$$

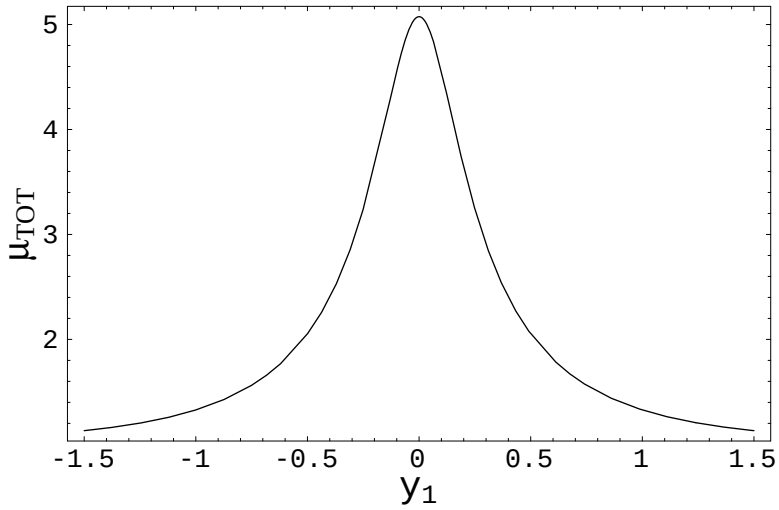

Figure 3.4: The Paczyński curve for a source moving with $y_2 = 0.2$.

Multiple images can be produced if $k^{\rm pN}(0) > 1$, i.e. $r < \sqrt{3/2}$. If $r < \sqrt{3/2}$, there are both a radial critical curve and a tangential critical curve. The radial critical curve is located at

$$x_{\rm r} = \frac{r}{2\sqrt{2}} \left[(48 - 32r^2 + r^8)^{\frac{1}{2}} - r^4 \right]^{1/2} . \tag{3.146}$$

If $r < 1$, the tangential curve is located at the Einstein radius, $x_{\rm t} = 1$; if $1 \leq r \leq \sqrt{3/2}$, it is

$$x_{\rm t} = \frac{r}{\sqrt{2}} \left[3 - r^4 - (r^2 - 1)^{3/2} (3 + r^2)^{1/2} \right]^{1/2} . \tag{3.147}$$

Point mass

Let us consider a point mass ($r = 0$) at the origin. This model is known as the Schwarzschild lens. The lensing quantities are like those of an homogeneous sphere, outside the radius. For a non rotating lens, the lens equation,

$$y = x - \frac{1}{x} \tag{3.148}$$

has two solutions

$$x_{\pm} = \frac{1}{2} \left(y \pm \sqrt{y^2 + 4} \right) ; \tag{3.149}$$

the lensed image x_+ lies outside the Einstein ring (on the same side of the source), while x_- is inside (on the side opposite the source). It is $x_+ + x_- = y$. The magnification is

$$\mu^{\rm pN} = \left(1 - \frac{1}{|x|^4} \right)^{-1} . \tag{3.150}$$

It is easy to verify that x_+ is a minimum and is magnified and x_- is a de-magnified saddle. As the light source moves to infinity $y \to \infty$, the lensed image x_+ goes

to infinity too and $\mu(x_+) \to 1$. The saddle image becomes dimmer and dimmer, $\mu(x_-) \to 0$, and it tends towards the point mass.

The difference in lensed image magnifications is the magnification of the unlensed light source, $|\mu(x_+)| - |\mu(x_-)| = 1$. The total magnification is the sum of the absolute values of the two magnifications. It can be expressed in terms of the source position as

$$\mu_{\rm TOT} = \mu(x_+) - \mu(x_-) = \frac{y^2+2}{y\sqrt{y^2+4}}. \tag{3.151}$$

When the source lies on the Einstein radius ($y = 1$), the total magnification becomes $\mu = 1.34$, corresponding to a brightening by 0.32 magnitudes.

Unless the lens is very massive ($M > 10^6 M_\odot$ for a cosmologically distant source), the angular separation of the two images is too small to be resolved and is is not possible to see the multiple images. However, a lensing event by a point mass can still be detected if the lens and the source move relative to each other, giving rise to lensing-induced time variability of the source [36, 75]. This kind of variability, when induced by stellar masses lens, is referred to as *microlensing*. Microlensing was first observed in the multiply-imaged quasar QSO 2237+0305 [92]. As first suggested by Paczyński [134], MACHOs in the galaxy can be searched monitoring millions of stars to look for a light magnification in a small fraction of the sources. The corresponding light curves, known as Paczyński curves, are described by the last term of Eq. (3.151). In Fig. (3.4), we plot the Paczyński curve for a source moving at $y_2 = 0.2$.

The time delay between the two images is

$$c\Delta T^{\rm pN} = \frac{4GM}{c^2}(1+z_{\rm d})\tau(y), \tag{3.152}$$

where

$$\tau(y) = \frac{y}{2}\sqrt{y^2+4} + \ln\frac{\sqrt{y^2+4}+y}{\sqrt{y^2+4}-y}. \tag{3.153}$$

If $y = 0$, the source appears as an infinitely magnified ring at the Einstein radius.

3.8.2 Perturbative analysis

To study how the positions of the images are perturbed by the gravito-magnetic term, we proceed as for the SIS case. Under the condition $U \ll 1$, we can obtain approximate solutions to the first-order in U, given by

$$\mathbf{x} \simeq \mathbf{x}_{(0)} + U\mathbf{x}_{(1)}, \tag{3.154}$$

where, again, $\mathbf{x}^{(0)}$ and $\mathbf{x}^{(1)}$ denote the zeroth-order solution and the correction to the first-order. Using the expressions for the unperturbed images, we obtain the first-order

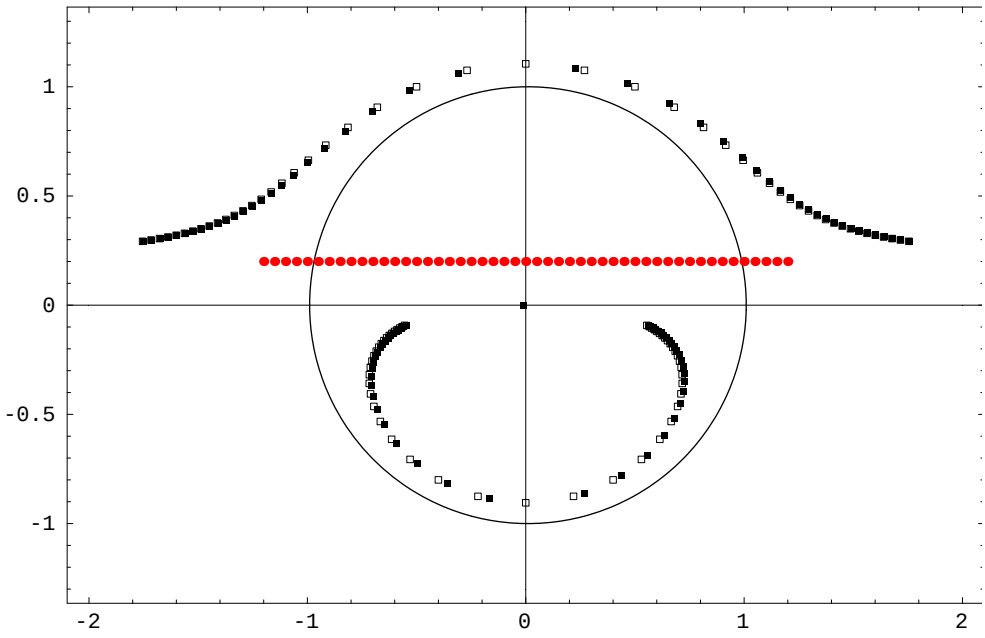

Figure 3.5: A source's track, $y_2 = 0.2$, and the corresponding images produced by a homogeneous rotating sphere. Grey circles indicates successive source positions. As the source moves, the centre of the coordinate-axes, the source (grey circle) and the two unperturbed images (empty boxes) lie on a straight line. For every source position, two images (filled boxes) are anticlockwisely rotated, about the centre, with respect to this line; a third image forms near the centre. The main critical curve is also plotted. It is $U = 10^{-2}$.

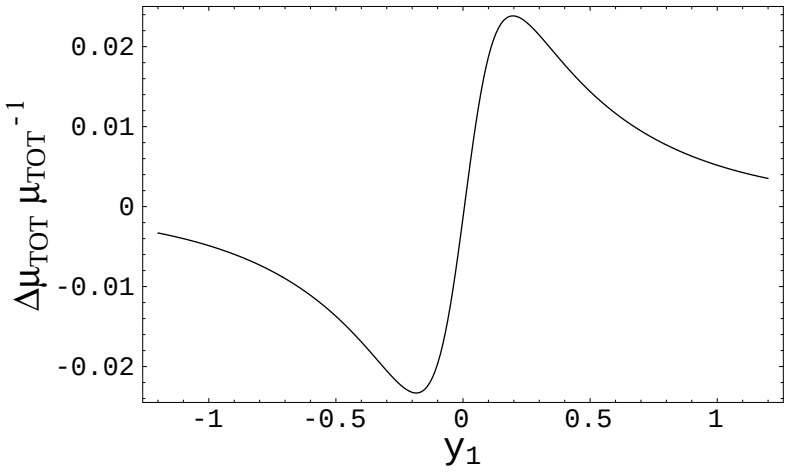

Figure 3.6: The relative variation in the total light amplification for a point source moving with $y_2 = 0.2$ with respect to the static case. It is $U = 10^{-2}$.

perturbation,

$$x_{(1)1} = \frac{x_{(0)2}^2 - x_{(0)1}^2 + 1}{x_{(0)}^4 - 1}, \tag{3.155}$$

$$x_{(1)2} = \frac{-2x_{(0)1}x_{(0)2}}{x_{(0)}^4 - 1}. \tag{3.156}$$

Together with these two perturbed images, a third, highly de-magnified image, is produced near the centre. When the source is at $(-U, 0)$, the third image is superimposed to the source. The corresponding magnification factor is $\sim U^4$. As can be numerically verified, for a large range of source positions, the third image forms near $(-U, 0)$.

The gravito-magnetic correction changes the number of critical curves: besides the main critical curve, which is a slight modification of the Einstein circle, a secondary critical curve forms. The equation for the main critical curve is

$$x_2(x_1) = \pm \left\{ -x_1^2 + \left[54U(U+x_1) + \sqrt{27}\sqrt{(108U(U+x_1))^2 - 1} \right]^{-\frac{1}{3}} \right. \tag{3.157}$$
$$\left. + \frac{1}{3}\left[54U(U+x_1) + \sqrt{27}\sqrt{(108U(U+x_1))^2 - 1} \right]^{\frac{1}{3}} \right\}$$
$$\simeq \pm \left\{ \sqrt{1-x_1^2} + U\frac{x_1}{\sqrt{1-x_1^2}} + U^2\frac{1-\frac{3}{2}x_1^2}{(1-x_1^2)^{3/2}} \right\}, \tag{3.158}$$

where the above approximate solution in Eq. (3.158) holds for $x_1 < 1$. The main critical curve intersects the x_1-axis in $x_1 \simeq -1 + U - \frac{3}{2}U^2$ and $x_1 \simeq 1 + U - \frac{3}{2}U^2$. The gravito-magnetic correction changes the width of the curve from 2 to $2(1 - \frac{3}{2}U^2)$. The maximum height is for $x_1 \simeq U$, when $x_2 \simeq \pm\left(1 + \frac{3}{2}U^2\right)$; the maximum total height changes to $\sim 2(1 + \frac{3}{2}U^2)$. So, the main critical curve is slightly compressed and its centre is shifted of U along the x_1-axis.

The main critical curve is mapped in a diamond-shaped caustic with four cusps. The main caustic is centred in $(y_1, y_2) = (U, 0)$ and its axes, parallel to the coordinate axes, are of semi-width $\sim 2U^2$.

A secondary critical curve forms. It is centred at $(x_1, x_2) = (-2U, 0)$, and has a width $\sim \mathcal{O}(U^3)$. It is mapped in a secondary caustic, far away from the central one, centred at $(y_1, y_2) \sim \left(\frac{1}{4U} - 2U \sim \frac{1}{4U}, 0\right)$.

A source moving inside a caustic changes the number of images from three to five. When a source is inside the main central caustic, four images form near the coordinate-axes, in a cross pattern; the fifth image forms near the centre. In Fig. (3.5), we plot the images of a source moving in the source plane. With respect to the non-rotating case, the images are rotated anti-clockwisely for $U > 0$.

Let us consider how the gravito-magnetic field perturbs the Paczyński curve. Numerically, we find that the maximum relative variation for a source moving parallelly

to the $\hat{y}_1$-axis, is $\sim \frac{1}{2}\left|\frac{U}{y_2}\right|$. In Fig. (3.6), we plot the relative variation in the total magnification, induced by a rotation with $U = 0.01$, for a source moving at $y_2 = 0.2$.

3.9 Point-mass in metric tensor theories

The simplicity of the point-like lens makes it possible a full treatment of its lensing properties in the general framework of metric tensor theories of gravity [180]. The Newtonian potential of a particle of mass M at the centre of the system of coordinates is

$$U = -G\frac{M}{|\mathbf{x}|}. \tag{3.159}$$

The lensing quantities, Eqs. (1.84,1.107), at the post-Newtonian order, reduce to

$$c\Delta T^{\rm pN}_{\rm pot} = -2(1+\gamma)(1+z_{\rm d})\frac{GM}{c^2}\ln\left(\frac{\xi}{\xi_0}\right), \tag{3.160}$$

and

$$\boldsymbol{\alpha}^{\rm pN}(\boldsymbol{\xi}) = 2(1+\gamma)\frac{GM}{c^2}\frac{\boldsymbol{\xi}}{\xi^2}. \tag{3.161}$$

The ppN correction is easily calculated. It is

$$\int_{observer}^{source} U^2 dl \simeq (GM)^2\int_{-\infty}^{+\infty}\frac{1}{\xi^2+l^2}dl = \pi\frac{(GM)^2}{\xi}. \tag{3.162}$$

Then,

$$c\Delta T^{\rm ppN}_{\rm pot} = \pi\left[\frac{3}{2} - \beta + \gamma\left(1-\frac{\gamma}{2}\right) + \frac{3}{4}\epsilon\right](1+z_{\rm d})\left(\frac{GM}{c^2}\right)^2\frac{1}{\xi}, \tag{3.163}$$

and

$$\boldsymbol{\alpha}^{\rm ppN}(\boldsymbol{\xi}) = \pi\left[\frac{3}{2} - \beta + \gamma\left(1-\frac{\gamma}{2}\right) + \frac{3}{4}\epsilon\right]\left(\frac{GM}{c^2}\right)^2\frac{\boldsymbol{\xi}}{\xi^3}. \tag{3.164}$$

As above remarked, since metric theories of gravity are classical non-quantized theories, the classical angular momentum of a particle goes to zero as its size goes to zero. In order to compare the effect of dragging of inertial frames on the deflection angle with the ppN contribution, we have to use the results for a finite homogeneous sphere. For a deflector rotating about the ξ_2-axis with angular momentum J, it is, outside the lens radius [181]

$$\alpha_1^{\rm GRM}(\xi,\theta) = \mu\frac{4G}{c^3}\frac{J}{\xi^2}\cos 2\theta, \tag{3.165}$$

$$\alpha_2^{\rm GRM}(\xi,\theta) = \mu\frac{4G}{c^3}\frac{J}{\xi^2}\sin 2\theta, \tag{3.166}$$

where ξ and θ are the polar coordinates in the lens plane. The gravito-magnetic field breaks the circular symmetry. Both the ppN and the gravito-magnetic contributions to the deflection angle decrease as ξ^{-2}.

The magnitudes of the different contributions to the deflection angle are considered by investigating real astrophysical systems acting as lenses. It is enough to use the values of the coefficients in general relativity, $\beta = \gamma = \epsilon = \mu = 1$. We will consider light rays in the equatorial plane ($\theta = 0$).

The post-Newtonian deflection angle for rays grazing the solar limb is 1.75 arcsec; $\alpha^{\rm ppN}$ is about 8 μarcsec, where the contribution of the non-standard ϵ coefficient is ~ 2 μarcsec. Given the angular momentum of the Sun, $J_\odot \simeq 1.6{\times}10^{48}$g cm^{2}s^{-1} [4], the gravito-magnetic correction is ~ 0.7 μarcsec. Very Long Baseline Interferometry (VLBI) has improved the accuracy of the measurements of the deflection of radio waves by the Sun to the milliarcsec level. This is not enough to measure the higher order ppN and gravito-magnetic contributions, so that the parameters β, ϵ and μ cannot be determined. However, strong constraints on γ can be put. It is $\gamma = 1.000 \pm 0.002$ [157], an impressive confirmation of the prediction by general relativity. In Brans-Dicke theory, this measurement constrains the ω parameter, $\omega \gtrsim 500$.

For an early type star, $J = 10^2 J_\odot \left(\frac{M}{M_\odot}\right)^{5/3}$ [106]. For $M = 1.4M_\odot$, $R = 1.1R_\odot$ and for a light ray grazing the star's limb, $\alpha^{\rm pN} \simeq 2.23$ arcsec, $\alpha^{\rm ppN} \simeq 13$ μarcsec, $\alpha^{\rm GRM} \simeq 0.10$ milliarcsec. The gravito-magnetic correction is $\sim 4{\times}10^{-3}\%$ of the zero order angle; it overwhelms the ppN one by an order of magnitude.

The gravito-magnetic field becomes even more significant for a fast rotating white dwarf, where $J \sim \sqrt{0.2GM^3R}$ [137]. For $M \sim M_\odot$, $R \sim 10^{-2}R_\odot$, $\xi \sim 6R$, $\alpha^{\rm pN} \simeq 29.2$ arcsec, $\alpha^{\rm ppN} \simeq 76$ μarcsec, $\alpha^{\rm GRM} \simeq 0.032$ arcsec. In this case, the gravito-magnetic correction is quite important. It is $\sim 0.1\%$ of the post-Newtonian term.

Now, we want to apply our approximation to a galaxy acting as a lens. We take $M = 10^{12}M_\odot$, $R \simeq 50$ kpc and $J \sim 0.1M_\odot$ kpc^{2}s^{-1}, as derived from numerical simulations [206]. It is $\alpha^{\rm pN} \simeq 0.80$ arcsec, $\alpha^{\rm ppN} \simeq 1.6$ μarcsec, $\alpha^{\rm GRM} \simeq 0.16$ milliarcsec. The gravito-magnetic correction overwhelms the ppN one by two orders of magnitude.

Chapter 4

Lensing by clusters of galaxies

Although the results listed in Section 1.8 are really compelling, it is still useful to develop new tools for the determination of the cosmological parameters. Many of the listed methods are affected by shortcomings, like poorly controlled systematic errors or large numbers of model parameters involved in the analysis. An independent constraint can improve the statistical significance of the statement about the geometry of the universe and can disentangle the degeneracy in the space of the cosmological parameters.

Gravitational lensing systems have been investigated as probes of dark energy. Gravitational lensing statistics [44, 208, 212, 228], effects of large-scale structure growth in weak lensing surveys [13] and Einstein rings in galaxy-quasar systems [68, 225] are very promising ways to test quintessence. Here, we investigate clusters of galaxies acting as lenses on background high redshift galaxies.

Clusters of galaxies are the largest gravitationally bound entities in the cosmos. They have the higher galaxy number density in the sky, with some hundreds up to a thousand galaxies. Several thousands of galaxy clusters are known today. Their masses can exceed $5\times10^{14}\mathrm{M}_{\odot}$, and their radii are typically 1.5 Mpc.

A hot, dilute plasma with temperature in the range $10^7 - 10^8$ K and density of 10^{-3} particles per cm^3 emits through thermal bremsstrahlung rendering the galaxy clusters the most luminous X-ray sources in the sky (10^{43}-10^{45} erg s^{-1}). Assuming that the intra-cluster gas is in hydrostatic equilibrium in the total gravitational potential, mass estimates can be derived from X-ray observations. Typical results agree up to a factor ~ 2 with the mass estimates from the kinematics of cluster galaxies based on the virial theorem.

The feasibility of clusters of galaxies, acting as lenses on background galaxies, to provide information on the universe is already known [23, 64, 69, 116, 117, 136]. Provided that the modeling of the lens is constrained, once both the position of a

critical line and the redshift of the corresponding source population are measured, it is possible to gain an insight into second-order cosmological parameters contained in angular diameter distances ratios [39, 74]. In addition to observations of arcs, a statistical approach based on magnification bias [25, 64, 121] can as well locate the critical lines (locations of maximum amplification) corresponding to background source populations.

In this Chapter, we will explore, following [178], the feasibility of clusters of galaxies in probing both the amount and the equation of state of quintessence in the universe. We assume general relativity holds and that the universe, assumed to be flat, expands according to the Friedmann's equations. We model the dark energy equation within the ansatz $w_{\rm X} = \text{const}$. These approximations have been discussed in Section 1.8.2.

The Chapter is as follows. In Section 1, we shortly review the lensing effects produced by a cluster of galaxies on background sources. In Sections 2 and 3, we discuss how the position of a critical line can be observationally detected. In Section 2, we shortly remember some features of the luminous giant arcs, highly elongated images of galaxies which form near critical curves. Section 3 discusses how the number density of background galaxies is affected by gravitational lensing; an analysis of a depletion curve, i.e. the radial variation in the surface number density, also allows to locate critical curves. In Section 4, we outline the method. Cosmological parameters enter the lens equation through the angular diameter distances. Once obtained independent information about the lensing system, some combinations of angular diameter distances can be determined. The method can help to distinguish between accelerating and decelerating models of the universe. Furthermore, since the position of critical lines is affected, especially in low-matter density universes, by the properties of quintessence, the observations of a suitable number of lensing clusters at intermediate redshifts can determine the equation of state. An application of the method to the cluster CL 0024+1654 is discussed in Section 5. It supports a flat accelerating universe dominated by dark energy. In Section 6, we discuss some systematics affecting the method.

4.1 Lensing regimes

The shape, brightness and number density of galaxies that are located behind clusters of galaxies are affected by the gravitational distortion of the massive galaxy cluster in the foreground. Three distinct modes of lensing phenomena are observed with clusters:

1. The strong regime. Rich centrally condensed clusters can occasionally produce giant luminous arcs, see Fig. (4.1), when a background galaxy happens to be aligned with one of the cluster's caustics. A fit to the observed images can be

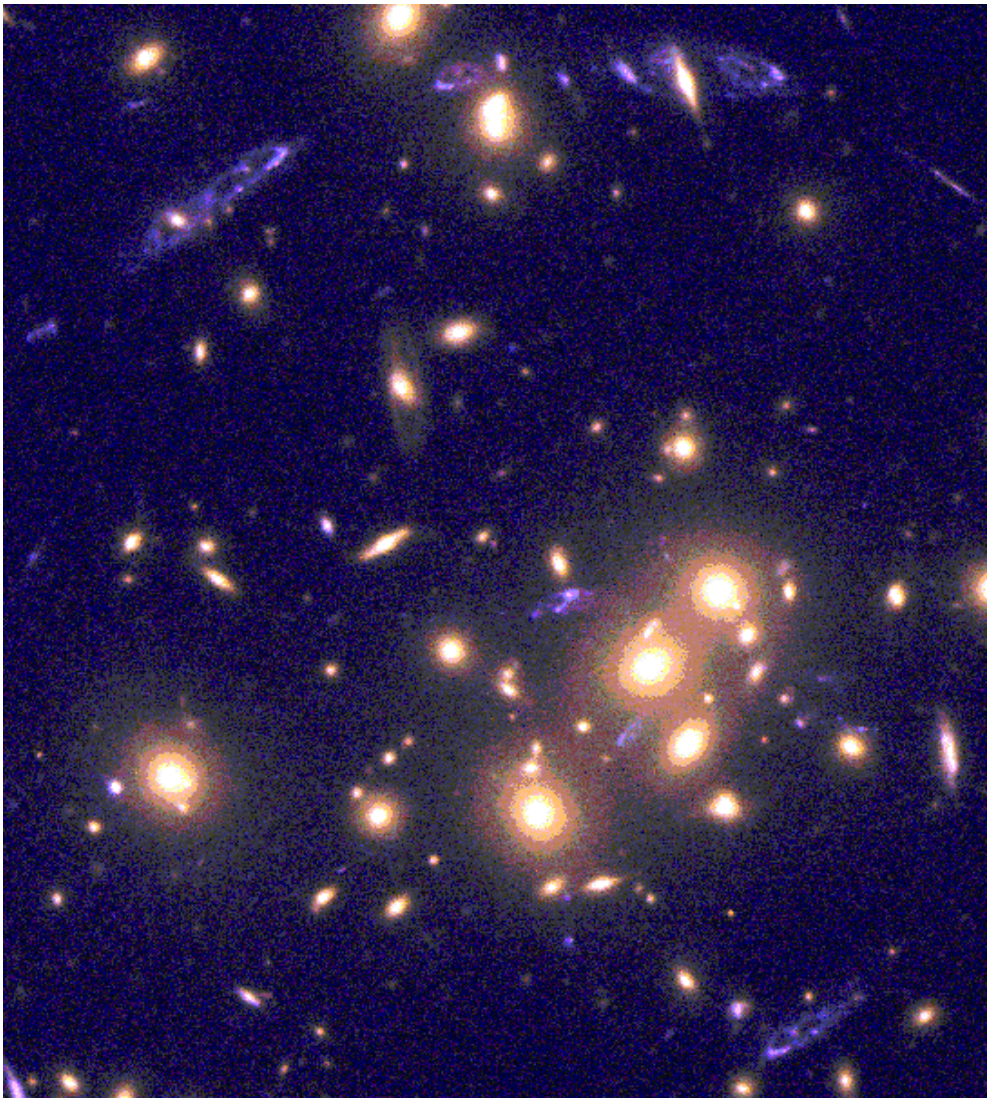

Figure 4.1: HST images of the galaxy cluster CL 0024+1654 with a multiple images of a blue background galaxy. From http://www.nasa.gov.

performed with a parameterized lens model.

2. Every cluster produces slightly distorted images of background galaxies, known as arclets [65, 201]. This phenomenon, referred to as weak lensing, acts on a large region of sky. The statistically coherent small deformation of the shape of the sources can be used to determine a parameter-free-two-dimensional mass map of the lensing cluster [95].

3. Number counts of background galaxies are depleted in the cluster centre. This effect provide a method for measuring the projected mass distribution of the lens, based solely on gravitational magnification of background population by the cluster gravitational potential.

Both observations in points 1 and 2 help to locate critical lines.

4.2 Giant luminous arcs

Rich clusters of galaxies at redshift beyond ~ 0.2 can be very effective lenses. In Fig. (4.1), one of the most spectacular systems of multiple arcs is represented. Einstein radii are, usually, of the order of 20 arcsec. Einstein rings can be produced only by lenses with spherical mass distribution in a perfect alignment with the source. However, intrinsic asymmetries and substructures increase the ability of clusters to produce arcs because they increase the shear and the number of cusps in caustics [142, 172]. The largest arcs, in fact, are formed from sources on cusp points, because three images of a source merge to form a curved arc. At the so called lips and beak-to-beak caustics similarly large arcs are formed [142, 172]. Sources on a fold caustic give rise to two images close to, and on the opposite sides, of the corresponding critical curve in the lens plane [142, 172]. They are elongated in the direction of their separation. When the source moves onto the caustic, a fusion of the two images occurs and a fairly straight, highly elongated image is produced.

4.3 Number density of images

Gravitational lensing by clusters of galaxies can affect the measured number counts of background galaxies [24, 25, 175]. This effect results from the competition between the gravitational magnification of faint sources above the observed magnitude limit (at least for marginally resolved objects) and the deviation of light beam towards the deflecting mass that spatially enlarge the observed area and thus decreases the apparent density of sources.

Let us assume a homogeneous distribution of the unlensed faint galaxies. Their number density $n_0(S, z)$, where S is the flux and z the redshift, can be expressed as

$$n_0(S, z) = p_z(z)F(S), \tag{4.1}$$

where $p_z(z)$ is the normalized redshift distribution and $F(S)$ is the distribution in flux. $n_0(S, z)$ is the intrinsic count in the absence of the lens, as can be obtained from counts in a nearby empty field. The factorization in Eq. (4.1) is not valid in general, but holds over a limited range of flux. However, since magnifications are large only in the very central parts of the cluster, Eq. (4.1) is applied over a quite small range. If Eq. (4.1) is not assumed, then the redshift distribution of sources locally will depend on the magnification.

The observed number density of galaxies with redshift z and flux larger than S is a function of the position. It is

$$n(>S,z,\boldsymbol{\theta}) = p_z(z)\frac{1}{|\mu(\boldsymbol{\theta},z)|}F\left(\frac{S}{|\mu(\boldsymbol{\theta},z)|}\right) \ ; \tag{4.2}$$

the factor $1/|\mu|$ account for the dilatation of the projected area. The total number density of galaxies with flux larger than S is obtained through integration in the redshift distribution,

$$n(>S,\boldsymbol{\theta}) = \int_0^\infty dz p_z(z)\frac{1}{|\mu(\boldsymbol{\theta},z)|}F\left(\frac{S}{|\mu(\boldsymbol{\theta},z)|}\right) \ . \tag{4.3}$$

If $F(>S) \propto S^{-\alpha}$, Then Eq. (4.3) becomes

$$n(>S,\boldsymbol{\theta}) = n_0(>S)\int_0^\infty dz p_z(z)|\mu(\boldsymbol{\theta},z)|^{\alpha-1} \equiv n_0(>S)\langle|\mu(\boldsymbol{\theta},z)|^{\alpha-1}\rangle_z. \tag{4.4}$$

From Eq. (4.4), we see that the number density does not change if $\alpha = 1$; in regions of magnification ($|\mu| > 1$), the number density increases (decreases) for $\alpha > 1$ ($\alpha < 1$) Averaging Eq. (4.4) over the data field $\mathcal{U}$, we obtain

$$\langle n(>S,\boldsymbol{\theta})\rangle_{\mathcal{U}} \equiv \frac{1}{U}\int_{\mathcal{U}} n(>S,\boldsymbol{\theta})d^2\theta = n_0(>S)\langle|\mu(\boldsymbol{\theta},z)|^{\alpha-1}\rangle_{z,\mathcal{U}}, \tag{4.5}$$

where U is the area of the data field. The ratio of the number of observed galaxies in the field $\mathcal{U}$ to the number $U\times n_0(>S)$ which would be observed in the absence of gravitational lensing gives $\langle|\mu(\boldsymbol{\theta},z)|^{\alpha-1}\rangle_{z,\mathcal{U}}$. $\langle|\mu(\boldsymbol{\theta},z)|\rangle_z$ is a local observable only given the ansatz in Eq. (4.1) with $F(>S) \propto S^{-\alpha}$. Without these assumptions, the observable quantity is, in general, a different one. Galaxy counting can give both local information, Eq. (4.4), or global information, Eq. (4.5), on the data field.

The above relations can be expressed in terms of the magnitude m of a source,

$$m = -2.5\log_{10} S + cost.$$

For a single source redshift, Eq. (4.4) becomes

$$n(<m,\boldsymbol{\theta},z) = n_0(<m)|\mu(\boldsymbol{\theta},z)|^{2.5\zeta-1} \ , \tag{4.6}$$

with ζ slope of the intrinsic counting of galaxies

$$\zeta \equiv \frac{d\log n(<m,z)}{dm} = \frac{\alpha}{2.5} \ . \tag{4.7}$$

With our hypotheses,

$$\frac{d\log n_0}{dm} = \frac{d\log n}{dm} \ .$$

The critical value $\alpha = 1$ corresponds to $\zeta = 0.4$.

The number density $n_0(>S)$ is regarded as an universal function and has been measured in several colours down to very faint magnitudes. For the counts in B at $26 < B < 27.5$, it is $\zeta_B = 0.17 \pm 0.02$ [64, 199]. I-galaxies at $24 < I < 26.5$ have $\zeta_I = 0.25 \pm 0.03$ [64, 186].

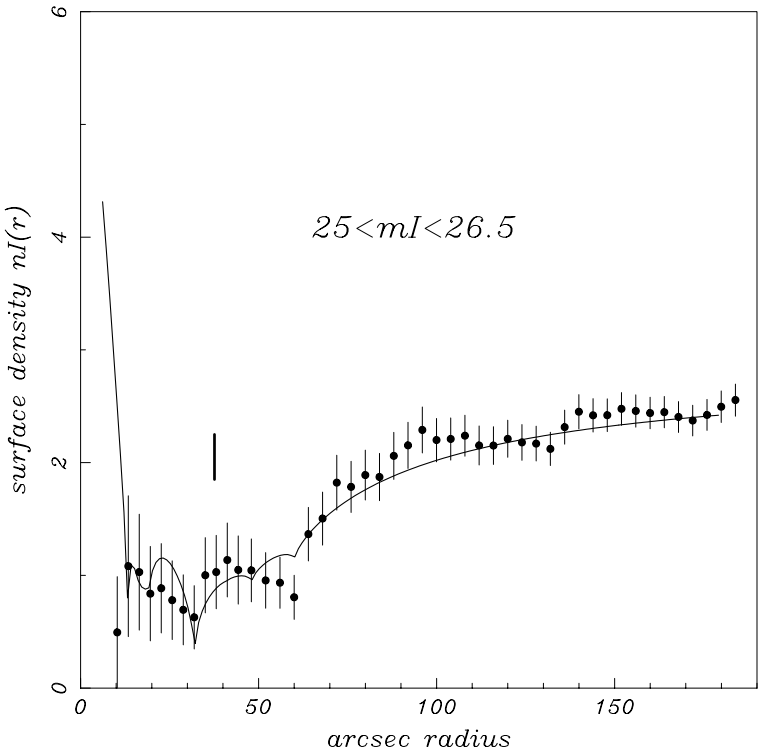

Figure 4.2: Depletion curve obtained in CL 0024+1654 in the range $25 < mI < 26.5$ for the I-selected galaxies. The data are the filled circles with error bars. A depletion, ending at $R_I = 60$ arcsec, is detected . The full line shows a fit. From [64].

4.3.1 Depletion curves

The depletion curve is the variation along the radial direction in the surface density of background galaxies around a massive cluster of galaxies. When $\zeta < 0.4$, a decrease of the number of galaxies is expected in region of magnification. The effect is maximum at the critical radius. In general, the critical radius increases with the redshift of the background sources. Galaxies at different redshift will show different radial depletion curves, with their minima deferring by an amount which depends on the respective locations of the critical curves. The overall depletion curve results from the superimposition of the depletion curves of galaxies at different redshift; the sharp minimum is replaced by a plateau ranging from the critical line of the lower redshift population to the critical line of the larger redshift one, see Fig. (4.2).

Let us consider a non rotating singular isothermal sphere (SIS) as a deflector. The projected density mass Σ of the SIS is, in angular variables, see Section (3.5),

$$\Sigma(\theta) = \frac{\sigma_{\rm v}^2}{2G}\frac{1}{D_{\rm d}\theta}, \tag{4.8}$$

where $\sigma_{\rm v}$ is the velocity dispersion and θ the angular position in the sky. The magni-

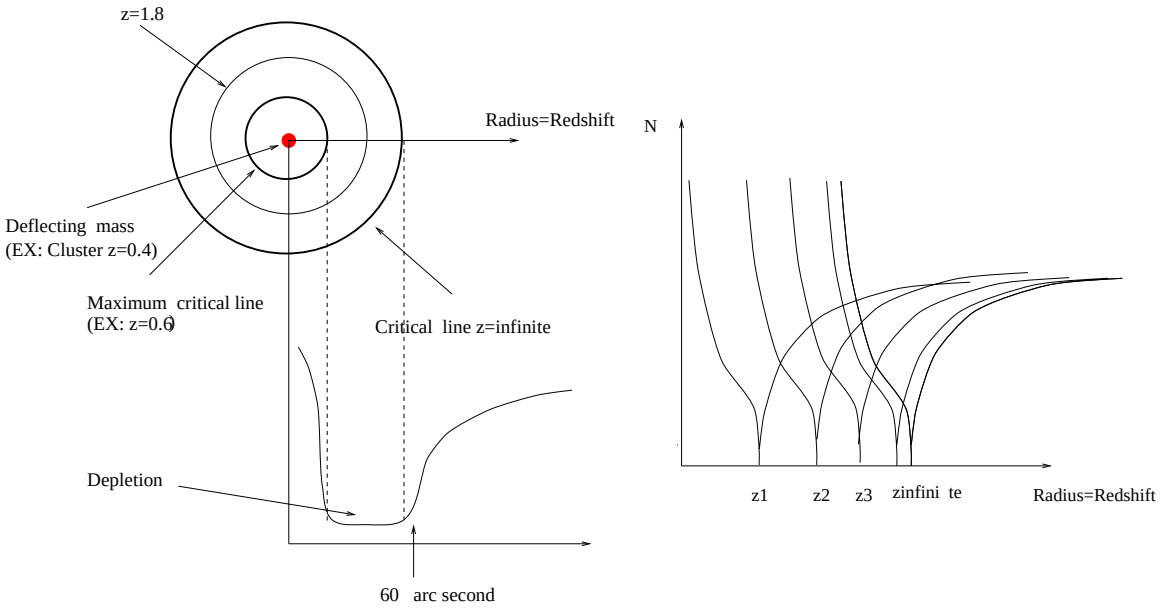

Figure 4.3: The left panel shows the depletion by a SIS. The top left panel shows the locations of the critical line for different source redshifts and the right panel shows the corresponding depletion curves. The bottom left panel is the overall depletion curve. A plateau appears instead of a single peaked minimum . From [122].

fication is

$$|\mu| = \left| \frac{\theta}{\theta - \theta_t} \right|, \tag{4.9}$$

where θ_t is the angular radius of the tangential critical curve. The depletion curve, see Fig. (4.3), turns out

$$n(\theta) = n_0 \left| 1 - \frac{\theta_{\rm t}}{\theta} \right|^{1-2.5\zeta_1} . \tag{4.10}$$

When $\zeta_1 < 0.4$, the number density vanishes at the critical radius $\theta_{\rm t}$, whereas, at large distances, it goes to n_0; in the very inner parts of the cluster ($\theta < \theta_{\rm t}$), the number of galaxies is increased.

A population source with $\zeta_2 > 0.4$ has an opposite behaviour. Let us compare its properties with those of a population with $\zeta_1 < 0.4$. We consider the ratio R,

$$R \equiv \frac{n_2(< m, \boldsymbol{\theta})}{n_1(< m, \boldsymbol{\theta})} = R_0 |\mu|^{2.5(\zeta_2 - \zeta_1)}(\boldsymbol{\theta}, z). \tag{4.11}$$

An example of population of type 2 are the bluest galaxies, $\zeta_B \approx 0.5$, whereas faint red source population have $\zeta_R \approx 0.15$ [24]. Near the tangential critical curve, the region where giant luminous arcs are formed, the ratio in Eq. (4.11) between blue and red galaxies is maximum: usually giant arcs are blue. On the other hand, in the inner region of a cluster, the colour of the de-magnified galaxies will be red.

We remind that the slope of the distribution in magnitude, $\zeta(< m, z)$, is an increasing function of the redshift [25].

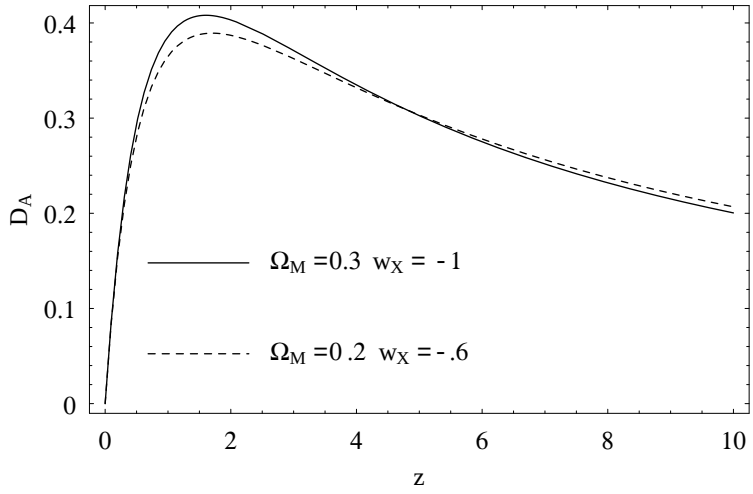

Figure 4.4: The angular diameter distance for two different flat, homogeneous FLRW universes. It is $z_{\rm d} = 0$. The distance is in units of c/H_0.

4.4 How critical lines depend on dark energy

The study of critical lines in a gravitational lensing system is a potentially important tool to probe the content of dark energy in the universe and to constrain its equation of state, as already shown in the case of galaxy-quasar lensing in [68, 225]. This type of cosmological investigations requires an accurate modeling of the lens, the observation of a critical line and the knowledge of the redshifts of both the lens and the deflected source [23, 64, 116].

For a spherically symmetric non rotating lens, the tangential critical line is determined by Eq. (3.34),

$$\theta_{\rm t} = \sqrt{\frac{4GM(\theta_{\rm t})}{c^2}\frac{D_{\rm ds}}{D_{\rm d}D_{\rm s}}}, \tag{4.12}$$

where c is the velocity of the light and $M(\theta)$ is the lens mass within the radius θ. As an example for our quantitative considerations, let us consider again as deflecting cluster a SIS. For the SIS, Eq. (4.12) reduces to

$$\theta_{\rm t} = 4\pi\left(\frac{\sigma_{\rm v}}{c}\right)^2\frac{D_{\rm ds}}{D_{\rm s}}. \tag{4.13}$$

Once $\theta_{\rm t}$ and $\sigma_{\rm v}$ are known, the ratio of distances $D_{\rm ds}/D_{\rm s}$ can be determined.

As seen in Chapter 1, the dependence on the cosmological parameters is contained in the angular diameter distance. In a flat FLRW universe, the angular diameter distance between an observer at $z_{\rm d}$ and a source at $z_{\rm s}$ is

$$D(z_{\rm d}, z_{\rm s}) = \frac{c}{H_0}\frac{1}{1+z_{\rm s}}\int_{z_{\rm d}}^{z_{\rm s}}\frac{dz}{\sqrt{\Omega_{\rm M0}(1+z)^3 + (1-\Omega_{\rm M0})(1+z)^{3(w_{\rm X}+1)}}}. \tag{4.14}$$

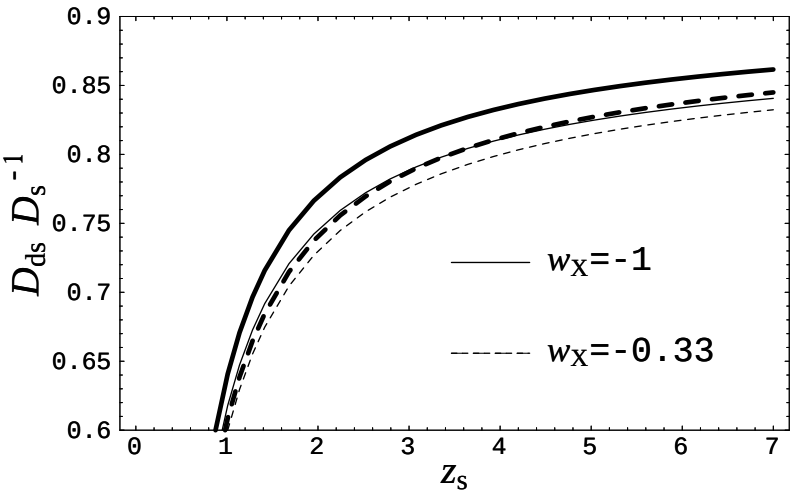

Figure 4.5: The ratio of distances $D_{\rm ds}/D_{\rm s}$ as a function of the source redshift for a deflector at $z_{\rm d} = 0.3$, for different sets of cosmological parameters. The thick lines correspond to $\Omega_{\rm M0} = 0.3$; the thin lines to $\Omega_{\rm M0} = 0.5$. The full and dashed lines correspond to, respectively, $w_{\rm X} = -1$ and $w_{\rm X} = -1/3$.

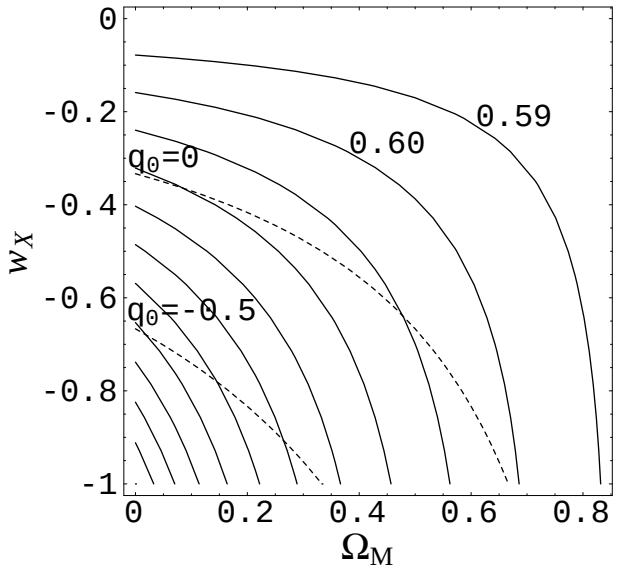

Figure 4.6: Contours of equal $D_{\rm ds}/D_{\rm s}$ on the $(\Omega_{\rm M0}, w_{\rm X})$ plane for $z_{\rm d} = 0.3$ and $z_{\rm s} = 1$. Each contour is drawn with a step of 0.01. The value of the contours increases from the top right corner to the bottom left corner. The thin dashed lines correspond to lines of constant q_0.

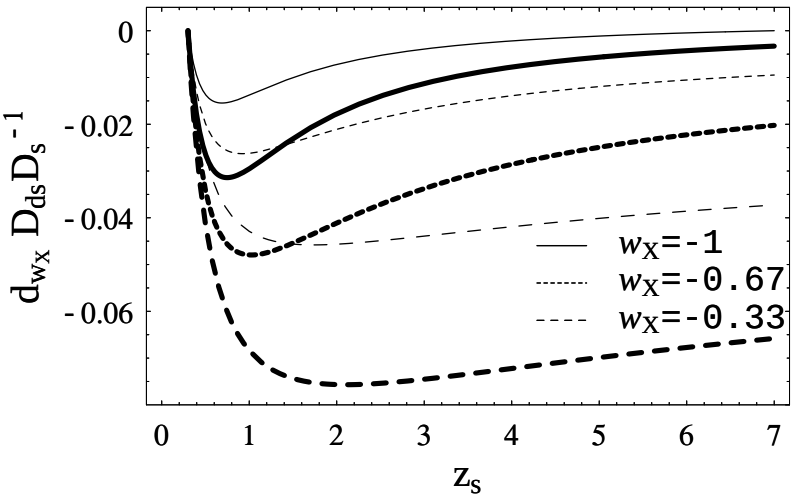

Figure 4.7: The derivative of the ratio of distances $D_{\rm ds}/D_{\rm s}$ with respect to $w_{\rm X}$ for a lens at $z_{\rm d} = 0.3$ as a function of the source redshift, for different values of the equation of state. The full lines correspond to $w_{\rm X} = -1$; the dashed lines to $w_{\rm X} = -2/3$; the long-dashed lines to $w_{\rm X} = -1/3$. The thick (thin) lines are for $\Omega_{\rm M0} = 0.3(0.5)$.

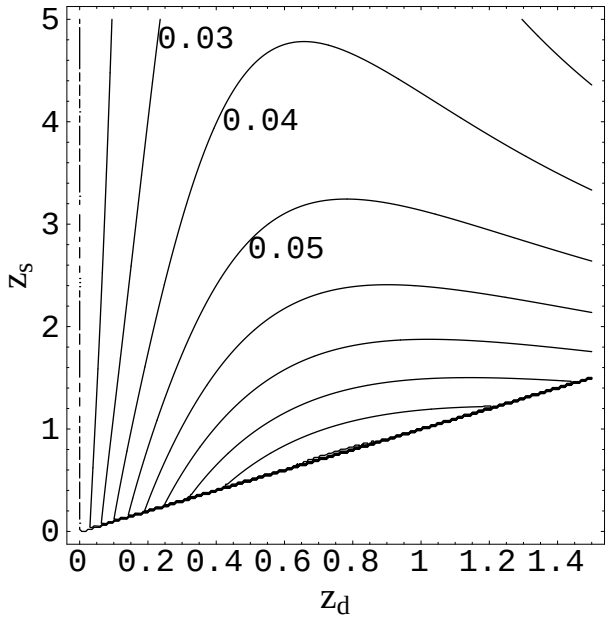

Figure 4.8: The relative variation between the ratio of distances $D_{\rm ds}/D_{\rm s}$ for two cosmological models, $(\Omega_{\rm M0} = 0.3, w_{\rm X} = -1)$ and $(\Omega_{\rm M0} = 0.3, w_{\rm X} = -1/3)$, in the $(z_{\rm d}, z_{\rm s})$ plane. Each contour is drawn with a step of 0.01.

At high redshift, the pressureless matter density overcomes the dark energy; for large $z_{\rm d}$ and small $w_{\rm X}$, $D_{\rm ds}$ is nearly insensitive to the equation of state. In Fig. (4.4), we plot the angular diameter distance in two flat FLRW universes.

Let us go, now, to examine the feasibility of determining $w_{\rm X}$ with observations of strong lensing events in clusters of galaxies by the study of the ratio of distances $D_{\rm ds}/D_{\rm s}$. Once the lens redshift is fixed, $D_{\rm ds}/D_{\rm s}$ first increases rapidly with the source redshift and, then, for $z_{\rm s}$ greater than 2.5, is nearly constant [5, 64], as can be seen in Fig. (4.5). The change with the cosmological parameters can be significant. The ratio increases with decreasing $\Omega_{\rm M0}$ and with dark energy with large negative pressure, i.e. it is maximum in the case of the cosmological constant. The variations with $\Omega_{\rm M0}$ and $w_{\rm X}$ are comparable. Changing $\Omega_{\rm M0}$ from 0.3 to 0.5 has the same effect of increasing $w_{\rm X}$ from -1 to $-1/3$, so that $D_{\rm ds}/D_{\rm s}$ is nearly indistinguishable in a universe with $\Omega_{\rm M0} = 0.3$ filled in with string networks and in a model with $\Omega_{\rm M0} = 0.5$ and cosmological constant.

To quantify the dependence of $D_{\rm ds}/D_{\rm s}$ with the cosmological parameters, we consider fixed redshifts for the lens and the source, see Fig. (4.6). The ratio is quite sensitive to $\Omega_{\rm M0}$. The variations due to changes in $\Omega_{\rm M0}$ for $w_{\rm X} = $ const. are greater than in the case of the constant deceleration parameter $q_0 \equiv (1 + 3w_{\rm X}(1 - \Omega_{\rm M0}))/2$. For $z_{\rm d} = 0.3$, $z_{\rm s} = 1$, and $\Omega_{\rm M0}$ ranging from 0 to 0.6, when $q_0 = 0$ the variation is $\sim 4\%$; when $w_{\rm X} = -1$, the variation is $\sim 15\%$. The dependence on the cosmological parameters is maximum for high negative values of q_0, i.e. the region today preferred by observations. For some particular pairs $(z_{\rm d}, z_{\rm s})$, i.e. for low lens redshifts and sources very near to the deflector, the ratio is nearly constant on lines of constant deceleration parameters; these properties suggest that the method of the critical line can help to distinguish between accelerating and decelerating universes. The dependence of $D_{\rm ds}/D_{\rm s}$ on the equation of state increases for low matter density universes and the sensitivity nearly doubles for small changes in $\Omega_{\rm M0}$: for $z_{\rm d} = 0.3$ and $z_{\rm s} = 1$, the relative variation from $w_{\rm X} = -1$ to $w_{\rm X} = -1/3$ is 1.9% (3.4%) when $\Omega_{\rm M0} = 0.5$ (0.3). The sensitivity is maximum for intermediate $w_{\rm X}$; for large negative pressure ($w_{\rm X} \lesssim -0.9$), the ratio is nearly independent of variations of the equation of state.

In Fig. (4.7), the derivative of the ratio $D_{\rm ds}/D_{\rm s}$ with respect to $w_{\rm X}$ is plotted as a function of the redshift of the source once the redshift of the deflector is fixed. The derivative is negative for a large range of redshifts of both source and deflector. Transitions from negative to positive values occur for very negative $w_{\rm X}$. The source redshift where the derivative cancels out decreases with increasing $\Omega_{\rm M0}$ and $z_{\rm d}$: for $z_{\rm d} = 0.3$ (0.6), $\Omega_{\rm M0} = 0.3$ and $w_{\rm X} = -1$, the derivative is null at $z_{\rm s} \simeq 7.0$ (2.1). The sign of the derivative determines when the equation of state changes as the angular position of the critical lines moves: when the derivative is negative (positive), as the equation of state increases (i.e. as $w_{\rm X}$ moves from -1 to 0), the angular radius in the sky of the critical line, for fixed source and deflector redshifts, decreases (increases).

The modulus of the derivative is an estimate of the dependence of the ratio on $w_{\rm X}$. Independently of the value of $z_{\rm d}$, $\Omega_{\rm M0}$ and $w_{\rm X}$, the dependence on $w_{\rm X}$ first increases and takes its maximum at an intermediate source redshift, and then decreases quite slowly. For dark energy in the form of a cosmological constant ($w_{\rm X} = -1$), $z_{\rm d} = 0.3$ and $\Omega_{\rm M0} = 0.3$, the maximum is at $z_{\rm s} \sim 0.75$. For increasing $w_{\rm X}$, the maximum moves to higher redshifts: for domain walls ($w_{\rm X} = -2/3$), the maximum is at $z_{\rm s} \sim 1.02$. From Fig. (4.7), we see that for a large range of $w_{\rm X}$ and $\Omega_{\rm M0}$ the maximum is at $z_{\rm s} \lesssim 2$. This trend of the derivative is connected to the properties of the ratio $D_{\rm ds}/D_{\rm s}$, that flattens at higher source redshifts.

Now, we want to search for the optimal lens and source configuration in order to discriminate among quintessence models. For illustration, we choose two universes with the same content of matter ($\Omega_{\rm M0} = 0.3$) but different $w_{\rm X}$; we consider a cosmological constant ($w_{\rm X} = -1$) and string networks ($w_{\rm X} = -1/3$). In Fig. (4.8), we scan the $(z_{\rm d}, z_{\rm s})$ plane plotting the relative variation between the two pairs of cosmological parameters. For a given lens redshift, the best $z_{\rm s}$ is very close to the deflector, i.e. a couple of redshifts corresponding to the rising part of the ratio $D_{\rm ds}/D_{\rm s}$; the sensitivity decreases for larger and larger source redshifts. So, the configurations with high sensitivity to the quintessence are those with very low cross section for strong lensing events. On the other hand, given a background population at $z_{\rm s} \gtrsim 1$, the optimal lens is a quite high redshift cluster at $z_{\rm d} \sim 0.7$; however, the dependence on the quintessence is nearly constant for lenses at $z_{\rm d} \gtrsim 0.6$

In order to estimate the accuracy of the determination of the equation of state, the variation induced on $D_{\rm ds}/D_{\rm s}$ by $w_{\rm X}$ must be compared to the error within which the parameters of the lens are known. For the SIS, the error in the estimate of the ratio of distances is

$$\left|\Delta\left(\frac{D_{\rm ds}}{D_{\rm s}}\right)\right| = \sqrt{4\left|\frac{\Delta\sigma_{\rm v}}{\sigma_{\rm v}}\right|^2 + \left|\frac{\Delta\theta_{\rm t}}{\theta_{\rm t}}\right|^2}\left|\frac{D_{\rm ds}}{D_{\rm s}}\right|, \tag{4.15}$$

where $\Delta\sigma_{\rm v}$ and $\Delta\theta_{\rm t}$ are the errors, respectively, on the velocity dispersion and $\theta_{\rm t}$. Usually, the largest uncertainty in the modeling of a lens comes from the error in the measurement of the velocity dispersion. Catalogues of galaxy velocities in lensing clusters are of the order of 50, so that the uncertainty on $\sigma_{\rm v}$ is $\sim 15\%$. $\Delta\theta_{\rm t}$ comes from the accuracy of the location of the arc and its radial thickness and from the uncertainty on the geometrical properties of the lens, i.e. the accuracy of the location of the centre, typically chosen to coincide with the brightest cluster galaxy, and the ellipticity of the mass distribution. For tangential arcs at $\theta_{\rm t} \sim 20$ arcsec [222], an error as large as ~ 1 arcsec can contribute a 5% error. The error on $\theta_{\rm t}$ is generally negligible with respect to the error in the mass normalization and will not be considered in the rest of this section. The variation on $D_{\rm ds}/D_{\rm s}$ connected to changes in the equation of

state can be expressed as

$$\left|\frac{\partial}{\partial w_{\rm X}}\left(\frac{D_{\rm ds}}{D_{\rm s}}\right)\right|\Delta w_{\rm X}, \tag{4.16}$$

and so, comparing Eq. (4.15) and Eq. (4.16), for N clusters we have a statistical error of

$$\begin{aligned}\Delta w_{\rm X} &\gtrsim \frac{2}{\sqrt{N}}\left|\frac{\Delta\sigma_{\rm v}}{\sigma_{\rm v}}\right|\left\langle\left|\frac{D_{\rm ds}}{D_{\rm s}}\right|\left|\frac{\partial}{\partial w_{\rm X}}\left(\frac{D_{\rm ds}}{D_{\rm s}}\right)\right|^{-1}\right\rangle \\ &= \frac{2}{\sqrt{N}}\left|\frac{\Delta\sigma_{\rm v}}{\sigma_{\rm v}}\right|\left\langle\left|\frac{\partial}{\partial w_{\rm X}}\ln\left(\frac{D_{\rm ds}}{D_{\rm s}}\right)\right|^{-1}\right\rangle,\end{aligned} \tag{4.17}$$

where the average is on the redshifts of the critical lines. The error in the determination of $w_{\rm X}$ increases with $\Delta\sigma_{\rm v}$ and decreases with the derivative. Since the error induced by the velocity dispersion is proportional to the ratio of distances $D_{\rm ds}/D_{\rm s}$, see Eq. (4.15), and the variation induced by $w_{\rm X}$ is proportional to the derivative, see Eq. (4.16), the uncertainty in the estimate of $w_{\rm X}$ is inversely proportional to the logarithmic derivative of $D_{\rm ds}/D_{\rm s}$, i.e. to the relative variation of $D_{\rm ds}/D_{\rm s}$. The properties of the logarithmic derivative with respect to the cosmological parameters $\Omega_{\rm M0}$ and $w_{\rm X}$ are the same of the ordinary derivative; the main difference is the disappearance of the minimum. As we have seen before, the uncertainty in the equation of state, given a deflector redshift, increases with $z_{\rm s}$ and decreases for quintessence with $w_{\rm X}$ far away from -1.

The case of the cosmological constant is the more problematic one since the derivative can cancel out (when $\Omega_{\rm M0}=0.3$ and $z_{\rm s}=1.5$, the derivative is null at $z_{\rm d}\simeq 1.13$). However, clusters at intermediate redshift ($z_{\rm d}\sim 0.4$) are quite stable with respect to the error in the equation of state.

As we shall see in the next section, it is possible to obtain information from a single cluster of galaxies on more than one critical line. So, using in Eq. (4.17) the number N of clusters, the lower limit on $\Delta w_{\rm X}$ is overestimated. Given a typical error of $\sim 15\%$ on $\sigma_{\rm v}$, we can use Eq. (4.17) to estimate the number of deflectors necessary for estimating $w_{\rm X}$ within a given uncertainty. For mean redshifts of $\langle z_{\rm d}\rangle = 0.4$ and $\langle z_{\rm s}\rangle = 1.2$, an uncertainty of $\Delta w_{\rm X}\simeq 0.25$ needs ~ 75 (~ 120) lensing clusters in a universe with $\Omega_{\rm M0}=0.3$ and $w_{\rm X}=-1/3$ (-0.5). N increases with dark energy with large negative pressure and large values of $\Omega_{\rm M0}$. As discussed, the method is unable to constrain the equation of state in the extreme case of a cosmological constant, when $\Delta w_{\rm X}\simeq 0.25$ needs ~ 800 clusters and $\Delta w_{\rm X}\simeq 0.5$ needs ~ 200 clusters. In general, to distinguish dark energy with an intermediate value of $w_{\rm X}$ from a cosmological constant at 95% confidence level, in a low matter density universe, we need 100-200 strong lensing events. These simple estimates are in agreement with the results in [225].

Together with spectroscopic analyses, X-ray observations of a lensing cluster can help to estimate the absolute mass of the deflector. The projected X-ray cluster mass, under the hypotheses of isothermal and hydrostatic equilibrium, is proportional to the

cluster gas temperature, $T_{\rm X}$, and $D_{\rm d}$ [223]: X-ray data alone cannot determine the mass without a prior knowledge of cosmological parameters. However, it has been shown that the relation between $\sigma_{\rm v}$ and $T_{\rm X}$ is not affected by cosmic evolution and is consistent with the isothermal scenario, $\sigma_{\rm v} \propto T_{\rm X}^{0.5}$ [224]. Once calibrated this relation, X-ray observations obtained with the new generation of telescopes can considerably enlarge the data sample of lensing clusters with known mass and help to disentangle the effect of cosmology and mass normalization of the deflector.

4.5 CL 0024+1654

Now, let us consider the application of the method outlined in Section 4.4 to a well studied cluster of galaxies, CL 0024+1654, in order to test the feasibility of what we are proposing, and how good the results can be.

CL 0024+1654, see Fig. (4.1), is one of the best investigated lenses in the universe. It is an optically rich cluster of galaxies, with a relaxed structure without a single central dominant cluster galaxy, at $z = 0.395$ and with a velocity dispersion of $\sigma_{\rm v} = 1050\pm75$ km s^{-1} [46, 47, 51]. This is the formal velocity dispersion estimated with the assumptions of virial equilibrium and random galaxy velocities, so that the reported error is a purely statistical one. We will consider the effect of some possible systematics in the next section. This value of $\sigma_{\rm v}$ is consistent with lensing observations [185]. X-ray data [17, 189] also support a regular morphology with no significant substructures. The measured value of $T_{\rm X} = 5.7^{+4.9}_{-2.1}$ is compatible with the observed velocity dispersion. A single background galaxy behind CL 0024+1654, at spectroscopic redshift $z = 1.675$ [26], is imaged in a well known multiple arc at $\theta_{\rm t} = 30.5$ arcsec [101, 187, 200, 209]. Images are characterized by a bright elongated knot, surrounded by a low surface brightness halo, see Fig. (4.1). The knot comprises two peaks, with separations ranging from 0.5 arcsec to 1.1 arcsec, roughly consistent with the relative lengths of the various arc components [187]. Given this peculiar morphology, we assume an indetermination on the critical radius $\Delta\theta_{\rm t} \sim 0.7$ arcsec. We do not take into account the error on the position of the centre; in the analyses considered here, it is determined as a free parameter in the lensing reconstruction. Based on deep images with the Hubble Space Telescope, Tyson et al. [200] performed a multi-parameter fit, including a number of small deflecting "mascons", to the mass profile. Each mascon was parameterized with a power-law model, see Section 3.7,

$$\Sigma(\theta) \propto \frac{1 + p\left(\frac{\theta}{\theta_{\rm c}}\right)^2}{\left[1 + \left(\frac{\theta}{\theta_{\rm c}}\right)^2\right]^{2-p}} \ , \tag{4.18}$$

where $\theta_{\rm c}$ is the core radius and p is the slope. Remarkably, they found that more than 98% of the cluster matter is well represented by a single power-law model centred

near the brightest cluster galaxies with $\theta_c = 10.0 \pm 0.9$ arcsec and $p = 0.57 \pm 0.02$, slightly shallower than an isothermal sphere ($p_{SIS} = 0.5$). To disentangle the effect of cosmology and absolute mass, we have to fix the central density Σ_0 independently of lensing data. It is [18],

$$\Sigma_0 = \frac{8\alpha\sigma_v^2}{3\pi G\theta_c}\frac{I^2_{(1+\alpha)/2}}{I_\alpha}\frac{1}{D_d}, \tag{4.19}$$

with $\alpha = 2(1-p)$ and $I_\beta = \int_0^\infty (1+u^2)^{-\beta} du$. For a power-law model, the angular position θ_t of the tangential critical line is related to the angular diameter distances and the parameters of the lens by

$$\left(\frac{\theta_t}{\theta_c}\right)^2 = \left(\frac{4\pi G}{c^2}\Sigma_0\frac{D_d D_{ds}}{D_s}\right)^{\frac{1}{1-p}} - 1. \tag{4.20}$$

Substituting in Eq. (4.20) for Σ_0 and using the fit parameters, we get an estimate for the ratio D_{ds}/D_s. It is

$$\frac{D_{ds}}{D_s}(z_d = 0.395, z_s = 1.675) = 0.76^{+0.18}_{-0.12}. \tag{4.21}$$

The main term in the error budget comes from the indetermination in the velocity dispersion which contributes $\sim 75\%$ of the total error. In Fig. (4.9), we show the dependence of D_{ds}/D_s on the cosmological parameters for a lens-source configuration as in CL 0024+1654; the values of (Ω_{M0}, w_X) compatible with the estimate in Eq. (4.21) are also plotted. Low matter density universes ($\Omega_{M0} \lesssim 0.55$), which are accelerating their expansion, are favoured. We find $-1 \leq w_X \lesssim -0.2$, with the lower values of Ω_{M0} corresponding to the higher values of the equation of state.

The method of the depletion curves, i.e. the variation along the radial direction in the surface density of background galaxies around a massive cluster of galaxies, has been employed to further study CL 0024+1654 [52, 64, 158, 203]. Observations of the magnification bias have been obtained in the B- and I-band [64] and in the U- and R-band [52, 158]. Extrapolating Hubble Space Telescope data to their detection limit, Dye et al. [52] obtained, for the background R-galaxies, a mean redshift of $\langle z_s \rangle = 1.2 \pm 0.3$. From a fit to the SIS profile of the depletion curve in the R-band, the location of the critical curve comes out at 15 ± 10 arcsec [52]. Using these estimates in Eq. (4.13), we can obtain a second constraint on the ratio D_{ds}/D_s; unfortunately, as can be seen in Fig. (4.10), the uncertainties completely hide the second order effect of the cosmological parameters on the ratio of distances D_{ds}/D_s.

A more interesting result can be obtained from the I-band, see Fig. (4.2). As discussed in [64], the angular radius where the depletion curve starts to increase locates the last critical line, that is the critical line corresponding to the farther source population. The last critical line at ~ 60 arcsec in the I-band corresponds to background galaxies at redshift $2.5 < z < 6.5$; however, about 20% of the very faint I selected

galaxies should be above $z = 4$. As noted in [203], given the very low density of the background I-galaxies, an appropriate radial binning to study the radial profile of the magnification bias is 30 arcsec. So, we will consider an error of 15 arcsec. This estimate of the location of the last critical line is independent of the assumed mass profile, and can be used in Eq. (4.20) to obtain a new constraint on $D_{\rm ds}/D_{\rm s}$, see Fig. (4.10). Since $D_{\rm ds}/D_{\rm s}$ is nearly flat for $z_{\rm s} \gtrsim 2.5$, the value of the ratio of distances is quite insensitive to the value of $z_{\rm s}$ corresponding to the last critical line.

Some interesting considerations are obtained from the variation of the ratio $D_{\rm ds}/D_{\rm s}$ with the redshift of the source. Figure (4.10) shows $D_{\rm ds}/D_{\rm s}$ for a lens at $z = 0.395$ and for various cosmological models. Models without dark energy are rejected, with no regard to the value of the pressureless matter density: both open ($\Omega_{\rm M0} < 1$) and flat (the Einstein-de Sitter model, with $\Omega_{\rm M0} = 1$) dark matter models are very poorly consistent with the experimental points. On the other hand, flat universes with quintessence are in agreement with the data. In particular, the data from the I-band analysis are marginally compatible (at the 68% confidence level) with a flat de Sitter universe ($\Omega_{\rm X0} = 1$ and $w_{\rm X} = -1$). Given the large uncertainties, we cannot draw definitive conclusions on this multi-band analysis. However, even if the data from the R-galaxies do not give information on the cosmology, the data from the multiple arc and the last critical line in the I-band prefer accelerating universes with subcritical matter density.

4.6 Systematics

In the previous section, we performed a statistical analysis based on the data found in the literature. We want now to address some systematics that can affect our results. A very accurate knowledge of the mass distribution of the lens is required to put meaningful constraints on cosmological parameters. One of the more important source of indetermination comes from the modeling of the mass profile of the lens [39]. In Eq. (4.15), we have considered only the error coming from a not very accurate mass normalization but, in general, we have also to face the indetermination on the cluster mass profile. As a general feature, the three-dimensional mass density of a clump, ρ, is proportional to a typical length scale, r_s, so that, with respect to the angular diameter distance, $\rho \propto D_{\rm d}^{-2}$. The mass enclosed within an angular radius θ comes out

$$M(\theta) \propto D_{\rm d}\sigma_{\rm v}^2\mathcal{P}\theta,$$

where $D_{\rm d}$ contains the cosmological dependence and $\sigma_{\rm v}^2$ stands for an overall normalization. $\mathcal{P}$ is a factor accounting for the deviations of the cluster mass profile from the SIS; $\mathcal{P}$ is a function of θ and of some parameters, such as a core radius. Substituting

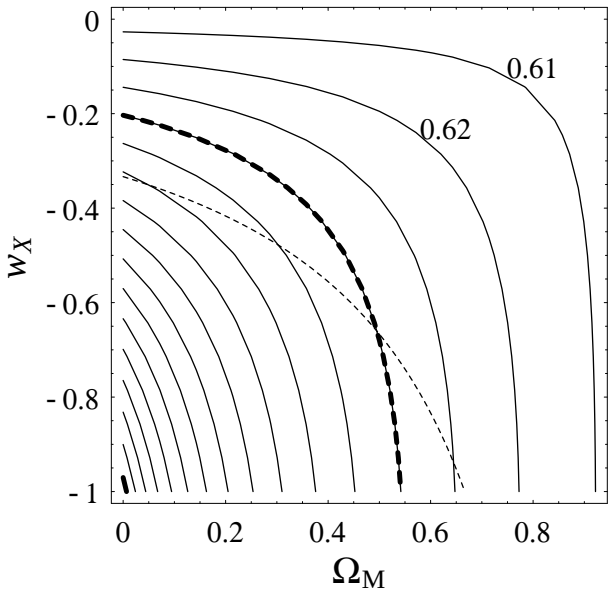

Figure 4.9: Contours of equal D_{ds}/D_s on the (Ω_{M0}, w_X) plane for CL 0024+1654 ($z_d = 0.395$) and its multiple arc ($z_s = 1.675$). Each contour is drawn with a step of 0.01. The value of the contours increases form 0.61 in the top right corner to 0.76 in the lower left corner. The thick lines correspond to the data in Eq. (4.21). The thick full line corresponds to the best parameters; the dashed one to the lower limit. The thin dashed line separates accelerating universes (below) from decelerating ones (above).

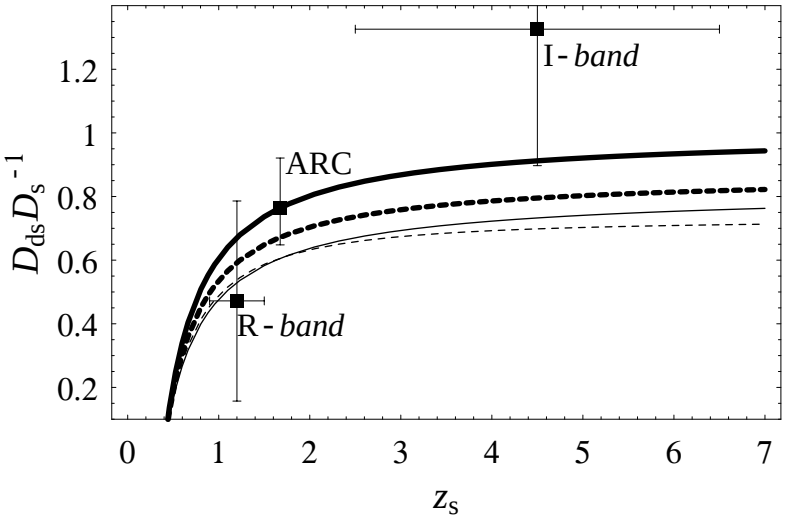

Figure 4.10: D_{ds}/D_s as a function of the source redshift for CL 0024+1654 ($z_d = 0.395$) for different cosmological models. The thick lines are for flat models with quintessence. The full thick line for $\Omega_{X0} = 1$ and $w_X = -1$ (de Sitter universe); the dashing thick line is for $\Omega_{M0} = 0.3$ and $w_X = -1$. The thin lines are for universes with pressureless matter alone. The full line is for an Einstein-de Sitter universe ($\Omega_{M0} = 1$); the thin dashed line is for an open universe ($\Omega_{M0} = 0.1$). "R-*band*" indicates the data derived from [52] (the error in σ_v is not considered); "ARC" is the data in Eq. (4.21); "I-*band*" indicates the data from the depletion curve in [64].

in Eq. (4.13), we get, for a spherically symmetric lens,

$$\frac{D_{\rm ds}}{D_{\rm s}} \propto \frac{\theta_{\rm t}}{\sigma_{\rm v}^2 \mathcal{P}}.$$

To consider the uncertainty in the profile, we have to add in quadrature to the right hand side of Eq. (4.15) an additional relative error of $\Delta\mathcal{P}/\mathcal{P}$. Usually, the main contribution to the error budget comes from the mass normalization but, in some extreme cases, the indetermination in the mass profile can be of the same order. $\Delta\mathcal{P}$ is maximum when calculated between a lens with a soft core and a halo with a singular density steeply rising towards the centre, as predicted by numerical simulations in the standard cold dark matter framework of structure formation and approximated by a Navarro-Frenk-White profile (NFW, [129, 130]).

A NFW model can match the mass distribution of CL 0024+1654 [26]. The required mass inside the arc's radius for such a model, reproducing the projected mass distribution outside the core radius, is 40% higher than the prediction of a power-law model [200]. Without an independent information, $\Delta\mathcal{P}$ would be a really large error. Fortunately, the NFW profile is discarded since it implies a velocity dispersion much higher than the measured value [185]. Once we can discard models with singular central density, the indetermination in the model can be accounted for by the errors within which we constrain the parameters of the mass profile (Δp and $\Delta\theta_{\rm c}$ in the power-law model used in Sect. 4.5). In general, an uncertainty in the cluster mass profile can significantly weaken the results on the cosmological parameters; but, in the case of CL 0024+1654, the degeneracy in the fit is not the main error.

Together with the overall mass profile, sub-structures must be considered. In the case of a lens with a rather regular morphology, even if a "not correct" potential shape is used in the reconstruction or the contribution of small sub-structures is neglected, the cosmological parameters are still retrieved, although with larger errors [74]. On the contrary, neglecting a sub-structure as large as 20% of the total mass in a bimodal cluster completely hides the effect of cosmology [74]. Adding the contribution of individual galaxy masses is also useful to tighten the confidence levels and can become critical in some extreme cases, as a galaxy strongly perturbing the location of multiple-images [74]. Deep imaging of CL 0024+1654 has made it possible to construct a high-resolution map of the projected mass distribution of the cluster and to take into account the effect of perturbing galaxies. The perturbing potentials of two galaxies near the middle segment of the arc have been considered in [101, 209]. Tyson et al. [200] assigned one or more mascons to each of the 118 cluster galaxies and 25 free mascons for the remaining cluster mass. However, all these studies in literature agree on a overall representation as the one in Eq. (4.18).

Some features in the 3-D space, as a possible merger scenario, can invalidate our estimation of the cosmological parameters. A recent analysis of the distribution of the

galaxies in the redshift space [46, 47] suggests a fairly complicated structure. A group of galaxies lying just in front of the main cluster could be the result of a high speed collision of two smaller clusters with a merger axis very nearly parallel to the line of sight [47]. In particular, a bulk velocity component present in the central velocity distribution would over-estimate the mass obtained from the formal central velocity dispersion. Furthermore, galaxies at large projected distance from the centre are also affected by the collision and cannot be used to derive $\sigma_{\rm v}$ [47]. The consequences on the dark energy constraint are quite dramatic since such a scenario could entail a systematic error on the estimation of the velocity dispersion of the same order of the statistical one. As can be seen from Fig. (4.9), this additional error would completely hide any dependencies on the cosmological parameters.

Even if, together with strong lensing observations, both a weak lensing analysis out to 10 arcmin [18] and X-ray observations [17, 189] favour a regular morphology, the points just discussed suggest caution in the interpretation of the results obtained in the previous section.

Chapter 5

Distances in the inhomogeneous universe

Light propagation through an inhomogeneous universe differs from that through a homogeneous one. The gravitational fields of inhomogeneities deflect and distort light bundles. The effect of gravitational lensing results in the appearance of shear and convergence in images of distant sources according to the different amount and distribution of matter along different lines of sight. As a consequence, cosmic distances in a locally inhomogeneous universe differ from those in a really smooth universe. In fact, light bundles, propagating far from clumps, experience a matter density less than the average matter density of the universe.

There is no known exact metric for a general relativistic universe that is homogeneous and isotropic on average, but includes density inhomogeneities. Owing to this lack, the framework of *on average Friedmann-Lemaître-Robertson-Walker (FLRW) models* is usually adopted. It is assumed that the relations on a large scale are the same of the corresponding FLRW universe, while inhomogeneities only affect local phenomena like the propagation of light. The so called *smoothness parameters* represent, in a phenomenological way, the magnification effect experienced by the light beam, that is the effective fraction of pressure and energy density in the beam connecting the observer and the source.

The importance of measurements of distances in cosmography makes necessary a complete study of all systematics. Observations of supernovae (SNe) of Type Ia are one of the main evidences of the acceleration of the universe's expansion. Observational data are taken in the inhomogeneous universe and sources most likely appear to be de-magnified relative to the standard Hubble diagram. The effect of amplification dispersion by gravitational lensing must be accurately considered.

In this Chapter, mainly based on [182, 183], we investigate the properties of cos-

mological distances in a locally inhomogeneous universe with pressureless matter and dark energy with constant equation of state, $w_{\rm X} = \text{const}$. In Section 1, we discuss the Hubble diagram and comment on some cosmological sources which have been explored to build the diagram. In particular, we present candidate standard candles, such as supernovae of type Ia, and other sources proposed as standard rods. Section 2 introduces the on average FLRW universes. In this framework, the gravitational lens equation is a powerful tool to study the properties of the cosmological distances. We first discuss as the angular diameter distance changes in presence of an intervening lens. Then we introduce the multiple lens-plane theory and show as the distance–redshift equation, known as generalized Dyer-Roeder (DR) equation, can be derived without referring to the focusing equation. In Section 3, we list exact solutions for angular diameter distances in a universe with a not specified value of the curvature. The case of only dark matter and of dark energy in the form of either a cosmological constant or topological defects of dimension one or two have been solved. The case of a flat universe is considered in Section 4, where we derive the general solution of the generalized DR equation in the case of homogeneous dark energy in terms of hypergeometric functions; the two extreme cases of both dark matter and dark energy homogeneously distributed or totally clumped are also treated. In Section 5, we show how the general framework of on average FLRW models makes distances degenerate with respect different cosmological parameters. Section 6 discusses how this degeneracy influences the critical redshift where the angular diameter distance takes its maximum.

Since the amplification of a source at a given redshift has a statistical nature, the smoothness parameters are direction-dependent. A dispersion in the observed flux of a standard candle must be considered. In Section 7, we discuss the main features of the magnification probability distribution function (pdf), such as a mode biased towards de-amplified values and a long tail towards large magnifications, and its dependence on the equation of state of the quintessence. We consider both microscopic and macroscopic dark matter. From the properties of the angular diameter distance in a clumpy universe, it follows that, with no regard to the nature of the dark matter, the dispersion increases with the redshift and is maximum for dark energy with very large negative pressure, being maximum for the case of the cosmological constant. In Section 8, the degenerate effects on the lensing dispersion of microscopic dark matter and quintessence with an intermediate $w_{\rm X}$, which both partially attenuate the effect of the clumpiness, are considered. The extraction of cosmological parameters from the Hubble diagram is the argument of Section 9. The noise due to gravitational lensing strongly affects the determination of the cosmological parameters. The effect is of the same order of the other systematics affecting observations of supernovae of type Ia.

5.1 The Hubble diagram

The Hubble diagram is the plot of the redshift of an object versus cosmological distance to it or viceversa. It is built by means of standard candles (rods), i.e. fictitious objects of constant luminosity (geometrical size) for which apparent magnitude (angular diameter) is directly related to the luminosity (angular diameter) distance.

By observationally identifying a cosmological source with the properties of a standard candle, it is possible to draw the Hubble diagram with very high precision and estimate the global cosmological parameters. Observations of standard sources at intermediate redshifts are sensitive to the deceleration parameter q_0.

Since in a generic space-time, the angular diameter distance $D_{\rm A}$ and the luminosity distance $D_{\rm L}$ are related by the Etherington's principle, $D_{\rm L} = (1+z)^2 D_{\rm A}$, see Section (1.5), in what follows we will switch between $D_{\rm A}$ and $D_{\rm L}$.

5.1.1 Supernovae

Supernovae (SNe) are the only individual objects that can be seen in distant galaxies. They are classified in two types [137, 138]. Type I SNe are explosions triggered by accretion in a binary system. They do not display absorption and emission lines of hydrogen but reveal the presence of other elements, with atomic masses ranging from helium through iron. The absence of hydrogen is understandable from the fact that progenitors are highly evolved stars that have lost almost all their hydrogen before the explosion.

Type I SNe are further divided in two varieties. Type Ia SNe are homogeneous in their properties. The mass of a white dwarf, accreted from a companion star, crosses the Chandrasekhar limit and explodes. Since the Chandrasekhar mass is a nearly universal quantity, the resulting thermonuclear explosions are of nearly constant luminosity. Their light curves present a characteristic rise to maximum, followed by a symmetric fall over roughly 30 days, after which the light decay becomes less rapid. Type Ib SNe also lack hydrogen lines but do not have any characteristic light curve. However, all SNe Ia show similar rates of decline of their brightness after the phase of maximum light. After 20 days, the rate is approximately 0.065 ± 0.007 mag day^{-1}; after ~ 50 days, the dimming rate slows and becomes 0.01 mag day^{-1}.

The SNe II do show hydrogen; they are associated with massive stars at the endpoint of their evolution, and are rather heterogeneous in their properties.

During the last years, two independent groups, the High-z SuperNova Search Team [171] and the Supernova Cosmology Project [140] have performed a strong effort in building the Hubble diagram with SNe of type Ia [156, 140].

SNe Ia are very luminous (of absolute magnitude ~ -19.5, typically comparable to the brightness of the entire host galaxy in which they appear) and have a small intrinsic dispersion in their peak absolute magnitude, $\delta M \lesssim 0.3$ [63]. These features make them an impressive candidate to be the long expected standard candles for cosmology.

An analysis of some parameters of the light curve makes it possible to further reduce the dispersion. SNe, where relative distances are known by some other independent methods, show as the height of the light curve (apparent luminosity at maximum light) and the width (time taken to reach maximum light, or equivalent measures) are correlated: the maximum output scales as roughly the 1.7 power of the characteristic timescale [143]. This relation is presumably based on the mass of the progenitor star. A more massive star generates a more energetic explosion, but the resulting fireball has to expand for longer in order for photons to escape, i.e. for the optical depth to reach unity. Given a good data sample, a dispersion of 0.17 mag in the peak magnitudes of SNe Ia, after the application of methods based on this considerations such as the "multi-colour light curve" method [155], can be achieved.

Evolutionary uncertainty should not affect SNe data since the laws of stellar evolution should be the same at all distances.

5.1.2 Other sources

Astrophysical sources other than SNe have been long investigated to draw the Hubble diagram. Modified standard rods, as compact radio sources [80, 102] or double radio galaxies [27, 77], have been used to evaluate the angular diameter distance to cosmological sources.

Extended radio sources which include the twin radio lobes surrounding a radio galaxy can have sizes ranging from a few Kpc to ~ 1000 Kpc. Classical double radio sources, in particular FR IIb radio sources, have been proposed as modified standard yardsticks [77]. They are characterized by a typical size that predicts the lobe-lobe separation at the end of the source lifetime. A comparison between an individual source and the properties of the parent population at the source redshift allows to built a standard rod.

Compact radio jets associated with quasars and active galactic nuclei (AGN) have also been considered as standard rods. They are typically less than a hundred parsec in extent [80, 102]. Their morphology and kinematics probably depends more on the nature of their central engine, controlled by a limited number of physical parameters (mass of the central black holes, the strength of the magnetic field..) confined within restricted ranges, than on the surrounding intergalactic medium. Furthermore, since compact radio jets have typical ages of only some tens of years, they are very young compared to the age of the universe, at any reasonable redshift. Therefore, compact

radio sources may be considered an evolution free sample. Usually, the characteristic angular size of these sources is defined as the distance between the strongest component (core) and the most distant component which has a peak brightness greater than or equal to 2% of the peak brightness of the core [102].

A recent proposal to estimate cosmological distances is based on Gamma-Ray Bursts (GRBs). Two independent luminosity estimators, the first one based on the variability of GRBs [153, 154] and the second one derived from the time lag between peaks in hard and soft energies [132], have been proposed to infer the luminosity distance to these sources. The physical origin of GRBs is still uncertain, but recent observations suggest that they are related to the violent death of massive stars. Under the hypothesis that GRBs trace the global star formation history of the universe, their assumed rate is strongly dependent on the expected evolution of the star formation rate with the redshift [146].

With no regard to their different physical origins, all these observations are affected by gravitational lensing of the sources.

5.2 The generalized Dyer-Roeder equation

The standard Hubble diagram is usually computed with relations that hold in FLRW models, that is assuming all gravitating energy density homogeneously distributed. Instead, observational data are taken in the inhomogeneous universe.

In general, both dark matter and quintessence are inhomogeneous. The observed matter content of the universe appears to be homogeneously distributed only on a large scale ($\gtrsim$ 500 Mpc), while the propagation of light is a local phenomena. A scalar field is not an ideal adiabatic fluid and the sound speed in it varies with the wavelength in such a way that high frequency modes remain stable still when $w_{\rm X} < 0$ [29, 76]. Moreover, smoothness is gauge dependent, and so a fluctuating inhomogeneous energy component is naturally defined [29]. Inhomogeneities, both in quintessence and CDM, make the relations for the distances derived in FLRW models not immediately applicable to the interpretation of experimental data both in measurements of luminosity distances and angular diameter distances.

Several attempts have addressed the problem of the redshift dependence of the distance in a clumpy universe: by relaxing the hypothesis of homogeneity and using the Tolman-Bondi metric instead of the RW one [35]; by quantifying the small deviations from the isotropy and homogeneity of the Ricci scalar [195]; by considering a local void [194]. In lack of a really satisfactory exact solution for inhomogeneous universes in the framework of general relativity [107], the usual, very simple framework we shall adopt for the study of distances is the *on average FLRW universe* [172, 176],

where: *i)* the relations on a large scale are the same of the corresponding FLRW universe; *ii)* the anisotropic distortion of the bundle of light rays contributed by external inhomogeneities is not significant.

A simple way to account for this scenario is to introduce the so called *smoothness parameters* α_i, each one describing the degree of homogeneity of the i-th component. In a phenomenological way, they represent the magnification effect experienced by the light beam [193, 213]: only a fraction α_i of the energy density and pressure of the i-th component contributes to the isotropic focusing of the bundle. In general, the smoothness parameters are redshift dependent since the degree of smoothness evolves with time.

Sources most likely appears to be de-magnified relative to the standard Hubble diagram. In fact, light bundles, propagating far from clumps along the line of sight from the source to the observer, experience a matter density less than the average matter density of the universe. Values of $\alpha_i < 1$, accounts for this defocusing effect; $\alpha_i = 0$ represents a totally clumped universe. This limiting case, sometimes known as "empty-beam approximation", corresponds to the maximum distance to a source for light bundles which have not passed through a caustic [172]. When $\alpha_i = 1$, we reduce to the FLRW case. Historically, $\alpha_{\rm M}$ is defined as the fraction of pressureless matter smoothly distributed. The distance recovered in on average FLRW models, sometimes known as DR distance, has been long studied [53, 54, 96, 105, 114, 176, 226], and now is becoming established as a very useful tool for the interpretation of experimental data [71, 97, 99, 140].

In this approximation, distances are functions of a family of parameters. We will consider a two components universe, filled in with pressureless matter and dark energy. Then, $\Omega_{\rm M0}$ and $\Omega_{\rm X0}$ describe the energy content of the universe on a large scale; $w_{\rm X}$ describes the equation of state of the quintessence and varies between -1 and 0; two clumpiness parameters, $\alpha_{\rm M}$ and $\alpha_{\rm X}$, represent the degree of homogeneity of the universe and characterize phenomena of local propagation.

5.2.1 Angular diameter distances and isolated lenses

As seen in Section (1.12), the distances which enter the gravitational lens equation are the angular diameter distances as measured by an observer in a strictly homogeneous universe. In the simpler gravitational lensing system, with only one deflector, light propagation is not perturbed between the source and the lens and between the lens and the observer. The distance to the source which enters the lens equation, D_s, refers to the homogeneous background. In this section, we will denote D_s as $D_{\rm A}^{\rm RW}$. However, the observer measures an angular diameter distance to the source which is affected by gravitational lensing, $D_{\rm A}^{\rm GL}$. The angular diameter distance is defined as the square

root of the area of the source as measured at the source, dA_S, divided by the solid angle under which we observe the source, $d\omega^{\rm GL}$. From the definition of magnification $|\mu| \equiv d\omega^{\rm GL}/d\omega^{\rm RW}$, where $d\omega^{\rm RW}$ is the solid angle subtended by the source in absence of lensing, we find

$$D_{\rm A}^{\rm GL} = \frac{1}{|\mu|^{1/2}} D_{\rm A}^{\rm RW} = |\det A|^{1/2} D_{\rm A}^{\rm RW}. \tag{5.1}$$

Gravitational lensing affects only the solid angle subtended by the source. Let us consider a light bundle propagating far away from mass inhomogeneity, $k = 0$: only shear affects the propagation. We have

$$D_{\rm A}^{\rm GL} = |1 - \gamma^2|^{1/2} D_{\rm A}^{\rm RW}. \tag{5.2}$$

In realistic situations, $|\gamma| < 2$, the angular diameter distance is reduced with respect to the absence of lensing.

Let us consider an homogeneous sheet with surface mass density $k_{\rm SH}$ added to an uniform background, with density $k_{\rm RW}$. The lensing effects derives from the variations of density. The Jacobian matrix reads

$$A = \begin{pmatrix} 1 - (k_{\rm SH} - k_{\rm RW}) & 0 \\ 0 & 1 - (k_{\rm SH} - k_{\rm RW}) \end{pmatrix}. \tag{5.3}$$

It is

$$D_{\rm A}^{\rm GL} = |1 - (k_{\rm SH} - k_{\rm RW})| D_{\rm A}^{\rm RW}; \tag{5.4}$$

in presence of an overdensity ($k_{\rm SH} > k_{\rm RW}$), the angular diameter is reduced ($D_{\rm A}^{\rm GL} < D_{\rm A}^{\rm RW}$); an underdensity ($k_{\rm SH} > k_{\rm RW}$) increases the angular diameter distance ($D_{\rm A}^{\rm GL} < D_{\rm A}^{\rm RW}$).

5.2.2 The multiple lens-plane equation

Let us consider N isolated thin matter distributions, with surface mass density Σ_i at redshift z_i, $i = 1, ..., N$, ordered such that $z_i < z_j$ if $i < j$; the source is at a redshift $z_{\rm s} > z_N$. At the present cosmic time, the index of refraction due to the i-th lens can be expressed as

$$n_i = 1 - \delta n_i, \tag{5.5}$$

where δn_i is a function of the gravitational potentials generated by the the i-th lens. The total index of refraction is

$$n_i = 1 - \sum_{i=1}^{N} \delta n_i. \tag{5.6}$$

The time delay measured at the observer of the lensed ray p, which travels from the source position $\boldsymbol{\eta}$ to the observer and impacts the i-th plane at $\boldsymbol{\xi}_i$, relative to the

unperturbed ray p_0 is

$$\Delta T(\boldsymbol{\xi}_1, ..., \boldsymbol{\xi}_N) = \frac{a_0}{c}\left[\Delta_{p_0}(p) - \sum_{i=1}^{N}\int_p \delta n_i dl_K\right]. \tag{5.7}$$

The geometrical time delay can be simple expressed as a sum. Let $p_{i,i+1}$ be the ray from $\boldsymbol{\xi}_{i+1}$ to $\boldsymbol{\xi}_i$ to the observer and p_i the unlensed ray from $\boldsymbol{\xi}_{i+1}$ to the observer. It is

$$\Delta_{p_0}(p) \equiv \sum_{i=1}^{N}\left[\mathrm{Length_K}(p_{i,i+1}) - \mathrm{Length_K}(p_i)\right]; \tag{5.8}$$

here $\boldsymbol{\xi}_{N+1} \equiv \boldsymbol{\eta}$. Then,

$$\Delta T(\boldsymbol{\xi}_1, ..., \boldsymbol{\xi}_N) = \sum_{i=1}^{N}\Delta T_{\boldsymbol{\xi}_{i+1}}(\boldsymbol{\xi}_i), \tag{5.9}$$

where the function $\Delta T_{\boldsymbol{\xi}_{i+1}}(\boldsymbol{\xi}_i)$ is the time delay measured at the observer of a ray from $\boldsymbol{\xi}_{i+1}$ to $\boldsymbol{\xi}_i$ to the observer, with deflection occurring only at $\boldsymbol{\xi}_i$ at the i-th lens plane. The multiple-plane time delay function reads [142]

$$\Delta T(\boldsymbol{\xi}_1, ..., \boldsymbol{\xi}_N) = \sum_{i=1}^{N}\frac{1+z_i}{c}\frac{D_i D_{i+1}}{D_{i,i+1}}\left\{\frac{1}{2}\left|\frac{\boldsymbol{\xi}_i}{D_i} - \frac{\boldsymbol{\xi}_{i+1}}{D_{i+1}}\right|^2 - \frac{D_{i,i+1}}{D_i D_{i+1}}\psi_i(\boldsymbol{\xi}_i)\right\}, \tag{5.10}$$

where $D_{i,i+1}$ is the angular diameter distance separating the i-th and $(i+1)$-st lens plane as measured in the background metric.

To derive the ray-trace equation, we apply the Fermat's principle. We get,

$$\boldsymbol{\eta} = \frac{D_s}{D_1}\boldsymbol{\xi}_1 - \sum_{i=1}^{N} D_{is}\hat{\boldsymbol{\alpha}}_i(\boldsymbol{\xi}_i), \tag{5.11}$$

where $\hat{\boldsymbol{\alpha}}_{\boldsymbol{i}}$ is the deflection angle a light ray undergoes if it traverses the i-th lens plane at $\boldsymbol{\xi}_i$. The impact vectors are obtained recursively from

$$\boldsymbol{\xi}_j = \frac{D_j}{D_1}\boldsymbol{\xi}_1 - \sum_{i=1}^{j-1} D_{ij}\hat{\boldsymbol{\alpha}}_i(\boldsymbol{\xi}_i). \tag{5.12}$$

Let us convert the lens equation to dimensionless form by introducing angular variables $\mathbf{x}_i = \boldsymbol{\xi}_i/D_i$. It is

$$\mathbf{x_j} = \mathbf{x_1} - \sum_{i=1}^{j-1}\frac{D_\mathrm{A}(z_i, z_j)}{D_\mathrm{A}(z_j)}\hat{\boldsymbol{\alpha}}_{\boldsymbol{i}}, \tag{5.13}$$

where $\mathbf{x_i}$ is the bidimensional angular position vector in the i-th lens plane.

The solid angle distortion is described by the 2×2 Jacobianes matrices of the mapping equation (5.13),

$$A_i \equiv \frac{\partial \mathbf{x_i}}{\partial \mathbf{x_1}}, \tag{5.14}$$

and by the derivatives of the scaled deflection angle $\boldsymbol{\alpha_i} = (D_1(z_i, z_s)/D_1(z_s))\hat{\boldsymbol{\alpha}}_{\boldsymbol{i}}$,

$$U_i \equiv \frac{\partial \boldsymbol{\alpha_i}}{\partial \mathbf{x_i}}. \tag{5.15}$$

By taking the derivative of equation (5.13) with respect to the independent variable $\mathbf{x_1}$, which represents the angular position of an image on the observer sky, we have the recursion relation

$$A_j = \mathcal{I} - \sum_{i=1}^{j-1} \frac{D_A(z_i, z_j) D_A(z_s)}{D_A(z_j) D_A(z_i, z_s)} U_i A_i, \tag{5.16}$$

with $A_1 = \mathcal{I}$, $\mathcal{I}$ being the two-dimensional identity matrix.

5.2.3 Derivation of the DR equation

As shown for a universe with pressureless matter [172, 173], it is possible to derive the DR equation from the multiple lens-plane theory, without referring to the focusing equation. In the framework of the on average FLRW universes, we can generalize this result to the case of inhomogeneous quintessence [182]. The basic idea is the simulation of the clumpiness by adding to a smooth homogeneous background a hypothetical density distribution of zero total mass, which is made of two components: a distribution of clumps (both in dust and dark energy) and a uniform negative energy density such that the mean density of the sum of both components is zero. After such an addition, the average properties of the universe on a large scale are still that corresponding to the background FLRW model. The gravitational surface density Σ of clumps in a shell of size Δz centred on the observer is then

$$\Sigma = \Delta z \frac{dr_P}{dz} T^{00}_{cl}, \tag{5.17}$$

where the relation between the redshift and the proper distance r_P is that valid in RW background,

$$\frac{dr_P}{dz} = \frac{c}{H(z)} \frac{1}{1+z}, \tag{5.18}$$

and T^{00}_{cl} is the gravitational contribution in clumps to the 0-0 element of the total energy-momentum tensor,

$$\begin{aligned} T^{00}_{cl}(z) &= (1-\alpha_M) T^{00}_M + (1-\alpha_X) T^{00}_X \\ &= (1-\alpha_M)\rho_M(z)c^2 + (1-\alpha_X)(1+w_X)\rho_X(z)c^2. \end{aligned} \tag{5.19}$$

We have assumed that a fraction α_M (α_X) of the pressureless matter (dark energy) is homogeneously distributed. In Eq. (5.19), we have assumed that the sum of the pressure and of energy density contributes to the focusing. In an on average FLRW

universe, the evolutions of densities of pressureless matter and quintessence are obtained by applying the conservation law in a RW background, see Section (1.7). We obtain

$$\rho_{\rm M}(z) = (1+z)^3\Omega_{\rm M0}\rho_{\rm cr}, \tag{5.20}$$
$$\rho_{\rm X}(z) = (1+z)^{n_{\rm X}}\Omega_{\rm X0}\rho_{\rm cr}, \tag{5.21}$$

where $\rho_{\rm cr} \equiv 3H_0^2/(8\pi G)$ is the today critical density and $n_{\rm X} \equiv 3(w_{\rm X}+1)$, $0 \leq n_{\rm X} < 3$. The dimensionless surface density k corresponding to equation (5.17) is

$$\begin{aligned} k\Delta z &\equiv \frac{4\pi G}{c^2}\frac{D_1(z)D_1(z,z_{\rm s})}{D_1(z_{\rm s})}\Sigma \\ &= \frac{H_0^2}{cH(z)}\frac{(1+z)^2}{2}\frac{D_1(z)D_1(z,z_{\rm s})}{D_1(z_{\rm s})} \\ &\times \left[3(1-\alpha_{\rm M})\Omega_{\rm M0} + n_{\rm X}(1-\alpha_{\rm X})\Omega_{\rm X0}(1+z)^{n_{\rm X}-3}\right]\Delta z, \end{aligned} \tag{5.22}$$

where, hereafter, the subscript 1 refers to angular diameter distances in FLRW universes and $z_{\rm s}$ is a hypothetical source redshift. The so constructed spherical shells will act as multiple lens-planes.

In our model of a clumpy universe, the matrices U_i are given by [173]

$$U_i = -k_i\mathcal{I}\Delta z - \mathcal{T}_i, \tag{5.23}$$

where the first term accounts for the negative convergence caused by the smooth negative surface density and $\mathcal{T}_i$ is the matrix that describes the deflection caused by the clumps. In the empty beam approximation (light rays propagating far away from clumps and vanishing shear), it is $\mathcal{T}_i = 0$ and then all the A_i are diagonal, $A_i = a_i\mathcal{I}$. From the properties of the uniform sheet, see Section (3.3), we see that no multiple images are considered. Equation (5.16) becomes

$$a_j = 1 + \sum_{i=1}^{j-1}\frac{D_1(z_i,z_j)D_1(z_{\rm s})}{D_1(z_j)D_1(z_i,z_{\rm s})}k_i a_i \Delta z, \tag{5.24}$$

where the dependence on $z_{\rm s}$ drops out in the product of the ratio of distances by k_i. In the continuum limit, $\Delta z \to 0$, equation (5.24) becomes

$$a(z) = 1 + \int_0^z \frac{D_1(y,z)D_1(z_{\rm s})}{D_1(z)D_1(y,z_{\rm s})}k(y)a(y)dy. \tag{5.25}$$

Multiplying equation (5.24) by $D_1(z)$ and letting $D_{\rm A}(z) = a(z)D_1(z)$, we obtain, substituting for the explicit expression of k given in equation (5.22),

$$\begin{aligned} D_{\rm A}(z) &= D_1(z) + \frac{1}{2}\left(\frac{H_0^2}{c}\right) \\ &\times \int_0^z \left\{\frac{(1+y)^2}{H(y)}\left[3(1-\alpha_{\rm M})\Omega_{\rm M0} + n_{\rm X}(1-\alpha_{\rm X})\Omega_{\rm X0}(1+y)^{n_{\rm X}-3}\right]\right. \\ &\times \left. D_1(y,z)D_{\rm A}(z)\right\}dy. \end{aligned} \tag{5.26}$$

Changing to $z_{\rm d}$ the lower limit of the integration in equation (5.26) and $D_{\rm A}(z)$ ($D_1(z)$) with $D_{\rm A}(z_{\rm d},z)$ ($D_1(z_{\rm d},z)$), we have the equation for generic initial conditions,

$$\begin{aligned} D_{\rm A}(z_{\rm d},z_{\rm d}) &= 0, \\ \left.\frac{d}{dz}D_{\rm A}(z_{\rm d},z)\right|_{z=z_{\rm d}} &= \frac{1}{1+z_{\rm d}}\frac{c}{H(z_{\rm d})}; \end{aligned} \tag{5.27}$$

$D_{\rm A}(z_{\rm d},z)$ is the angular diameter distance between $z_{\rm d}$ (that, in general, can be different from zero, as occurs in gravitational lensing for the deflector) and the source at z. The second initial condition is obtained by applying the Hubble law to a fictitious observer at $z_{\rm d}$ [172]. Equation (5.26), already derived with a different way of proceeding in [114], has here been found only using the multiple lens-plane theory [182]. It is easy to verify that equation (5.26) is equivalent to the so called the generalized DR equation

$$\begin{aligned} H^2(z)\frac{d^2D_{\rm A}}{dz^2} + \left[\frac{2H^2(z)}{1+z} + \frac{1}{2}\frac{dH^2}{dz}\right]\frac{dD_{\rm A}}{dz} \\ + \frac{1}{2}(1+z)\left[3\alpha_{\rm M}\Omega_{\rm M0} + n_{\rm X}\alpha_{\rm X}\Omega_{\rm X0}(1+z)^{n_{\rm X}-3}\right]D_{\rm A} = 0. \end{aligned} \tag{5.28}$$

The isotropic focusing effect in equation (5.28) is simply represented by the multiplicative factor to $D_{\rm A}$; this coefficient increases with $\alpha_{\rm M}$, $\alpha_{\rm X}$ and $n_{\rm X}$. Changing to the expansion factor $a \equiv 1/(1+z)$, equation (5.28) reads

$$\begin{aligned} a^2\left[\Omega_{\rm M0} + \Omega_{\rm X0}a^{3-n_{\rm X}} + \Omega_{\rm K0}a\right]\frac{d^2D_{\rm A}}{da^2} - a\left[\frac{3}{2}\Omega_{\rm M0} + \frac{n_{\rm X}}{2}\Omega_{\rm X0}a^{3-n_{\rm X}} + \Omega_{\rm K0}a\right]\frac{dD_{\rm A}}{da} \\ + \left[\alpha_{\rm M}\frac{3}{2}\Omega_{\rm M0} + \alpha_{\rm X}\frac{n_{\rm X}}{2}\Omega_{\rm X0}a^{3-n_{\rm X}}\right]D_{\rm A} = 0, \end{aligned} \tag{5.29}$$

a form which will be useful in the next sections.

Equation (5.26) is a Volterra integral equation of the second kind [196] whose solution is

$$D_{\rm A}(z) = D_1(z) + \int_0^z \mathcal{H}(y,z)D_1(y)dy, \tag{5.30}$$

where the resolvent kernel $\mathcal{H}(y,z)$ is given by the series of iterated kernels

$$\mathcal{H}(y,z) = \sum_{i=0}^{\infty} K_i(y,z), \tag{5.31}$$

with

$$\begin{aligned} K_1(y,z) = \frac{1}{2}\left(\frac{H_0^2}{c}\right)\frac{(1+y)^2}{H(y)} \\ \times \left[3(1-\alpha_{\rm M})\Omega_{\rm M0} + n_{\rm X}(1-\alpha_{\rm X})\Omega_{\rm X0}(1+y)^{n_{\rm X}-3}\right]D_1(y,z) \end{aligned} \tag{5.32}$$

if $y \leq z$ or $K_1 = 0$ elsewhere; the iterated kernels K_i are defined by the recurrence formula

$$K_{i+1}(y,z) \equiv \int_0^y K_1(y,x)K_i(x,z)dx. \tag{5.33}$$

Since for all i, $K_i(y,z)$ and $D_1(y)$ are non negative, we see from equations (5.30-5.32) that the angular diameter distance $D_{\rm A}(z)$ is a decreasing function of both $\alpha_{\rm M}$ and $\alpha_{\rm X}$,

$$D_{\rm A}(z,\alpha_{\rm M}^{(1)}) \leq D_{\rm A}(z,\alpha_{\rm M}^{(2)}) \text{ for } \alpha_{\rm M}^{(1)} \geq \alpha_{\rm M}^{(2)}, \tag{5.34}$$

$$D_{\rm A}(z,\alpha_{\rm X}^{(1)}) \leq D_{\rm A}(z,\alpha_{\rm X}^{(2)}) \text{ for } \alpha_{\rm X}^{(1)} \geq \alpha_{\rm X}^{(2)}.$$

The above considerations apply equally well to weak lensing by large scale structure density perturbations. The basic idea is to divide the inhomogeneous matter distribution into cubes at varying redshift and project the matter in each cube to the middle-plane of the cube. In this multi-plane lensing model, the surface mass density can be positive ($\alpha_i > 1$) or negative ($\alpha_i < 1$).

5.2.4 The focusing equation

Equation (5.28) is usually derived from the focusing equation [164, 172]. The equation for the angular diameter distance $D_{\rm A}$ in terms of an affine parameter λ, is

$$\frac{d^2 D_{\rm A}}{d\lambda^2} = -\left[|\sigma(\lambda)|^2 - \mathcal{R}(\lambda)\right] D_{\rm A}, \tag{5.35}$$

where $\mathcal{R}$ is the Ricci focusing and σ is the optical shear. In an on average FLRW model, Eq. (5.35) becomes

$$\frac{d^2 D_{\rm A}}{d\lambda^2} + \frac{1}{2}(1+z)^2\left[3\alpha_{\rm M}\Omega_{\rm M0}(1+z)^3 + n_{\rm X}\alpha_{\rm X}\Omega_{\rm X0}(1+z)^{n_{\rm X}}\right] D_{\rm A} = 0, \tag{5.36}$$

where the relation between λ and the redshift z, in terms of the generalized Hubble parameter is

$$\frac{dz}{d\lambda} = (1+z)^2 \frac{H(z)}{H_0}. \tag{5.37}$$

Substituting for λ in equation (5.36) by using equation (5.37), we get the same form of Eq. (5.28).

5.3 Exact solutions of the DR equation for $\Omega_{\rm K0} \neq 0$

The observational data presently available are in agreement with the hypothesis of a flat universe, but are also compatible with a non zero, although small, value of $\Omega_{\rm K0}$. A small value of $\Omega_{\rm K0}$ is also allowed by some inflationary theories. These circumstances make useful the study of the effect of the curvature on the cosmological distances since today technology allows to put strong constraints on the cosmological parameters.

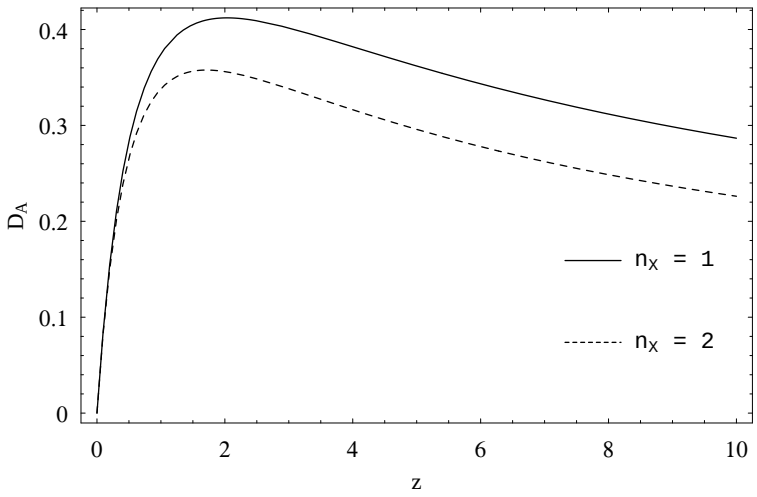

Figure 5.1: The angular diameter distance for two universes with $\Omega_{\rm M0} = 0.2$, $\Omega_{\rm X0} = 0.7$, $\alpha_{\rm M} = 0.7$ and $\alpha_{\rm X} = 1$. The full and dashed lines correspond respectively to $n_{\rm X} = 1$ and $n_{\rm X} = 2$. The unit of distance is taken to be c/H_0.

In what follows, we will consider the DR equation with constant smoothness parameters. For $\alpha_{\rm X} = 1$, equation (5.29) reduces to

$$a^2\left[\Omega_{\rm M0}+\Omega_{\rm K0}a+\Omega_{\rm X0}a^{3-n_{\rm X}}\right]\frac{d^2D_{\rm A}}{da^2}-a\left[\frac{3}{2}\Omega_{\rm M0}+\Omega_{\rm K0}a+\frac{n_{\rm X}}{2}\Omega_{\rm X0}a^{3-n_{\rm X}}\right]\frac{dD_{\rm A}}{da} + \left[\frac{3}{2}\alpha_{\rm M}+\frac{n_{\rm X}}{2}\Omega_{\rm X0}a^{3-n_{\rm X}}\right]D_{\rm A}=0. \tag{5.38}$$

To solve equation (5.38), we proceed as in [49]. First, we look for a solution in the power form a^s when $\Omega_{\rm X0} = \Omega_{\rm K0} = 0$. The parameter s is constrained to fulfil the algebraic equation

$$s^2-\frac{5}{2}s+\frac{3}{2}\alpha_{\rm M}=0, \tag{5.39}$$

which has the solutions

$$s_\pm=\frac{5}{4}\pm\frac{1}{4}\sqrt{25-24\alpha_{\rm M}}\equiv\frac{5}{4}\pm\beta; \tag{5.40}$$

we have introduced the parameter β,

$$\beta\equiv\frac{\sqrt{25-24\alpha_{\rm M}}}{4}.$$

When $\Omega_{\rm X0} \neq 0$, $\Omega_{\rm K0} \neq 0$, we choose to impose the form $D_{\rm A} = a^s f(a)$ to the solution, being f a generic function. Inserting this expression into equation (5.38) we have for $f(a)$

$$\begin{aligned}0 = {} & a\left[\Omega_{\rm M0}+\Omega_{\rm K0}a+\Omega_{\rm X0}a^{3-n}\right]\frac{d^2f}{da^2}\\ & -\left[\Omega_{\rm M0}\left(2s-\frac{3}{2}\right)+\Omega_{\rm K0}(2s-1)a\left(s(s-1)-\frac{n_{\rm X}}{2}s\right)\Omega_{\rm X0}a^{3-n_{\rm X}}\right]\frac{df}{da}\\ & +\left[\Omega_{\rm K0}s(s-2)+\Omega_{\rm X0}\left(s^2-s\left(1+\frac{n_{\rm X}}{2}\right)\right)a^{2-n_{\rm X}}\right]f.\end{aligned} \tag{5.41}$$

The initial conditions at $a = 1$ for the auxiliary function f come out from equation (5.27) evaluated at $z = 0$,

$$\begin{aligned} f(1) &= 0, \\ \left.\frac{d}{da}f(a)\right|_{a=1} &= \frac{c}{H_0}. \end{aligned} \tag{5.42}$$

Equation (5.41) is very useful to obtain some exact solutions of the DR equation, corresponding to integer values of the quintessence parameter $n_{\rm X}$.

5.3.1 Only dust

The solution for a model of universe with only dust ($\Omega_{\rm X0} = 0$ or $n_{\rm X} = 3$) is well known in terms of Legendre functions [174]. In this case, the DR equation reads

$$(z+1)(\Omega_{\rm M0}z+1)\frac{d^2D_{\rm A}}{dz^2} + \left(\frac{7}{2}\Omega_{\rm M0}z + \frac{\Omega_{\rm M0}}{2} + 3\right)\frac{dD_{\rm A}}{dz} + \frac{3}{2}\alpha_{\rm M}\Omega_M(1+z)D_{\rm A} = 0,$$

and the boundary conditions reduce to

$$\begin{aligned} D_{\rm A}(z_d, z_{\rm d}) &= 0 \\ \left.\frac{dD_{\rm A}}{dz}(z_{\rm d}, z)\right|_{z=z_{\rm d}} &= \frac{c}{H_0}\frac{1}{(1+z_{\rm d})^2\sqrt{1+\Omega_{\rm M0}z_{\rm d}}}. \end{aligned}$$

Let us consider $0 < \Omega_{\rm M0} < 1$. Through a transformation of the independent and dependent variables,

$$y = \sqrt{\frac{1+\Omega_{\rm M0}z}{1-\Omega_{\rm M0}}}; \quad D_{\rm A} = \frac{c}{H_0}\frac{1}{y^2-1}f, \tag{5.43}$$

we obtain the Legendre differential equation for $f(y)$,

$$(1-y^2)\frac{d^2f}{dy^2} - 2y\frac{df}{dy} + \left[\nu(\nu+1) - \frac{\mu^2}{1-y^2}\right]f = 0\ , \tag{5.44}$$

where

$$\mu = 2\ ;\ \nu = \frac{4\beta-1}{2}. \tag{5.45}$$

Two independent solutions of Eq. (5.44) are the associated Legendre functions of first and second type [1], $P^\mu_\nu(y)$ and $Q^\mu_\nu(y)$ respectively, unless $\nu = 0$ or $\nu = 1$. When $2/3 \neq \alpha_{\rm M} \neq 1$, we get

$$\begin{aligned} D_{\rm A}(z_{\rm d}, z) = \frac{c}{H_0}&\frac{1}{6(1-\alpha_{\rm M})(2-3\alpha_{\rm M})\sqrt{1-\Omega_{\rm M0}}}\frac{1}{1+z} \\ &\times \left[Q^\mu_\nu(y_d)P^\mu_\nu(y) - Q^\mu_\nu(y)P^\mu_\nu(y_d)\right], \end{aligned} \tag{5.46}$$

where $y_d = y(z_{\rm d})$. Let us introduce the dimensionless angular diameter distance r,

$$D_{\rm A} \equiv \frac{c}{H_0} r.$$

Equation (5.85) reduces to the hypergeometric equation through the transformations [54],

$$x = \frac{1+\Omega_{\rm M0} z}{1-\Omega_{\rm M0}} \ , \ r(z) = r[x]; \tag{5.47}$$

we find

$$x(1-x)\frac{d^2 r}{dx^2} + [c - (1+a+b)x]\frac{dr}{dx} - abr = 0 \ , \tag{5.48}$$

where

$$a = \frac{5+4\beta}{4} \ , \ b = \frac{5-4\beta}{4} \ , \ c = \frac{1}{2} \ . \tag{5.49}$$

In terms of the hypergeometric functions, the dimensionless angular diameter distance reads[174],

$$r(z_{\rm d}, z) = 2(1+z_{\rm d})[V_1(z_{\rm d})V_2(z) - V_1(z)V_2(z_{\rm d})] \ , \tag{5.50}$$

where

$$\begin{aligned} V_1(z) &= \Omega_{\rm M0}(1+\Omega_{\rm M0} z)^{\frac{-(4\beta+5)}{4}} {}_2F_1\left[\frac{4\beta+7}{4}, \frac{4\beta+5}{4}; \frac{4\beta+2}{2}; \frac{1-\Omega_{\rm M0}}{1+\Omega_{\rm M0} z}\right], \\ V_2(z) &= \frac{\Omega_{\rm M0}}{4\beta}(1+\Omega_{\rm M0} z)^{\frac{4\beta-5}{4}} {}_2F_1\left[\frac{7-4\beta}{4}, \frac{5-4\beta}{4}; \frac{2-4\beta}{2}; \frac{1-\Omega_{\rm M0}}{1+\Omega_{\rm M0} z}\right], \end{aligned} \tag{5.51}$$

where ${}_2F_1$ is the hypergeometric function of the second type.

The expression for the dimensionless angular diameter distance in Eq. (5.50) is general. It still holds in the particular cases $\Omega_{\rm M0} = 1$, $\alpha_{\rm M} = 2/3$ or $\alpha_{\rm M} = 1$. Let us consider these cases. The homogeneous universe is described by $\alpha_{\rm M} = 1$ ($\beta = 1/4$). It is

$$V_1(z) = \frac{\sqrt{1+\Omega_{\rm M0} z}}{\Omega_{\rm M0}(1+z)^2} \ , \ V_2(z) = \frac{2-\Omega_{\rm M0}+\Omega_{\rm M0} z}{\Omega_{\rm M0}(1+z)^2}; \tag{5.52}$$

then

$$\begin{aligned} r(z_{\rm d}, z) = \frac{2}{\Omega_{\rm M0}^2(1+z_{\rm d})(1+z)^2} \Big[& \sqrt{1+\Omega_{\rm M0} z_{\rm d}}(2-\Omega_{\rm M0}+\Omega_{\rm M0} z) \\ & - \sqrt{1+\Omega_{\rm M0} z}(2-\Omega_{\rm M0}+\Omega_{\rm M0} z_{\rm d})\Big]; \end{aligned} \tag{5.53}$$

for $z_{\rm d} = 0$, Eq. (5.53) becomes

$$r(z) = \frac{2}{\Omega_{\rm M0}^2(1+z)^2}\left[\Omega_{\rm M0} z - (2-\Omega_{\rm M0})\left(\sqrt{\Omega_{\rm M0} z + 1} - 1\right)\right] \ . \tag{5.54}$$

When $\alpha_{\rm M} = 2/3$, it is $\beta = 3/4$. We get

$$V_1(z) = \frac{1}{\Omega_{\rm M0}(1+z)^2} \ , \ V_2(z) = \frac{\sqrt{1+\Omega_{\rm M0} z}(\Omega_{\rm M0} z + 3\Omega_{\rm M0} - 2)}{3\Omega_{\rm M0}(1+z)^2}. \tag{5.55}$$

The dimensionless angular diameter distances reads

$$r(z_{\rm d},z) = \frac{2}{3\Omega_{\rm M0}^2(1+z_{\rm d})(1+z)^2} \times \left[\sqrt{1+\Omega_{\rm M0}z}(\Omega_{\rm M0}z+3\Omega_{\rm M0}-2) - \sqrt{1+\Omega_{\rm M0}z_{\rm d}}(\Omega_{\rm M0}z_{\rm d}+3\Omega_{\rm M0}-2)\right]; \tag{5.56}$$

When $z_{\rm d}=0$, Eq. (5.56) reduces to

$$r(z) = \frac{2}{3\Omega_{\rm M0}^2(1+z)^2}\left[\frac{1}{3}\Omega_{\rm M0}z\sqrt{\Omega_{\rm M0}z+1} - \left(\frac{2}{3}-\Omega_{\rm M0}\right)\left(\sqrt{\Omega_{\rm M0}z+1}-1\right)\right]. \tag{5.57}$$

In the Einstein-de Sitter, we have $\Omega_{\rm M0}=1$. Then,

$$V_1(z) = (1+z)^{-(4\beta+5)/4}\ ,\ V_1(z) = \frac{1}{4\beta}(1+z)^{(4\beta-5)/4}; \tag{5.58}$$

$$r(z_{\rm d},z) = \frac{2}{\beta}\left[\frac{(1+z)^{(\beta-5)/4}}{(1+z_{\rm d})^{(\beta+1)/4}} - \frac{(1+z_{\rm d})^{(\beta-1)/4}}{(1+z)^{(\beta+5)/4}}\right]; \tag{5.59}$$

$$r(z) = \frac{2}{\beta}(1+z)^{(4\beta-5)/4}\left[1+(1+z)^{-2\beta}\right]. \tag{5.60}$$

Let us consider the case $\Omega_{\rm M0}>1$. We perform the transformation [174],

$$y = \sqrt{\frac{1+\Omega_{\rm M0}z}{\Omega_{\rm M0}(1+z)}}\ ,\ r = \left(\frac{\Omega_{\rm M0}-1}{\Omega_{\rm M0}(1+z)}\right)^{5/4} f\ . \tag{5.61}$$

Once again, $f(y)$ is a solution of the Legendre equation (5.44), with

$$\mu = 2\beta;\ \nu = \frac{3}{2}\ .$$

With the same procedure as in the case $\Omega_{\rm M0}<1$, we find

$$r(z_{\rm d},z) = \frac{2}{\sqrt{\Omega_{\rm M0}}}\frac{\Gamma\left(\frac{5-4\beta}{2}\right)}{\Gamma\left(\frac{5+4\beta}{2}\right)}\frac{1}{(1+z_{\rm d})^{\frac{1}{4}}(1+z)^{\frac{5}{4}}}\left[Q_\nu^\mu(y_d)P_\nu^\mu(y) - Q_\nu^\mu(y)P_\nu^\mu(y_d)\right], \tag{5.62}$$

where $y_d = y(z_{\rm d})$ and $\Gamma(x)$ denotes the Gamma function [1]. Again, the solution can be expressed in terms of hypergeometric functions as

$$r(z_{\rm d},z) = 2(1+z_{\rm d})\left[W_1(z_{\rm d})W_2(z) - W_1(z)W_2(z_{\rm d})\right], \tag{5.63}$$

where

$$W_1(z) = \left(\frac{\Omega_{\rm M0}-1}{\Omega_{\rm M0}}\right)^{2\beta}(1+z)^{\frac{-(5+4\beta)}{4}}F\left[\frac{5+4\beta}{4},\frac{\beta-3}{4};\frac{1}{2};\frac{1+\Omega_{\rm M0}z}{\Omega_{\rm M0}(1+z)}\right], \tag{5.64}$$

$$W_2(z) = \frac{\sqrt{1+\Omega_{\rm M0}z}}{\Omega_{\rm M0}}(1+z)^{\frac{-(7+4\beta)}{4}}F\left[\frac{7+4\beta}{4},\frac{4\beta-1}{4};\frac{1}{2};\frac{1+\Omega_{\rm M0}z}{\Omega_{\rm M0}(1+z)}\right].$$

As shown in [174], the pairs of equations (5.50, 5.51) and (5.63, 5.64) are analytic continuations of each other.

5.3.2 The cosmological constant

The solution for the case of the cosmological constant ($n_{\rm X} = 0$) is already known in terms of Heun functions [97].

Let us perform the transformation of the dependent and independent variables,

$$\zeta = \frac{\Omega_{\rm M0}(1+z) + \Omega_{\rm K0} y_1}{\Omega_{\rm K0}(y_2 - y_1)} \ , \ h = (1+z)r; \tag{5.65}$$

in Eq. (5.65), y_1 is the real root, whereas y_2 e y_3 are the complex solutions of the third order equation

$$y^3 + y^2 + \frac{\Omega_{\rm M0}^2 \Omega_{\Lambda 0}}{\Omega_{\rm K0}^3} = (y - y_1)(y - y_2)(y - y_3) = 0; \tag{5.66}$$

the roots are constrained by the relations

$$y_1 y_2 y_3 = -\frac{\Omega_{\rm M0}^2 \Omega_{\Lambda 0}}{\Omega_{\rm K0}^3} \ , \ y_1 + y_2 + y_3 = -1 \ , \ y_1 y_2 + y_2 y_3 + y_1 y_3 = 0. \tag{5.67}$$

By introducing

$$\begin{aligned} \tilde{a} &= \frac{y_3 - y_1}{y_2 - y_1}, \\ \nu &= \frac{4\beta - 1}{2}, \\ q &= \frac{1 + (1/4)\nu(\nu+1) y_1}{y_2 - y_1}, \end{aligned}$$

the DR equation can be rewritten as a standard Heun equation,

$$\frac{d^2 h}{d\zeta^2} + \frac{1}{2}\left(\frac{1}{\zeta} + \frac{1}{\zeta - 1} + \frac{1}{\zeta - \tilde{a}}\right)\frac{dh}{d\zeta} - \frac{(1/2)\nu(1/2)(\nu+1)\zeta + q}{\zeta(\zeta-1)(\zeta-\tilde{a})} h = 0. \tag{5.68}$$

Equation (5.68) is the Heun equation [61, 83], which is slightly more complicated than the hypergeometric equation, possessing four points of regular singularity in the entire complex plain, rather than three. For

$$|\zeta_0| = \left|\frac{\Omega_{\rm M0} + \Omega_{\rm K0} y_1}{\Omega_{\rm K0}(y_2 - y_1)}\right| < 1,$$

it is

$$\begin{aligned} D(z) = &-\frac{c}{H_0}\frac{2}{(1+z)\Omega_{\rm K0}\sqrt{\Omega_{\rm M0}}}\sqrt{\frac{\Omega_{\rm M0}(\Omega_{\rm M0} - \Omega_{\rm K0} y_1)}{y_1(2+3y_1)}} \\ &\times \left\{ \mathrm{H1}\left[a, \frac{1 + (1/4)\nu(\nu+1) y_1}{\sqrt{y_1(2+3y_1)}}\sqrt{a}; -\frac{\nu}{2}, \frac{\nu+1}{2}, \frac{1}{2}, \frac{1}{2}; \frac{\Omega_{\rm M0}(1+z) - \Omega_{\rm K0} y_1}{\Omega_{\rm K0}\sqrt{y_1(2+3y_1)}}\sqrt{a}\right] \right. \end{aligned}$$

$$\times \,\mathrm{H1}\left[a, \frac{3+(\nu^2+\nu-3)y_1}{4\sqrt{y_1(2+3y_1)}}\sqrt{a}; -\frac{\nu-1}{2}, \frac{\nu+2}{2}, \frac{3}{2}, \frac{1}{2}; \frac{\Omega_{\mathrm{M0}}-\Omega_{\mathrm{K0}}y_1}{\Omega_{\mathrm{K0}}\sqrt{y_1(2+3y_1)}}\sqrt{a}\right]$$
$$-\sqrt{\frac{\Omega_{\mathrm{M0}}(1+z)-\Omega_{\mathrm{K0}}y_1}{\Omega_{\mathrm{M0}}-\Omega_{\mathrm{K0}}y_1}} \tag{5.69}$$
$$\times \,\mathrm{H1}\left[a, \frac{3+(\nu^2+\nu-3)y_1}{4\sqrt{y_1(2+3y_1)}}\sqrt{a}; -\frac{\nu-1}{2}, \frac{\nu+2}{2}, \frac{3}{2}, \frac{1}{2}; \frac{\Omega_{\mathrm{M0}}(1+z)-\Omega_{\mathrm{K0}}y_1}{\Omega_{\mathrm{K0}}\sqrt{y_1(2+3y_1)}}\sqrt{a}\right]$$
$$\times \,\mathrm{H1}\left[a, \frac{1+(1/4)\nu(\nu+1)y_1}{\sqrt{y_1(2+3y_1)}}\sqrt{a}; -\frac{\nu}{2}, \frac{\nu+1}{2}, \frac{1}{2}, \frac{1}{2}; \frac{\Omega_{\mathrm{M0}}-\Omega_{\mathrm{K0}}y_1}{\Omega_{\mathrm{K0}}\sqrt{y_1(2+3y_1)}}\sqrt{a}\right]\right\},$$

where H1 are the Heun functions; although they contain complex parameters, they are real function of the real variable z [97]. For the case $|\zeta_0| > 1$ and for further details, we refer to [97].

5.3.3 String networks

Let us consider dark energy in the form of string networks ($n_{\mathrm{X}} = 2$) [182], when equation (5.41) reduces to

$$a(c_1 + c_2 a)\frac{d^2 f}{da^2} + (c_3 + c_2 c_4 a)\frac{df}{da} + c_5 f = 0, \tag{5.70}$$

being

$$\begin{aligned} c_1 &= \Omega_{\mathrm{M0}}, \\ c_2 &= \Omega_{\mathrm{K0}} + \Omega_{\mathrm{X0}}, \\ c_3 &= c_2\left(2s - \frac{3}{2}\right), \\ c_4 &= 2s - 1, \\ c_5 &= \Omega_{\mathrm{K0}}s(s-2) + \Omega_{\mathrm{X0}}\left(s\left(s - \frac{3}{2} + \frac{1}{2}\right)\right). \end{aligned} \tag{5.71}$$

Equation (5.70) is of hypergeometric type, i.e. it has three regular singularities [91], and so, for $n_{\mathrm{X}} = 2$, f is the hypergeometric function. If we indicate with f_{s_+} and f_{s_-} two independent solutions for, respectively, $s = s_+$ and $s = s_-$, we can write the general solution of equation (5.38) for $n_{\mathrm{X}} = 2$ as

$$\begin{aligned} D_{\mathrm{A}} &= A_+ a^{s_+} f_{s_+}(a) + A_- a^{s_-} f_{s_-}(a) \\ &= \frac{1}{(1+z)^{5/4}}\left\{A_+(1+z)^{-\beta} f_{s_+}\left(\frac{1}{1+z}\right) + A_-(1+z)^{\beta} f_{s_-}\left(\frac{1}{1+z}\right)\right\}, \end{aligned} \tag{5.72}$$

where A_+ and A_- are constants determined by the initial conditions. In equation (5.72) we have expressed the scale factor, a, in terms of the redshift.

5.3.4 Domain walls

Let us consider now the case of domain walls, $n_{\rm X} = 1$ ($w_{\rm X} = -2/3$) [182]. The equation for f becomes

$$a\left[\frac{\Omega_{\rm M0}}{\Omega_{\rm X0}} + \frac{\Omega_{\rm K0}}{\Omega_{\rm X0}}a + a^2\right]\frac{d^2f}{da^2} + \left[\frac{\Omega_{\rm M0}}{\Omega_{\rm X0}}\left(2s - \frac{3}{2}\right) + \frac{\Omega_{\rm K0}}{\Omega_{\rm X0}}(2s-1)\,a + \left(2s - \frac{1}{2}\right)a^2\right]\frac{df}{da} + \left[\frac{\Omega_{\rm K0}}{\Omega_{\rm X0}}s\,(s-2) + \left(s\,(s-2) + \frac{1}{2}\right)a\right]f = 0. \tag{5.73}$$

Equation (5.73) is a fuchsian equation with three finite regular points plus a regular singularity at ∞ [91]. The regular points in the finite part of the complex plane are

$$\begin{aligned} a_1 &= 0, \\ a_2 &= \frac{-\Omega_{\rm K0} - \sqrt{\Omega_K^2 - \Omega_{\rm M0}\Omega_{\rm X0}}}{2}, \\ a_3 &= \frac{-\Omega_{\rm K0} + \sqrt{\Omega_K^2 - \Omega_{\rm M0}\Omega_{\rm X0}}}{2}. \end{aligned} \tag{5.74}$$

The transformation $y = a/a_2$ sends $a_2 \to 1$ and $a_2 \to \zeta = \frac{a_3}{a_2}$. In terms of y, equation (5.73) reads

$$y\,(y-1))\,(y-\zeta)\frac{d^2f}{dy^2} + \left[\frac{\Omega_{\rm M0}}{\Omega_{\rm X0}}\left(2s - \frac{3}{2}\right) + \frac{\Omega_{\rm K0}}{\Omega_{\rm X0}}(2s-1)\,a_2 y + \left(2s - \frac{1}{2}\right){a_2}^2 y^2\right] \times \frac{df}{dy} + \left[\frac{\Omega_{\rm K0}}{a_2\Omega_{\rm X0}}s\,(s-2) + \left(s\,(s-2) + \frac{1}{2}\right)a_2 y\right]f = 0, \tag{5.75}$$

which can be reduced to the standard form

$$\frac{d^2f}{dy^2} + \left(\frac{\gamma}{y} + \frac{\delta}{y-1} + \frac{\epsilon}{y-\zeta}\right)\frac{df}{dy} + \left(\frac{\theta\lambda y - q}{y\,(y-1)\,(y-\zeta)}\right)f = 0, \tag{5.76}$$

where

$$\begin{aligned} \gamma + \delta &= \left(2s - \frac{1}{2}\right)a_2^2, \\ \frac{\Omega_{\rm K0}}{\Omega_{\rm X0}}(2s-1)\,a_2 &= \gamma\,(1+\zeta) + \delta\zeta + \epsilon, \\ \gamma\zeta &= \frac{\Omega_{\rm M0}}{\Omega_{\rm X0}}\left(2s - \frac{3}{2}\right), \\ q &= \frac{\Omega_{\rm K0}}{\Omega_{\rm M0}}s\,(s-2), \\ \theta\lambda &= s\left(s - \frac{3}{2}\right) + \frac{1}{2}. \end{aligned} \tag{5.77}$$

The constant q is the so called *accessory parameter*, whose presence is due to the fact that a fuchsian equation is not completely determined by the position of the singularities and the indices. The Heun equation can be characterized by a $\mathcal{P}$ symbol,

and the solutions can be expanded in series of hypergeometric functions. Thus, the solution of the equation (5.38) for $n_{\rm X}=1$ can be formally written as equation (5.72), once the functions f_{s_+} and f_{s_-} are interpreted as Heun functions.

In Fig. (5.1), we plot some of the solutions found above.

5.4 Exact solutions of the DR equation for $\Omega_{\rm K0}=0$

The DR equation for a flat universe has already been treated in the limiting case of the cosmological constant in [49, 97, 99, 100]. Here, in presence of generic dark energy, we propose the general solution in terms of hypergeometric functions [182, 183] and, then, list particular solutions in terms of elementary functions [182]. Let us first consider the case $\alpha_{\rm X}=1$. For flat universes, $\Omega_{\rm M0}+\Omega_{\rm X0}=1$, it is

$$(1+z)^2\left[1+\mu(1+z)^{3w_{\rm X}}\right]\frac{d^2D_{\rm A}}{dz^2}+\frac{(1+z)}{2}\left[7+(3w_{\rm X}+7)\mu(1+z)^{3w_{\rm X}}\right]\frac{dD_{\rm A}}{dz} + \frac{3}{2}\left[\alpha_{\rm M}+(w_{\rm X}+1)\mu(1+z)^{3w_{\rm X}}\right]D_{\rm A}=0, \quad (5.78)$$

where $\mu\equiv\frac{1-\Omega_{\rm M0}}{\Omega_{\rm M0}}$. The boundary conditions of Eq. (5.78), for $z_{\rm d}=0$, reduce to, see Eqs. (5.27),

$$\begin{aligned} D_{\rm A}(0) &= 0, \\ \left.\frac{dD_{\rm A}}{dz}\right|_{z=0} &= \frac{c}{H_0}. \end{aligned} \quad (5.79)$$

It is straightforward to obtain the corresponding equation for the luminosity distance. Using the Etherington principle [62], $D_{\rm L}=(1+z)^2D_{\rm A}$, we can substitute in Eq. (5.78),

$$(1+z)^2\left[1+\mu(1+z)^{3w_{\rm X}}\right]\frac{d^2D_{\rm L}}{dz^2}-\frac{(1+z)}{2}\left[1+(1-3w_{\rm X})\mu(1+z)^{3w_{\rm X}}\right]\frac{dD_{\rm L}}{dz} + \left[\frac{3\alpha_{\rm M}-2}{2}+\frac{1-3w_{\rm X}}{2}\mu(1+z)^{3w_{\rm X}}\right]D_{\rm L}=0; \quad (5.80)$$

the boundary conditions are, again,

$$\begin{aligned} D_{\rm L}(0) &= 0, \\ \left.\frac{dD_{\rm L}}{dz}\right|_{z=0} &= \frac{c}{H_0}. \end{aligned} \quad (5.81)$$

The solution of Eq. (5.80), satisfying the boundary conditions in Eq. (5.81), takes the form

$$D_{\rm L}(z)=\frac{c}{H_0}\frac{D_1(0)D_2(z)-D_1(z)D_2(0)}{W(0)}, \quad (5.82)$$

where $D_1(z)$ and $D_2(z)$ are two linearly independent solutions of Eq. (5.80) and $W(z)\equiv D_1(z)\frac{D_2(z)}{dz}-\frac{dD_1(z)}{dz}D_2(z)$ is the Wronskian of the solutions system.

To solve Eq. (5.80), we perform the transformation of both the independent and dependent variables,

$$u \equiv -\mu(1+z)^{3w_{\rm X}}, \quad D_{\rm L}(z) \equiv u^{\frac{3+4\beta}{12w_{\rm X}}} R_L(z). \tag{5.83}$$

With such a transformation, Eq. (5.80) reduces to the hypergeometric equation for R_L,

$$\begin{aligned}\frac{d^2R_L}{du^2} + \left[\left(1+\frac{2\beta}{3w_{\rm X}}\right)\frac{1}{u} - \frac{1}{2(1-u)}\right]\frac{dR_L}{du} \\ - \left(\frac{4\beta-1}{12w_{\rm X}}\right)\left(\frac{4\beta+1}{12w_{\rm X}}+\frac{1}{2}\right)\frac{1}{u(1-u)}R_L = 0.\end{aligned} \tag{5.84}$$

A pair of independent solutions of Eq. (5.84) is

$$\begin{aligned}R_1(u) &= {}_2F_1\left[\frac{4\beta-1}{12w_{\rm X}}, \frac{4\beta+1}{12w_{\rm X}}+\frac{1}{2}, \frac{2\beta}{3w_{\rm X}}+1, u\right], \\ R_2(u) &= u^{-\frac{2\beta}{3w_{\rm X}}}\ {}_2F_1\left[-\frac{4\beta+1}{12w_{\rm X}}, \frac{-4\beta+1}{12w_{\rm X}}+\frac{1}{2}, -\frac{2\beta}{3w_{\rm X}}+1, u\right].\end{aligned} \tag{5.85}$$

Inserting the expressions for R_1 and R_2 in Eq. (5.29) and substituting in Eq. (5.27), we have the final expression for the luminosity distance,

$$\begin{aligned}D_{\rm L}(z) = \frac{c}{H_0}\frac{1}{2\beta\sqrt{\Omega_{\rm M0}}} \\ \times \left\{(1+z)^{\frac{3}{4}+\beta}\ {}_2F_1\left[-\frac{4\beta+1}{12w_{\rm X}}, \frac{1}{2}+\frac{1-4\beta}{12w_{\rm X}}, 1-\frac{2\beta}{3w_{\rm X}}, \frac{\Omega_{\rm M0}-1}{\Omega_{\rm M0}}\right]\right. \\ \times\ {}_2F_1\left[\frac{4\beta-1}{12w_{\rm X}}, \frac{1}{2}+\frac{4\beta+1}{12w_{\rm X}}, 1+\frac{2\beta}{3w_{\rm X}}, \frac{\Omega_{\rm M0}-1}{\Omega_{\rm M0}}(1+z)^{3w_{\rm X}}\right] \\ - (1+z)^{\frac{3}{4}-\beta}\ {}_2F_1\left[-\frac{4\beta+1}{12w_{\rm X}}, \frac{1}{2}+\frac{1-4\beta}{12w_{\rm X}}, 1-\frac{2\beta}{3w_{\rm X}}, \frac{\Omega_{\rm M0}-1}{\Omega_{\rm M0}}(1+z)^{3w_{\rm X}}\right] \\ \left.\times\ {}_2F_1\left[\frac{4\beta-1}{12w_{\rm X}}, \frac{1}{2}+\frac{4\beta+1}{12w_{\rm X}}, 1+\frac{2\beta}{3w_{\rm X}}, \frac{\Omega_{\rm M0}-1}{\Omega_{\rm M0}}\right]\right\}.\end{aligned} \tag{5.86}$$

For the case of a cosmological constant, $w_{\rm X}=-1$, Eq. (5.86) reduces to equation (16) in [99], as we can see by using the property of the hypergeometric function

$${}_2F_1\left[a,b,c,x\right] = \frac{1}{(1-x)^a}\ {}_2F_1\left[a, c-b, c, \frac{x}{x-1}\right], \tag{5.87}$$

and noting that the clumping parameter ν in [99] corresponds to $(\beta-1)/2$. The case of the cosmological constant is also studied in [49, 97, 100].

Now, let us consider values of $\alpha_{\rm X} \neq 1$. We can proceed as in the previous section. When $\Omega_{\rm K0}=0$, equation (5.29) reduces to [182]

$$\begin{aligned}a^2\left[\Omega_{\rm M0}+(1-\Omega_{\rm M0})a^{3-n_{\rm X}}\right]\frac{d^2D_{\rm A}}{da^2} - a\left[\frac{3}{2}\Omega_{\rm M0}+\frac{n_{\rm X}}{2}(1-\Omega_{\rm M0})a^{3-n_{\rm X}}\right]\frac{dD_{\rm A}}{da} \\ + \left[\frac{3}{2}\alpha_{\rm M}\Omega_{\rm M0}+\frac{n_{\rm X}}{2}\alpha_{\rm X}(1-\Omega_{\rm M0})a^{3-n_{\rm X}}\right]D_{\rm A} = 0;\end{aligned} \tag{5.88}$$

dividing equation (5.88) by $\Omega_{\rm M0}$, we have

$$a^2\left[1+\mu a^{3-n_{\rm X}}\right]\frac{d^2D_{\rm A}}{da^2}-a\left[\frac{3}{2}+\frac{n_{\rm X}}{2}\mu a^{3-n_{\rm X}}\right]\frac{dD_{\rm A}}{da} + \left[\frac{3}{2}\alpha_{\rm M}+\frac{n_{\rm X}}{2}\alpha_{\rm X}\mu a^{3-n_{\rm X}}\right]D_{\rm A}=0. \tag{5.89}$$

To solve equation (5.89), we first look for a solution in the power form a^s when $\mu=0$. The parameter s is constrained to fulfil equation (5.39). When $\mu\neq 0$, we choose to impose the form $D_{\rm A}=a^s f(a)$ to the solution, where f is generic. Inserting this expression into equation (5.89) and changing to $x\equiv a^{3-n_{\rm X}}$, we have for f

$$x(3-n_{\rm X})(1+\mu x)\frac{d^2f}{dx^2}+\left[\left(2s-n_{\rm X}+\frac{1}{2}\right)+\left(2-\frac{3}{2}n_{\rm X}+2s\right)\mu x\right]\frac{df}{dx} + \frac{\mu}{2}\left[s-\frac{3\alpha_{\rm M}-n_{\rm X}\alpha_X}{3-n_{\rm X}}\right]f=0. \tag{5.90}$$

Again, this equation can be solved in terms of hypergeometric functions. Denoting with f_{s_+} and f_{s_-} two of such independent solutions for, respectively, $s=s_+$ and $s=s_-$, we can write the general solution of equation (5.88) as

$$\begin{aligned} D_{\rm A} &= A_+ a^{s_+} f_{s_+}[x(a)]+A_- a^{s^-} f_{s_-}[x(a)] \\ &= \frac{1}{(1+z)^{\frac{5}{4}-\beta}}\left\{A_+ f_{s_+}\left[\frac{1}{(1+z)^{3-n_{\rm X}}}\right]+A_-(1+z)^{2\beta}f_{s_-}\left[\frac{1}{(1+z)^{3-n_{\rm X}}}\right]\right\}, \end{aligned} \tag{5.91}$$

where A_+ and A_- are constants determined by the initial conditions.

Once we have the general solution of the DR equation (5.88) in terms of hypergeometric functions, we go now to list some expressions of the angular diameter distance in terms of elementary functions in two extremal cases.

5.4.1 Homogeneous universe

In this case, we have that $\alpha_{\rm M}=\alpha_{\rm X}=1$. Eq. (5.80) is solved by

$$D_{\rm L}(z)=\frac{c}{H_0}(1+z)\int_0^z\frac{1}{\sqrt{\Omega_{\rm M0}(1+z')^3+(1-\Omega_{\rm M0})(1+z')^{3(w_{\rm X}+1)}}}dz'. \tag{5.92}$$

This expression is equivalent to Eq. (5.86) when $\beta=1/4$,

$$D_{\rm L}(z)=\frac{c}{H_0}\frac{2(1+z)}{\sqrt{\Omega_{\rm M0}}}\left\{{}_2F_1\left[-\frac{1}{6w_{\rm X}},\frac{1}{2},1-\frac{1}{6w_{\rm X}},\frac{\Omega_{\rm M0}-1}{\Omega_{\rm M0}}\right]\right. \tag{5.93}$$

$$\left.-\frac{1}{\sqrt{1+z}}\,{}_2F_1\left[-\frac{1}{6w_{\rm X}},\frac{1}{2},1-\frac{1}{6w_{\rm X}},\frac{\Omega_{\rm M0}-1}{\Omega_{\rm M0}}(1+z)^{3w_{\rm X}}\right]\right\}.$$

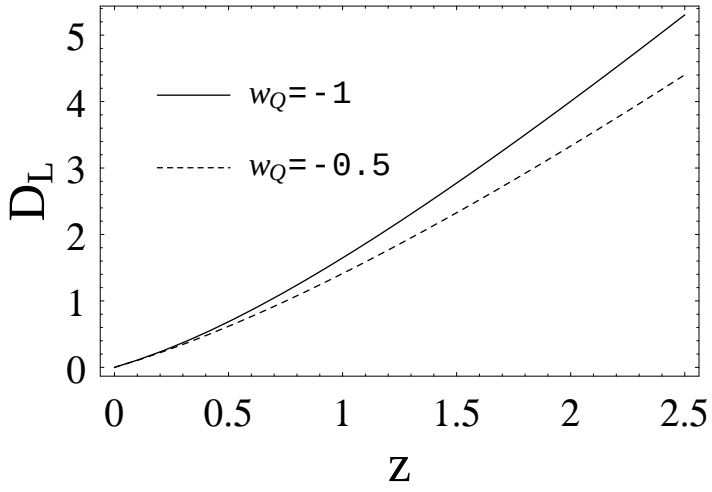

Figure 5.2: The luminosity distance in a flat and smooth universe with $\Omega_{\rm M0} = 0.3$. The distance is in units of c/H_0.

Our Eq. (5.93) is equivalent to the expression found in [16], see also [71]. In the Einstein-de Sitter case ($\Omega_{\rm M0} = 1$ or $w_{\rm X} \to 0$), Eq. (5.93) reduces to

$$D_{\rm L}(z) = 2\frac{c}{H_0}(1+z)\left(1 - \frac{1}{\sqrt{1+z}}\right), \tag{5.94}$$

as can also be seen directly by solving the integral in Eq. (5.92). Figure (5.2) plots the luminosity distance for different equations of state: the distance increases for decreasing $w_{\rm X}$.

The integral in Equation (5.92) can be expressed in terms of elementary functions for particular values of $n_{\rm X}$. It is the integral of the differential binomial

$$\tilde{x}^{\tilde{\mu}}(\tilde{a} + \tilde{b}\tilde{x}^{\tilde{\nu}})^{\tilde{\rho}}, \tag{5.95}$$

where $\tilde{x} = 1+z,\ \tilde{a} = \Omega_{\rm M0},\ \tilde{b} = 1 - \Omega_{\rm M0},\ \tilde{\mu} = -3/2,\ \tilde{\nu} = n_{\rm X} - 3$ and $\tilde{\rho} = -1/2$. We can put this integral in rational form when

$$n_{\rm X} = \frac{3s-1}{s},\ s \in \mathcal{Z} - \{0\}, \tag{5.96}$$

performing the substitutions [144]

$$t = \sqrt{\Omega_{\rm M0} + (1+\Omega_{\rm M0})(1+z)^{n_{\rm X}-3}}$$

when s is even, and

$$t = \sqrt{\frac{\Omega_{\rm M0} + (1+\Omega_{\rm M0})(1+z)^{n_{\rm X}-3}}{(1+z)^{n_{\rm X}-3}}}$$

for odd s. Equation (5.96) includes all and only the rational values of $n_{\rm X}$ for which equation (5.92) can be solved in terms of elementary functions. $n_{\rm X}$ varies from 2

($w_{\rm X} = -1/3$), when quintessence evolves like curvature, to 4 ($w_{\rm X} = 1/3$)(*hot dark matter*); for $s \to \pm\infty$, $n_{\rm X}$ tends to 3, giving ordinary pressureless matter. For $n_{\rm X} = 2$, see also [113], we get

$$D_{\rm L}(z_{\rm d}, z) = \frac{c}{H_0}\frac{2}{\sqrt{1-\Omega_{\rm M0}}}(1+z)\left[\mathrm{Arctanh}\left(\frac{\sqrt{1+\Omega_{\rm M0}z}}{\sqrt{1-\Omega_{\rm M0}}}\right)\right]_{z=z_{\rm d}}^{z}; \tag{5.97}$$

we note that with respect to the dynamical equations, a flat universe with $n_{\rm X} = 2$ behaves like an open one with $\Omega_{\rm K0} = 1 - \Omega_{\rm M0} \neq 0$, but, on the other hand, while quintessence contributes to the Ricci focusing, a geometric term does not. For $n_{\rm X} = 4$, it is

$$D_{\rm L}(z_{\rm d}, z) = \frac{c}{H_0}\frac{2}{\Omega_{\rm M0}}(1+z)\left[\frac{\sqrt{1+z-\Omega_{\rm M0}z}}{(1+z)^{1/2}}\right]_{z}^{z=z_{\rm d}}. \tag{5.98}$$

Equation (5.98) holds in the past history of the universe at the epoch of matter-radiation equality ($z_{eq} \sim 10^4$). Other solutions with $2 < n_{\rm X} < 4$ are easily found. Even if they can be physically interesting when related to other behaviours of the scale factor, they cannot explain the today observed accelerated universe. So, we will not mention them here.

5.4.2 Totally clumpy universe

We now study very particular models of universe in which both matter and quintessence are totally clumped, that is $\alpha_{\rm M} = \alpha_{\rm X} = 0$. In this case, the DR equation reduces to a first order equation and the expression for the angular diameter distance becomes

$$D_{\rm A}(z_{\rm d}, z) = \frac{c}{H_0}(1+z_{\rm d})\int_{z_{\rm d}}^{z}\frac{dz'}{(1+z')^2\sqrt{\Omega_{\rm M0}(1+z')^3 + \Omega_{\rm X0}(1+z')^{n_{\rm X}}}}. \tag{5.99}$$

The energy density supplied by a cosmological constant is homogenously distributed; but, even if $\alpha_\Lambda = 1$, when $n_{\rm X} = 0$ ($w_{\rm X} = -1$) and $\alpha_{\rm M} = 0$, the DR equation becomes again of the first order independently of the values of $\Omega_{\Lambda 0}$, and so the distance takes the form

$$D_{\rm A}(z_{\rm d}, z) = \frac{c}{H_0}(1+z_{\rm d})\int_{z_{\rm d}}^{z}\frac{dz'}{(1+z')^2\sqrt{\Omega_{\rm M0}(1+z')^3 + \Omega_{\Lambda 0}}}. \tag{5.100}$$

Once again, in equation (5.99) there is the integral of a differential binomial of the form given in equation (5.95), with, this time, $\tilde{a} = \Omega_{\rm M0}$, $\tilde{b} = 1 - \Omega_{\rm M0}$, $\tilde{\mu} = -7/2$, $\tilde{\nu} = n_{\rm X} - 3$ and $\tilde{\rho} = -1/2$. When $n_{\rm X}$ is rational, all and only the solutions of equation (5.99) in terms of elementary functions occur when

$$n_{\rm X} = \frac{3s-5}{s},\ s \in \mathcal{Z} - \{0\}; \tag{5.101}$$

for any such s we can perform the same substitutions already described for homogeneous universes in the previous subsection. Now, we have values of $n_{\rm X} < 2$: for $s = 2,\ 3,\ 4$, respectively, we find $n_{\rm X}\ (w_{\rm X}) = 1/2\ (-5/6),\ 4/3\ (-5/9),\ 7/4\ (-5/12)$. For $n_{\rm X} = 1/2$, it is

$$D_{\rm A}(z_{\rm d}, z) = \frac{c}{H_0}\frac{4(1+z_{\rm d})}{5(1-\Omega_{\rm M0})}\left[\sqrt{\Omega_{\rm M0} + \frac{1-\Omega_{\rm M0}}{(1+z_{\rm d})^{5/2}}} - \sqrt{\Omega_{\rm M0} + \frac{1-\Omega_{\rm M0}}{(1+z)^{5/2}}}\right]; \quad (5.102)$$

for $n_{\rm X} = 4/3$, we get

$$\begin{aligned} D_{\rm A}(z_{\rm d}, z) = \frac{c}{H_0}(1+z_{\rm d})\Bigg[&\frac{6}{5}\Omega_{\rm M0}\sqrt{1-\Omega_{\rm M0}+\Omega_{\rm M0}(1+z)^{5/3}} \\ &\times \Bigg((\Omega_{\rm M0}-1)^2 + \frac{2}{3}(\Omega_{\rm M0}-1)^2\left(1-\Omega_{\rm M0}+\Omega_{\rm M0}(1+z)^{\frac{5}{3}}\right) \\ &+ \frac{1}{5}\left(1-\Omega_{\rm M0}+\Omega_{\rm M0}(1+z)^{\frac{5}{3}}\right)^2\Bigg)\Bigg]_{z=z_{\rm d}}^{z}, \end{aligned} \quad (5.103)$$

and, for $n_{\rm X} = 7/4$,

$$\begin{aligned} D_{\rm A}(z) = &\frac{c}{H_0}\frac{8}{5(1-\Omega_{\rm M0})^2} \\ &\times\left\{\frac{1}{3} - \Omega_{\rm M0} - \frac{1}{3}\left(\frac{1-\Omega_{\rm M0}}{(1+z)^{\frac{5}{4}}} + \Omega_{\rm M0}\right)^{\frac{3}{2}} + \Omega_{\rm M0}\sqrt{\frac{1-\Omega_{\rm M0}}{(1+z)^{\frac{5}{4}}} + \Omega_{\rm M0}}\right\}. \end{aligned} \quad (5.104)$$

Other interesting results are obtained when $n_{\rm X} = 2$ ($s = 5$) and $n_{\rm X} = 4$ ($s = -5$). For $n_{\rm X} = 2$ (string networks), the angular diameter distance is

$$\begin{aligned} D_{\rm A}(z_{\rm d}, z) = &2\frac{c}{H_0}(1+z_{\rm d})\Omega_{\rm M0}^2\mathcal{E} \\ &\times\left[(\Omega_{\rm M0}-1)^3 + (\Omega_{\rm M0}-1)^2\mathcal{E} + \frac{3}{5}(\Omega_{\rm M0}-1)\mathcal{E}^2 + \frac{1}{7}\mathcal{E}^3\right]_{z=z_{\rm d}}^{z}, \end{aligned} \quad (5.105)$$

where $\mathcal{E} \equiv \sqrt{1-\Omega_{\rm M0}+(1+z)\Omega_{\rm M0}}$; for $n_{\rm X} = 4$ (hot dark matter), it is

$$\begin{aligned} D_{\rm A}(z_{\rm d}, z) = &\frac{c}{H_0}\frac{1+z_{\rm d}}{\Omega_{\rm M0}^3(\Omega_{\rm M0}-1)} \\ &\times\left[\frac{\mathrm{Arctan}\left(\sqrt{\frac{1+z-\Omega_{\rm M0}z}{(1+z)(\Omega_{\rm M0}-1)}}\right)}{\sqrt{1-\Omega_{\rm M0}}} + \sqrt{\frac{(1+z)(1+z-z\Omega_{\rm M0})}{\Omega_{\rm M0}}}\right]_{z}^{z=z_{\rm d}}. \end{aligned} \quad (5.106)$$

In the limit $s \to \pm\infty$, $n_{\rm X}$ goes to 3 (cold dark matter).

5.5 Parameter degeneracy

As seen, the consideration of the DR equation in its full generality, with respect to the case of a homogeneous cosmological constant, demands the introduction of new

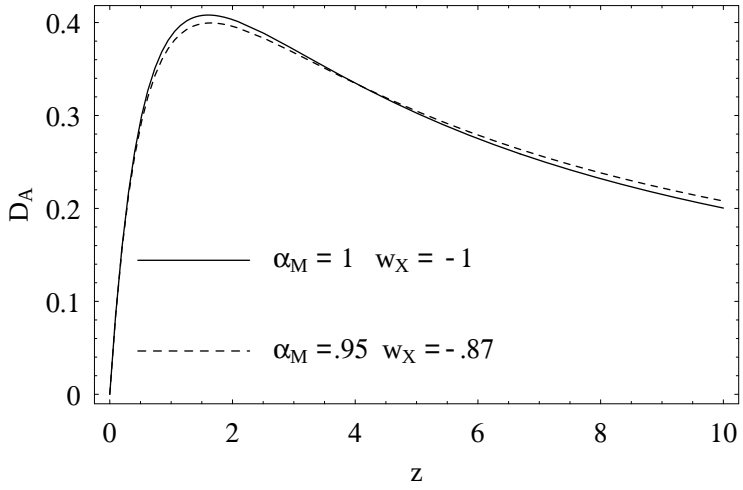

Figure 5.3: The angular diameter distance for different values of $\alpha_{\rm M}$ and $w_{\rm X}$. We assume a flat universe with $\Omega_{\rm M0} = 0.3$. The unit of distance is taken to be c/H_0.

parameters. Let us study the case of homogeneous dark energy ($\alpha_{\rm X} = 1$). For $\alpha_{\rm X} = 1$, equation (5.30), in units of c/H_0, simplifies to

$$D_{\rm A}(z) = D_1(z) + \int_0^z \sum_{i=1}^{\infty} K_i(y,z) D_1(y) dy, \tag{5.107}$$

while equation (5.32) reduces, for $y \leq z$, to

$$K_1(y,z) = \frac{3}{2}(1-\alpha_{\rm M})\Omega_{\rm M0}\frac{H_0}{H(y)}(1+y)^2 D_1(y,z). \tag{5.108}$$

Some monotonical properties with respect to the cosmological parameters are then easily derived. Accelerated universes demands $w_{\rm X} < -1/3$; then, it is

$$\frac{\partial}{\partial\Omega_{\rm X0}}\frac{1}{H(z)} > 0, \ \frac{\partial}{\partial\Omega_{\rm X0}} D_1(z) > 0 \text{ if } w_{\rm X} < -1/3, \tag{5.109}$$

and so, for every value of the clumpiness parameter $\alpha_{\rm M}$, the angular diameter distance increases with increasing $\Omega_{\rm X0}$,

$$\frac{\partial}{\partial\Omega_{\rm X0}} D_{\rm A}(z) > 0 \text{ if } w_{\rm X} < -1/3. \tag{5.110}$$

When $w_{\rm X} > -1/3$, the inequalities in equation (5.109) are reversed and the distance decreases with increasing $\Omega_{\rm X0}$. With respect to the equation of state $w_{\rm X}$, it is

$$\frac{\partial}{\partial w_{\rm X}}\frac{1}{H(z)} < 0, \ \frac{\partial}{\partial w_{\rm X}} D_1(z) < 0; \tag{5.111}$$

and so

$$\frac{\partial}{\partial w_{\rm X}} D_{\rm A}(z) < 0; \tag{5.112}$$

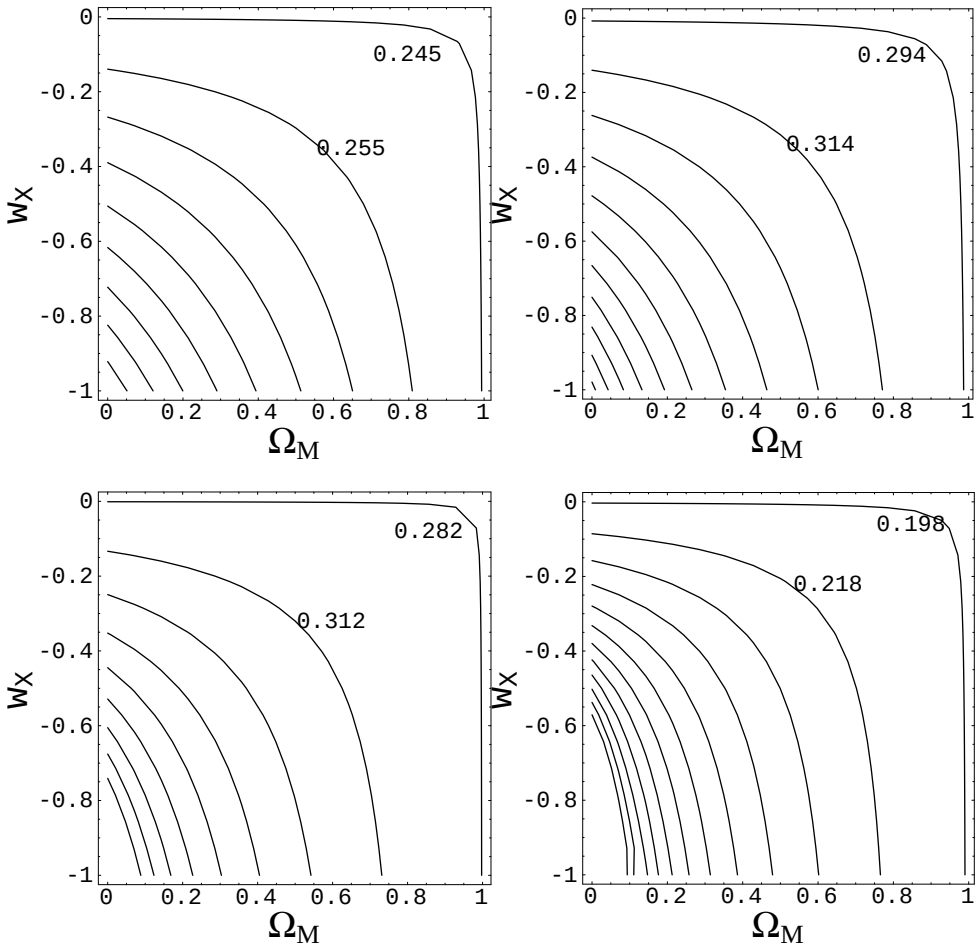

Figure 5.4: The angular diameter distance in the $\Omega_{\rm M0} - w_{\rm X}$ plane, when $\alpha_{\rm M} = \alpha_{\rm X} = 1$. The distance increases from the top-right to the bottom-left corner. *a)* We assume $z = 0.5$; each contour is drawn with steps of 0.01. *b)* We assume $z = 1$; the step is 0.02. *c)* We assume $z = 2$; the step is 0.03. *d)* We assume $z = 5$; the step is 0.02. The unit of distance is taken to be c/H_0.

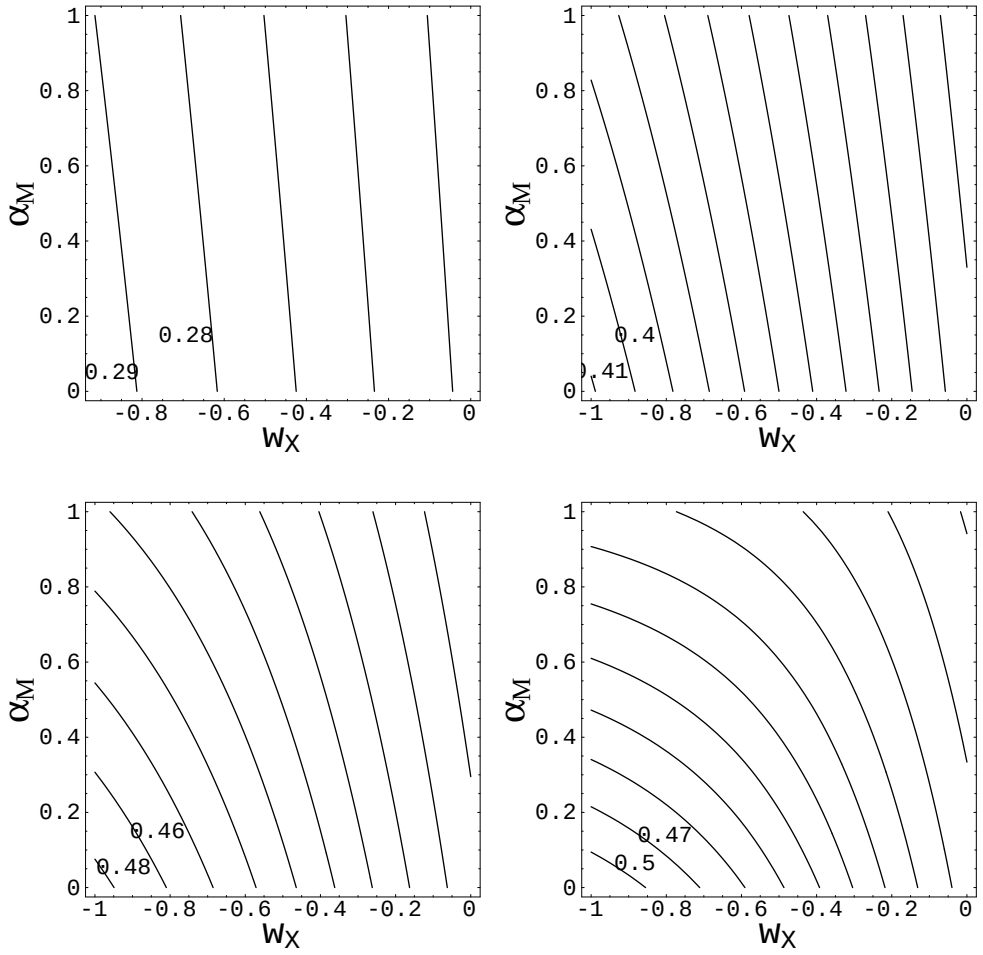

Figure 5.5: The angular diameter distance in the $w_{\rm X} - \alpha_{\rm M}$ plane, when $\Omega_{\rm M0} = 0.3$ and $\alpha_{\rm X} = 1$. The distance increases from the top-right to the bottom-left corner. *a)* We assume $z = 0.5$; each contour is drawn with steps of 0.01. *b)* We assume $z = 1$; the step is 0.01. *c)* It is $z = 2$; the step is 0.02. *d)* it is $z = 5$; the step is 0.03. The unit of distance is taken to be c/H_0.

large values of the distances correspond to strongly negative values of the pressure of quintessence: for fixed $\Omega_{\rm M0}$, $\Omega_{\rm X0}$ and $\alpha_{\rm M}$, the angular diameter distance takes its maximum when the dark energy is in the form of a cosmological constant.

We now want to stress the dependence of the angular diameter distance on $w_{\rm X}$, $\Omega_{\rm M0}$ and $\alpha_{\rm M}$ in flat universes with $\alpha_{\rm X} = 1$. As Fig. (4.4) and Fig. (5.3) show, the angular diameter distance is degenerate with respect to different pairs of parameters: the distance in the ΛCDM model with $\Omega_{\rm M0} = 0.3$ is not distinguishable, within the current experimental accuracy [140], from the one in a FLRW universe with less pressureless matter but a greater value of $w_{\rm X}$ or from an inhomogeneous universe with greater $w_{\rm X}$ and the same content of matter.

In Fig. (5.4), we plot the degenerate values of the distance in the $\Omega_{\rm M0} - w_{\rm X}$ plane when universe is homogeneous for four different source redshifts: as expected, the dependence of the distance on the cosmological parameters increases with the redshift of the source. A general feature is that the distance is less sensitive to the components of the universe when $\Omega_{\rm M0}$ is near unity and $w_{\rm X}$ goes to 0. This is easily explained: when $\Omega_{\rm M0}$ is large, quintessence density $\Omega_{\rm X0}$ is not, and the pressureless matter characterizes almost completely the universe; moreover, a value of $w_{\rm X}$ near zero describes a dark energy with an equation of state very similar to that of the ordinary matter. So, increasing $w_{\rm X}$ mimics a growth in $\Omega_{\rm M0}$. On the other side, for low values of $\Omega_{\rm M0}$ ($w_{\rm X}$) the distance is very sensitive to $w_{\rm X}$ ($\Omega_{\rm M0}$) and this effect increases with the redshift. We see from Fig. (5.4) that the effects of $w_{\rm X}$ and $\Omega_{\rm M0}$ are of the same order for a large range of redshifts.

In Fig. (5.5) we compare, for $\Omega_{\rm M0}$ fixed to 0.3 and for different source redshifts, the compelling effects of $\alpha_{\rm M}$ and $w_{\rm X}$ on the distance. When $\alpha_{\rm M}$ goes away from the usually assumed value ($\alpha_{\rm M} = 1$), once fixed the redshift, the distance increases; on the contrary, for $w_{\rm X}$ that goes away from the value corresponding to the cosmological constant ($w_{\rm X} = -1$), the distance decreases. The dependence of the distance on $\alpha_{\rm M}$ increases very rapidly with z, and, when $z = 5$, the effects of $\alpha_{\rm M}$ and $w_{\rm X}$ are of the same order. From Fig. (5.5), we deduce that the dependence on $\alpha_{\rm M}$ increases when $w_{\rm X}$ goes to -1, since values of $w_{\rm X}$ near zero have the effect to smooth the universe. In fact, when $w_{\rm X} = -1$, both a fraction $\alpha_{\rm M}$ of the pressureless matter and of the cosmological constant are uniformly distributed; when $w_{\rm X} \to 0$, quintessence behaves like ordinary matter, and so, for the same value of $\alpha_{\rm M}$, the pressureless matter homogeneously distributed is $\alpha_{\rm M}\Omega_{\rm M0} + \Omega_{\rm X0} = 1 - (1 - \alpha_{\rm M})\Omega_{\rm M0}$. Intermediate values of $w_{\rm X}$ interpolate between these two extreme cases.

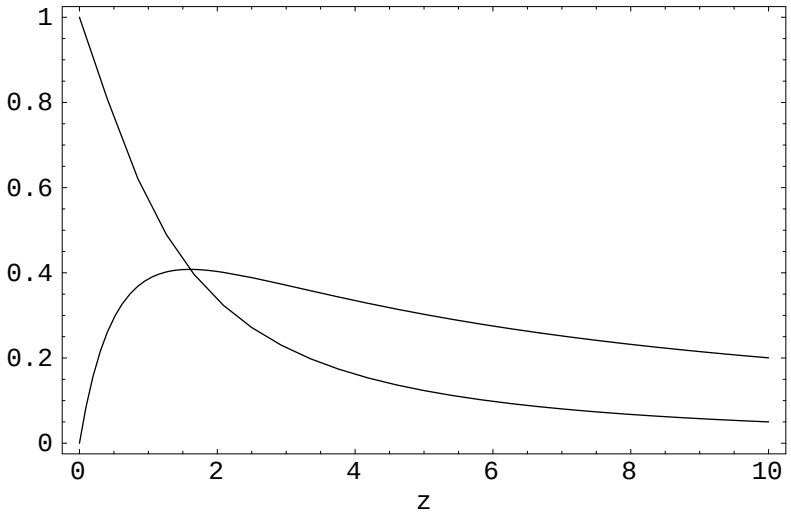

Figure 5.6: For flat homogeneous universes $z_{\rm m}$ is determined by the intercept between the angular diameter distance and the always decreasing Hubble distance. The values on the ordinate axis are in units of c/H_0. It is $\Omega_{\rm M0} = 0.3,\ w_{\rm X} = -1$.

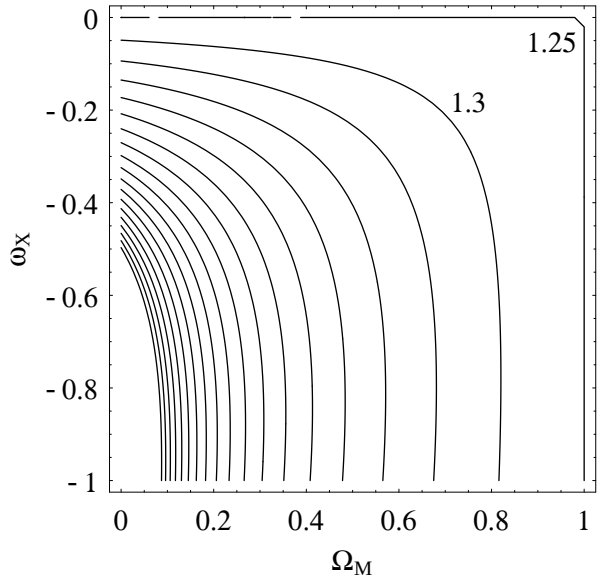

Figure 5.7: Contours of equal $z_{\rm m}$ on the $\Omega_{\rm M0} - w_{\rm X}$ plane for flat homogeneous universes. Each contour is drawn with a step of 0.05.

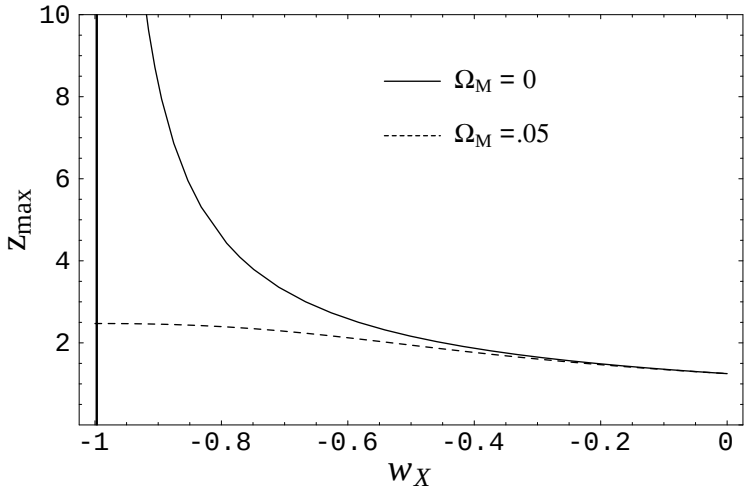

Figure 5.8: $z_{\rm m}$ as a function of $w_{\rm X}$ for two values of $\Omega_{\rm M0}$. For $\Omega_{\rm M0} = 0.05$, $z_{\rm m}$ nearly halves itself (from 2.47 to 1.25) when $w_{\rm X}$ goes from -1 to 0.

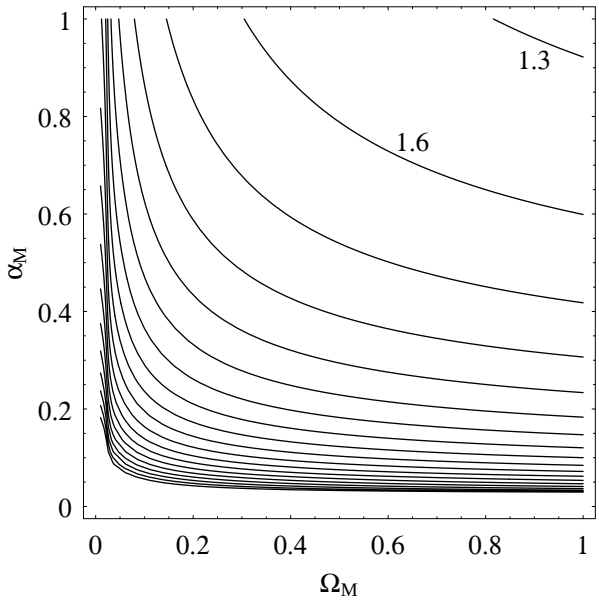

Figure 5.9: Contours of equal $z_{\rm m}$ on the $\Omega_{\rm M0} - \alpha_{\rm M}$ plane for universes with a cosmological constant. Contours are drawn with steps of 0.03.

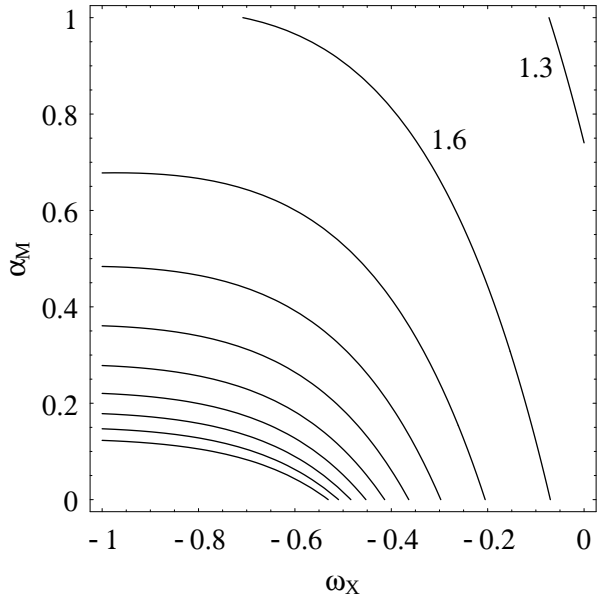

Figure 5.10: Contours of equal $z_{\rm m}$ on the $w_{\rm X} - \alpha_{\rm M}$ plane for flat universes with $\Omega_{\rm M0} = 0.3$ and $\alpha_{\rm X} = 1$. Contours are drawn with steps of 0.03.

5.6 The critical redshift

The critical redshift at which the angular diameter distance of an extragalactic source takes its maximum value has already been studied for the case of a flat universe with a cosmological constant in [108] and for a flat universe with quintessence in [113]. In this section, we will find again their results with a new approach and will extend the analysis to inhomogeneous flat universes [182]. Without being explicitly stated, we assume will $\alpha_{\rm X} = 1$.

Let us first consider the Einstein-de Sitter model. As can be easily seen, the maximum redshift is

$$z_{\rm m} = \left(\frac{5+4\beta}{5-4\beta}\right)^{\frac{1}{2\beta}} - 1 \ ; \tag{5.113}$$

when $\alpha_{\rm M}$ moves from 1 to 0, (β from 1/4 to 5/4), $z_{\rm m}$ goes from 1.25 to ∞. The maximum of the angular diameter distance is directly related to the mass within the light bundle [54, 226].

We want now evaluate the effect of the dark energy. As can be seen cancelling out the derivative of the right hand of equation (5.92) with respect to z, the critical redshift $z_{\rm m}$ for a flat homogeneous universe occurs when

$$D_{\rm A}(z_{\rm d}, z_{\rm m}) = \frac{c}{H(z_{\rm m})}, \tag{5.114}$$

so that, the angular diameter distance between an observer at $z = z_{\rm d}$ and a source at $z_{\rm m}$ is equal to the Hubble distance for $z = z_{\rm m}$, as you can see in Fig. (5.6). Equation (5.114)

is an implicit relation that gives the dependence of $z_{\rm m}$ on $z_{\rm d}, \Omega_{\rm M0}$ and $w_{\rm X}$. Throughout this section, we will put $z_{\rm d} = 0$. In Fig. (5.7) we show $z_{\rm m}$ for a homogeneous flat universe. For a given value of $w_{\rm X}$ ($\Omega_{\rm M0}$), $z_{\rm m}$ decreases with increasing $\Omega_{\rm M0}$ ($w_{\rm X}$); when $\Omega_{\rm M0} = 0$, $z_{\rm m}$ diverges for $w_{\rm X} = -1$, but also a small value of $\Omega_{\rm M0}$ is sufficient to eliminate this divergence, see Fig. (5.8). The minimum value of $z_{\rm m}$ corresponds to the Einstein-de Sitter universe ($\Omega_{\rm M0} = 1$ or $w_{\rm X} = 0$), when $z_{\rm m} = 1.25$. As you can see from Fig. (5.7), for values of $w_{\rm X}$ in the range $(-1, -0.8)$, once fixed $\Omega_{\rm M0}$, $z_{\rm m}$ is nearly constant and this trend increases with $\Omega_{\rm M0}$; on the contrary, for small $\Omega_{\rm M0}$ ($\lesssim 0.4$) and $w_{\rm X} \gtrsim -0.4$, $z_{\rm m}$ is very sensitive to $w_{\rm X}$. The small changes of $z_{\rm m}$ in the region of large $\Omega_{\rm M0}$ and $w_{\rm X}$ are explained with considerations analogous to those already made in the previous section for the values of the distance in the $\Omega_{\rm M0} - w_{\rm X}$ plane.

Let us go now to analyse the effect of $\alpha_{\rm M}$ on $z_{\rm m}$. By differentiating equation (5.99) and equation (5.100) with respect to z, we see that the derivatives are zero only for $z \to \infty$: i.e., in flat universes with totally inhomogeneous quintessence or in a generic model with cosmological constant, the critical redshift is not finite when $\alpha_{\rm M} = 0$. So with respect to $z_{\rm m}$, a totally clumpy universe, independently of $\Omega_{\rm M0}$ and $w_{\rm X}$, behaves like a FLRW model completely dominated by the vacuum energy. In fact, the cosmological constant, differently from dark energy with $w_{\rm X} > -1$, does not give contribution to the Ricci focusing and the same occurs for the pressureless matter with $\alpha_{\rm M} = 0$. In Fig. (5.9), we show $z_{\rm m}$ in the $\Omega_{\rm M0} - \alpha_{\rm M}$ plane for $w_{\rm X} = -1$. The critical redshift decreases with increasing $\Omega_{\rm M0}$ and $\alpha_{\rm M}$, and takes its minimum for the Einstein-de Sitter universe ($\Omega_{\rm M0} = \alpha_{\rm M} = 1$), that is when the focusing is maximum. On the other side, $z_{\rm m}$ is very sensitive to $\alpha_{\rm M}$, especially for large values of $\Omega_{\rm M0}$ since $\alpha_{\rm M}$ appears in the DR equation as a multiplicative factor of $\Omega_{\rm M0}$. For $\Omega_{\rm M0} = 0.3$, $z_{\rm m} = 1.61$ and 3.23 for, respectively, $\alpha_{\rm M} = 1$ and 0.2, a variation of 100%. So, combining different cosmological tests to constrain the other cosmological parameters, we can use the redshift-distance relation to guess the smoothness parameter $\alpha_{\rm M}$ in a quite efficient way.

We conclude this section comparing the influence of $\alpha_{\rm M}$ and $w_{\rm X}$ on the critical redshift. Fig. (5.10) displays $z_{\rm m}$ in the $\alpha_{\rm M} - w_{\rm X}$ plane, for $\Omega_{\rm M0}$ fixed to 0.3 and with $\alpha_{\rm X} = 1$. As expected, $z_{\rm m}$ increases when the focusing decreases, that is for small values of $\alpha_{\rm M}$ and $w_{\rm X}$. We can see that the effects of $\alpha_{\rm M}$ and $\Omega_{\rm M0}$ are of the same order.

5.7 The magnification probability distribution function

The amplification of a source at a given redshift has a statistical nature. For narrow light-beams, the effect of gravitational lensing results in the appearance of shear and

convergence in images of distant sources according to the different amount and distribution of matter along different lines of sight. So, gravitational lensing increases the level of errors in the Hubble diagram [10, 67, 85, 86, 98, 97, 123, 145, 211]. In the framework of the on average FLRW universe, we can account for this effect by considering a direction dependent smoothness parameter $\alpha_{\rm M}$. Now, $\alpha_{\rm M}$ represents the effective fraction of matter density in the beam connecting the observer and the source and depends on the distribution of matter in the beam [213]; values of $\alpha_{\rm M}$ greater than one account for amplification effects. We will consider homogeneously distributed dark energy ($\alpha_{\rm X} = 1$).

There is a unique mapping between the magnification μ of a standard candle at redshift z and the direction-dependent smoothness parameter at z [213]. According to Eq. (1.17), the magnification μ of the source with respect to the maximum empty-beam case ($\alpha_{\rm M} = 0$) is

$$\mu = \left[\frac{D_{\rm L}(\alpha_{\rm M} = 0)}{D_{\rm L}(\alpha_{\rm M})}\right]^2 . \tag{5.115}$$

Once derived the magnification (that is, once found the distance by integrating the null-geodesic equation or using ray-tracing techniques along a line of sight) of a source at epoch z, the corresponding smoothness parameter is determined in comparison with the DR distance: the solution of the DR equation for that constant value of $\alpha_{\rm M}$ matches, at redshift z, that given value of the distance [193, 213].

The shape of the magnification probability distribution function (pdf) depends on the redshift of the source, on the cosmological parameters and on the nature of the dark matter (DM). The dark matter can be classified according to its clustering properties [124, 126, 177]: microscopic DM consists of weakly interacting massive particles (WIMPs), such as neutralinos [78, 79] and clumps on galaxy halo-scales; macroscopic DM consists of compact objects, such as massive compact halo objects (MACHOs) or primordial black holes.

According to N-body simulations of large scale structures in cold dark matter models, galactic halos are expected to contain a large number of small substructures besides their overall profile. However, this type of small-scale structure does not act as a compact object and only clumps of galaxy-size contribute appreciably to the lensing [126].

In the framework of the on average FLRW models, the μ-pdf is characterized by some general features with no regard to the nature of the DM. Under the assumption that the area of a sphere at redshift z centred on the observer is not affected by the mass distribution, the photon number conservation implies that the mean apparent magnitude of a source at z is identical to the FLRW value [172, 215],

$$\langle\mu\rangle = \mu_{\rm FL} \equiv \mu(\alpha_{\rm M} = 1) > 1. \tag{5.116}$$

Since the matter is clumped, most of the narrow light-beams from distant sources do not intersect any matter along the line of sight resulting in a dimming of the image with respect to the filled-beam case: the mode of the pdf, $\mu_{\rm peak}$, is biased towards the empty beam value,

$$\mu_{\rm peak} < \langle \mu \rangle. \tag{5.117}$$

The third feature is a tail towards large amplifications which preserves the mean. In terms of the magnification relative to the mean,

$$\delta\mu \equiv \left[\frac{D_{\rm L}(\alpha_{\rm M}=0)}{D_{\rm L}(\alpha_{\rm M})}\right]^2 - \left[\frac{D_{\rm L}(\alpha_{\rm M}=0)}{D_{\rm L}(\alpha_{\rm M}=1)}\right]^2, \tag{5.118}$$

the $\delta\mu$-pdf has the mean at $\delta\mu = 0$, the peak value at $\delta\mu_{\rm peak} < 0$ and a long tail for $\delta\mu > 0$, with no regard to the source redshift and to the cosmological parameters. It follows from these very general considerations that a simple way to characterize the pdf is to consider the parameter $\Delta\mu$, defined as the difference in amplification between the mean FLRW value and the magnification in the empty beam case ($\alpha_{\rm M} = 0$), $\Delta\mu \equiv -\delta\mu(\alpha_{\rm M} = 0)$. When $\Delta\mu$ increases, the mode value moves towards greater de-magnification: to preserve the total probability and the mean value, the pdf must both reduce its maximum and enlarge its high amplification tail. From the properties of the angular diameter distance in a clumpy universe discussed in the previous sections, it follows that $\Delta\mu$ increases with the redshift of the source and with dark energy with large negative pressure. So, the dispersion in the μ-pdf due to gravitational lensing increases with z and it is maximum for the case of the cosmological constant, see also [14]: quintessence with $w_{\rm X} > -1$ reduces the bias towards large de-amplifications of the peak value of the pdf, partially attenuating the effect of the clumpiness.

5.7.1 Lensing by microscopic dark matter

The gravitational lensing effect by large-scale structures on the apparent luminosity of distant sources in the universe has been studied either with N-body simulations [10, 11, 94, 193, 211] or with the integration of the geodesic deviation equation [14, 86] in a universe filled with either isothermal spheres or Navarro-Frenk-White profiles [129, 130].

The μ-pdf for the smoothly distributed DM is characterized by two main trends with increasing redshift: an increase in the dispersion and an increasing gaussianity. As we look back to earlier times, the universe becomes smoother on average and lines of sight become more filled in with matter: light bundles intersect more independent regions along their paths and the resulting μ-pdf approaches a gaussian by the central limit theorem [177, 213]. The corresponding $\alpha_{\rm M}$-pdf also becomes symmetric but it reduces its dispersion and its mode goes to the filled-beam value [11, 193, 213].

The trends in dispersions in the μ-pdf and $\alpha_{\rm M}$-pdf are opposite since, with increasing redshift, a large variation in the distance corresponds to a small variation in the smoothness parameter [182]. Wambsganss et al. [211] used the ray-tracing method for large-scale simulations in a cold dark matter universe, normalized to the first year COBE data with $\Omega_{\rm M0} = 0.4$, $\Omega_{\rm X0} = 0.6$, $w_{\rm X} = -1$, with a spatial resolution on small scales of the order of the size of a halo, to derive the μ-pdf at different redshifts. Wang [213] was able to find empirical formulae for the fitting of the μ-pdf and of the corresponding $\alpha_{\rm M}$-pdf,

$$p_\mu(\mu, z) = p_{\alpha_{\rm M}}(\alpha_{\rm M}, z) \left| \frac{\partial \alpha_{\rm M}}{\partial \mu} \right| = p_{\alpha_{\rm M}}(\alpha_{\rm M}, z) \frac{D_{\rm A}(\alpha_{\rm M} = 0)}{2\mu^{3/2}} \left| \frac{\partial D_{\rm A}}{\partial \alpha_{\rm M}} \right|^{-1} . \tag{5.119}$$

As noted in [193], the angular diameter distance depends on $\alpha_{\rm M}$ linearly for $0 \leq z \lesssim 5$ and, with high precision, we can approximate

$$\frac{\partial D_{\rm A}}{\partial \alpha_{\rm M}} \simeq D_{\rm A}(\alpha_{\rm M} = 1) - D_{\rm A}(\alpha_{\rm M} = 0). \tag{5.120}$$

In Fig. (5.11), we plot the $\delta\mu$ corresponding to the mode of the $\alpha_{\rm M}$-pdf (as plotted in figure (2b) in [213]) as a function of the redshift: while the mode value of the $\alpha_{\rm M}$-pdf goes to the filled-beam value for increasing redshift, the variation in magnification with respect to the FLRW mean increases; that is, the bias increases with z.

To study the role of the quintessence in the magnification dispersion of standard candles, we consider the same matter content [213], that is the same $\alpha_{\rm M}$-pdf, for different equations of state. Models with different cosmological parameters produce, in general, different $\alpha_{\rm M}$-pdf, predictable by numerical simulations; but, to consider the influence of the dark energy on the μ-pdf, it suffices to use the same matter distribution in Eq. (5.119). This is equivalent to assume that the dependence on quintessence enters Eq. (5.119) through the angular diameter distances and that the effect on $p_{\alpha_{\rm M}}$ is of the second order. So, for analytical convenience, we can use the same $p_{\alpha_{\rm M}}$ derived in [213] for several cosmological models with the same $\Omega_{\rm M0}$ but different equations of state. In Fig. (5.12), the μ-pdf is plotted for two source redshifts and for two different equations of state: the μ-pdf becomes more and more symmetric with z and the dark energy reduces both the dispersion and the bias.

The effect of gravitational lensing by large-scale structures affects significantly the determination of the cosmological parameters from observations of standard candles. Observed SNe Ia represent individual sources at each redshift and do not sample evenly the probability distribution: at a fixed redshift, we will observe the mode value of the distribution and not the mean one [211, 10]. For $\Omega_{\rm M0} = 0.4$, $w_{\rm X} = -1$ and $z = 1$, the mode is $\mu_{\rm peak} = 1.14$ and the magnification values above and below which 97.5% of all of the lines of sight fall are $\mu_{\rm low} = 1.11$ and $\mu_{\rm high} = 1.28$. This dispersion induces uncertainties in determining $\Omega_{\rm M0}$ and the equation of state. Assuming a flat universe

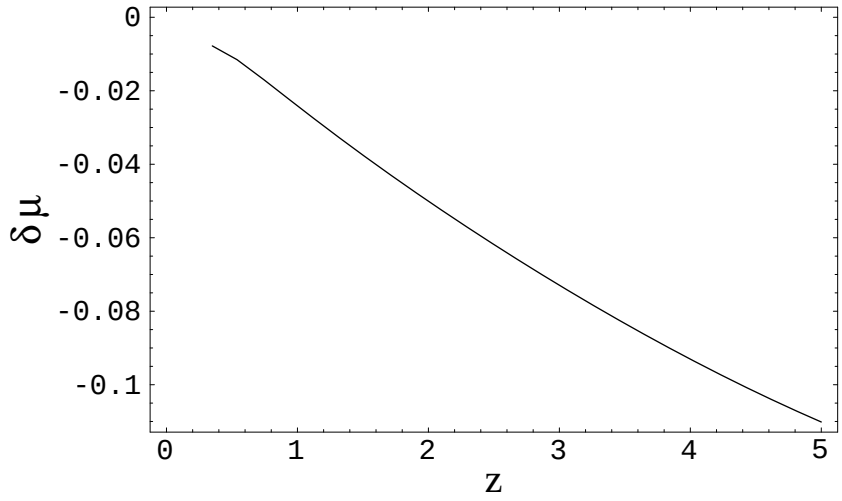

Figure 5.11: The magnification relative to the mean calculated for the peak value of the $\alpha_{\rm M}$-pdf as found in Wang (1999). It is $\Omega_{\rm M0} = 0.4$, $\Omega_{\rm X0} = 0.6$ and $w_{\rm X} = -1$.

with cosmological constant, a universe with $\Omega_{\rm M0} = 0.4$ will be interpreted as a model with $\Omega_{\rm M0} = 0.42^{+0.03}_{-0.11}$ only because of the gravitational lensing noise. Here and in what follows, the error bars represent 2-σ limits. With the constraint of $\Omega_{\rm M0} = 0.4$, a cosmological constant might be interpreted as dark energy with $w_{\rm X} < -0.84$.

For a flat universe with $\Omega_{\rm M0} = 0.4$ and $w_{\rm X} = -0.5$, at $z = 1$ it is $\mu_{\rm peak} = 1.11$, $\mu_{\rm low} = 1.09$ and $\mu_{\rm high} = 1.23$. With the constraint $w_{\rm X} = -0.5$, we should estimate $\Omega_{\rm M0} = 0.43^{+0.05}_{-0.18}$; assuming $\Omega_{\rm M0} = 0.4$, it is $w_{\rm X} = -0.46^{+0.05}_{-0.24}$.

Although the lensing dispersion is reduced in a quintessence cosmology, the errors induced on the cosmological parameters increase. The reason is that in this models the luminosity distance is less sensitive to the cosmology [182].

5.7.2 Lensing by compact objects

The effect of gravitational lensing is maximum when the matter in the universe consists of point masses [86]; as seen above, this case is not included in the small-scale structures in the microscopic DM [126]. The universal fraction of macroscopic DM is still unknown. The average cosmological fraction in macroscopic DM could be significantly different from local estimates obtained through microlensing surveys.

The properties of the μ-pdf are essentially independent of both the mass spectrum of the lenses (this statement is strictly true for point sources [173]) and the clustering properties of the point masses, provided that the clustering is spherically symmetric [86]. The dispersion in luminosity of standard candles is non-gaussian, sharply peaked at the empty beam value and has a long tail towards large magnifications falling as

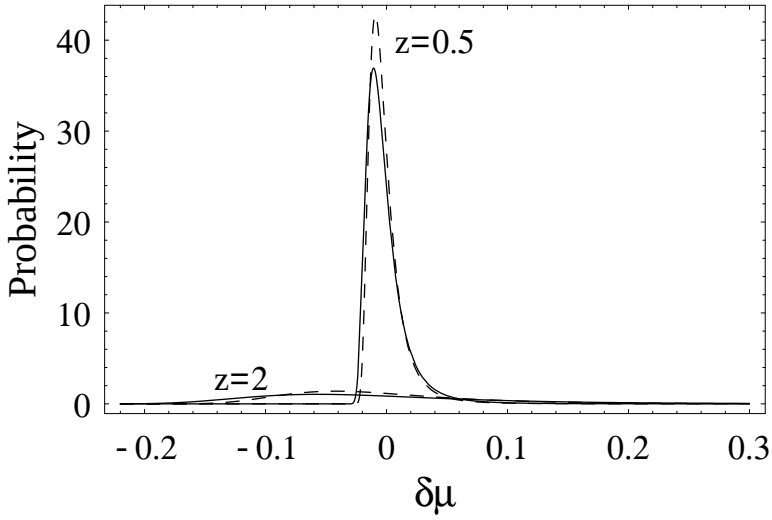

Figure 5.12: The amplification pdf for microscopic DM as a function of $\delta\mu$, the magnification relative to the mean. The sharply peaked line are for $z = 0.5$, the smoother ones for $z = 2$. Solid and dashed lines correspond, respectively, to $w_{\rm X} = -1$ and $-1/2$. It is $\Omega_{\rm M0} = 0.4$ and $\Omega_{\rm X0} = 0.6$. Solid and dashed lines have the same matter distribution but different cosmological backgrounds.

μ^{-3} [134, 150, 86], caused by small impact parameter lines of sight near the compact objects; so, its second moment is logarithmically divergent and the law of large numbers fails: if strongly lensed events are removed from the data sample, a bias will be introduced towards smaller apparent luminousities [86].

A comparative analysis of the μ-pdf in the case of either microscopic DM or compact objects has put in evidence two main differences: the high magnification tail is larger for macroscopic DM and the mode of the distribution is nearer the average value in the case of lensing by large-scale structures [126, 177].

The μ-pdf in a universe filled with a uniform comoving density of compact objects depends on a single parameter, the mean magnification $\langle\mu\rangle$ [150, 177]. Based on Monte-Carlo simulations, Rauch [150] gives the fitting formula

$$p(\mu) \propto \left[\frac{1 - e^{b(\mu-1)}}{\mu^2 - 1}\right]^{3/2}, \tag{5.121}$$

where the parameter b is related to the mean magnification by

$$b = 247\exp\left[-22.3(1 - \langle\mu\rangle^{-\frac{1}{2}})\right].$$

The approximation holds for $\langle\mu\rangle^{-1/2} \gtrsim 0.8$, a condition verified up to $z \sim 2$ in a universe with low matter density, with no regard to the equation of state $w_{\rm X}$.

The $\alpha_{\rm M}$-pdf corresponding to the distribution in Eq. (5.121) is highly non-gaussian, see Fig. (5.13). The pdf decreases monotonically from the empty beam value to high

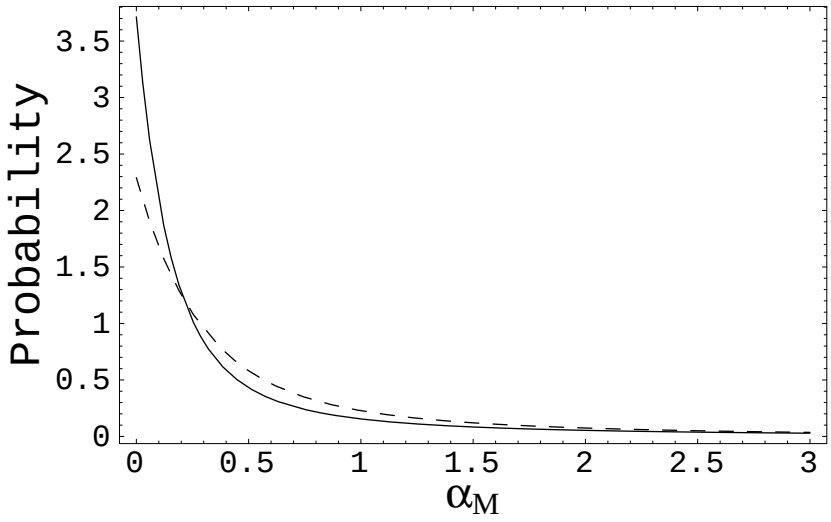

Figure 5.13: The $\alpha_{\rm M}$-pdf for macroscopic dark matter. Solid and dashed lines correspond respectively to $z = 0.8$ and 1.5. It is $\Omega_{\rm M0} = 0.3$, $\Omega_{\rm X0} = 0.7$ and $w_{\rm X} = -1$.

values of the smoothness parameter. With increasing redshift, the $\alpha_{\rm M}$-pdf tends to flatten and the probability for the filled-beam case and for high values of $\alpha_{\rm M}$ grows.

In Fig. (5.14), we show the $\delta\mu$-pdf for two source redshifts and for two values of $w_{\rm X}$: quintessence with $w_{\rm X} > -1$ reduces the effect of clumpiness. For $z = 0.5$, the variation in the distance modulus from the empty-beam case to the filled-beam one is 0.033 (0.039) mag for $w_{\rm X} = -1/2$ (-1); for $z = 1$, it is 0.108 (0.138) mag for $w_{\rm X} = -1/2(-1)$; for $z = 1.5$, it is 0.205 (0.268) mag for $w_{\rm X} = -1/2$ (-1). For $z \gtrsim 1$, the bias towards the empty-beam value can be compared with the dispersion of 0.17 mag in the peak magnitudes of SNe Ia after the application of methods as the "multi-colour light curve" method [155]. The effect of gravitational lensing is of the same order of magnitude as the other systematic uncertainties that limit the conclusions on the cosmological parameters based on SNe Ia Hubble diagram [63]. The correlation between host galaxy type and both luminosity and light-curve shape of the source; interstellar extinction occurring in the host galaxy and the Milky Way; selection effects in the comparison of nearby and distant SNe; sample contamination by SNe that are not SNe Ia can produce changes as large as 0.1 mag in the measured luminosities of SNe Ia.

The effect on the estimate of the cosmological parameters of gravitational lensing by a totally clumped model with only macroscopic DM is quite dramatic. For a source redshift of $z = 1$, a universe with $\Omega_{\rm M0} = 0.3$ and a cosmological constant can be interpreted as a model with $\Omega_{\rm M0} = 0.42$ and $w_{\rm X} = -1$ or as one with $\Omega_{\rm M0} = 0.3$ and $w_{\rm X} = -0.71$. These systematic errors increase in a quintessence cosmology with $w_{\rm X} > -1$. For $z = 1$, a universe with $\Omega_{\rm M0} = 0.3$ and $w_{\rm X} = -2/3$ will be interpreted as a model with $\Omega_{\rm M0} = 0.45$ and $w_{\rm X} = -2/3$ or one with $\Omega_{\rm M0} = 0.3$ and $w_{\rm X} = -0.46$.

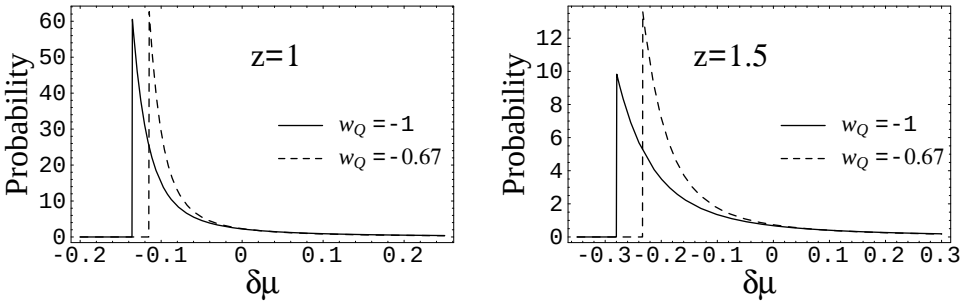

Figure 5.14: The magnification pdf for macroscopic dark matter as a function of $\delta\mu$, the magnification relative to the mean. Solid and dashed lines correspond, respectively, to $w_{\rm X} = -1$ and $-2/3$. It is $\Omega_{\rm M0} = 0.3$, $\Omega_{\rm X0} = 0.7$. Left panel: the source redshift is $z = 1$; right panel: it is $z = 1.5$

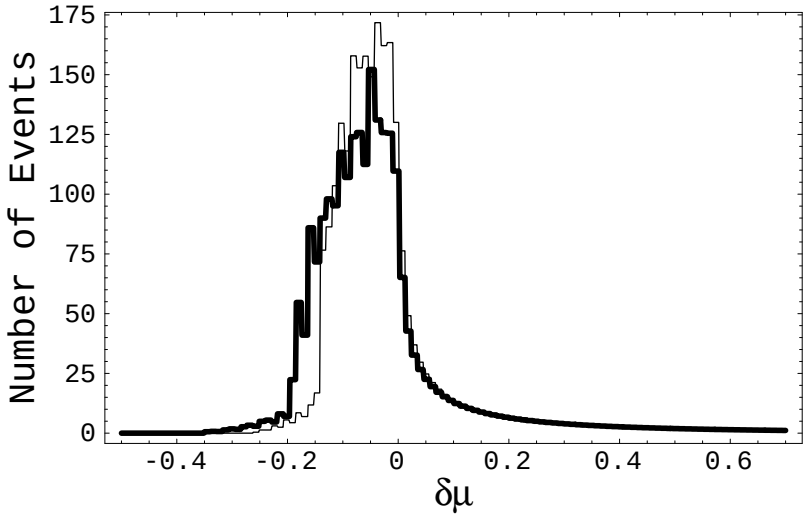

Figure 5.15: Amplification dispersion relative to the mean due to gravitational lensing by macroscopic DM for the projected 1-year SNAP sample. Thick and thin lines correspond, respectively, to $w_{\rm X} = -1$ and $-1/2$. It is $\Omega_{\rm M0} = 0.3$, $\Omega_{\rm X0} = 0.7$. Intrinsic dispersion of SN luminosities is not considered.

5.8 Dark matter and lensing dispersion

Although the lensing dispersion on the luminosity of standard candles represents a noise in the determination of the cosmological parameters, it can also be considered as a probe of the clustering properties of the DM. Lensing dispersion has been investigated to search for the presence of compact objects in the universe [115, 124, 150, 177]. The possibility of determining the fraction of macroscopic DM using future samples of SNe Ia has also been explored [126]. The planned mission SuperNova Acceleration Probe (SNAP - Http://snap.lbl.gov) should intensively observe SNe up to $z \sim 1.7$. In one year of study, this space-born mission should be able to discover ~ 2350 SNe, most of which in the region $0.5 \lesssim z \lesssim 1.2$. The discrimination of models of universe with different fractions of compact objects is mainly based on the shift in the peak of the lensing dispersion [177, 126]: a shift of ~ 0.01 mag in the peak of the lensing dispersion in the projected SNAP sample towards lower amplifications corresponds to a growth of 20% in the fraction of macroscopic DM in a flat universe with $\Omega_{\rm M0} = 0.3$ and a cosmological constant (see figure (4) in [126]). In Fig. (5.15), we plot the dispersion in amplification, for the projected redshift distribution of SNe according to the SNAP proposal, in a universe with $\Omega_{\rm M0} = 0.3$ filled in with macroscopic DM . High de-amplification are preferred in the case of a cosmological constant, when the maximum of the distribution is depleted and the mode is shifted away from the mean with respect to dark energy with $w_{\rm X} > -1$. Changing from $w_{\rm X} = -1$ to $w_{\rm X} = -1/2$, the peak of the distribution moves for ~ 0.015 mag towards higher amplifications. So, a significant reduction in the fraction of compact object can be mimed by quintessence with $w_{\rm X} > -1$. Since quintessence reduces the dispersion of gravitational lensing, it also reduces the ability to distinguish between microscopic and macroscopic DM from the shape of the amplification dispersion. Both quintessence and microscopic DM reduce the bias towards the empty beam value and the high magnification tail and their effect is of the same order. A universe with an high fraction of macroscopic objects can be misleadingly interpreted as one with dark energy with large negative pressure.

5.9 Determining cosmological parameters with the Hubble diagram

Observations of SNe Ia are strongly affected by inhomogeneities in the universe. For redshifts $z \gtrsim 1$, the variation in the distance modulus from a standard flat FLRW model to a clumpy universe with the same content of pressureless matter can be considerably greater than other systematic effects. The effect of amplification dispersion by gravitational lensing must be accurately considered. The prospects of future space-

born missions, like SNAP and the Next Generation Space Telescope, of determining properties of the dark energy have been discussed [70, 73, 217, 218]. According to these studies, SNAP data should only distinguish between a cosmological constant and quintessence with $w_{\rm X}$ relatively far from -1. When SNe observations are combined with an independent estimate of $\Omega_{\rm M0}$, for example from galaxy clustering [204], the degeneracies among the quintessence models can be significantly reduced and some constraints on the time evolution of the equation of state can be put [70, 218]. However, these studies only consider measurement errors and intrinsic dispersion of the sources, neglecting the systematic and redshift dependent error induced by gravitational lensing. We have shown how, also assuming an exact knowledge of $\Omega_{\rm M0}$, in the redshift range covered by future missions a cosmological constant can be interpreted as dark energy with $w_{\rm X} > -1$. For $\Omega_{\rm M0} = 0.4$ and $z = 1$, a constant Λ-term may be interpreted as quintessence with $w_{\rm X} < -0.84$, only due to the lensing by large-scale structure. A fraction of DM in form of compact objects will make the situation even more dramatic. So, also with a prior knowledge of the remaining cosmological parameters, gravitational lensing can make the statements on the properties of dark energy based on SNe data significantly less certain.

The effect of inhomogeneities dominates at high redshifts and should be one of the main systematics in attempting to build the Hubble diagram with GRBs [132, 153, 154, 169]. While some scenarios prefer a redshift distribution of the GRB comoving rate peaked between $z = 1$ and 2, according to other ones the comoving rate remains roughly constant at $z \gtrsim 2$ and out to very high redshift [146]. Furthermore, the lack of strong lensing events in the fourth BATSE GRBs catalog [87] suggests that, at the 95% confidence level, the upper limit to the average redshift of GRBs is $\lesssim 3$ in a flat, low-matter density universe with cosmological constant. According to these considerations, the effect of gravitational lensing would be really dominant in the Hubble diagram built with GRBs.

As an example, we consider the GRB redshift distribution derived from a combined analysis of two independent luminosity indicators [169]. Examining a sample of 112 GRBs from the BATSE catalog, Schaefer et al. [169] found redshifts varying between 0.25 and 5.9 with a median of 1.5. At $z = 1.5$, gravitational lensing by large-scale structures, in a model with $\Omega_{\rm M0} = 0.4$ and $w_{\rm X} = -2/3$, induces a magnification distribution with $\mu_{\rm peak} = 1.25$, $\mu_{\rm low} = 1.20$ and $\mu_{\rm high} = 1.46$. Assuming $w_{\rm X} = -2/3$, we will estimate $\Omega_{\rm M0} = 0.43^{+0.05}_{-0.16}$; assuming $\Omega_{\rm M0} = 0.4$, we will estimate $w_{\rm X} < -0.51$.

Conclusions

The gravitational lens equation has been discussed. Theoretical developments and phenomenological applications have been performed.

I have considered the gravitational lens equation in the framework of metric theories of gravity. To this aim, I used an approximate metric element generated by an isolated mass distribution in the weak field regime and slow motion approximation, expanded up to the ppN order, and with non diagonal components which include the effects of gravity by currents of mass. Fermat's principle has been applied under the usual assumptions of small deflection angles and geometrically thin lenses. The time delay function and the deflection angle for a single lens plane have been derived. Simple formulae for a general deflector have been obtained for the post-Newtonian order and the gravito-magnetic correction. The post-post-Newtonian order has also been included in the analysis.

Very simple expressions for the ppN corrections to the lensing quantities have been derived for the point-like lens. This approximation for the deflector is quite rough, but, some of the times, astrophysics can be tough. The gravito-magnetic correction and the ppN contribution to the deflection angle are of the same order for intermediate main sequence stars, like the Sun. For early type stars, white dwarfs and galaxies acting as lenses, the gravito-magnetic term overwhelms the ppN one.

Ground based instrumentations, such as VLBI, or satellites, such as Hipparcos, can measure deflection angles, respectively in the radio-wave regime and optical band, with accuracy of nearly milliarcsec. Since the γ parameter appears in the post-Newtonian expression of the lensing quantities, this accuracy put strong constraints on it. However, the other parameters which enter the approximate metric element, that is the standard β term and the non-standard ϵ and μ coefficients, need more accurate measurements. Lensing by fast rotating stars, such as white dwarfs, could give some hints on the dragging of inertial frames, whose strength is determined by the μ parameter.

New generation space interferometric missions, such as SIM by NASA (scheduled for launch in 2009), should greatly improve the experimental accuracy, so that gravitational lensing could address, in the near future, two very interesting topics in gravi-

tation: the detection of gravito-magnetism and possible discrepancies of gravity from general relativity. We remark that a full analysis of higher order corrections to the lensing theory makes possible a comparison between general relativity and viable relativistic theories of gravity. An analysis to the lowest order might hide such differences.

The formalism of the lensing mapping has been generalized to include viable theories of gravity up to the post-Newtonian order and also considering the effect of dragging of inertial frames. Classical results, such as the theorems about the number of images and the minimum magnification, up till now derived only in the case of static deflectors in the framework general relativity, have been stated in a more general context.

I have considered several gravitational lens models of astrophysical interest. For spherically symmetric lenses in rigid rotation, a general expression for the deflection angle, to the order c^{-3}, has been derived. I have explicitly considered isothermal spheres, power law models and the homogeneous sphere. A perturbative approach has made it possible to discuss critical lines, caustics and image positions. Both for galaxies and white dwarfs, the gravito-magnetic correction to the deflection angle can be as large as 0.1%. I have also considered some gravitational lensing phenomena, such as detections of microlensing signatures in stellar light curves and measurements of time delays in multiple quasars. The gravito-magnetic correction is usually negligible with respect to other systematics but in some limiting cases it can become important.

Phenomenological applications of the gravitational lens equation have been also considered.

I have explored the feasibility of reconstructing the properties of the dark energy in the universe by using strong lensing systems in which a cluster of galaxies acts as deflector. With respect to other lensing systems, for cluster of galaxies, it is possible to determine the position of the critical lines in two independent ways: with giant arcs or with depletion curves. Provided that the properties of the background source populations are well constrained, it is possible, in principle, to use multi-band depletion measurements to obtain several independent estimates, each one probing a different source redshift. These circumstances allow to study the ratio of angular diameter distances that characterizes the angular position of the critical lines over a large range of source redshifts, just for a single lensing cluster.

For a flat universe, the sensitivity of the angular positions of the critical lines on quintessence becomes higher in low-density pressureless matter universes and for dark energy with intermediate equation of state. While the analysis of only a few lensing clusters suffices to distinguish between accelerating and decelerating models of universe (also without a prior knowledge of $\Omega_{\rm M0}$), a considerably larger sample ($N \sim 200$) and an accurate estimate of $\Omega_{\rm M0}$ are needed to constrain the equation of state within an

uncertainty of $\Delta w_{\rm X} \sim 0.25$ and discriminate, at the 95% confidence limit, between a cosmological constant and an evolving quintessence.

Analyses of magnification bias in multi-band photometry can be combined with observations of giant arcs to obtain some insight on cosmological parameters. A first application of the method to the cluster CL 0024+1654 has given interesting results. My analysis disfavours models of a universe without dark energy and favours flat accelerating universes. These estimates agree with the currently favoured constraints from other independent measurements. However, some features in the redshift space of CL 0024+1654, as a possible merger scenario, could invalidate my results. Indeed, a very accurate knowledge of the absolute mass distribution of the deflector and a correct understanding of the pattern of sub-structures are necessary to obtain secure constraints on the cosmological parameters.

The method which I have discussed is quite general and can be applied to several strong lensing systems. For example, a single galaxy, whose stellar velocity dispersion can be accurately measured, can multiply image a background quasar. Clusters of galaxies need an accurate modelling of the pattern of substructures and present a quite problematic measurement of $\sigma_{\rm v}$ but allow one to study the ratio $D_{\rm ds}/D_{\rm s}$ at different source redshifts. Furthermore, a multiple images system of galaxies with known redshift makes possible an absolute calibration of the total mass of the cluster.

Gravitational lensing affects cosmological distances. Shear and convergence affect images of distant sources according to the different amount and distribution of matter along different lines of sight. By iterating the gravitational lens equation, I have obtained, in the framework of on average Friedmann-Lemaître-Robertson-Walker models, the distance–redshift relation in an inhomogeneous universe. Analytic expressions for luminosity distance–redshift relations in a universe with dark energy have been corrected for the effects of inhomogeneities. This is what is necessary to study the gravitational lensing dispersion on the Hubble diagram of standard candles. The amplification probability distribution function in the observed luminosity of standard candles has been discussed. It is strongly dependent on the equation of state, $w_{\rm X}$, of the quintessence. With no regard to the nature of the dark matter (microscopic or macroscopic), the dispersion increases with the redshift of the source and is maximum for dark energy with very large negative pressure.

Since observational data are taken in the inhomogeneous universe, the noise in the Hubble diagram induced by gravitational lensing strongly affects the determination of the cosmological parameters from observations of Supernovae of type Ia. The importance of these observations makes necessary a complete study of all systematics. The errors on the pressureless matter density parameter, $\Omega_{\rm M0}$, and on $w_{\rm X}$ are maximum for quintessence with not very negative pressure, since in these models the luminosity distance is less sensitive to the cosmology. The effect of the gravitational lensing is of

the same order of the other systematics affecting observations of SNe Ia. Due to lensing by large-scale structures, in a flat universe with $\Omega_{\rm M0} = 0.4$, at $z = 1$ a cosmological constant ($w_{\rm X} = -1$) can be interpreted as dark energy with $w_{\rm X} < -0.84$ (at 2-sigma confidence limit).

Appendix A

Some useful numbers

Constants

vacuum speed of light	c	=	$2.9979250(10)\times10^{10}$cm s^{-1}
Newton gravitational constant	G	=	$6.6732(31)\times10^{-8}$dyn cm^2 g^{-2}
Planck constant	$\hbar$	=	$1.0545919(80)\times10^{-27}$ erg s
Boltzmann constant	$k_{\rm B}$	=	$1.380622(59)\times10^{-16}$ erg $^{\rm o}$K^{-1}

Astronomical constants

Parsec	1pc	=	$3.0856(1)\times10^{18}$ cm
Solar Mass	$M_\odot$	=	$1.989(2)\times10^{33}$ g
	$\frac{GM_\odot}{c^2}$	=	1.475×10^5 cm
Solar Radius	$R_\odot$	=	$6.9598(7)\ \times10^{10}$ cm
Superficial potential	$\frac{GM_\odot}{R_\odot c^2}$	=	2.12×10^{-6}
Solar luminosity	$L_\odot$	=	$3.90(4)\times10^{33}$ erg s^{-1}

List of Figures

Ringraziamenti

Ringrazio il prof. Ruggiero de Ritis, che il mio ringraziamento non può ricevere, per avermi introdotto alla materia di questa tesi. Molti degli argomenti trattati sono stati ispirati da conversazioni con lui. E tutti avrei voluto con lui discuterli.

Ringrazio il prof. Massimo Capaccioli per il supporto fornitomi in questi anni. I proff. Claudio Rubano e Paolo Scudellaro per il consiglio costante. Vincenzo F. Cardone, Ester Piedipalumbo ed il prof. Mikhail V. Sazhin per la collaborazione nello sviluppo di alcune idee. Il prof. Salvatore Capozziello, il prof. Giuseppe Longo, il prof. Giovanni Platania per le utili discussioni.

Ringrazio il Dipartimento di Scienze Fisiche e l'I.N.F.N. per le strutture messe a disposizione. Parte del lavoro è stato finanziato dal "Progetto Giovani Ricercatori" (art.3, D.M. 21.6.1999), annualità 2000 e 2001.

Ringrazio il coordinatore del dottorato, prof. Antonino Sciarrino, e la segreteria, per la continua disponibilità.

Ringrazio i miei amici.

Ringrazio la mia famiglia.

Ringrazio la mia amata.

Ringrazio chi mi ha aiutato.

Bibliography

[1] Abramowitz, M., Stegun, I.A., 1965, Handbook of mathematical functions, Dover, New York.

[2] Alcock, C., Akerlof, C.W., Allsman, R.A., Alves, D.R., Bennett, D.P., Chan, S., Cook, C.H., Freeman, K.C., Griest, K., Marshall, S.L., Park, H.S., Perlmutter, S., Peterson, B.A., Pratt, M.R., Quinn, P.J., Rodgers, A.W., Stubbs, C.W., Sutherland, W., 1993, Nature, 365, 621.

[3] Alcock, C., Allsman, R.A., Alves, D.R., Axelrod, T.S., Becker, A.C., Bennett, D. P., Cook, K.H., Dalal N., Drake, A.J., Freeman, K.C., Geha, M., Griest, K., Lehner, M. J., Marshall, S.L., Minniti, D., Nelson, C.A., Peterson, B.A., Popowski, P., Pratt, M.R., Quinn, P. J., Stubbs, C.W., Sutherland, W., Tomaney, A.B., Vandehei, T., Welch, D., ApJ, 542, 281.

[4] Allen, C.W., Astrophysical Quantities, 1983, The Athlone Press, London.

[5] Asada, H., 1997, ApJ, 485, 460.

[6] Asada, H., Kasai, M., 2000, Prog. Th. Phys., 104, 95.

[7] Aubourg, E., Bareyre, P., Brehin, S., Gros, M., Lachieze-Rey, M., Laurent, B., Lesquoy, E., Magneville, C., Milsztajn, A., Moscoso, L., Queinnec, F., Rich, J., Spiro, M., Vigroux, L., Zylberajch, S., Ansari, R., Cavalier, F., Moniez, M., Beaulieu, J.P., Ferlet, R., Grison, P., Madjar, A. Vidal, Guibert, J., Moreau, O., Tajahmady, F., Maurice, E., Prevot, L., Gry, C., 1993, Nature, 365, 623.

[8] Bachall, N.A., & Fan, X., 1998, ApJ, 504, 1.

[9] Balbi, A., Ade, P., Bock, J., Borrill, J., Boscaleri, A., De Bernardis, P., Ferreira, P.G., Hanany, S., Hristov, V., Jaffe, A. H., Lee, A.T., Oh, S., Pascale, E., Rabii, B., Richards, P. L., Smoot, G.F., Stompor, R., Winant, C.D., Wu, J.H.P., 2000, ApJ, 545, L1.

[10] Barber, A.J., 2000, MNRAS, 318, 195.

[11] Barber, A.J., Thomas, P.A., Couchman, H.M.P., Fluke, C.J., 2000, MNRAS, 319, 267.

[12] Bean, R., Melchiorri, A., 2002, Phys. Rev. D, 65, 041302.

[13] Benabed, K., & Bernardeau, F., 2001, Phys. Rev.D, 64, 083501.

[14] Bergström, L., Goliath, M., Goobar, A., Mörtsell, E., 2000, A&A, 385, 13.

[15] Binney, J., Tremaine, S., 1987, Galactic Dynamics, Princeton Univ. Press, Princeton.

[16] Bloomfield Torres, L.F., Waga, I., 1996, MNRAS, 279, 712.

[17] Böhringer, H., Soucail, G., Mellier, Y., Ikebe, Y., & Schuecker, P., 2000, A&A, 353, 124.

[18] Bonnet, H., Mellier, Y., & Fort, B., 1994, ApJ, 427, L83.

[19] Bourassa, R.R., Kantowski, R., Norton, T,D., 1973, ApJ, 185, 747.

[20] Bourassa, R.R., Kantowski, R., 1975, ApJ, 195, 13.

[21] Bourassa, R.R., Kantowski, R., 1976, ApJ, 205, 674.

[22] Bozza, V., 2000, A&A, 355, 423.

[23] Breimer, T.G., & Sanders, R.H., 1992, MNRAS, 257, 97.

[24] Broadhurst, T.J., 1995, [astro-ph/9511150].

[25] Broadhurst, T.J., Taylor, A.N., Peacock, J.A., 1995, ApJ, 438, 49.

[26] Broadhurst, T., Huang, X., Frye, B., Ellis, R., 2000, ApJ, 534, L15.

[27] Buchalter, A., Helfand, D.J., Becker, R.H., White, R.L., 1998, ApJ, 494, 503.

[28] Calchi Novati, S., Iovane, G., Marino, A.A., Aurière, M., Baillon, P., Bouquet, A., Bozza, V., Capaccioli, M., Capozziello, S., Cardone, V., Covone, G., De Paolis, F., de Ritis, R., Giraud-Héraud, Y., Gould, A., Ingrosso, G., Jetzer, Ph., Kaplan, J., Lambiase, G., Le Du, Y., Mancini, L., Piedipalumbo, E., Re, V., Roncadelli, M., Rubano, C., Scarpetta, G., Scudellaro, P., Sereno, M., Strafella, F., 2002, A&A, 381, 848, [astro-ph/0110706].

[29] Caldwell, R.R., Dave, R., & Steinhardt, P.J., 1998, Phys. Rev. Lett., 80, 1582.

[30] Capozziello, S., Lambiase, Papini, G., Scarpetta, G., 1999, Phys. Lett. A, 254, 11.

[31] Capozziello, S., Cardone, V.F., Piedipalumbo, E., Sereno, M., Troisi, A., 2002, Int. J. Mod. Phys. D, in press; [astro-ph/0209610].

[32] Carlberg, R.G., Yee, H.K.C., Morris, S.L., Lin, H., Ellingson, E., Patton, D., Sawicki, M., Shepherd, C.W., 1998, ApJ, 516, 552.

[33] Carroll, S.M., 2001, The cosmological constant, Living Rev. Rel. 4, 1, URL: http://www.livingreviews.org; [astro-ph/0004075].

[34] Carroll, S.M., Press, W.H., 1992, ARA&A 30, 499.

[35] Célérier, M.N., 2000, A&A, 353, 63.

[36] Chang, K., Refsdal S., 1979, Nature, 282, 561.

[37] Chiba, T., & Nakamura, T., 2000, Phys. Rev. D, 62, 121301.

[38] Chiba, T., Sugiyama, N., & Nakamura, T., 1997, MNRAS, 289, L5.

[39] Chiba, T., & Takahashi, R., 2002, Prog. Theor. Phys., 107, 625.

[40] Chwolson, O., 1924, Astron. Nachr., 221, 329.

[41] Ciufolini I., Wheeler J.A., 1995, Gravitation and Inertia, Princeton University Press, Princeton.

[42] Clark, E.E., 1972, MNRAS, 158, 233.

[43] Cook, J.H., Kantowski, R., 1975, ApJ, 195, L11.

[44] Cooray, A.R., & Huterer, D., 1999, ApJ, 513, L95.

[45] Corasaniti, P.S., & Copeland, E.J., 2002, Phys. Rev. D, 65, 043004.

[46] Czoske, O., Kneib, J.-P., Soucail, G., Bridges, T., Mellier, Y., Cuillandre, J.-C., 2001, A&A, 372, 391.

[47] Czoske, O., Moore, B., Kneib, J.-P., Soucail, G., 2002, A&A, 386, 31.

[48] de Bernardis, P., Ade, P.A.R., Bock, J.J., Bond, J. R., Borrill, J., Boscaleri, A., Coble, K., Crill, B.P., De Gasperis, G., Farese, P.C., Ferreira, P. G., Ganga, K., Giacometti, M., Hivon, E., Hristov, V.V., Iacoangeli, A., Jaffe, A.H., Lange, A.E., Martinis, L., Masi, S., Mason, P.V., Mauskopf, P.D., Melchiorri, A., Miglio, L., Montroy, T., Netterfield, C.B., Pascale, E., Piacentini, F., Pogosyan, D., Prunet, S., Rao, S., Romeo, G., Ruhl, J. E., Scaramuzzi, F., Sforna, D., Vittorio, N., 2000, Nature, 404, 955.

[49] Demianski M., de Ritis R., Marino A.A. & Piedipalumbo E., 2000, [astro-ph/0004376].

[50] de Ritis, R., Marino, A.A., Rubano, C., & Scudellaro, P., 2000, Phys. Rew. D, 62, 043506.

[51] Dressler, A., Smail, I., Poggianti, B.M., Butcher, H., Couch, W.J., Ellis, R.S., Oemler Jr., A., 1999, ApJS, 122, 51.

[52] Dye, S., Tayolor, A.N., Greve, T.R., Rögnvaldsson, Ö.E., van Kampen, E., Jakobsson, P., Sigmundsson, V.S., Gudmundsson, E.H., Hjorth, J., 2002, A&A, 386, 12.

[53] Dyer, C.C., Roeder, R.C., 1972, ApJ, 174, L115.

[54] Dyer, C.C., Roeder, R.C., 1973, ApJ, 180, L31.

[55] Dymnikova, I., 1986, Relativity in Celestial Mechanics and Astrometry, eds. Kovalevsky J., Brumberg A., 411.

[56] Eddington, A.S., 1920, Space, Time and Gravitation, University Press, Cambridge.

[57] Einstein, A., 1911, Annalen der Physik, 35, 898.

[58] Einstein, A., 1915, Sitzungsber. Preu. Akad. Wissensch., erster Hallband, 831.

[59] Einstein, A., 1936, Sci., 84, 506.

[60] Epstein, R., Shapiro, I., 1980, Phys. Rev. D 22, 2947.

[61] Erdélyi, A., Magnus, W., Oberhettinger, F., Tricomi, F.G., 1955, Higher Trascendental Functions Vol.3, McGraw Hill Book Company, New York.

[62] Etherington, I.M.H., 1933, Phil. Mag., 15, 761.

[63] Filippenko, A.V., Riess, A.G., 2000, in "Type Ia Supernovae: Theory and Cosmology", edited by J.C. Niemeyer and J.W. Truran, Cambridge University Press, Cambridge.

[64] Fort, B., Mellier, Y., & Dantel-Fort, M., 1997, A&A, 321, 353.

[65] Fort, B., Prieur, J.L., Mathez, G., Mellier, Y., Soucail, G., 1988, A&A, 200, L17.

[66] Freeman, K.C., 1970, ApJ, 160, 811.

[67] Frieman, J.A., 1997, Comments Astrophys., 18, 323.

[68] Futamase, T., & Yoshida S., 2001, Prog. Theor. Phys., 105, 887.

[69] Gautret, L., Fort, B., & Mellier Y., 2000, A&A, 353, 10.

[70] Gerke, B.F., Efstathiou, G., 2002, [astro-ph/0201336].

[71] Giovi, F., Amendola, L., 2001, MNRAS, 325, 1097.

[72] Glicenstein, J.F., 1999, A&A, 343, 1025.

[73] Goliath, M., Amanullah R., Astier, P., Goobar, A., Pain, R., 2001, A&A, 380, 6.

[74] Golse, G., Kneib, J.-P., & Soucail, G., 2002, A&A, 387, 788.

[75] Gott, J.R., 1981, ApJ, 243, 140.

[76] Grishchuk, L.P., 1994, Phys. Rev. D, 50, 7154.

[77] Guerra, E.J., Daly, R.A., Wan, L., 2000, ApJ, 544, 659.

[78] Gurevich, A.V., Zybin, K.P., 1995, Phys. Lett. A, 208, 276.

[79] Gurevich, A.V., Zybin, K.P., & Sirota, V.A., 1997, Sov. Phys. Usp., 167, 913.

[80] Gurvits, L.I., Kellermann, K.I., Frey, S., 1999, A&A, 342, 378.

[81] Hamana, T., Hattori, M., Ebeling, H., Henry, J.P., Futamase, T., Shioya, Y., 1997, ApJ, 484, 574.

[82] Harun-or-Rashid, S.M., & Roos, M., 2001, A&A, 373, 369.

[83] Heun, K., 1889, Math. Annu., 33, 161.

[84] Hewitt, J.N., Turner, E.L., Schneider, D.P., Burke, B.F., Langston, G.I., 1988, Nature, 333, 537.

[85] Holz, D.E., 1998, ApJ, 506, L1.

[86] Holz, D.E., & Wald, R.M., 1998, Phys. Rev. D, 58, 063501.

[87] Holz, D.E., Miller, M.C., Quashnock, J.M., 1999, ApJ, 510, 64.

[88] Huterer, D., & Turner, M.S., 2001, 20th Texas Symposium on relativistic astrophysics, AIP conference proceedings, Vol. 586, Edited by J.C. Wheeler and H. Martel, p.297.

[89] Ibáñez, J., 1983, A&A, 124, 175.

[90] Ibáñez, J., Martín, J., 1982, Phys. Rev. D, 26, 384.

[91] Ince, E.L., 1956, Ordinary Differential Equations, Dover, New York.

[92] Irwin, M.J., Webster, R.L., Hewett, P.C., Corrigan, R.T., Jedrzejewski, R.I., 1989, AJ, 98, 1989.

[93] Jaffe, A.H., Ade, P.A.R., Balbi, A., Bock, J.J, Bond, J.R., Borrill, J., Boscaleri, A., Coble, K., Crill, B.P., de Bernardis, P., Farese, P., Ferreira, P.G., Ganga, K., Giacometti, M., Hanany, S., Hivon, E., Hristov, V.V., Iacoangeli, A., Lange, A.E., Lee, A.T. , Martinis, L., Masi, S., Mauskopf, P.D., Melchiorri, A., Montroy, T., Netterfield, C.B., Oh, S., Pascale, E., Piacentini, F., Pogosyan, D., Prunet, S., Rabii, R., Rao, S., Richards, P.L., Romeo, G., Ruhl, J.E., Scaramuzzi, F., Sforna, D., Smoot, G.F., Stompor, R., Winant, C.D., Wu, J.H.P., 2001, Phys. Rev. Lett., 86, 3475.

[94] Jain, B., Seljak, U., White, S., 2000, ApJ, 530, 547.

[95] Kaiser, N., Squires, G., 1993, ApJ, 404, 441.

[96] Kantowski, R., 1969, ApJ, 155, 89.

[97] Kantowski, R., 1998, ApJ, 507, 483.

[98] Kantowski, R., Vaughan, T., Branch, D., 1995, ApJ, 447, 35.

[99] Kantowski, R., Thomas, R.C., 2001, ApJ, 561, 491.

[100] Kantowski, R., Kao, J.K., Thomas, R.C., 2000, ApJ, 545, 549.

[101] Kassiola, A., Kovner, I., & Fort, B., 1992, ApJ, 400, 41.

[102] Kellerman K.I., 1993, Nature, 361, 134.

[103] Kolb E.W., Turner M.S., 1990, The Early Universe, Addison-Wesley, Redwood City, California.

[104] Konno, K., Kojima, Y., 1999, Prog. Theor. Phys., 101, 885.

[105] Korolev, V.A., Sazhin, M.V., 1986, Preprint ISR, N 1060.

[106] Kraft R.P., 1967, ApJ, 150, 551.

[107] Krasiński A., 1997, Inhomogeneous Cosmological Models, Cambridge University Press.

[108] Krauss L.M., Schramm D.N., 1993, ApJ, 405, L43.

[109] Landau L.D., Lifshits E.M., 1985, Teoria dei Campi, Editori Riuniti, Roma.

[110] Laplace, P.S., 1796, Exposition du systéme du monde, vol. II, De l'Imprimierie du Circle Social Paris.

[111] Lasserre, T., Afonso, C., Albert, J. N., Andersen, J., Ansari, R., Aubourg, É., Bareyre, P., Bauer, F., Beaulieu, J.P., Blanc, G., Bouquet, A., Char, S., Charlot, X., Couchot, F., Coutures, C., Derue, F., Ferlet, R., Glicenstein, J.F., Goldman, B., Gould, A., Graff, D., Gros, M., Haissinski, J., Hamilton, J. C., Hardin, D., de Kat, J., Kim, A., Lesquoy, É., Loup, C., Magneville, C., Mansoux, B., Marquette, J.B., Maurice, É., Milsztajn, A., Moniez, M., Palanque-Delabrouille, N., Perdereau, O., Prévot, L., Regnault, N., Rich, J., Spiro, M., Vidal-Madjar, A., Vigroux, L., Zylberajch, S., 2000, A&A, 355, L39.

[112] Liebes, S., 1964, Phys. Rev. B, 133, 835.

[113] Lima, J.A.S., Alcaniz, J.S., 2000, A&A, 357, 393.

[114] Linder, E.V., 1988, A&A, 206, 190.

[115] Linder, E.V., Schneider, P., Wagoner, R.V., 1988, ApJ, 324, 786.

[116] Link, R., & Pierce, M.J., 1998, ApJ, 502, 63.

[117] Lombardi, M., & Bertin, G., 1999, A&A, 342, 337.

[118] Lynds, R., Petrosian, V.,1986, Bull. Am. Astron. Soc., 18, 1014.

[119] Maor, I., Brustein, R., & Steinhardt, P.J., 2001, Phys. Rev. Lett., 86, 6.

[120] Marino A.A., Capozziello S., de Ritis R., Scudellaro P., 2000, Lezioni di Lensing Gravitazionale, Bibliopolis, Napoli.

[121] Mayen, C., & Soucail, G., 2000, A&A, 361, 415.

[122] Mellier, Y., Fort, B., 1996, [astro-ph/9608105].

[123] Metcalf, R.B., 1999, MNRAS, 305, 746.

[124] Metcalf, R.B., Silk, J., 1999, ApJ, 519, L1.

[125] Michell, J., 1784, Philo. Trans. R.Soc. Lon., 74, 35.

[126] Mörtsell, E., Goobar, A., Bergström, L., 2001, ApJ, 559, 53.

[127] Nakamura, T., & Chiba, T., 2001, ApJ, 550, 1.

[128] Narayan, R., Bartelmann, M., 1997, Lectures on gravitational Lensing, in Proceedings of the 1995 Jerusalem Winter School; [astro-ph/9606001].

[129] Navarro, J.F., Frenk, C.S., White, S.D.M., 1995, MNRAS, 275, 56.

[130] Navarro, J.F., Frenk, C.S., White, S.D.M., 1996, ApJ, 462, 563.

[131] Newton, I., 1730, Optiks.

[132] Norris, J.P., Marani, G., & Bonnell, J., 2000, ApJ, 534, 248.

[133] Paczyński, B., 1986, ApJ, 301, 503.

[134] Paczyński, B., 1986, ApJ, 304, 1.

[135] Paczyński, B., 1986, Nature, 325, 572.

[136] Paczyński, B., & Gorski, K., 1981, ApJ, 248, L101.

[137] Padmanabhan, T., 2001, Theoretical Astrophysics Vol. II, Cambridge University Press, Cambridge.

[138] Peacock, J.A., 1999, Cosmological Physics, Cambridge University Press, Cambridge.

[139] Peacock, J.A., Cole, S., Norberg, P., Baugh, C.M., Bland-Hawthorn, J., Bridges, T., Cannon, R.D., Colless, M., Collins, C., Couch, W., Dalton, G., Deeley, K., De Propris, R., Driver, S.P., Efstathiou, G., Ellis, R.S., Frenk, C.S., Glazebrook, K., Jackson, C., Lahav, O., Lewis, I., Lumsden, S., Maddox, S., Percival, W.J., Peterson, B.A., Price, I., Sutherland, W., Taylor, K., 2001, Nature, 410, 169.

[140] Perlmutter, S., Aldering, G., Goldhaber, G., Knop, R.A., Nugent, P., Castro, P.G., Deustua, S., Fabbro, S., Goobar, A., Groom, D.E., Hook, I.M., Kim, A.G., Kim, M.Y., Lee, J.C., Nunes, N. J., Pain, R., Pennypacker, C.R., Quimby, R., Lidman, C., Ellis, R.S., Irwin, M., McMahon, R. G., Ruiz-Lapuente, P., Walton, N., Schaefer, B., Boyle, B.J., Filippenko, A.V., Matheson, T., Fruchter, A.S., Panagia, N., Newberg, H.J.M., Couch, W.J., 1999, ApJ, 517, 565.

[141] Perlmutter, S., Turner, M.S., & White, M., 1999, Phys. Rev Lett., 83, 670.

[142] Petters, A.O., Levine, H., Wambsganss, J., 2001, Singularity Theory and Gravitational Lensing, Birkhäuser, Boston.

[143] Phillips, M.M., 1993, ApJ, 413, L105.

[144] Picone, M., Miranda, C., 1943, Esercizi di analisi matematica, Studium Urbis, Roma.

[145] Porciani, C., & Madau, P., 2000, ApJ, 532, 679.

[146] Porciani, C., & Madau, P., 2001, ApJ, 548, 522.

[147] Press, W.H., Gunn, J.E., 1973, ApJ, 185, 397.

[148] Pryke, C., Halverson, N.W., Leitch, E.M., Kovac, J., Carlstrom, J.E., Holzapfel, W.L., Dragovan, M., 2002, ApJ, 568, 46.

[149] Ratra, B., & Peebles, P.J., 1998, Phys. Rev. D, 37, 3406.

[150] Rauch, K.P., 1991, ApJ, 374, 83.

[151] Refsdal, S., 1964, MNRAS, 128, 295.

[152] Refsdal, S., 1964, MNRAS, 128, 307.

[153] Reichart, D.E., Lamb, D.Q., 2001, 20th Texas Symposium on relativistic astrophysics, AIP conference proceedings, Vol. 586. Edited by J. C. Wheeler and H. Martel., p.599; [astro-ph/0103255].

[154] Reichart, D.E., Lamb, D.Q., Fenimore, E.E., Ramirez-Ruiz, E., Cline, T.L., Hurley, K., 2001, ApJ, 552, 57.

[155] Riess, A.G., Press, W.H., Kirshner, R.P., 1996, ApJ, 473, 88.

[156] Riess, A.G., Filippenko, A.V., Challis, P., Clocchiatti, A., Diercks, A., Garnavich, P.M., Gilliland, R.L., Hogan, C.J., Jha, S., Kirshner, R.P., Leibundgut, B., Phillips, M.M., Reiss, D., Schmidt, B.P., Schommer, R.A., Smith, R.C., Spyromilio, J., Stubbs, C., Suntzeff, N.B., Tonry, J., 1998, AJ, 116, 1009.

[157] Robertson, D.S., Carter, W.E., Dillinger, W.H., 1991, Nature, 349, 768.

[158] Rögnvaldsson, Ö.E., Greve, T.R., Hjorth, J., Gudmundsson, E.H., Sigmundsson, V.S., Jakobsson, P., Jaunsen, A.O., Christensen, L.L., van Kampen, E., Taylor, A.N., 2001, MNRAS, 322, 131.

[159] Roulet, E., Mollerach, S., 1997, Phys. Rep., 279, 67; [astro-ph/9603119].

[160] Rubano, C., & Scudellaro, P., 2002, Gen. Rel. Grav., 34, 307.

[161] Rubano, C., Sereno, M., 2002, in Proceedings of the Ninth Marcel Grossmann Meeting on General Relativity, edited by V.G. Gurzadyan, R.T. Jantzen and R. Ruffini, World Scientific, Singapore.

[162] Rubano, C., Sereno, M., 2002, MNRAS, 335, 30; [astro-ph/0203205].

[163] Russel, H.N., 1936, Sci. Am., 156, 76.

[164] Sachs, R.K., 1961, Proc. Roy. Soc. London A, 264, 309.

[165] Sahni, V., Starobinski, A.A., 2000, Int. J. M. Ph., 9, 4.

[166] Saini, T.D., Raychaudhury, S., Sahni, V., & Starobinsky, A.A., 2000, Phys. Rev. Lett., 85, 1162.

[167] Sandage, A., 1970, Phys. Today, February, 24.

[168] Sazhin, M.V., Yagola, A.G., Yakubov, A.V., 1995, Phys. Lett. A, 208, 276.

[169] Schaefer, B.E., Deng, M., Band, D.L., 2001, ApJ, 563, L123.

[170] Schmidt, M., 1963, Nature, 197, 1040.

[171] Schmidt, B.P., Suntzeff, N.B., Phillips, M.M., Schommer, R.A., Clocchiatti, A., Kirshner, R.P., Garnavich, P., Challis, P., Leibundgut, B., Spyromilio, J., Riess, A.G., Filippenko, A.V., Hamuy, M., Smith, R.C., Hogan, C., Stubbs, C., Diercks, A., Reiss, D., Gilliland, R., Tonry, J., Maza, J., Dressler, A., Walsh, J., Ciardullo, R., 1998, ApJ, 507, 46.

[172] Schneider, P., Ehlers, J., Falco, E.E., 1992, Gravitational Lenses, Springer-Verlag, Berlin.

[173] Schneider, P., Weiss, A., 1988, ApJ, 327, 526.

[174] Seitz, S., Schneider, P., 1994, A&A, 287, 349.

[175] Seitz, C., Schneider, P., 1997, A&A, 318, 687.

[176] Seitz, S., Schneider, P., Ehlers, J., 1994, Class. Quant. Grav., 11, 2345.

[177] Seljak, U., Holz, D.E., 1999, A&A, 351, L10.

[178] Sereno, M., 2002, A&A, 393, 757; [astro-ph/0209210].

[179] Sereno, M., 2002, Phys. Lett. A., in press; [astro-ph/0209148].

[180] Sereno, M., 2002, Phys. Rev. D, submitted.

[181] Sereno, M., Cardone, V.F., 2002, A&A, in press; [astro-ph/0209297].

[182] Sereno, M., Covone, G., Piedipalumbo, E., de Ritis, R., 2001, MNRAS, 327, 517.

[183] Sereno, M., Piedipalumbo, E., Sazhin, M.V., 2002, MNRAS, 335, 1061; [astro-ph/0209181].

[184] Shapiro, I., 1964, Phys. Rev. Lett., 13, 789.

[185] Shapiro, P.R., & Iliev, I.T., 2000, ApJ, 542, L1.

[186] Smail, I., Hogg, D.W., Yan, L., Cohen, J.G., 1995, ApJ, 449, L105.

[187] Smail, I., Dressler, A., Kneib, J.-P., Ellis, R.S., Couch, W.J., Sharples, R.M., Oemler Jr., A., 1996, ApJ, 469, 508.

[188] Soucail, G., Fort, B., Mellier, Y., Picat, J.P., 1987, A&A, 172, L14.

[189] Soucail, G., Ota, N., Böhringer, H., Czoske, O., Hattori, M., Mellier, Y., 2000, A&A, 355, 433.

[190] Soucail, G., Mellier, Y., Fort, B., Mathez, G., Cailloux, M., 1988, A&A, 191, L19.

[191] Spergel, D., & Pen, U., 1997, ApJ, 491, L67.

[192] Straumann, N. 1998, in "Topics on Gravitational Lensing", Bibliopolis, Napoli.

[193] Tomita, K., 1998, Prog. Theor. Phys., 100, 79.

[194] Tomita, K., 2001, MNRAS, 326, 287.

[195] Trentham, N., 2001, MNRAS, 326, 1328.

[196] Tricomi F.G., 1985, Integral Equations, Interscience Publishers, Inc., New York.

[197] Turner, M.S., 2000, Physica Scripta, 85, 210.

[198] Turner, M.S., & White, M., 1997, Phys. Rev. D, 56, 4439.

[199] Tyson, J.A., 1988, AJ, 96, 1.

[200] Tyson, J.A., Kochanki, G.P., & Dell'Antonio, I.P., 1998, ApJ, 498, L107.

[201] Tyson, J.A., Valdes F., Wenk R.A., 1990, ApJ, 349, L1.

[202] Udalski, A., Szymanski, M., Kaluzny, J., Kubiak, M., Krzeminski, W., Mateo, M., Preston, G.W., Paczynski, B., 1993, Acta. Astron., 43, 289.

[203] van Kampen, E., 1998, MNRAS, 301, 389.

[204] Verde, L., Heavens, A.F., Percival, W.J., Matarrese, S., Baugh, C.M., Bland-Hawthorn, J., Bridges, T., Cannon, R., Cole, S., Colless, M., Collins, C., Couch, W., Dalton, G., De Propris, R., Driver, S.P., Efstathiou, G., Ellis, R.S., Frenk, C.S., Glazebrook, K., Jackson, C., Lahav, O., Lewis, I., Lumsden, S., Maddox, S., Madgwick, D., Norberg, P., Peacock, J.A., Peterson, B.A., Sutherland, W., Taylor, K., 2002, MNRAS, 335, 432; [astro-ph/0112161].

[205] Vilenkin, A., 1984, Phys. Rev. Lett., 53, 1016.

[206] Vitviska, M., Klypin, A., Kravtsov, A.V., Wechsler, R.H., Primack, J.R., Bullock J.S., 2001, ApJ, in press; [astro-ph/0105349].

[207] von Soldner, J., 1804, Berliner Astron. Jahrb, 161.

[208] Waga, I., & Miceli A.P.M.R., 1998, Phys. Rev. D, 59, 1035.

[209] Wallington, S., Kochanek, C.S., & Koo D.C., 1995, ApJ, 441, 58.

[210] Walsh, D., Carswell, R.F., Weymann, 1979, Nature, 279, 381.

[211] Wambsganss, J., Cen, R., Xu, G., Ostriker, J.P., 1997, ApJ, 475, L81.

[212] Wang, L., Caldwell, R.R., Ostriker, J.P., & Steinhardt P.J., 2000, ApJ, 530, 17.

[213] Wang, Y., 1999, ApJ, 525, 651.

[214] Wang, Y., & Garnavich, P.M., 2001, ApJ, 552, 445.

[215] Weinberg, S., 1976, ApJ, 208, L1.

[216] Weinberg, S., 1992, Gravitation and Cosmology, Wiley, New York.

[217] Weller, J., Albrecht, A., 2001, Phys. Rev. Lett., 86, 1939.

[218] Weller, J., Albrecht, A., 2002, Phys. Rev. D, 65, 103512, [astro-ph/0106079].

[219] Wetterich, C., 1988, Nuclear Phys. B, 302, 668.

[220] Will, C.M., 1988, Am. J. Phys., 56, 413.

[221] Will, C.M., 1993, Theory and Experiment in Gravitational Physics, rev. ed., Cambridge University Press, Cambridge.

[222] Williams, L.L.R., Navarro, J.F., Bartelmann, M., 1999, ApJ, 527, 535.

[223] Wu, X.-P., 2000, MNRAS, 316, 299.

[224] Wu, X.-P., Chiueh, T., Fang, L.-Z., & Xue, Y.J., 1998, MNRAS, 301, 861.

[225] Yamamoto, K., & Futamase, T., 2001, Prog. Theor. Phys., 105, 707.

[226] Zel'dovich, Ya.B., 1964, Sov. Astr., 8, 13.

[227] Zel'dovich, Ya.B., 1968, Sov. Phys.-Uspekhi, 11, 381.

[228] Zhu, Z.-H., 2000, Mod. Phys. Lett. A, 15, 1023.

[229] Zwicky, F., 1933, Helv. Phys. Acta, 6, 110.

[230] Zwicky, F., 1937, Phys. Rev. Lett., 51, 290.

[231] Zwicky, F., 1937, Phys. Rev. Lett., 51, 679.